THE UNIVERSITY
of EDINBURGH

Polymers, Proteins, and Cells

Yichuan Zhang

Doctorate of Philosophy

The University of Edinburgh

2019

Lay Abstract

Many synthetic polymers have been developed for clinical applications, and include synthetic bone scaffolds or artificial corneas with these materials made *en masse* and used clinically. In the first part of my thesis I report how artificial polymers can be made inside cells. Cells were found to be fully viable following polymer formation but behaved slightly differently to untreated cells. The formation of polymers inside cells provided cells with a variety of new functions such as fluorescence and nanoparticle generation.

Many techniques have been developed to help surgeons efficiently delineate cancerous tissue from non-cancerous, with fluorescence-guided surgery a powerful new approach to "mark" or label cancer cells to allow surgeons to visualise tumour tissues and remove them. However, the brightness of the label is often insufficient while a wash step is typically needed to remove unbound fluorescent molecules from healthy tissues. In the second part of my thesis a polymer based fluorescent probe was generated that targets tumour cells and carry multiple fluorescent molecules while generating over 80-fold higher brightness. To promote the signal to noise ratio, a non-fluorescent molecule that specifically reacted with the probe and became fluorescent was developed removing the need of the wash and amplifying the signal.

Abstract

Biopolymers such as proteins, nucleic acids and polysaccharides are essential components in living systems and enabling the modification and modulation of various cellular functions and cellular behaviour. Many synthetic polymers have been used in a cellular context mimicking these natural polymers. However, few studies have focused on polymerisation chemistry within the complicated biological environment inside cells. In the first part of this thesis, a new method of synthesising synthetic polymers in cells was developed, enabling the introduction of artificial components to tune cellular behaviour. Several biocompatible acrylic and styrene monomers were polymerised intracellularly and shown to control the cell cycle, alter the cytoskeleton and influence cell motility. Moreover, the introduction of specific functional monomers enabled the *in situ* formation of fluorescent polymers and nanoparticles which may contribute to further applications such as fluorescent imaging and cargo delivery.

Chemical modifications of native biomacromolecules provides access to novel functions such as macromolecule based cargo delivery and imaging probes. In the second part of this thesis, linear acrylamide polymer scaffolds, bearing norbornene reactive centres for tetrazine ligation and a hexahistidine tag for ease of purification, were synthesised and conjugated to a clinical antibody. This enabled the selective labelling of cancer cells with amplified fluorescent signal. Simultaneously "switching on" and amplification of a fluorescent signal "*in situ*" were achieved by utilising a tetrazine quenched fluorophore, reacting with norbornenes on the polymer–antibody conjugate. This fluorescence signal amplification method has the potential to improve real-time tumour detection and fluorescence-guided surgeries while the amplification strategy can be expanded to enhance radio-therapy performances.

Table of Contents

Declaration of Authorship

All research performed in this thesis was carried out under the supervision of Professor Mark Bradley at the University of Edinburgh from September 2015 to January 2019. The work, data, and interpretation presented here are those of the author unless there was significant collaborative contribution made, in which case it has been clearly recognised. No part of this thesis has been previously submitted for any other degree or professional qualification.

Parts of the presented work in this thesis are currently in press or ready for submission:

Yichuan Zhang†, Alessia Gambardella†, (equal contribution) Muhammed Ucuncu, Jin Geng, Annamaria Lilienkampf and Mark Bradley. Polymer–protein conjugates – signal amplification. Ready for submission.

Jin Geng†, Weishuo Li†, Yichuan Zhang†, (equal contribution) Neelima Thottappillil, Jessica Clavadetscher, Annamaria Lilienkampf, Mark Bradley. Radical polymerisation inside living cells. *Nat. Chem.* Accepted. 2019.

Signed:

Yichuan Zhang

Date:

Acknowledgements

First and foremost, I would like to thank Professor Mark Bradley for giving me the opportunity to carry out my PhD within his research group. I really appreciated for all your support and guidance. Thank you for affording me such a great opportunity to work and live in such a big and warm family – the Bradley group.

I would like to thank Nanna, Jin, Muhammed, Matt, Alicia, Sarah and Matteo for mentoring me and the kind advice during the past 3.5 years. I have learnt a lot from you about how to be a good chemist. It is really nice to working with all the group members, past and present, as my friends: Andrea, Antonio, Clarissa, Dan, Durgadas, Eva, Fuad, Gavin, Hua, Jess, Jingjing, Kevin, Mithun, Neelima, Patricia, Paul, Sara, Sesha, Shuo, Vikki and Weishuo. Thank you for encouraging and supporting me all the time.

A big thank to Ale, thank you for sharing both the successes and failure with me. It was really nice to collaborate with you. It was not possible for me to finish the projects without your huge efforts. By the way, I will always remember the magic pink compounds you have made.

As a foreigner, the language was a big barrier when I was first here. A big thank to Matt, Jess, Sara, Sesha, and Sarah, for trying a lot to talk to me and encourage me. Also, I very much appreciated the proofreading by Nanna, Matt and Sarah. Thank you!

On the personal side, I would like to thank my family, especially my wife Jie for always being on my side. I am thankful for my Chinese friends, especially Daye, Chao, Peilei, Meng and Zhengyi. Thank you for sharing the happiness with me and being patient with me when I wa sad.

Four years time in Edinburgh has passed fast. I believe it was the best choice I have ever made to come to Edinburgh. I enjoyed a lot, learnt a lot and gained a lot. Thank you!

Abbreviation

AIBN: 2,2′-azobis(2-methylpropionitrile);

AEMA: 2-aminoethyl methacrylate;

AOTCRhB: acryloxyethyl thiocarbamoyl rhodamine B;

BSA: bovine serum albumin;

DCFH-DA: dichloro-dihydro-fluorescein diacetate;

DIPEA: *N*,*N*-diisopropylethylamine;

DMAA: *N*,*N*-dimethylacrylamide;

DMEM: Dulbecco's modified eagle's medium;

DNA: deoxyribonucleic acid;

ECM: extracellular matrix;

EDC: *N*-(3-dimethylaminopropyl)-*N*′-ethylcarbodiimide hydrochloride;

FBS: fetal bovine serum;

FMMA: ferrocenylmethyl methacrylate;

GPC: gel permeation chromatography;

HEMA: 2-hydroxyethyl methacrylate;

HPLC: high-performance liquid chromatography;

HPMA: *N*-(2-hydroxypropyl) methacrylamide;

ICP-MS: inductively coupled plasma mass spectrometry;

MALDI-TOF: matrix-assisted laser desorption/ionization-time of flight;

MBA: *N,N*′-methylene bis(acrylamide);

NaSS: sodium 4-styrenesulfonate;

NHS: *N*-hydroxysuccinimide

O-HPMA: *O*-2-hyroxypropyl methacrylate;

PBS: phosphate buffered saline;

PEG-DA: poly(ethylene glycol) diacrylate;

PEG-MA: polyethylene glycol methyl ether methacrylate;

PET: photoinduced electron transfer;

PFA: paraformaldehyde;

PS: polystyrene;

RAFT: reversible addition–fragmentation chain transfer;

TEM: transmission electron microscopy;

VAN: 4-vinylaniline;

VBA: 4-vinylbenzoic acid.

Chapter 1. Introduction

Synthetic polymers have rapidly developed over the past few decades with many polymeric materials now used in clinical applications. For instance, polymers have been used as tissue engineering scaffolds to support cell growth (see Figure 1). An "artificial skin" was commercialised (Dermagraft®), enabling human neonatal dermal fibroblasts on a bioabsorbable polyglactin mesh to help wound closure[1] for burn patients (Figure 1a).[2] An injectable implant using poly(L-lactic acid) (Sculptra® Aesthetic), was approved by the Food and Drug Administration in 2004 and is used today as a filling material in plastic surgery (Figure 1b).[3, 4] RESOMER®, biodegradable polyesters (*e.g.* poly(L-lactic acid), polycaprolactone and poly(lactic acid-*co*-glycolic acid)), are shaped to give *e.g.* microparticles, rods, fibres and meshes, for bone fracture patients (Figure 1c).[5]

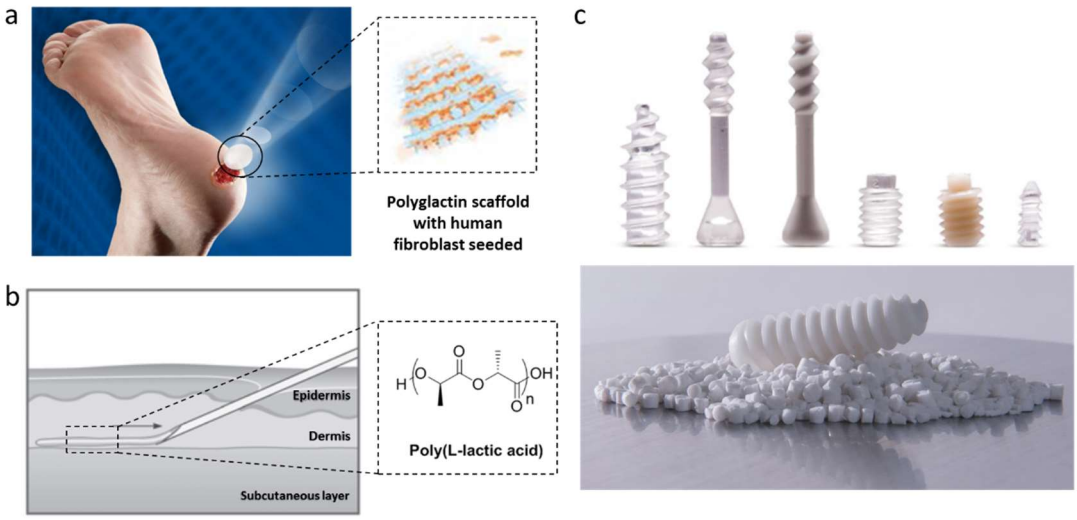

Figure 1. Examples of polymers used as biomaterials for medical applications. (a) Human fibroblasts seeded onto a polyglactin scaffold and allowed to proliferate give the medical product Dermagraft®.[2] (b) Poly(L-lactic acid) macroparticles are used as a filling material for injection into dermis of the patient.[4] (c) Several polyester based RESOMER® products are shaped into different shapes and used as biodegradable scaffolds.[5]

Polymers have been used for drug delivery and controlled release. Poly(lactic-*co*-glycolic) based materials (RESOMER® Sterile), have been approved by the Food and Drug

Administration for drug encapsulation allowing precisely controlled release *(e.g.* therapeutic peptides and proteins) release.[5] Myocet®, marketed by Teva, encapsulates Doxorubicins in polymeric vesicles to improve the water solubility of the hydrophobic drug and reduce the dosage.[6]

The attractiveness of polymers has driven much research towards understanding how artificial polymers interact with live cells, how polymerisation chemistry influences cells, and whether such polymerisations can be conducted in the presence of cells. In Chapter 3, several successful polymerisation systems in cellular contexts are review. The possibility of synthesising synthetic polymers in cells is demonstrated and the influence of the polymerisation chemistry on cells is evaluated with several examples showing the possibility of introduction of new functions into cells.

Besides medical applications, polymers also play an important role in biological research. For example, expansion microscopy was established recently that utilises the swelling effect of polymeric hydrogels in water to "expand" biological samples for fluorescence microscopy (see Figure 2).[7] Specifically, fluorescent markers are decorated with "molecular handles" which enable them to bind to a polymer hydrogel, and incubated with the fixed tissue to mark the features of interest. The tissue is then immersed in a solution containing monomers, *e.g.* sodium acrylate and acrylamide, crosslinkers, *e.g. N*,*N*'-methylenebisacrylamide and initiators to form a densely crosslinked hydrogel with the fluorescent markers covalently attached. The polymerised tissue sample is homogenised by denaturation (by heating or enzymatic digestion) minimising the interactions between biomolecules, and then swells in water to achieve the expansion.[7, 8] The biological samples can be expanded by approximately 100-fold in volume permitting the imaging of tissues and organs in 3D with a nanoscale resolution. This technique, for example, enabled visualisation of an entire mouse brain in 3D with high resolution, with quantitative measurement of organelle volume and morphological parameters such as dendritic spin and protein expression within the whole brain region.[9]

Super resolution microscopy is also a powerful fluorescent imaging technique widely used in biology, because it can bypass the resolution limitation of traditional optical microscopy (around 250 nm, known as Abbe limit[10]) caused by the diffraction limit of light. The use of unique fluorophores which are switchable or have a non-continuous emitting property (*i.e.* not all of the fluorophores emit at the same time), enables neighbouring fluorescent

molecules to be in different states ("on" and "off") to be resolved from each other. The "on" fluorophores then can be imaged individually using high resolution fluorescent microscopy. By stacking images from different time points, super resolution images can be achieved (Figure 3).[11, 12]

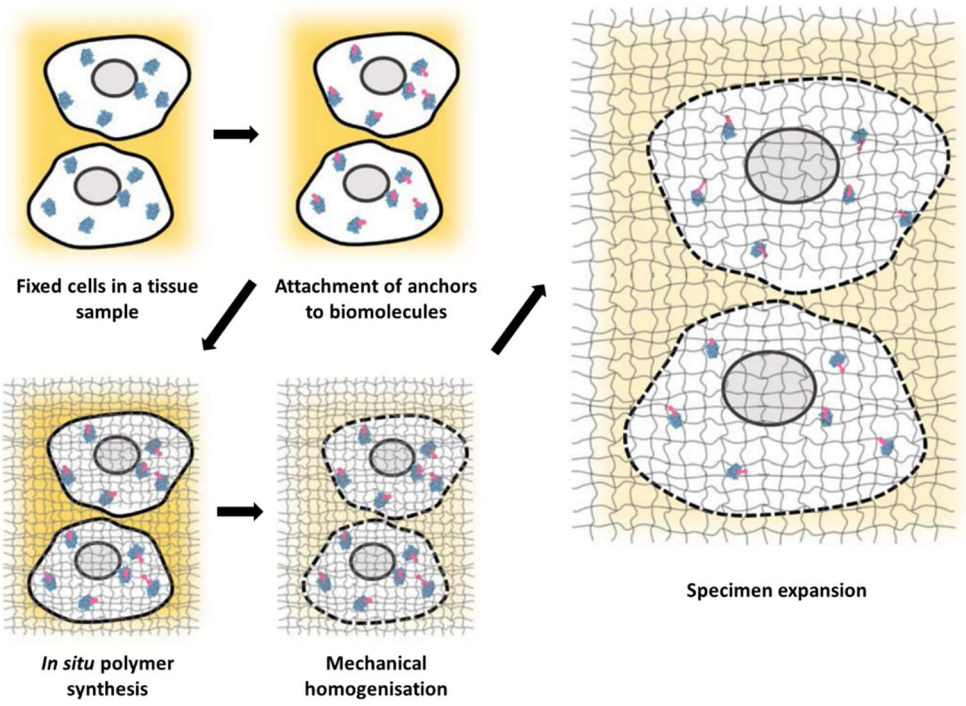

Figure 2. Principle of expansion microscopy.[8] The tissue sample was fixed and labelled with fluorescent markers. A polymeric hydrogel was formed *in situ* and swelled in water to achieve an expanded feature to allow conventional fluorescent microscopy analysis.

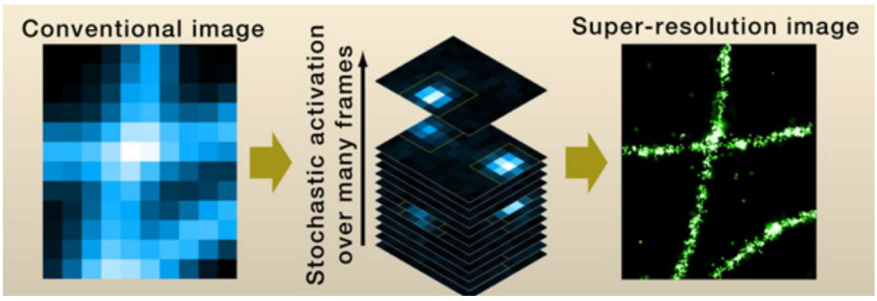

Figure 3. Principle of the super-resolution imaging approach. Separate images of single molecules are taken and overlapped spatially to construct a super-resolution image.[11]

This technique has allowed it to be used for investigation of plasma membrane proteins and membrane microdomains which are too small to be resolved by conventional light microscopy.[13, 14] Visualisation of internal structures in bacteria (typically 1 μm^3 in volume), much smaller than mammalian cells, were challenging for conventional light microscopy, but now can be achieved using super resolution microscopy.[15]

However, limited fluorescence intensity of many markers may lead to low sensitivity, and narrow detection range particularly with low abundance targets.[16, 17] Therefore, signal amplification methods are required for improving fluorescence detection. In Chapter 4, a number of commonly used signal amplification methods are reviewed and the approach of polymer–protein conjugate based amplifications is explored and shown to give up to 80-fold increase in fluorescent signal.

Chapter 2. Aims and Objectives

Applications of polymers are found across chemistry and material science and used extensively in medicine and impact on all aspects of daily life. Although the mechanisms of many polymerisation reactions have been studied in depth, there are only a few examples of looking at “organic chemistry-based” polymerisations in living systems. The first work in this thesis shows the possibility of conducting free radical polymerisation chemistry in cells with an evaluation of its influence on cells with examples given of introducing new functions into cells.

The second aspect of this thesis shows how polymers can serve as a platform for multiple functional motifs for amplification. By conjugating a targeting moiety, such as an antibody, a polymeric scaffold will be shown to act as a site for specific fluorescent probe amplification, targeting and visualisation of cancer with simultaneous “turn on” and amplification of fluorescent signals.

Chapter 3. Radical Polymerisation inside Living Cells

3.1. Introduction

3.1.1. Natural Polymers in Cells

The chemical composition of cells is huge, encompassing macromolecules, such as proteins, nucleic acids, polysaccharides, and small molecules including water, metal ions and lipids and everything in between. These molecules interact with each other in multiple ways to drive function (*e.g.* proliferation, movement, apoptosis). Macromolecules (ranging from 10^3 to 10^{12} Da), as defined by Staudinger in 1920s,[18] contribute to distinct functionalities in biological systems, *e.g.* polynucleotides have the function of information storage; polypeptides have the function of catalysis and polysaccharides contribute to energy storage, although these functions are widely mixed.[18, 19]

Polynucleotides, including deoxyribonucleic acids (DNA) and ribonucleic acids (RNA) are fundamental biomacromolecules of all known living organisms.[20] Chemically, they are linear polymers constructed of nucleotides containing nitrogen based heterocyclic bases and sugar phosphate esters (see Figure 1). In mammalian cells, these polynucleotides comprise some 10% of the dry mass of a cell, are essential components for information storage and information translation by which the genetic code guides the synthesis of proteins.[21, 22]

Polypeptides are also fundamental macromolecular building units in cells,[23] based on polymers constructed by α-amino acids (see Figure 1), that can be assembled into unique 3D structures by covalent crosslinking (*e.g.* disulfide bond) and/or physical interactions, *e.g.* hydrogen bonds, salt bridges and hydrophobic-hydrophobic interactions. They are the major component of cells (60% dry mass), with diverse functions, such as binding (*e.g.* membrane protein binding to signalling molecules), catalysis (*e.g.* enzymes) and structure (*e.g.* collagen and actin, the building blocks of the cytoskeleton).[19]

Polysaccharides are another type of biopolymer commonly found in/on cells based on sugars covalently linked by glycosidic linkages (Figure 4).[24] The functions of these biopolymers included energy storage (*e.g.* starch and glycogen used for energy storage in plant and animal,

respectively), structure (*e.g.* cellulose, a fundamental structural component of cell walls in plants) and surface recognition (*e.g.* glycocalyx).[25]

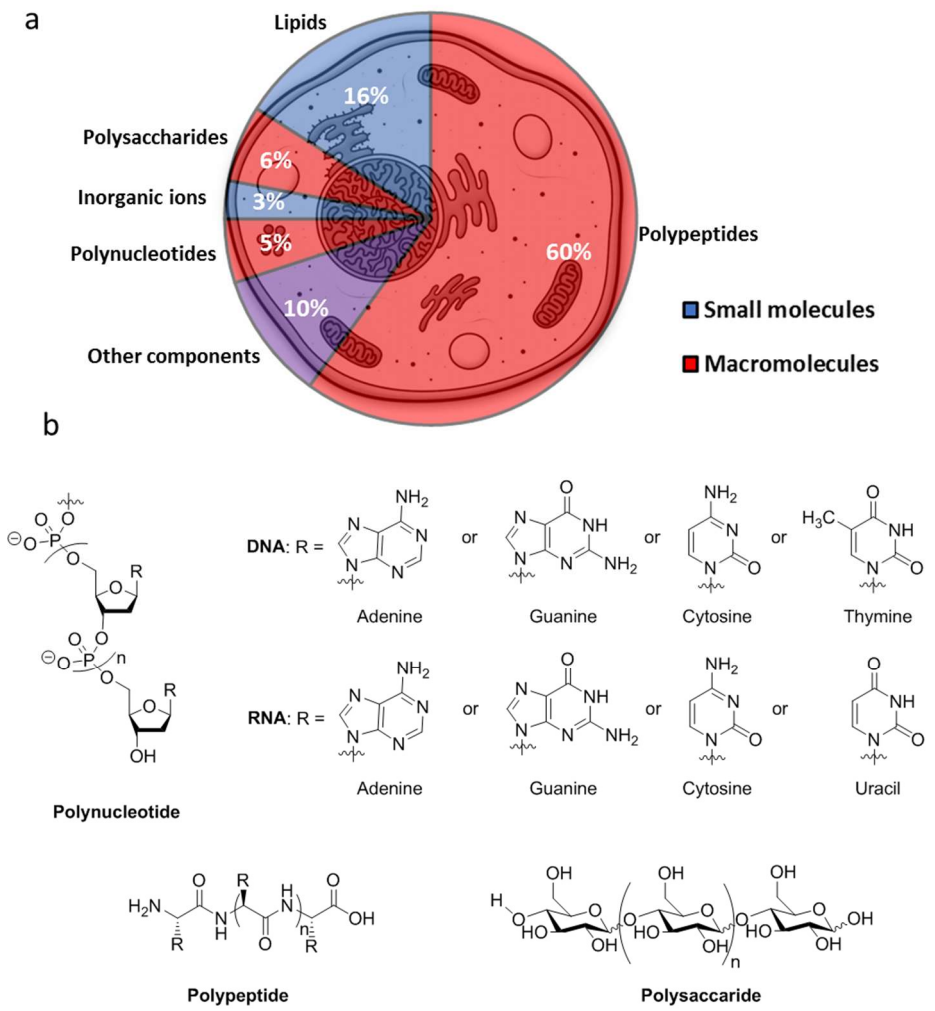

Figure 4. (a) Composition (by mass) of a typical mammalian cell.[26] (b) Chemical structures of biomacromolecules: polynucleotide, polypeptide and polysaccharide.

Other polymers such as polyesters and polyphosphates are also found in some organisms. For example, poly(hydroxyalkanoates), polyesters, are produced by many bacteria as intracellular granules and used as energy storage material, while polyphosphates, constructed with phosphoanhydride bond linked phosphates, have been found in the stress response in some bacteria.[27, 28]

3.1.2. Synthetic Polymers Used in a Cellular Context

With the development of biology and medical science, the demand for advanced functional macromolecular materials has been continuously expanding.[29] The development of polymer science allows various synthetic polymers with well controlled chemical compositions and molecular weights to be fabricated into materials with desired sizes, mechanical properties and surface morphologies. These are widely used in biological research and medical applications, such as tissue engineering, cargo delivery and cancer therapy to name but three.

For example, human coronary artery smooth muscle cells were seeded on nanofibers (produced by electrospinning of biodegradable polycaprolactone with collagen) with the cell shape guided by the fibre orientation. The stem cells were found to be directed to migrate towards the inside of the fibres and differentiated to smooth muscle cells with sufficient growth and proliferation rate (comparing to cells cultured in tissue culture plate), showing the potential to form muscle tissues and blood vessels *in vitro* for transplantations.[30] Transition metal, such as palladium can be trapped within polystyrene microparticles to allowed the catalysis of various artificial chemical reactions intracellularly, which is of importance in chemical biology (*e.g.* imaging) and pharmacology (*e.g.* prodrug activation).[31] Additionally, nanoparticles containing anticancer drugs have been synthesised with positively charged surfaces (for cell membrane penetration and degradation in acidic organelles, *i.e.* lysosomes) and used for delivery of drug molecules. The rapid release of drugs intracellularly allows efficient inhibition of drug-resistant cancer cells.[32]

3.1.3. Synthetic Polymers Synthesised in a Cellular Context

3.1.3.1. Polymers Synthesised around Cells

The *in situ* synthesis of unnatural polymers either around, on or in cells (Figure 5) is challenging due to the complicated environment in biological systems and the limited choices of bioorthogonal reactions for polymer synthesis.[33] Successful applications of *in situ* synthesised polymers have been reported, *e.g.* bioinks for bioprinting, but challenges still exist.[34, 35]

As a new possible tool in biology and medical science, bioprinting techniques potentially allowing the rapid and precise constructions of 3D scaffolds with live cell seeding.[34] Multiple

challenges exist such as the viabilities and functionality of the cells post printing, but bioprinting techniques have been rapidly developed driven by the attractive potential applications of such biofabrication approaches for both biological research and medical applications (*e.g.* tissue engineering).

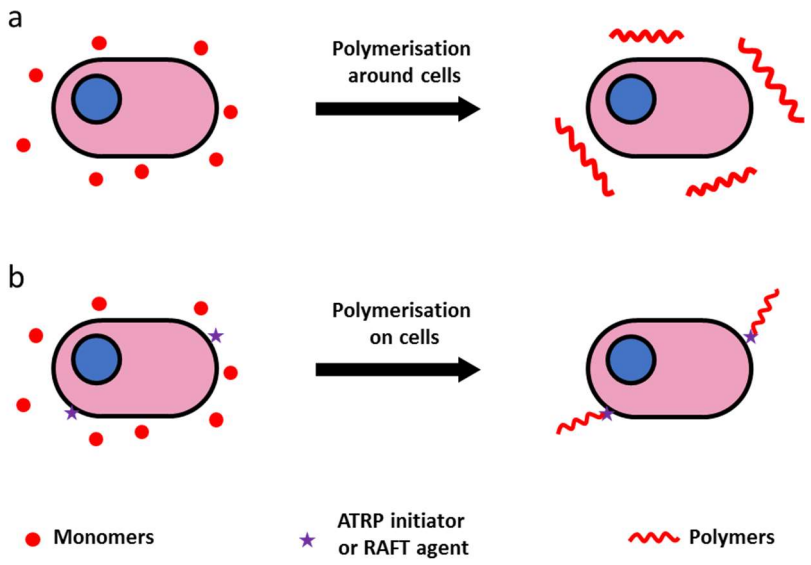

Figure 5. Examples of applying polymerisation around and on live cells. (a) Biocompatible monomers can be introduced into the culture media with cells. Subsequent polymerisation generates polymers around the cells. (b) For synthesising controlled and targeted polymers on cell surfaces via living polymerisation, initiating moieties, *e.g.* ATPR initiators and RAFT agents, are grafted onto the cell surfaces to allow *in situ* polymerisation giving grafted polymer chains on the cell surfaces.

The most commonly used method for bioprinting has been to print alternative layers of supporting materials (*e.g.* hydrogel) and cell suspensions with simultaneous photo/thermal polymerisation/crosslinking process to fabricate desired structures and functions of the materials.[36] For example, various types of cells have been 3D-printed with gelatin methacrylate and photopolymerised to give synthetic scaffolds with desired structures and mechanical strength.[37, 38] By precisely control the chemical component at different positions, an "artificial corneal" was successfully fabricated via the 3D printing of collagen based hydrogel and cell binding peptide together with live human limbal epithelial stem cells. The

"artificial corneal" was demonstrated to be similar to the natural corneal in terms of cell and collagen organization, stiffness, cell phenotype.[39]

Despite the successful applications of synthetic macromonomers (*e.g.* poly(ethylene glycol) diacrylate[36, 40, 41]) and natural product derived monomers (*e.g.* glycidyl acrylate-modified hyaluronic acid[42] and gelatin methacrylate[43-45]) used as substrates for bioprinting, the number of alternative monomers with different functional groups is limited because of the uncertain toxicity of the monomers, the polymerisation process, and the resulting polymers and side products to the cells.[34, 46]

3.1.3.2. Polymers Synthesised on Cells

In nature, some cells (*e.g.* bacteria and fungi) form hard shells to preserve their species under unfavourable harsh environments. Recent strategies have emerged to encapsulate cells with synthetic polymers as scaffolds to greatly prolong the viable period of the cells as well as providing additional functions to the cells.[47, 48] One of the key clinical applications is to encapsulate pancreatic islets which allows transplantation without immunosuppression.[49] The artificial membranes (e.g. alginate, chitosan, agarose and poly(ethylene glycol)) can protect the transplanted tissue/cells from the host immune system so that permit the use of foreign donor cells and even animal and stem cell derived islets for diabetic patients.[50-52] For example, the first reported encapsulation of islet (using alginate) permitted the cells to maintain their biofunctions in rats for up to 15 week.[52]

To achieve the encapsulated "artificial cells", many efforts have focused on developing the coating materials for live cell encapsulations.[53] For instance, dopamine has been polymerised onto cell surfaces (adhering to the cells following oxidation and reactions with free thiols and amines of surface proteins) of Saccharomyces cerevisiae which formed a robust and stable artificial shell protecting the yeast cells. Further functionalisation with streptavidin by similar polydopamine–protein interactions allowed isolation of encapsulated cells with a biotin decorated substrate (*e.g.* a glass slide). The possibility of introducing additional functionalities demonstrated the possibilities of conducting chemical reactions on the cell surface which may be challenging with unmodified native cells.[48]

Due to the uncontrolled dopamine polymerisation reaction, the "artificial polydopamine shell" was not homogenous. Another approach using a well-defined synthetic polymer *i.e.*

poly(ethylene glycol), overcame such issue and achieved a stable polymer shell on Hela cells.[47] The cells were firstly coated with positively charged gelatin by electrostatic interactions to provide an extracellular matrix like environment for the cells. Multibranched PEG molecules then crosslinked the gelatin by reacting with the free thiols on the gelatin chains through thiol–maleimide 1,4-addition chemistry and the rigid encapsulations promoted the long term viability of Hela cells under harsh environments (such as trypsin). Subsequent introduction of glutathione drove the cleavage of the thiosuccinimides (thiol–maleimide adduct) through the retro-Michael reaction and achieved "on-demand" degradation of the "polymeric shell" (Figure 6).

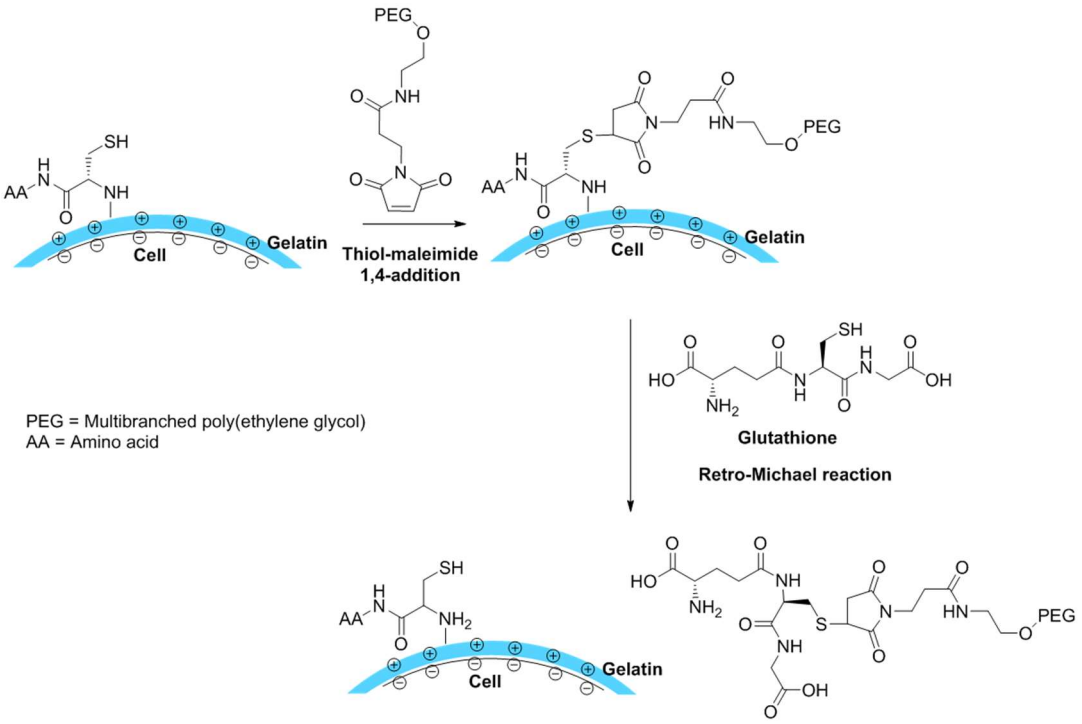

Figure 6. Living cell encapsulation by crosslinking of gelatin using maleimide functionalised multibranched poly(ethylene glycol). A layer of positively charged gelatin was firstly deposited on the negatively charged Hela cell surface and the maleimide functionalised multibranched poly(ethylene glycol) was added and reacted with free thiols on the gelatin to achieve the crosslinking. By introducing glutathione, the thiol group can attack the thiosuccinimides and undergo a retro-Michael reaction to degrade the crosslinked structure and release the encapsulated cells.

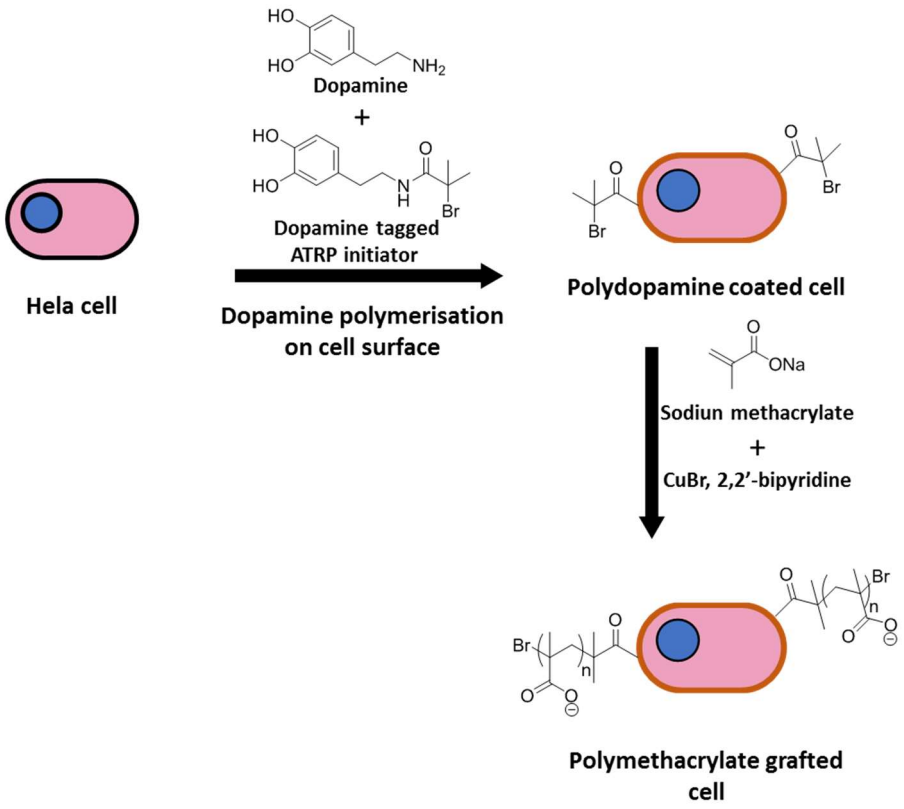

Figure 7. Polymerisation of sodium methacrylate on Hela cell surfaces. Hela cells were incubated in a solution of dopamine and dopamine tagged ATRP initiator (in Tris buffer, pH = 8.4) for 4 h to allow dopamine oxidation (by oxygen in the air) and polymerisation on cell surfaces. The isobutyl bromide moiety anchored on the cells allows ATRP of sodium acrylate (catalysed by CuBr-bipryidine complex) to generate poly(sodium methacrylate) on the cell surface.

However, direct encapsulation of cells with rigid polymer shells may affect molecular uptake, *e.g.* nutrient and oxygen, which may be overcome by controlled *in situ* polymerisation on cell surfaces to give polymeric shells with tuneable densities and mophologies.[54] Thus studies of controlled living radical polymerisations on cells have been studied. For example, yeast cell surfaces were functionalised with a dopamine tagged ATRP initiator (dopamine can polymerise in the presence of oxygen and strongly bind to surface proteins through covalent bond and hydrogen bond) followed by copper catalysed ATRP giving uniformly distributed linear polymer chains on cell surfaces (Figure 7).[55]

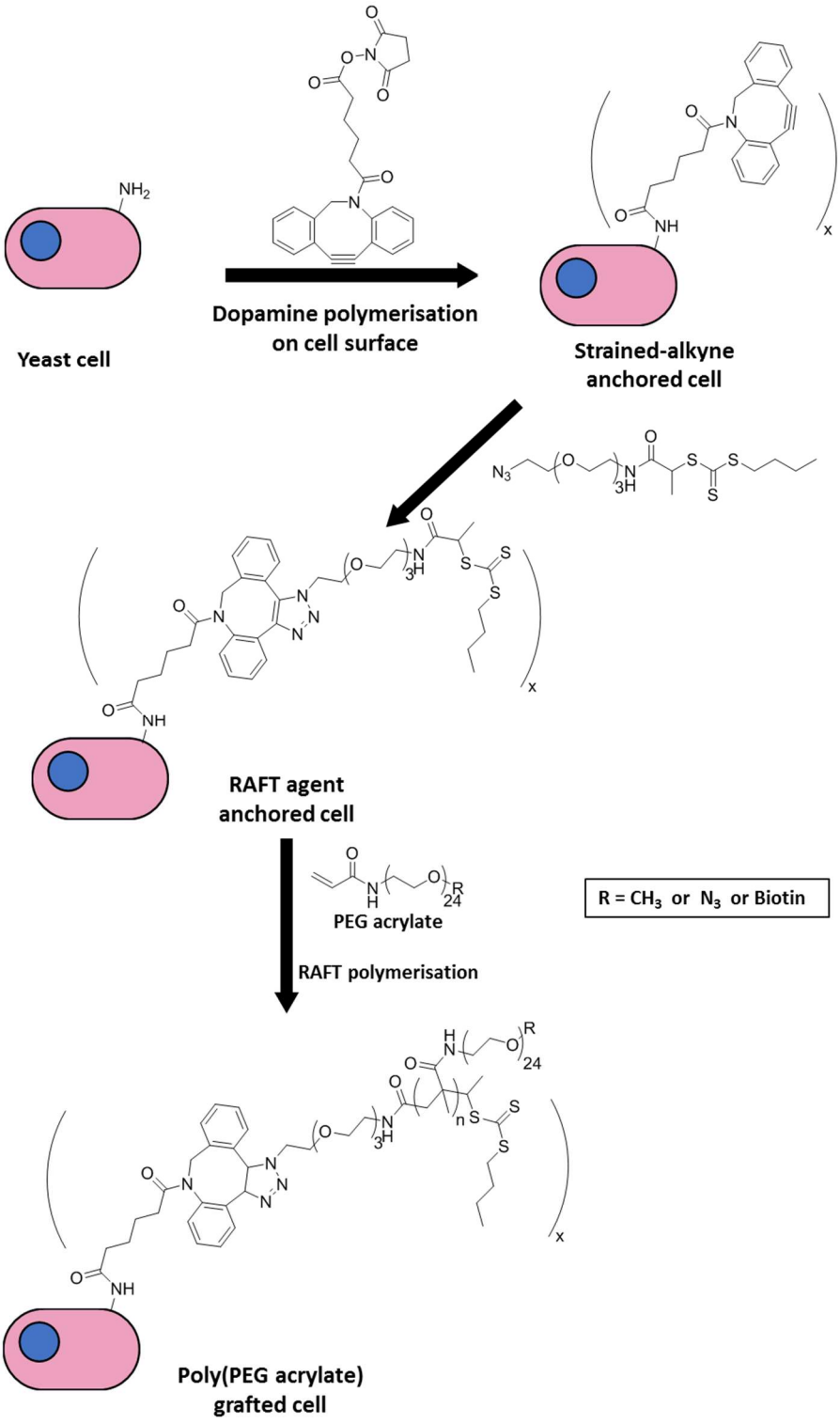

Figure 8. Polymerisation of PEG acrylate on the surface of yeast. The yeast were incubated with an active ester functionalised strained alkyne (in PBS, pH = 7.4) and then with an azide tagged RAFT agent to introduce the RAFT agent on the cell surface. The polymerisation of PEG acrylate could then be conducted by photoinduced electron transfer RAFT polymerisation to generate polymer grafted yeast.

However, the utilisation of copper ions may cause direct cytotoxicity, although the authors stated cell viability >60% after polymerisation due to the protection offering by the polydopamine shells.[55] An improvement was achieved by applying photoinduced electron transfer RAFT polymerisations. The chain transfer agents were anchored onto the yeast by conjugation of an active ester functionalised strained alkyne attached (to the lysine moieties on cell surfaces through active ester–amine coupling reaction) and then an azide tagged RAFT agent (through alkyne–azide cycloaddition) (Figure 8). The polymerisation of PEG acrylamides gave controlled polymers (Đ < 1.3, analysed by GPC) with different molecular weight (10-20 kDa) with almost full viabilities of yeast (determined by MTT assay).[54]

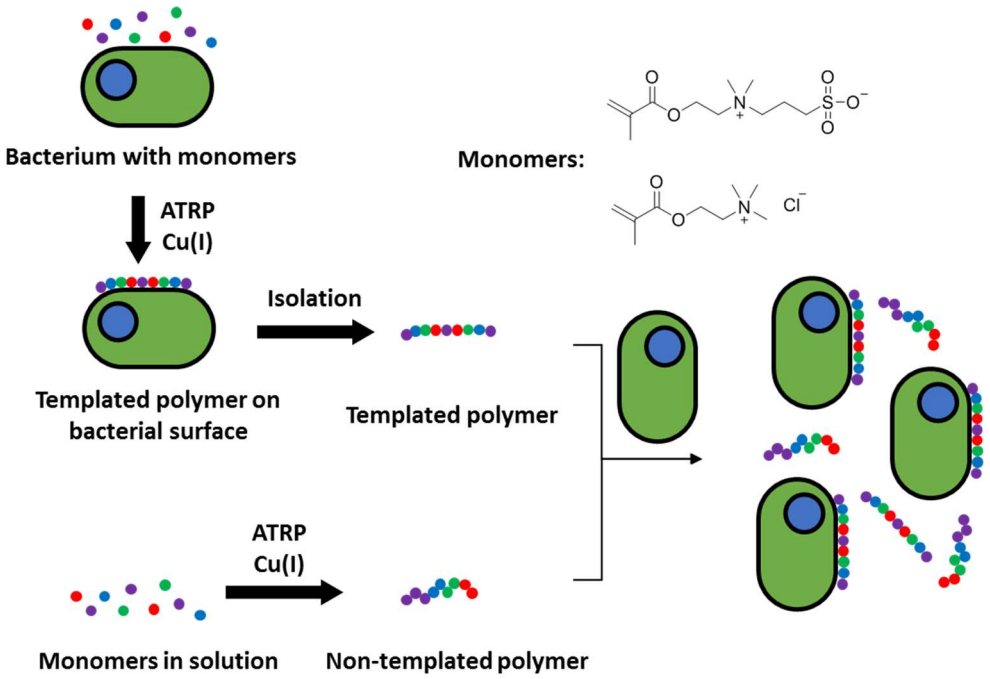

Figure 9. Templated polymer synthesised on bacterial surfaces. 2-(Methacryloyloxy)-*N*,*N*,*N*-trimethylethan amonium chloride and 2-(*N*-3-sulphopropyl-*N*, *N*-dimethyl ammonium) ethyl methacrylate were incubated with *E. coli* for 30 min and polymerised by adding the catalyst precursor $CuBr_2$ (which was reduced on the bacterial surfaces) and the ligand tris(2-pyridylmethyl) amine. The template polymers were isolated by washing the mixture with NaCl solution (0.15M) and dialysis. In comparison to non-templated polymer showing no specific binding, the template polymer could specifically bind to the same kind of bacteria upon which they were synthesised.

On bacteria, polymerisation of methacrylates was carried out through a copper catalysed ATRP reaction with the *in situ* reduced copper ions catalysing the chain propagation of the controlled polymerisation (see Figure 9).[56] The active copper species was only generated and localised on cell surfaces, avoiding chain propagation reactions in solution. The isolated polymers were shown to selectively recognise and bind specifically to the same kind of bacteria they were synthesised on (a molecular imprinting type approach). Such a strategy could act as a novel approach for bacterial/cell targeting and may aid the development of cell specific diagnostics and therapies.

In this chapter the first strategy for free radical polymerisation in an intracellular environment is reported. Biocompatible monomers and initiators were screened and used for synthesis of the synthetic polymers intracellularly with the successful polymerisation demonstrated by isolation of polymers from the "polymerised" cells and analysis by NMR and GPC. The mechanisms of the polymerisations were investigated and the influence of the polymerisation on the cells were evaluated in terms of cell viability, proliferation ability, cell cycle, cell mobility and cytoskeleton. The *in situ* generation of fluorescent polymers from non-fluorescent monomers and polymeric nanoparticles from soluble small molecules demonstrated possible applications utilising such an intracellular polymerisation strategy.

3.2. Results and Discussions

3.2.1. Biocompability of Photopolymerisation in Cells

3.2.1.1. Biocompability of Monomers and Initiators (with Dr W. Li and Dr J. Geng)

Acrylate, acrylamide, methacrylate, methacrylamide and styrene-based monomers readily undergo free radical polymerisation to give polymers with various structures and functions.[57, 58] These monomers have typically been believed to be highly toxic,[59, 60] and therefore before application in cell-based assays their biocompatibilities had to be evaluated. Thus a range of monomers with various functional groups (*e.g.* hydroxyl, carboxylic acid, sulfonic acid, amine, ferrocene and poly(ethylene glycol) chain), were screened on Hela cells using an MTT assay and their IC_{50} values (Table 1). Interestingly, the monomers displayed a broad range of toxicities but with no obvious relationship observed between monomer structure and cytotoxicity. From the screening, *N*-(2-hydroxypropyl) methacrylamide (HPMA), sodium 4-styrenesulfonate (NaSS), 4-vinylaniline (VAN) and ferrocenylmethyl methacrylate (FMMA) were selected for further studies.

Photoinitiators Irgacure2959 and BAPO-ONa[61] (Figure 10) have been reported to be well tolerated by many cell types (including human fetal osteoblasts, corneal epithelial cells, human mesenchymal stem cells, and human embryonic germ cells) and have been used in multiple biomedical and tissue engineering applications.[62-64] For example, Irgacure2959 was utilised for photopolymerisation of monomers into hydrogels (aided with of 365 nm illumination) with minimum effect on cell viability.[62, 63] BAPO-ONa showed even higher polymerisation reactivity and water solubility and has been used for 3D printing of hydrogels in aqueous solutions.[64] Here good biocompatibility of both photoinitiators were observed (with nearly full viability of Hela cells after 48 h incubation at 5 μM, Figure 10b and 10c), which was in good agreement with literatures.

Table 1. Chemical structures and the IC_{50} values of the monomers evaluated as part of this work. Hela cells were treated with the monomers at a set of concentrations (typically from 1 mM to 1000 mM). The concentration range was reset to 1 µM to 1 mM if the viability was lower than 80% at 1 mM) for 48 h and the viability was measured by an MTT assay.

Monomer abbreviation	Monomer name	Monomer structure	IC50
HPMA	*N*-(2-Hydroxypropyl) methacrylamide	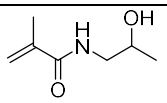	>250 mM
NaSS	Sodium 4-styrenesulfonate	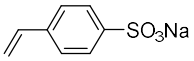	>100 mM
VAN	4-Vinylaniline	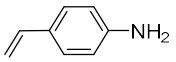	56 mM
FMMA	Ferrocenylmethyl methacrylate	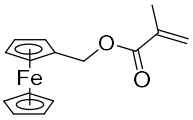	68 mM
AEMA	2-Aminoethyl methacrylate	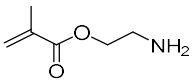	20 mM
VBA	4-Vinylbenzoic acid	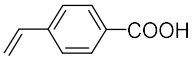	15 mM
MBA	*N*,*N*'-Methylene bis(acrylamide)	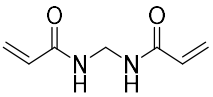	20 mM
PEGDA (Mn = 575 Da)	Poly(ethyleneglycol) diacrylate (Mn = 575 Da)	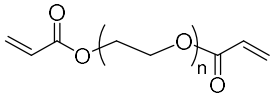 n = 12	4 mM
PEGDA (Mn = 10 kDa)	Poly(ethyleneglycol) diacrylate (Mn = 10 kDa)	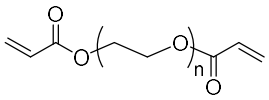 n = 2300	25 mM
AOTCRhB	Acryloxyethyl thiocarbamoyl rhodamine B	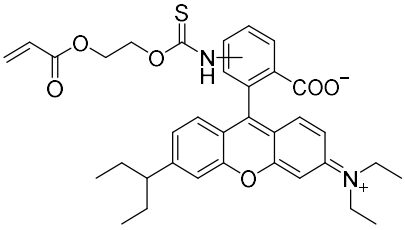	20 µM
Acrylamide	Acrylamide	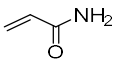	1 µM
PEGMA (Mn = 480 Da)	Poly(ethylene glycol) methyl ether methacrylate (Mn = 480 Da)	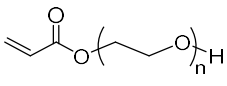 n = 12	1 mM
HEMA	2-Hydroxyethyl methacrylate	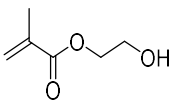	7 mM
O-HPMA	*O*-2-Hyroxypropyl methacrylate	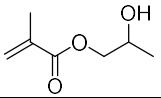	8 mM

The tolerance of Hela cells to 365 nm illumination (5 mW/cm^2) was also investigated with over 80% cells viable after 10 min illumination at 365 nm (see Figure 11).

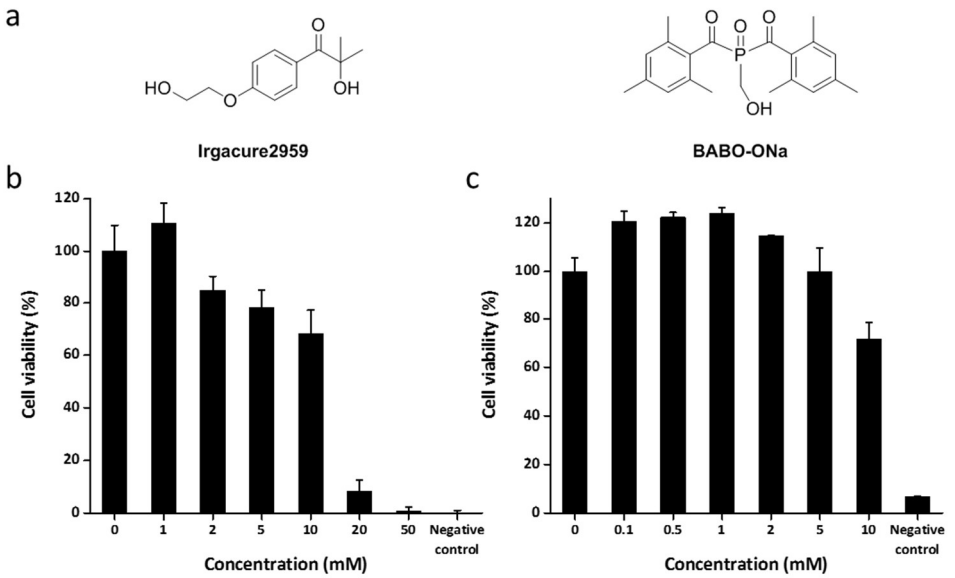

Figure 10. (a) Chemical structures of the two initiators used and HeLa cell viability after incubation for 48 h with (b) Irgacure2959 (1 mM to 50 mM) and (c) BAPO-ONa (0.1 mM to 10 mM). Viability measured using an MTT assay, n = 6. As a negative control the cells were treated with 50% DMSO in DMEM.

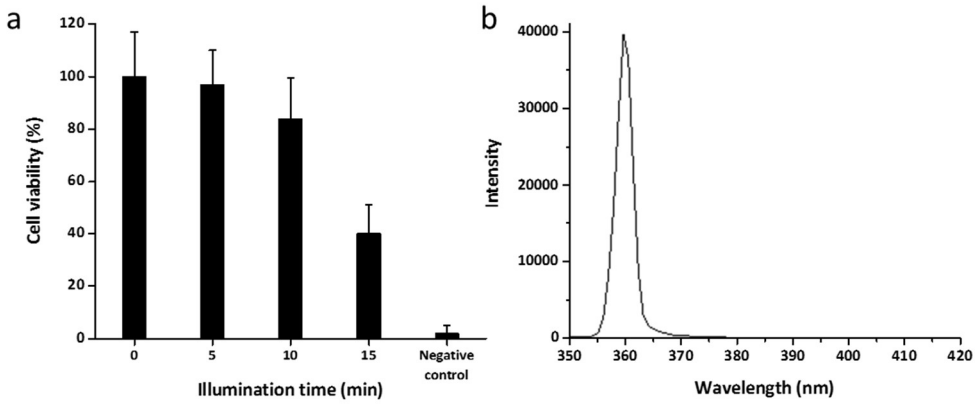

Figure 11. (a) HeLa cell viability after 5, 10, 15 min illumination (365 nm, 5 mW/cm^2). The cells were incubated for a further 48 h before the viability was measured by an MTT assay, n = 3. As a negative control the cells were treated with 50% DMSO in DMEM. (b) The emission spectrum of the Blak-ray UV lamp used for the intracellular polymerisation (maximum emission at 365 nm).

3.2.1.2. Biocompability of the Polymerisation Process

The effect of the polymerisation process on cell viability was investigated. Treatment of cells with HPMA (1 mM to 100 M) and Igracure2959 (2 mM) followed by 365 nm illumination (5 min) showed low cytotoxicity with over 85% viability (up to 100 mM HPMA). This indicates the tolerance of Hela cells to the radical polymerisation conditions (Figure 12a), which is in agreement with previous studies that suggested that radicals generated intracellularly are not directly relevant to cell viability (*e.g.* a series of photoinitiators producing benzoyl radicals were shown to be tolerated by fibroblasts (NIH/3T3) and chondrocytes following UV/visible light irradiation (>80% viability), with up to 0.3 mM of radical forming in the cells (theoretically calculated)).[63-65]

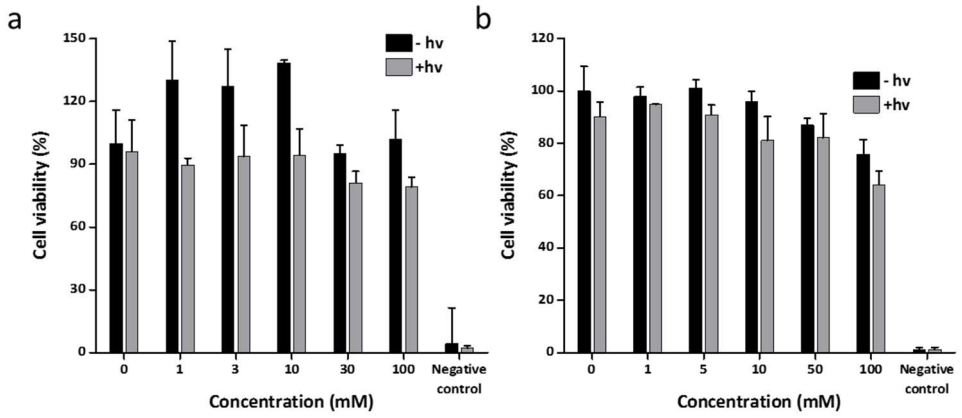

Figure 12. (a) HeLa cell and (b) human adipogenesis mesenchymal stem cell viability after "polymerisation". The cells were incubated with HPMA (1 mM to 1 M) and initiator Irgacure2959 (2 mM) for 4 h followed by illumination for 5 min at 365 nm and were incubated for further 48 h before the viability measured by an MTT assay, n = 6. As a negative control the cells were treated with 50% DMSO in DMEM.

The negligible effect on cell viability of the polymerisation was also confirmed by the same viability assay on human adipogenesis mesenchymal stem cells (Figure 12b), which also showed tolerance to the photo-polymerisation.

To investigate the long term effect of the *in situ* polymerisation, Hela cells were "polymerised" (treated with 50 mM of monomers HPMA, NaSS, VAN or FMMA, initiator Igracure2959 (2 mM) and 365 nm illumination) and were evaluated after 7 days using a cell viability assay (CellTiter-Glo® assay, which quantified the amount of ATP generated) and a proliferation assay (Click-iT™ EdU assay, which quantified the ratio of cells proliferating by quantification of cells synthesising DNAs) (Figure 13 and 14).

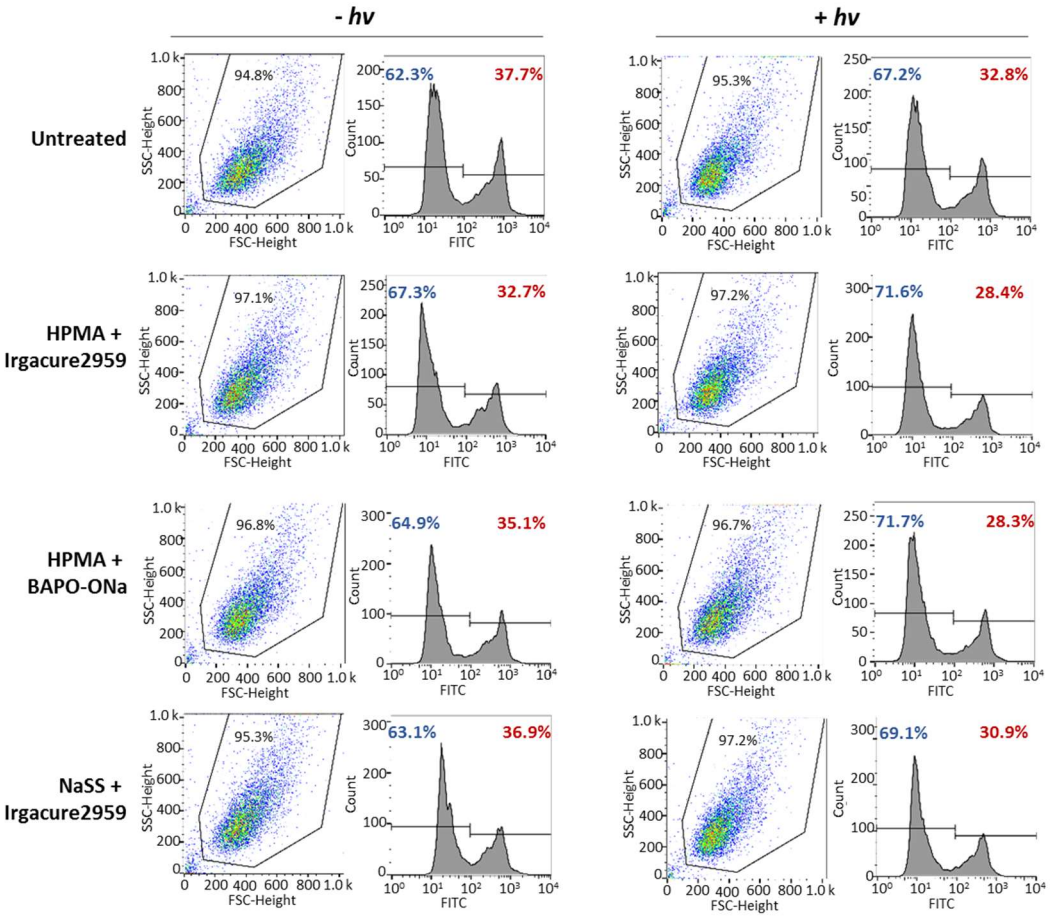

Figure 13. Cell proliferation of Hela cells incubated with monomers (50 mM) and initiator (2 mM) for 4 h, washed and illuminated for 5 min at 365 nm. The cells were then incubated at 37 °C for 7 days and analysed by the Click-iT EdU flow cytometry assay (the cells were incubated with an alkyne labelled 5-ethynyl-2'-deoxyuridine (EdU) for 2 h, and subsequently labelled with an azide-fluorescein according to the manufacturer's instructions). 4-vinylaniline treated cells showed a significant reduction in the number of intact cells and therefore the flow cytometry based proliferation assay could not be carried out.

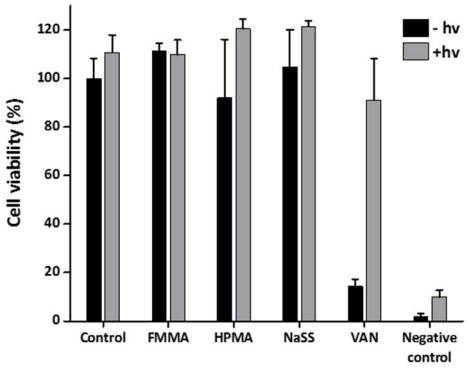

Figure 14. Cell viability of HeLa cells following intracellular polymerisation (CellTiter-Glo 2.0 assay). The cells were treated with monomers (ferrocenylmethyl methacrylate (FMMA), N-(2-hydroxypropyl) methacrylamide (HPMA), sodium 4-styrenesulfonate (NaSS) and 4-vinylaniline (VAN), 50 mM) and Irgacure2959 (2 mM) for 4 h, washed, and illuminated for 5 min. Cell viability was measured after a 7 day incubation at 37 °C. As a negative control the cells were treated with 50% DMSO in DMEM, n = 6.

Cells treated with HPMA, NaSS and FMMA and "polymerisation chemistry" showed negligible direct cytotoxicity to Hela cells (Table 1) and no significant viability decreases were observed upon expanding the incubation time to 7 d, indicating no effect of polymerisation on cell growth or proliferation. 4-vinylaniline (50 mM) was found toxic to the cells when incubated for 7 d after monomer treatment (without polymerisation). However, when the polymerisation was conducted, cell viability improved showing much reduced toxicity of the generated polymers compared to the monomer. Results from proliferation assays (Figure 13) showed no significant changes in the amount of cells synthesising DNAs (shown in red) following polymerisation with HPMA, NaSS and FMMA (28%, 28% and 31% cells in the FITC positive gated regions compared to 32% for cells that just underwent illumination and 37% for totally untreated cells).

3.2.2. Monomer and Initiator Uptake

The cellular uptake of the monomers and initiators were evaluated by quantifying compound uptaken from lysed cells by high-performance liquid chromatography (HPLC). Hela cells were treated with the various monomers and initiator Irgacure2959 for 4 h, washed and then lysed. The monomers and initiators were extracted by DCM and the compounds were analysed by HPLC (compared to a calibration curve (see Experimental, Figure 75 to 82)) (Figure 15). All monomers and initiator Irgacure2959 showed high cellular uptake (the intracellular amounts

of HPMA, NaSS, VAN, FMMA and Irgacure2959 were 0.26, 0.82, 0.10, 0.20 and 0.01 pmol/cell, respectively). For Hela cells with typical cell volume of 3×10^3 μm^3,[66] the molar concentrations of the monomers and initiators were all in the millimolar range (87, 273, 33, 67 and 3 mM for HPMA, NaSS, VAN, FMMA and Irgacure2959, respectively). To evaluate whether these concentrations were sufficient for the photopolymerisation system, the evaluation of the polymerisation conditions was carried out (see Section 3.5).

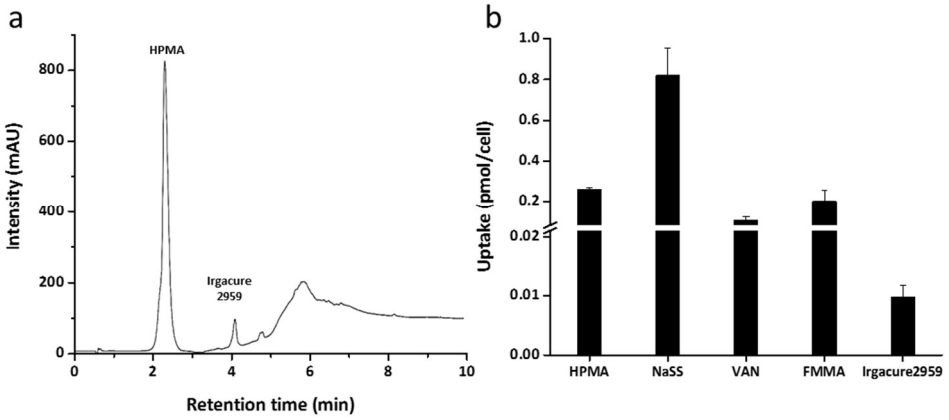

Figure 15. (a) HPLC trace of the initiator Irgacure2959 (40 µM) and the monomer HPMA (10 mM) recovered from the cells after 4 h incubation with compounds (lysed samples were extracted with DCM 3 times). HPLC was performed using a reverse phase column with 10 µL injections, using water/MeCN (95:5 to 5:95 over 10 min, *v*/*v*, with 0.1% formic acid) as the mobile phase and UV detection at 254 nm. The peak at 2.11 min corresponds to HPMA and the peak at 4.06 min to Irgacure2959. (b) Intracellular monomer concentrations determined after 4 h incubation with 50 mM HPMA, NaSS or VAN, 20 mM FMMA or 2 mM Irgacure2959 and extracted.

3.2.3. Evaluation of the Polymerisation Mechanism

In order to confirm the mechanism of the polymerisation, a dichloro-dihydro-fluorescein diacetate (DCFH-DA) assay was carried out to detect the generation of free radicals. The DCFH-DA assay is a well-developed method to directly detect free radicals and reactive oxygen species in living systems, *e.g.* detection of hydroxy radicals.[67, 68] The fluorescin (reduced fluorescein) has negligible fluorescence, but the fluorescence is regenerated when oxidised by free radical species (or reactive oxygen species) and then hydrolysed intracellularly by esterases (Figure 16). The cells treated with the initiator Irgacure2959 (with

and without the monomer HPMA) gave a remarkable increase in fluorescence intensity (389 and 406-fold increase, respectively as analysed by flow cytometry) in comparison to untreated cells. This data thus confirmed the light-mediated generation of free radicals in the cellular system (Figure 16b).

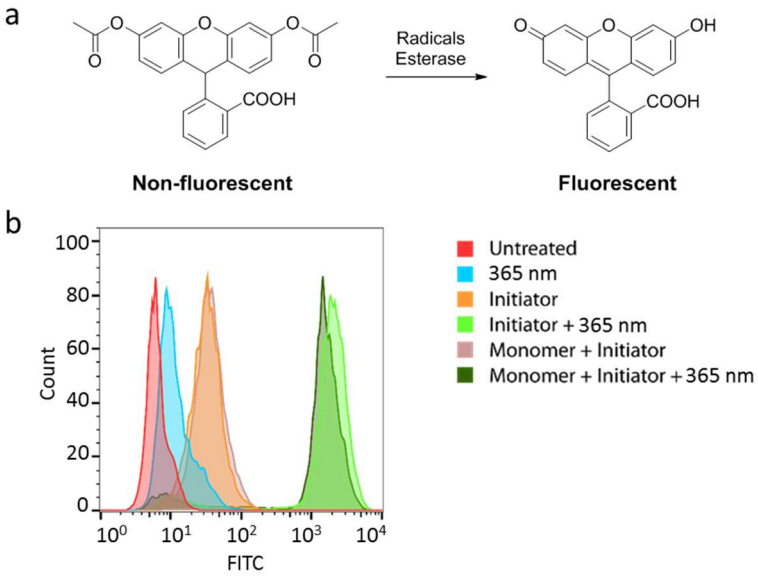

Figure 16. Identification of free radicals using a DCFH-DA assay. (a) Fluorescence "turn on" of a DCFH-DA by oxidation with free radials and hydrolysis. (b) Flow cytometry histograms of HeLa cells incubated with HPMA (50 mM) and/or initiator (2 mM) for 3.5 h, and then DCFH-DA (10 µM) for another 30 min (cells kept in the dark after DCFH-DA addition) before illumination at 365 nm for 5 min. Untreated cells were used as a control. The cells were harvested and analysed by flow cytometry with $\lambda_{ex/em}$ = 488/525 nm.

3.2.4. Polymerisation Evaluation

To optimise the polymerisation conditions in living cells, polymerisation of HPMA (1–500 mM) with various initiator concentrations (0.5–5 mM, with photo-activation at 365 nm for 5 min) were conducted in different systems (PBS (pH = 7.4), cell lysate, and cell lysate with 50 mM glutathione), with and without the presence of air.

The degree of polymerisation was measured by ^{1}H NMR (Table 2 and 3). In PBS, polymerisation was only observed at monomer concentrations ≥ 50 mM and initiator concentrations ≥ 600 µM. Polymerisation of HPMA (50 mM) in the presence of Irgacure2959

(2 mM) with illumination at 365 nm for 5 min resulted in 48% conversion in PBS with the same degree of polymerisation remarkably achieved in cell lysate. Another biocompatible photoinitiator BAPO-ONa[61] gave similar conversions (48 % conversion in PBS) (see Table 3). There were no detectable conversions of HPMA observed with low concentrations of either photoinitiator, consistent with the results of the mechanism evaluation that the free radical initiators were essential for initiating the polymerisation (see Section 1.4).

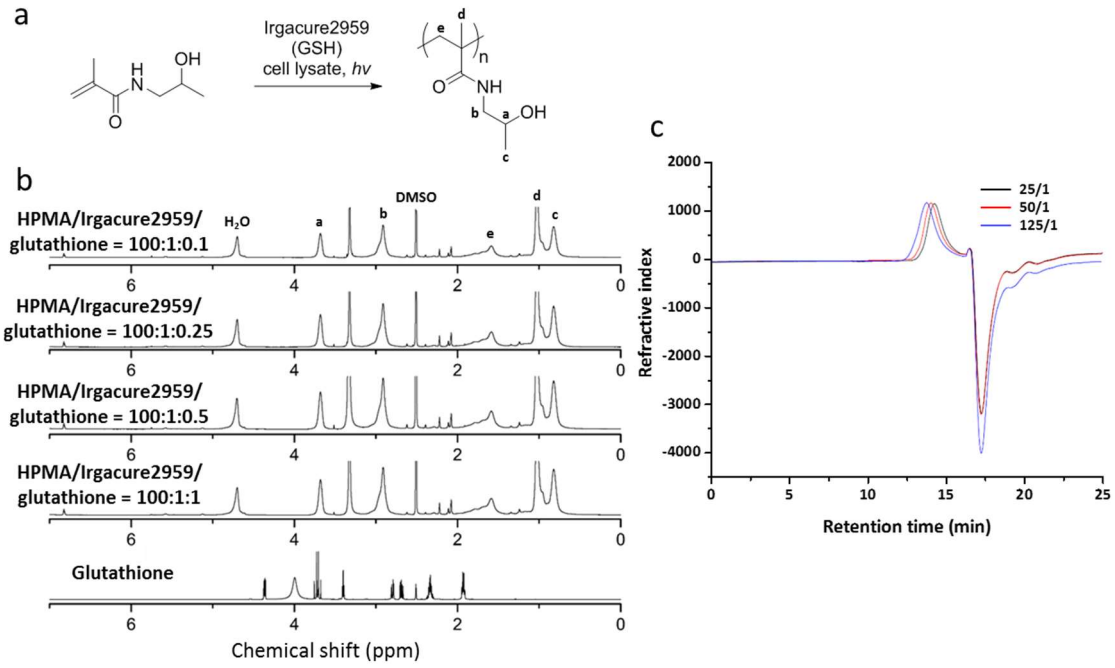

Figure 17. (a) Poly(HPMA) was synthesised by polymerisation of HPMA using Irgacure2959 as a photoinitiator and illuminated at 365 nm for 5 min in cell lysate with additional glutathione (HPMA/initiator/glutathione = 100:1:1; 100:1:0.5; 100:1:0.25; 100:1:0.1, molar ratio). (b) ^{1}H NMR spectra (in DMSO-d_6) of the isolated poly(HMPA) (by dialysis (molecular weight cut off 1000 Da) and centrifugation in MeOH (to remove proteins)), with polymerisation in the presence of different concentrations of glutathione in cell lysate. Bottom spectrum is glutathione in DMSO-d_6. (c) GPC traces following the polymerisation of HPMA with Irgacure2959 in cell lysate with 5 min illumination at 365 nm. GPC traces was performed by using two PLgel MIXED-C columns and a reflective index detector, using DMF with 0.1% *w/v* LiBr at 60 °C at 1 mL min^{-1} as an eluent. The ratios of monomer to initiator were 25:1 (50 mM, 2 mM), 50:1 (100 mM, 2 mM), and 125:1 (250 mM, 2 mM) and gave the following molecular weights (and Đ): 15 kDa (1.7), 18 kDa (1.7), 19 kDa (1.8), respectively.

Table 2. Reaction screening for the free radical polymerisation of HPMA with initiators Irgacure2959 in PBS and cell lysate with conversion monitored by ^{1}H NMR. (Conversions were calculated based on the integration ratio between the polymer and the monomer resonances)

HPMA	Irgacure2595	Degassed	Solvent	Conversion (%)
1 M	40 mM	No	PBS	62
500 mM	20 mM	No	PBS	57
200 mM	8 mM	No	PBS	54
100 mM	4 mM	No	PBS	52
50 mM	2 mM	No	PBS	48
50 mM	600 µM	No	PBS	18
50 mM	200 µM	No	PBS	< 1
50 mM	60 µM	No	PBS	< 1
15 mM	2 mM	No	PBS	< 1
5 mM	2 mM	No	PBS	< 1
1.5 mM	2 mM	No	PBS	< 1
500 µM	2 mM	No	PBS	< 1
15 mM	600 µM	No	PBS	< 1
15 mM	200 µM	No	PBS	< 1
5 mM	600 µM	No	PBS	< 1
5 mM	200 µM	No	PBS	< 1
1 M	40 mM	Yes	PBS	65
50 mM	2 mM	Yes	PBS	46
5 mM	200 µM	Yes	PBS	< 1
1 M	40 mM	No	Cell Lysate	85
50 mM	2 mM	No	Cell Lysate	48
5 mM	200 µM	No	Cell Lysate	< 1
1 M	40 mM	No	Cell Lysate + glutathione (50 mM)	75
50 mM	2 mM	No	Cell Lysate + glutathione (50 mM)	45
5 mM	200 µM	No	Cell Lysate + glutathione (50 mM)	< 1

Importantly, the polymerisation was also shown to be tolerant to both oxygen in the air (see highlighted rows in Table 2 that degassing did not affect the conversion) and the antioxidants found in biological systems, such as glutathione (see Table 2). Even when additional glutathione (50 mM) was added, the polymerisation gave similar level of conversion (45%), thus confirming the glutathione did not act as chain transfer agent for the polymerisation. This was also evident from ^{1}H NMR with no glutathione resonances observed in the NMR spectra of the isolated polymers (Figure 17a). This further indicated the chemical and biological robustness of the monomer/initiator system. The polymers from the cell lysate were isolated with a M_n of 14 kDa and a dispersity of 1.78 as determined by GPC (Table 4). Polymers with higher M_n were obtained with increasing monomer concentration (from 50 mM to 1 M with 25/1 monomer/initiator ratio) (Table 4, Figure 17b), although higher monomer and initiator concentrations gave better conversion (up to 62%). The polymerisation conditions (50 mM monomer and 2 mM initiator with illumination at 365 nm for 5 min) were used for further polymerisation studies to minimise potential cytotoxicity.

Table 3. Reaction screening for the free radical polymerisation of HPMA with the initiator BAPO-ONa in PBS with conversion monitored by ^{1}H NMR.

HPMA	BAPO-ONa	Degassed	Solvent	Conversion (%)
50 mM	2 mM	No	PBS	48%
20 mM	800 µM	No	PBS	< 1
10 mM	400 µM	No	PBS	< 1
5 mM	200 µM	No	PBS	< 1
2 mM	80 µM	No	PBS	< 1
1 mM	40 µM	No	PBS	< 1

Table 4. Characterisation of polymers prepared in cell lysate. HPMA was polymerised with Irgacure2959 as a photoinitiator at different concentrations and was isolated by dialysis (molecular weight cut off 1000 Da). The resulting polymers were analysed by GPC with DMF with 0.1% *w*/*v* LiBr as an eluent. The molecular weights and dispersity were calibrated with narrow dispersed PMMA standards.

HPMA	Irgacure2959	Degassed	M_n	Đ
20 mM	800 µM	No	15 KDa	1.6
50 mM	2 mM	No	15 kDa	1.7
100 mM	4 mM	No	18 kDa	1.8
1 M	40 mM	No	19 kDa	1.8

In order to demonstrate the compatibility of other monomers to the polymerisation conditions, polymerisations of monomers NaSS, VAN and FMMA (50 mM) with Irgacure2959 (2 mM) in cell lysate were conducted and the resulting polymers were directly characterised by ^{1}H NMR and GPC (see Figure 18). Representative broad polymer peaks of each polymers were observed in the ^{1}H NMR spectra and polymer peaks (retention time <18 min) observed on the GPC. To eliminate the influences of biomolecules, ^{1}H NMR and GPC analyses for cell lysate were conducted with no “polymer like” peaks observed. These results indicate the compatibility of the polymerisation system to diverse monomers.

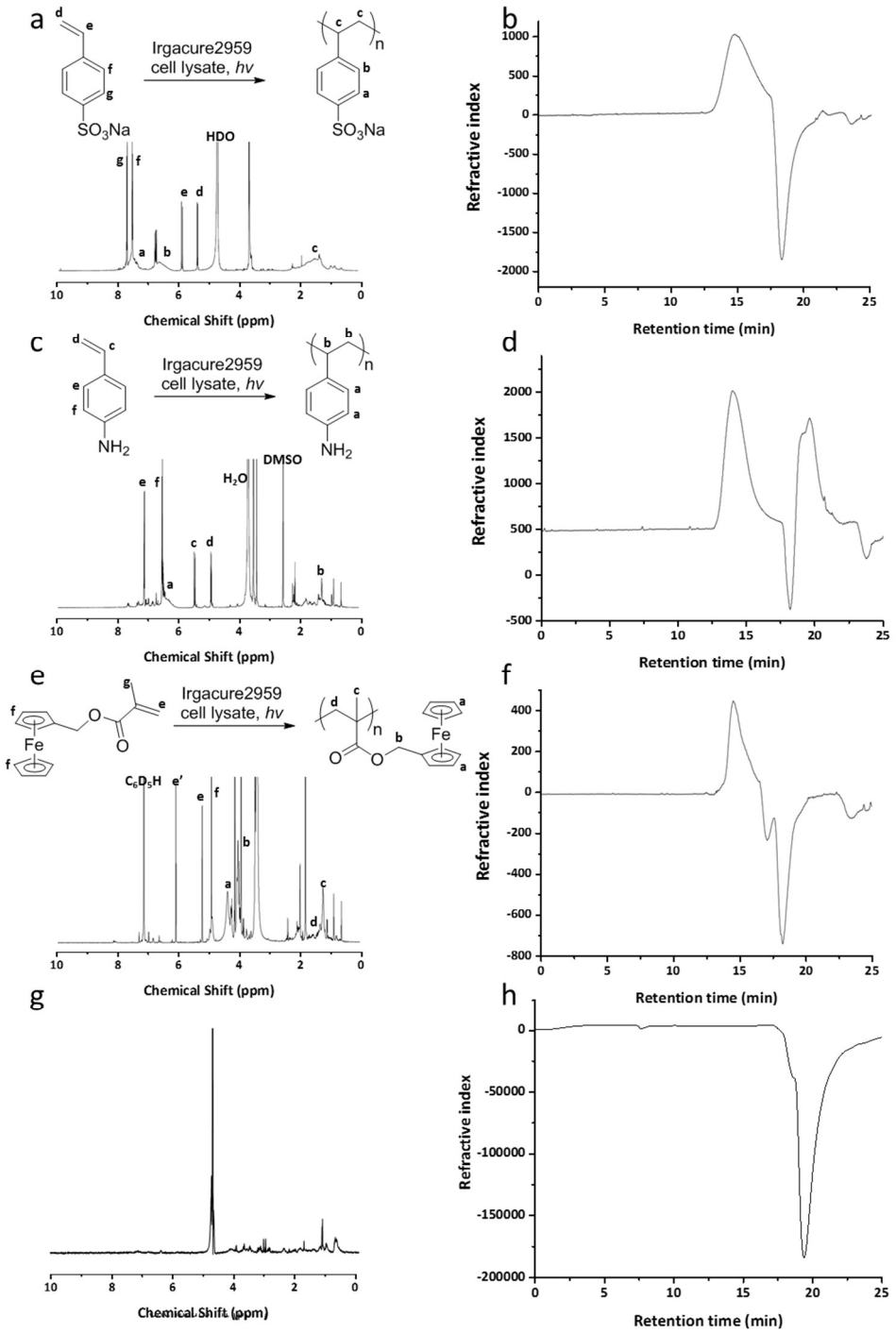

Figure 18. (a) and (b) Polymerisation of NaSS in cell lysate with resulting ^{1}H NMR spectrum (in D_2O) and GPC trace. GPC trace gave M_n (and Đ) = 10 kDa (1.8). (c) and (d) Polymerisation of VAN in cell lysate with resulting ^{1}H NMR spectrum (in DMSO-d_6) and GPC trace. GPC trace gave M_n (and Đ) = 14 kDa (2.0). (e) and (f) Polymerisation of FMMA in cell lysate with resulting ^{1}H NMR spectrum (in C_6D_6) and GPC trace. GPC trace gave M_n (and Đ) = 12 kDa (1.3). (g) and (h) ^{1}H NMR spectrum (in D_2O) and GPC trace of cell lysate. Reaction mixtures analysed directly without purification. GPC traces were performed using DMF with 0.1% *w*/*v* LiBr as an eluent.

3.2.5. Isolation of Polymers from Cells

To confirm the generation of polymers inside cells, a monomer was used that would enable the isolation of the *in situ* polymerised polymer from cells. Thus biotin-PEG-methacrylate (biotin-PEGMA)[69] was synthesised (Figure 19) and used to provide a handle for streptavidin directed magnetic nanoparticle isolation. Thus an esterification reaction was conducted using EDC as the activator and DMAP as the catalyst, to give the biotin-PEGMA in 30% yield. The synthesised biotinylated PEG-methacrylate monomer was purified by silica gel column chromatography to give a narrow mass range of the monomers for intracellular experiments.

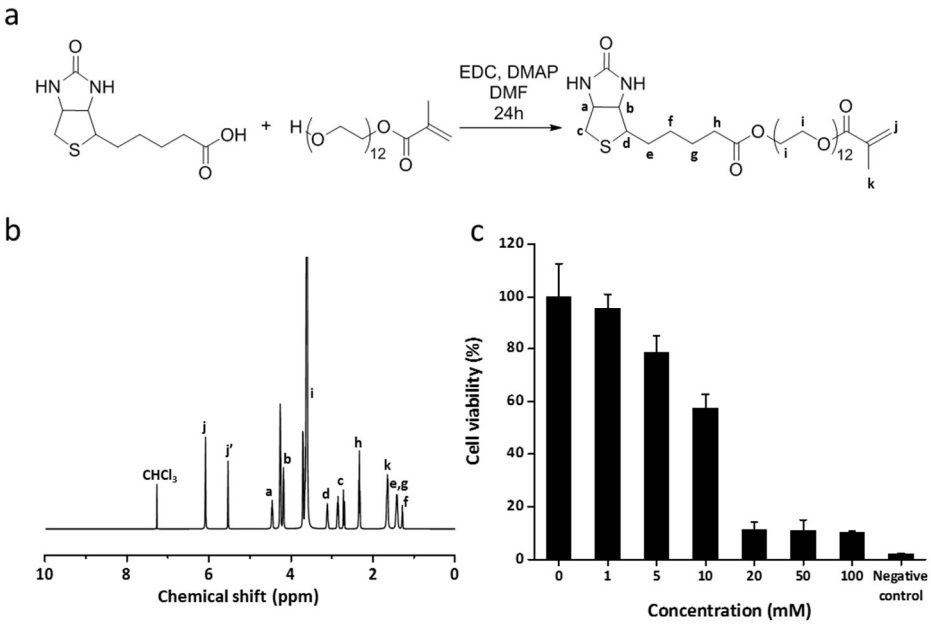

Figure 19. (a) Synthesis of biotin-PEGMA. Biotin was activated by EDC (1.5 equivalent) with DMAP (0.15 equivalent) as a catalyst, and coupled to hydroxyl terminated PEGMA (M_n = 560) followed by column chromatography purification to give biotin-PEGMA in 30% yield. (b) ^{1}H NMR spectrum of biotin-PEGMA in $CDCl_3$. (c) Evaluation of cell viability of biotin-PEGMA using an MTT assay with cells incubated for 48 h, n = 6. As a negative control, the cells were treated with 50% DMSO in DMEM.

The biotin-PEGMA had an IC_{50} of 11 mM (Figure 19c). HeLa cells were thus "polymerised" using biotin-PEGMA (5 mM) and HPMA (50 mM) as the monomers and the cells were lysed and the poly(biotin-PEGMA-*co*-HPMA) polymers extracted using streptavidin functionalised magnetic nanoparticles (Figure 20). To allow non-specifically bound natural proteins to be

removed, a temperature gradient (40 °C, 60 °C, 80 °C and 97 °C) was applied for polymer elution from the particles with > 80% (weight percentage) released at 60 °C (see ^{1}H NMR spectra in experimental Figure 83). The released polymers were analysed by MALDI-TOF MS, GPC and ^{1}H NMR (Figure 21), with the mass of the repeating unit (HPMA, 143 g/mol) clearly observed in the MS spectra. The molecular weight of the polymer (calculated from MALDI) was in good agreement with the GPC data (M_n = 2.8 kDa). The streptavidin nanoparticle isolation process was repeated for the cell lysate without polymerisation and the elution was analysed by GPC to eliminate the potential influence of natural polymers (see Figure 21e). There was no obvious polymer peaks detected, indicating the absence of synthetic polymers. Comparison of the ^{1}H NMR spectrum of poly(biotin-PEGMA-*co*-HPMA) isolated from living cells to the polymer synthesised in PBS, showed no significant differences, again indicating the effectiveness of the polymerisation process within biological conditions.

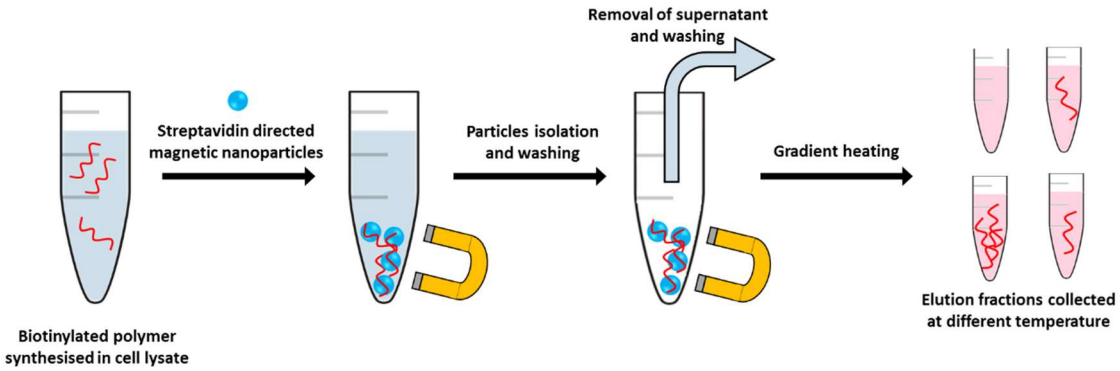

Figure 20. Isolation of biotinylated polymer poly(biotin-PEGMA-*co*-HPMA) using streptavidin magnetic nanoparticles. "Polymerised" cells were lysed and the lysate incubated with streptavidin magnetic nanoparticles. The nanoparticles were collected by a magnet and the unbound fractions discarded. The nanoparticles were then washed with PBS and heated at 40 °C, 60 °C, 80 °C and 97 °C with the buffer changed at each steps to give the poly(biotin-PEGMA-*co*-HPMA).

However, the location of the generated polymers, *i.e.* whether the extracted polymers are from the inside of the cells or the plasma membrane, need to be further confirmed. Therefore, evaluation of the polymer locations were conducted utilising two *in situ* generated fluorescent polymers and analysed by confocal microscopy (see details in Chapter 3.2.7).

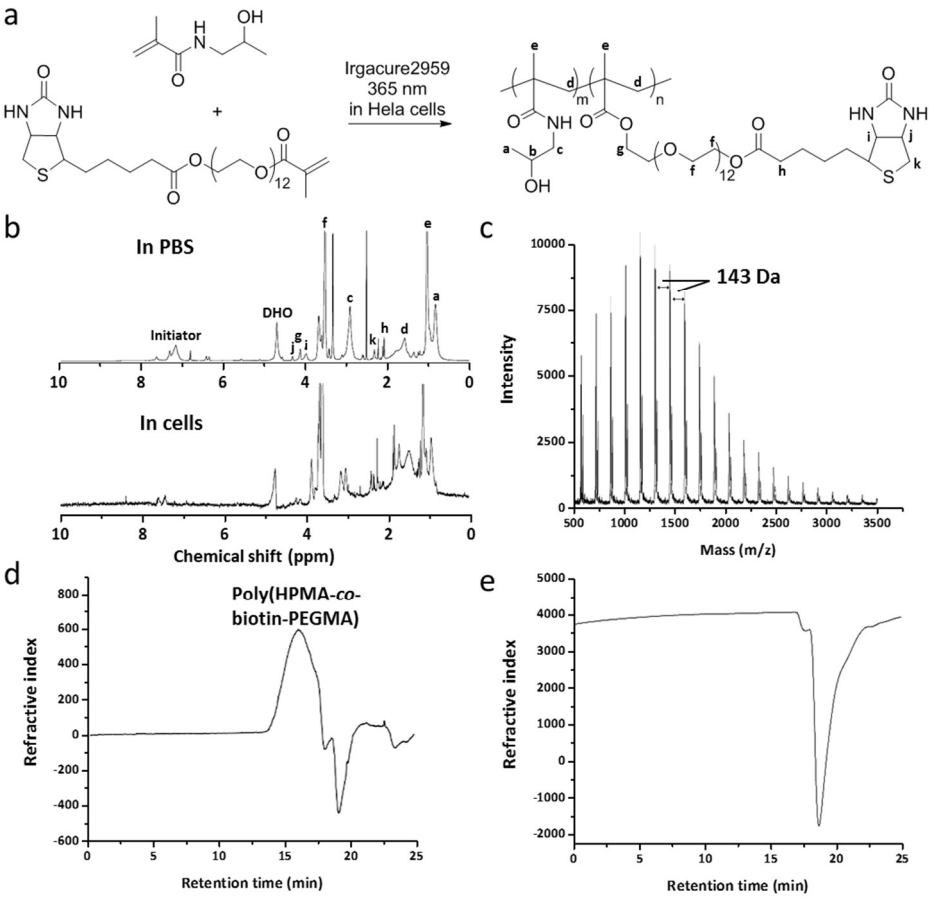

Figure 21. Characterisation of the poly(HPMA-*co*-biotin-PEGMA) extracted from Hela cells. (a) Synthesis of poly(HPMA-*co*-biotin-PEGMA) and (b) ^{1}H NMR spectrum (in D_2O) of isolated poly(HPMA-*co*-biotin-PEGMA) polymerised in PBS (upper) and in cells (lower). The polymer synthesised in PBS was isolated by dialysis against water, (molecular weight cut off 1000). The polymer synthesised in cell lysate was isolated using streptavidin magnetic beads and released at 60 °C (in water). (c) MALDI-TOF MS spectrum of poly(HPMA-*co*-biotin-PEGMA) extracted from the cell lysate. (d) GPC trace of poly(HPMA-*co*-biotin-PEGMA) extracted from the Hela cell lysate (giving M_n = 9 kDa and Đ = 1.7) and (e) GPC trace of the extraction from the HeLa cell lysate (without polymerisation).

3.2.6. Intracellular Polymerisation Changed the Cell Cycle Behaviour, the Cell Mobility and the Cytoskeleton Structure

3.2.6.1. Evaluation of the Cell Cycle

Although the proliferation assay (see Section 1.2) demonstrated that the photopolymerisation did not have any effect to the total amount DNA synthesised by the

cells, it was important to gain insight into the effect of intracellular polymerisation on the cell cycle. Flow cytometry based cell cycle analysis is one of the most widely used methodologies for quantifying cell numbers in different phases of the cell cycle.[70] DNA binding fluorophores can be used to label cells in different phases based on the differences in fluorescence intensities and then quantified by flow cytometry. Cells in the G2 and M phases have almost double the amount of DNA comparing to the cells in G0 and G1 phases while any cells having fluorescence intensities in between can be attributed as being in the S phase where the DNA is being synthesised. Thus, Hela cells were "polymerised" using the monomer HPMA and cultured under normal cell culture conditions for 2 h, 24 h, 48 h and 72 h before analysis by flow cytometry using a Vybrant DyeCycle Green ($\lambda_{ex/em}$ = 488/534 nm) nuclear stain (Figure 22 to 25).

Flow cytometry data (Figure 26) showed that there were no significant differences in the G_0 and G_1 phases between the "polymerised" and "untreated" cells with around 50% cells found in these phases for both the "polymerised" and untreated cells (Figure 26a). However, the number of cells in S phase was observed to be affected by the polymerisation. After 2 h incubation, the "polymerised" cell (15%) population showed a significant increase in quantity over the untreated cells (10%), but decreased to 8% and 5% when the incubation time was extended to 24 h and 48 h (12% for untreated cells at both time point). These changes indicated the influences of the polymerisation to the DNA synthesis in the cells, however the influence was observed to be recovered after 72 h where the "polymerised" cells had a similar DNA content after 72 h (Figure 26b). Although it is believed that DNA damage induces cell death by apoptosis,[71] here the reduced number of cells in S phase was not accompanied by an increased apoptotic response following polymerisation, where the number of apoptotic cells were all in a similar range from 6%-17% and 5%-11% for the "polymerised" cells and the untreated cells, respectively (Figure 26d). For the G_2/M phases, the ratio of both the "polymerised" cells and the untreated cells were stable (26%-33% and 23%-30% for the "polymerised" cells and the untreated cells, respectively) after 72 h (Figure 26c). In addition, there were no notable differences in cell cycle progression when comparing cells with and without illumination where the ratio of cells in S phase was in the range of 10%-12% and 10%-13% for untreated cells and cells illuminated at 365 nm for 5 min. This indicated that the illumination did not result in any changes in DNA synthesis (Figures 22 to 25).

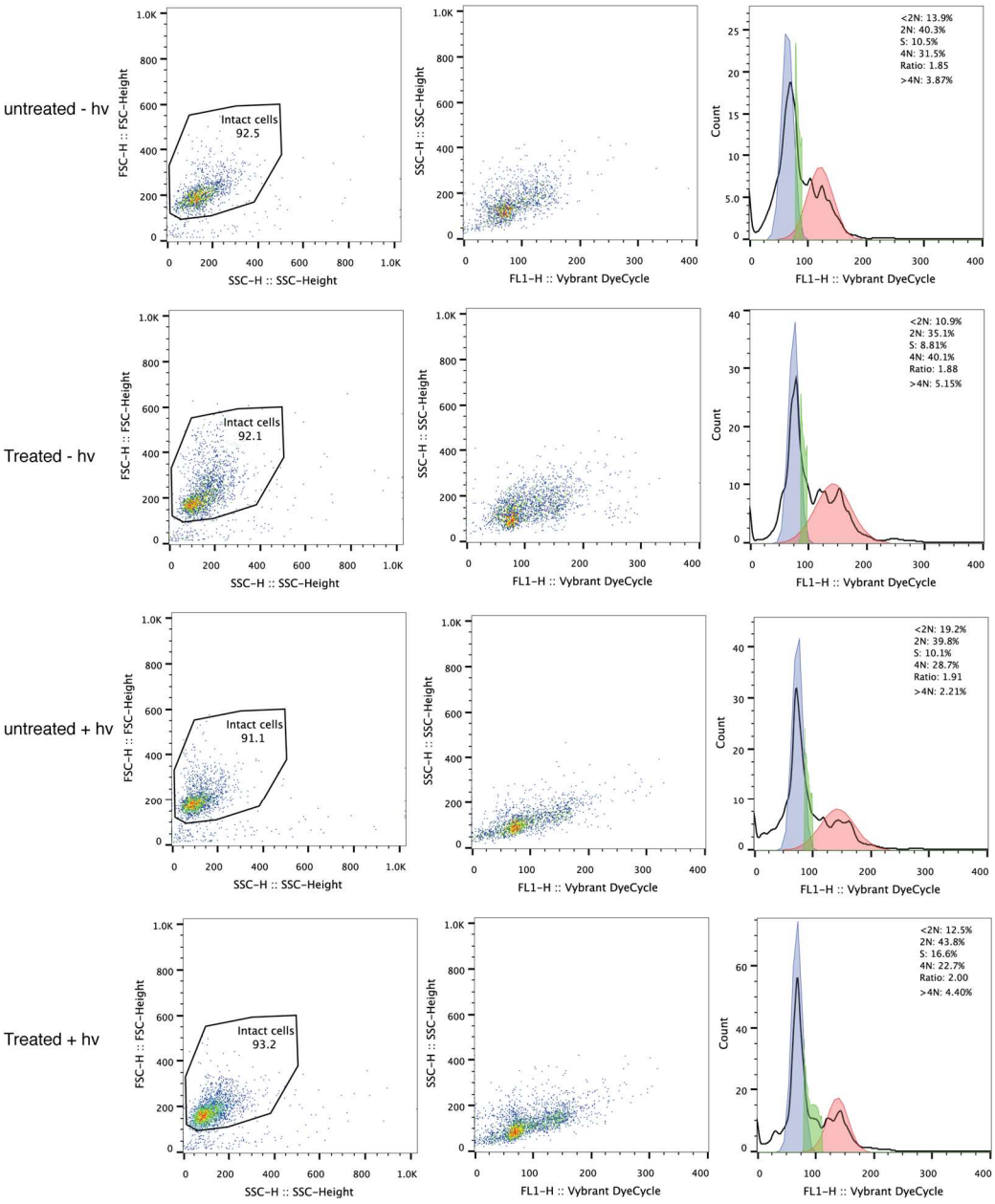

Figure 22. Cell cycle analysis using flow cytometry. Hela cells were treated (HPMA, 50 mM and Irgacure2959, 2 mM) or untreated, with or without illumination at 365 nm for 5 min. The cells were then washed and incubated for 2 h at 37 °C in fresh media. Cell cycle and cell death were quantified by cell staining using Vybrant DyeCycle Green following the manufacturer's instruction, and analysed on a flow cytometer ($\lambda_{ex/em}$ = 488/525 nm). Forward versus side scatter profiles were used to gate intact cellular materials. All flow cytometry analyses are based on analysis of 10,000 cells.

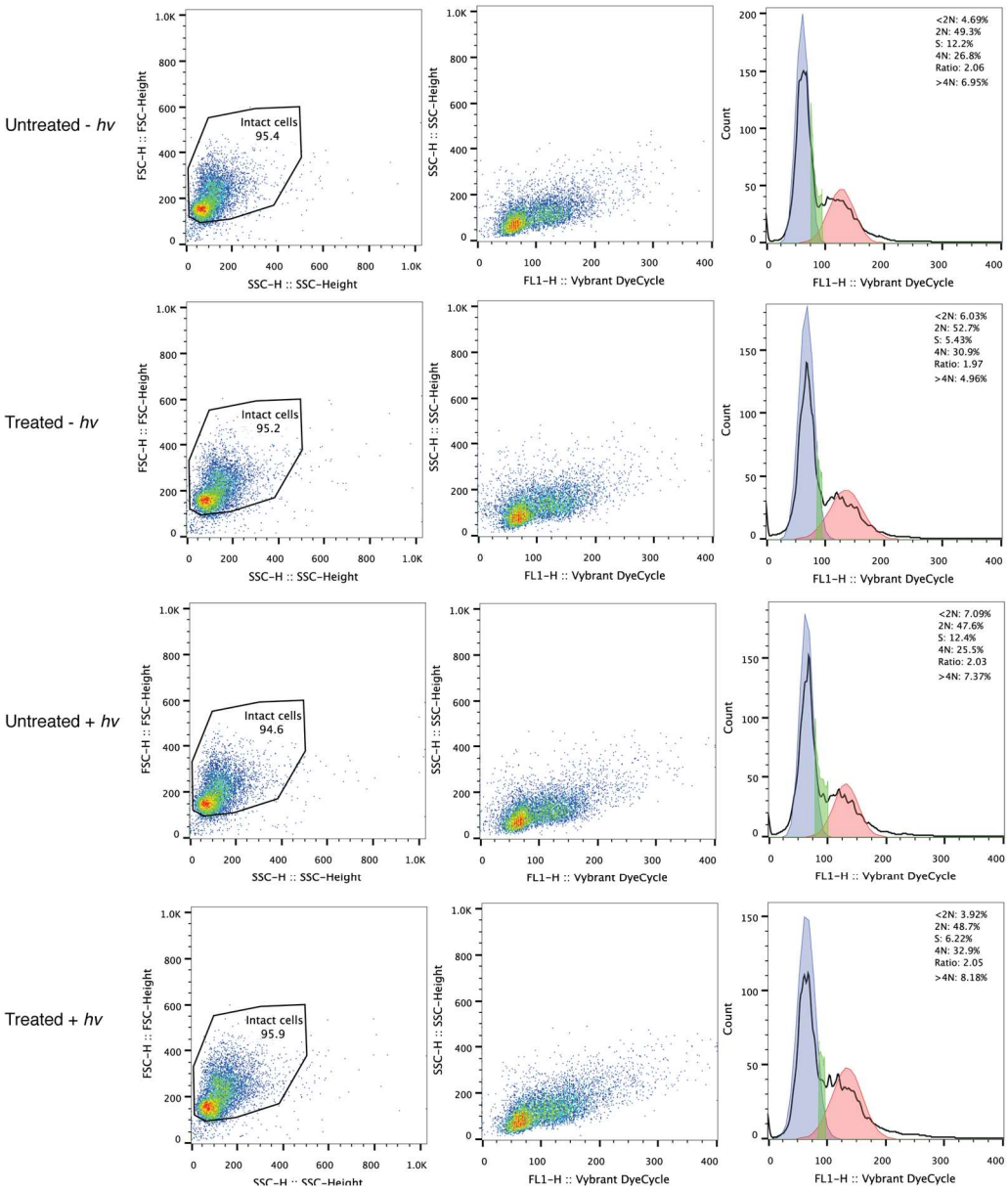

Figure 23. Cell cycle analysis using flow cytometry. Hela cells were treated (HPMA, 50 mM and Irgacure2959, 2 mM) or untreated, with or without illumination at 365 nm for 5 min. The cells were then washed and incubated for 24 h at 37 °C in fresh media. Cell cycle and cell death were quantified by cell staining using Vybrant DyeCycle Green following the manufacturer's instruction, and analysed on a flow cytometer ($\lambda_{ex/em}$ = 488/525 nm). Forward versus side scatter profiles were used to gate intact cellular materials. All flow cytometry analyses are based on analysis of 10,000 cells.

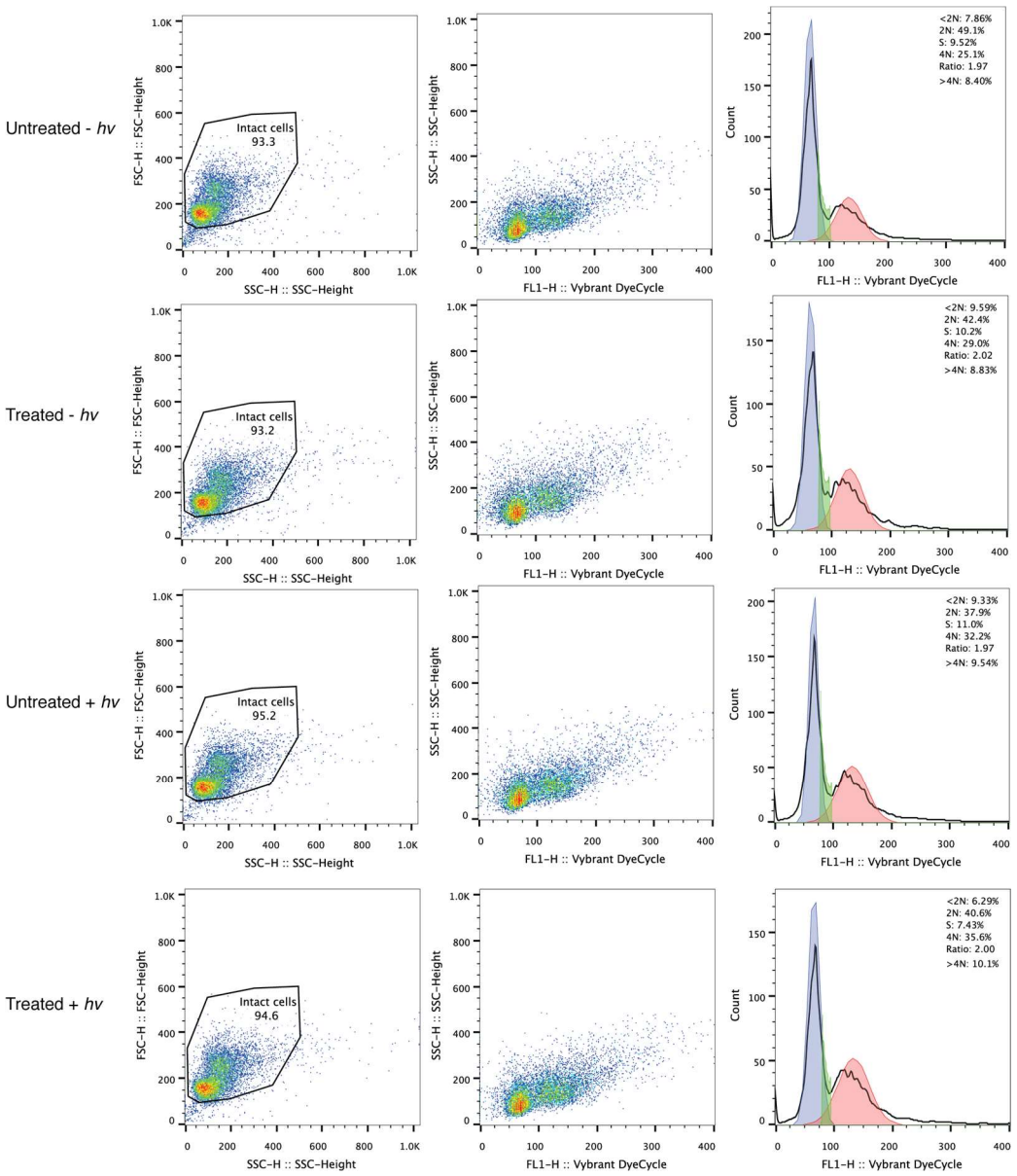

Figure 24. Cell cycle analysis using flow cytometry. Hela cells were treated (HPMA, 50 mM and Irgacure2959, 2 mM) or untreated, with or without illumination at 365 nm for 5 min. The cells were then washed and incubated for 48 h at 37 °C in fresh media. Cell cycle and cell death were quantified by cell staining using Vybrant DyeCycle Green following the manufacturer's instruction, and analysed on a flow cytometer ($\lambda_{ex/em}$ = 488/525 nm). Forward versus side scatter profiles were used to gate intact cellular materials. All flow cytometry analyses are based on analysis of 10,000 cells.

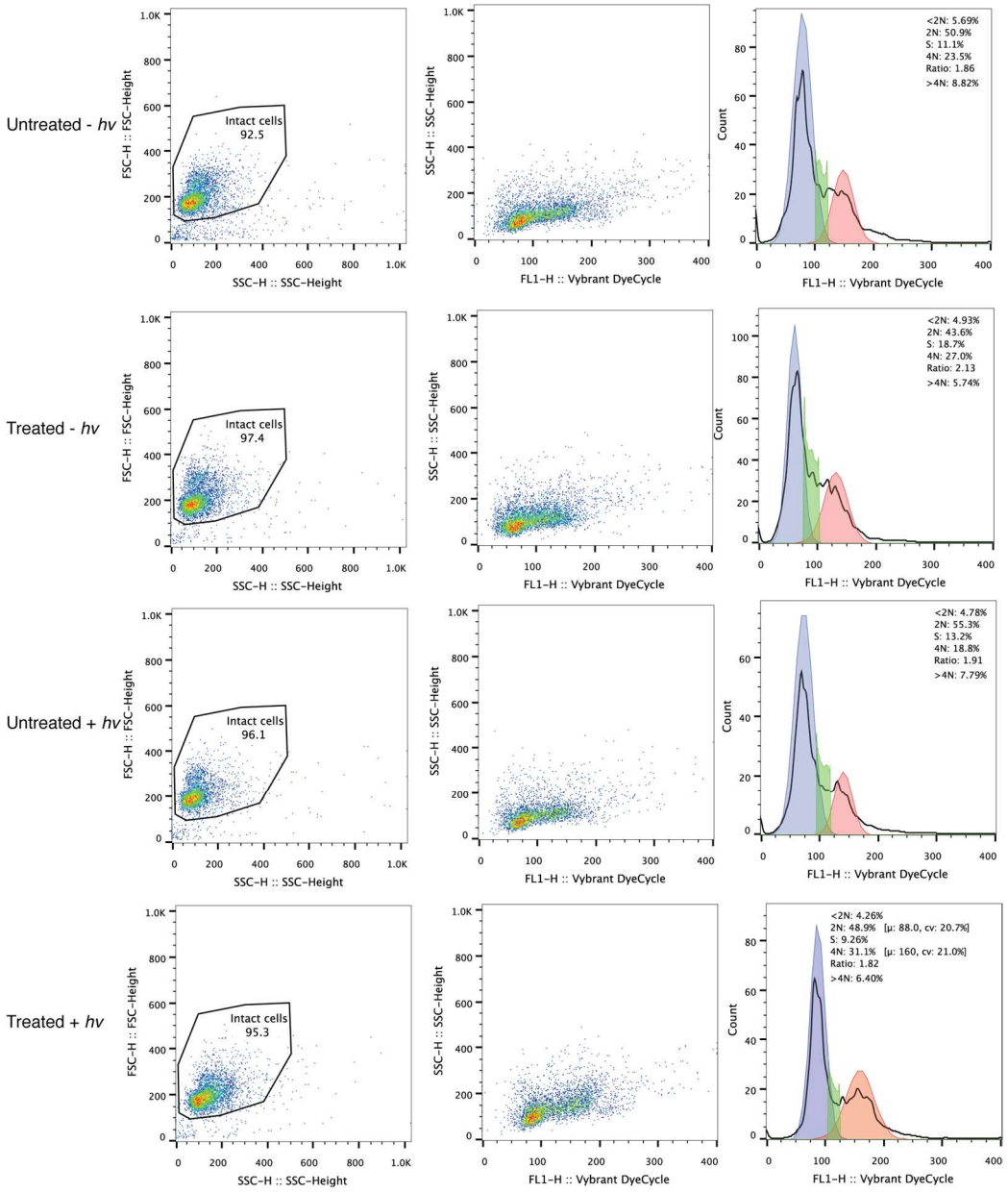

Figure 25. Cell cycle analysis using flow cytometry. Hela cells were treated (HPMA, 50 mM and Irgacure2959, 2 mM) or untreated, with or without illumination at 365 nm for 5 min. The cells were then washed and incubated for 72 h at 37 °C in fresh media. Cell cycle and cell death were quantified by cell staining using Vybrant DyeCycle Green following the manufacturer's instruction, and analysed on a flow cytometer ($\lambda_{ex/em}$ = 488/525 nm). Forward versus side scatter profiles were used to gate intact cellular materials. All flow cytometry analyses are based on analysis of 10,000 cells.

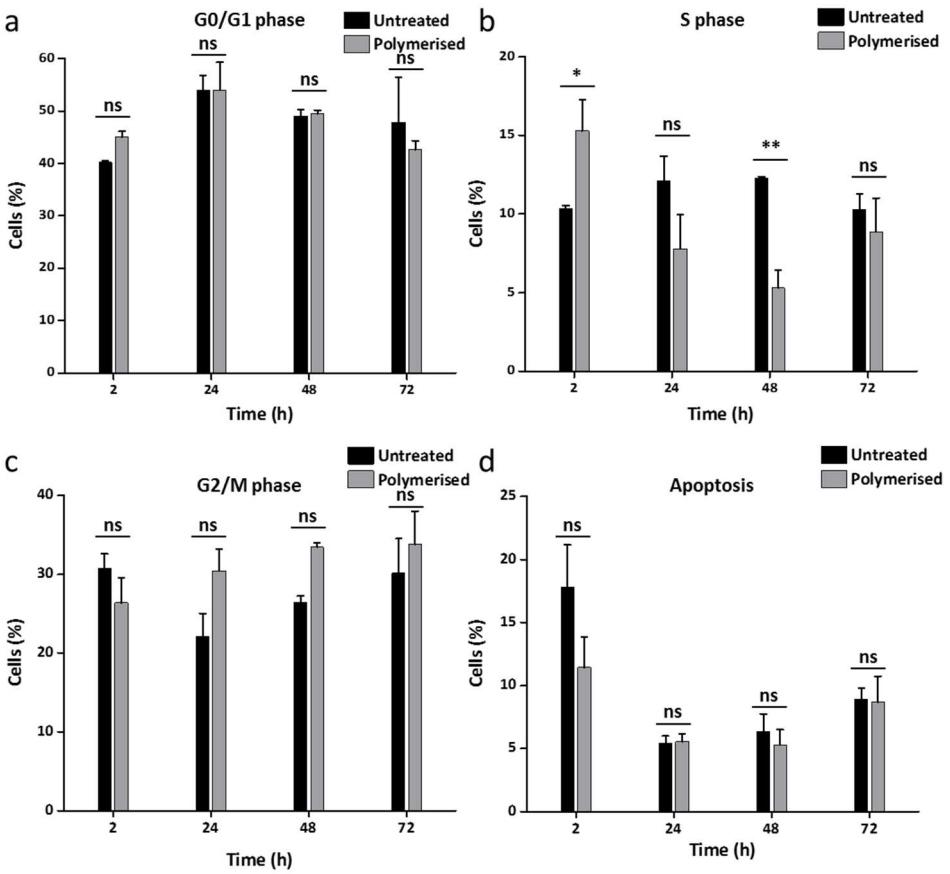

Figure 26. Data extracted from the flow cytometry graphs (Figure 22 to 25). The data is presented as a mean ± standard deviation (n = 3 for each group). Significant differences were analysed using two-way analysis of variance followed by Sidak's multiple comparison test compared to an untreated control group (* $P < 0.05$, ** $P < 0.01$).

In summary, the intracellular polymerisation altered cell cycle by affecting DNA replication in S phase, although no apoptotic responses were observed, indicating the polymerisation chemistry do not affect cell viability.

3.2.6.2. Evaluation of the Cell Mobility

Cell movement is a fundamental process of all cellular organisms and contributes to tissue repair and regeneration, and is also related to diseases such as cancer.[72, 73] To investigate the role synthetic "intracellular polymers" play in altering cellular migration, a wound healing migration assay was utilised (Figure 27). Hela cells were seeded in the two wells of the removable insert mode in a culture dish (Ibidi insert) and allowed to attach to the bottom of

the wells. The mode were then removed and a "wound" (500 µm) was generated between the two groups of cells. The migration was quantified by measuring the "wound area" at different time points in comparison to the original area (at 0 h).

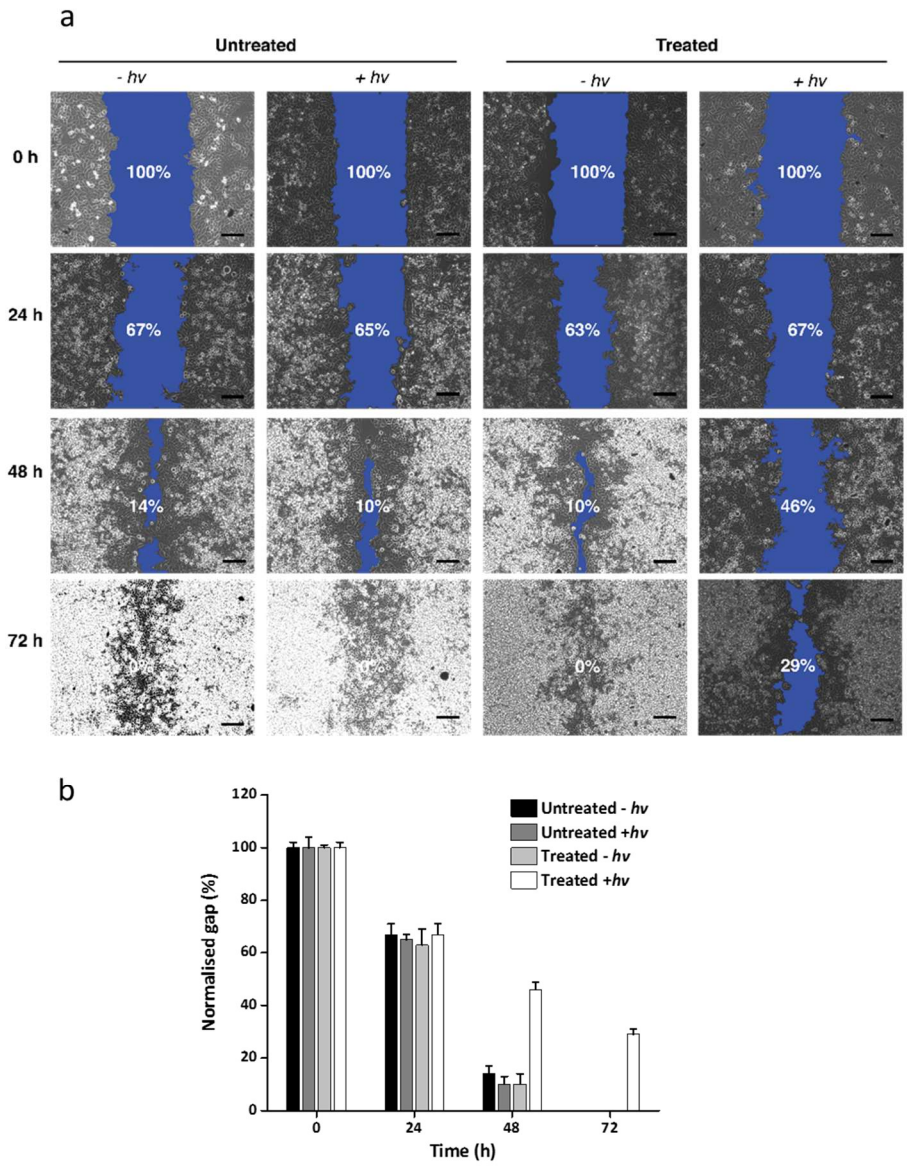

Figure 27. (a) Cell migration was analysed by a wound-healing assay using a HeLa cell monolayers. "Wounds" were created using the Ibidi insert kits and "wound closure" was monitored by bright-field microscopy at 24 h, 48 h, and 72 h with untreated cells and treated cells (incubated with HPMA (50 mM) and Irgacure2959 (2 mM) for 4 h) with and without 5 min illumination at 365 nm. Wound areas were measured using ImageJ and are coloured in blue. Scale bar = 100 µm. (b) The normalised wound area *vs* time (calculated as the ratio of the remaining wound area at the given time point and at t = 0 h) (data represent the mean ± SD, n = 3).

For the cells polymerised using the monomer HPMA, the percentage of wound closure was similar to untreated cells after 24 h (67% and 65%, respectively). However, after 48 h and 72 h the "polymerised" cells showed significantly reduced motility compared to untreated HeLa cells (46% and 29% area remaining for "polymerised" cells comparing to 14% and 0% for untreated cells, after 48 and 72 h respectively). The "polymerised" cells presumably migrating more slowly as a consequence of the "internal polymer" resulting in a phenotype that had reduced translocation ability.[72] Individual treatments of UV illumination or monomer/initiator did not cause any significant differences in the wound healing rate/migration, with the wound area remaining at 10% for both the illuminated cells and the monomer/initiator treated cells while an area of 14% was left for untreated cells after 48 h incubation and full closure observed for all three cases after 72 h (see Figure 27).

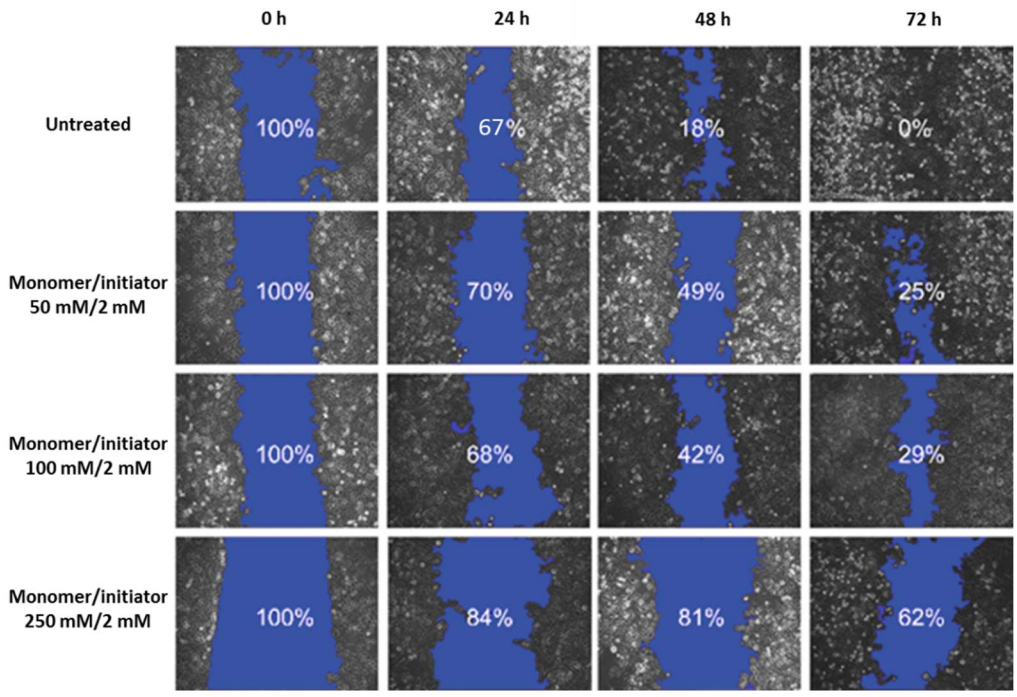

Figure 28. Cell migration experiments using a wound-healing assay of a HeLa cell monolayer. Untreated cells were used as a control and compared with "polymerised" cells using HPMA and Irgacure2959 as the monomer and the initiator, respectively.

The effect of molecular weight of polymer on cell migration was evaluated by applying different monomer/initiator ratios (25:1, 50:1 and 125:1) in the wound healing assay (Figure 27). As described previously (see Section 1.5), lower initiator ratios generate larger polymers (Table 4, Figure 17) and here contributed to slower migration of the cells (Figure 28). Thus, a monomer to initiator ratio of 125:1 (250 mM and 2 mM) gave wound areas of 81% and 62% after 48 and 72 h, respectively, whereas with a ratio of 25:1 (50 mM and 2 mM) and 50:1 (100 mM and 2 mM) gave gaps of 49% and 42% after 48 h and 25% and 29% after 72 h, compared to 18% and 0% for untreated cells after 48 and 72 h incubation. There were no significant changes in cell proliferation for the "polymerised" cells compared to the untreated cells (Figure 13), but the formation of polymers inside the cells did modify their migration abilities.

3.2.6.3. Evaluation of Alternations in Cytoskeleton Structure

The cell migration was shown be affected by the intracellular polymerisation which is directly related to the cytoskeleton, which is a network of proteins responsible for most of the mechanical activities in cells. Therefore, the cytoskeleton is essential to cells and directly related to many cell functions, such as the generation of force, motion, sensing of force and cell division.[74, 75] Affecting cytoskeleton artificially can contribute to the inhibition of migration and proliferation and inducing apoptosis to cancer cells. Thus such chemicals (e.g. DNA and organic small molecules) interacting with cytoskeleton proteins may be used as anticancer drugs.[76] For example, the gene PTEN (or MMAC1) can be used as a tumour suppressor by reducing the tyrosine phosphorylation of the focal adhesion kinase FAK and therefore negatively regulates cancer cell regatation with extracellular matrix.[77] Paclitaxel (also known as Taxol) is used for treating cancers by binding to the β subunit of tubulin, preventing tubulin chain depolarisation and thus inducing apoptosis.[76]

Understanding how intracellular polymerisation affects cytoskeleton may offer a deep insight to the functions of cytoskeleton and may contribute to new therapeutic method development. Actin, a linear polyanionic protein, is one of the most important structural proteins of the cytoskeleton.[78, 79] Since intracellular polymerisation will increase intracellular viscosity, it may alter G-actin polymerisation and result in structural changes in the cytoskeleton.[80] It was worthwhile to get further insight into the influences of the polymerisation on cytoskeleton structures and functions.

Hela cells “polymerised” with HPMA as monomer and were stained with a Alexa Fluor 488 labelled phalloidin (a bicyclic peptide that specifically binds to F-actin[81]). Because of the inaccessibility of phalloidin to plasma membranes, the Hela cells were fixed and the cell membranes were removed using a surfactant (Triton X100) prior to the actin reorganisation by phalloidin and the cells were analysed by confocal microscopy (Figure 29).[82, 83] Remarkable differences were observed between “polymerised” cells and untreated cells.

In comparison to the untreated cells, the “polymerised” cells showed a “well-spread” phenotype and an elongated and polarised morphology. The actin fibres were observed to be aligned with each other (orientation close to 0 degree) and cluster into large locally ordered microdomains, while the untreated cells correlated with an orthoradial actin distribution, together with small adhesion complexes mostly distributed at the cell edge (Figure 29).[83] In addition, an increased area containing intracellular microdomains was observed to be 30% total cell area after 48 h incubation (comparing to 18% for untreated cells) and further increased to 40% after 72 h incubation (Figure 30). The anisotropy of the actin was observed to be significantly higher for “polymerised” cells after 72 h which was scored as 0.18 comparing to 0.03 for untreated cells and 0.04 for illuminated cells (365 nm, 5 min) (Figure 30).[84]

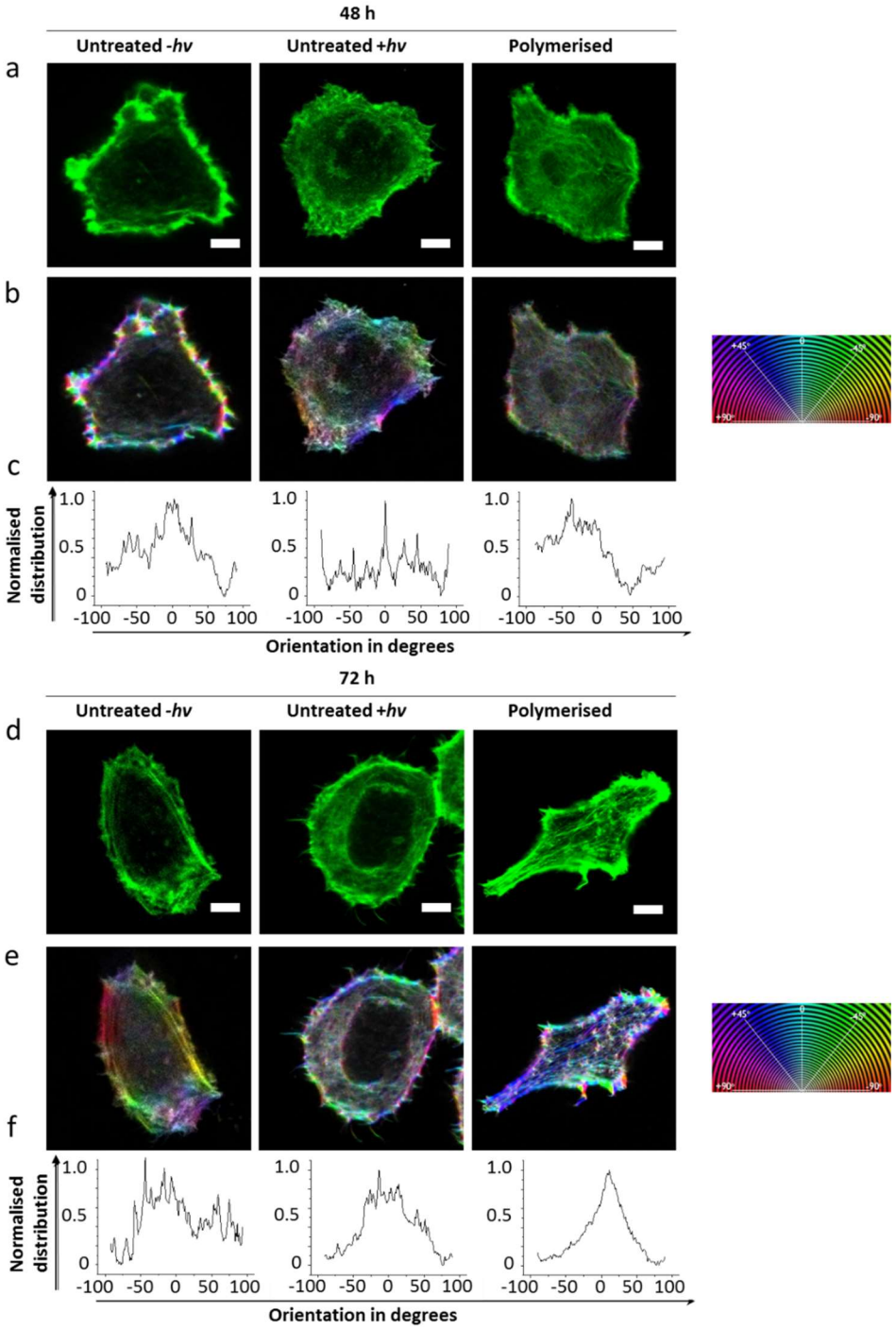

Figure 29. Confocal images of untreated cells, with and without illumination, and "polymerised" cells stained for actin filaments (F-actin, after removal of cellular membranes) after (a) 48 h and (d) 72 h. Scale bar = 10 µm. (b) and (e) Corresponding orientation plots for actin staining, where the different colours indicate different orientations of actin filaments, as per the given colour map. The actin orientations were quantified in (c) and (f) (the convention of anisotropy score: 0 for no order (purely isotropic) and 1 for perfect order (perfect alignment)).

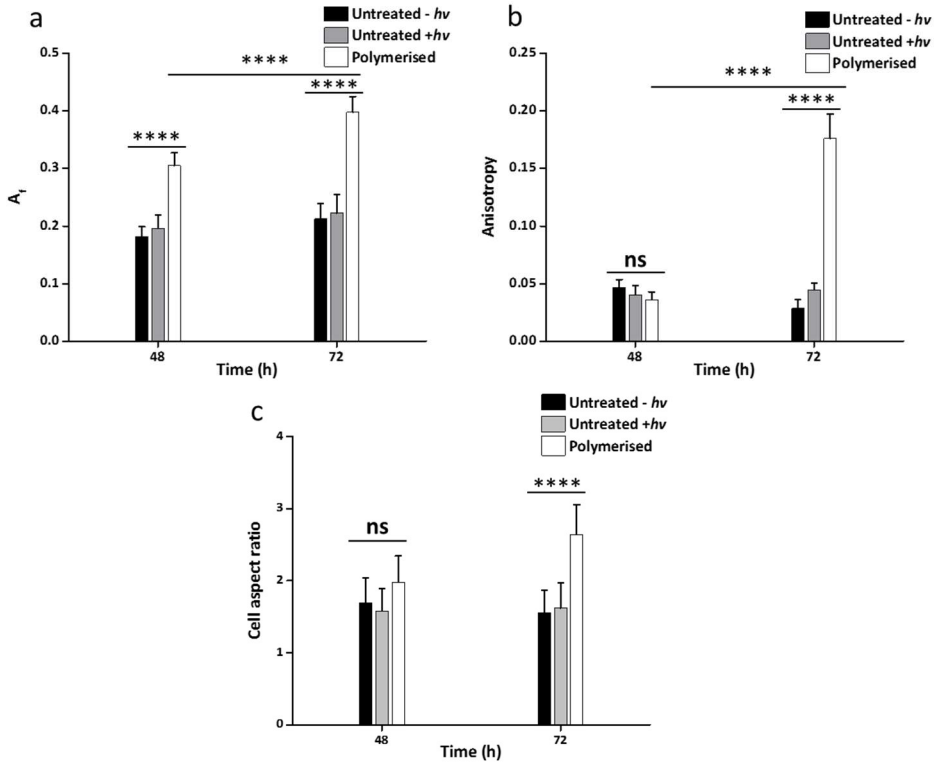

Figure 30. Data from the confocal microscope images in Figure 29. (a) Area of actin microdomains relative to cell area (A_r) for untreated cells with and without illumination (5 min at 356 nm), and "polymerised" cells incubated for 48 h and 72 h (data represent the mean ± SD, with each data point corresponding to 20 cells.) (b) Quantitative analysis of the anisotropy of actin from confocal images of HeLa cells (n ≥ 20 cells per condition, mean ± SD). (c) Aspect ratio of cell shape for untreated and "polymerised" cells after incubation for 48 h and 72 h. At least 20 cells were analysed for each experiment. Significance was analysed by two-way analysis of variance followed by Sidak's multiple comparison test compared to untreated cells with and without illumination (* $P < 0.05$, ** $P < 0.01$, *** $P < 0.001$, **** $P < 0.0001$).

3.2.7. Polymerisation Induced Fluorescence

Fluorescent imaging techniques are widely used in biology and diagnostics.[85-87] In comparison to small molecular fluorescent markers, polymer based fluorophores can provide improved biocompatibility and fluorescence intensity and contribute to long-term stability in living systems.[88, 89] I*n situ* generation of fluorescent polymers would open up the window to enable a wash-free method for labelling cells. Poly(NaSS) and poly(VAN) are known fluorescent polymers generated from non-fluorescent styrene monomers.[90-92]

To confirm the properties of these fluorescent polymers, NaSS (50 mM) was initially polymerised in PBS using the same condition as for polymerisations in cells (Irgacure2959 (2mM) as photoinitiator and illumination at 365 nm for 5 min). The representative broad resonance peaks (7.85-6.97 ppm and 2.36-1.63 ppm) together with the peak in the GPC trace indicated the formation of polymers. The fluorescence property of the poly(NaSS) was evaluated by the fluorescence emission spectra recorded in PBS before and after photopolymerisation and showing a 3.4-fold increase in fluorescence intensity of the polymerised NaSS compared to the solution before illumination (see Figure 31).

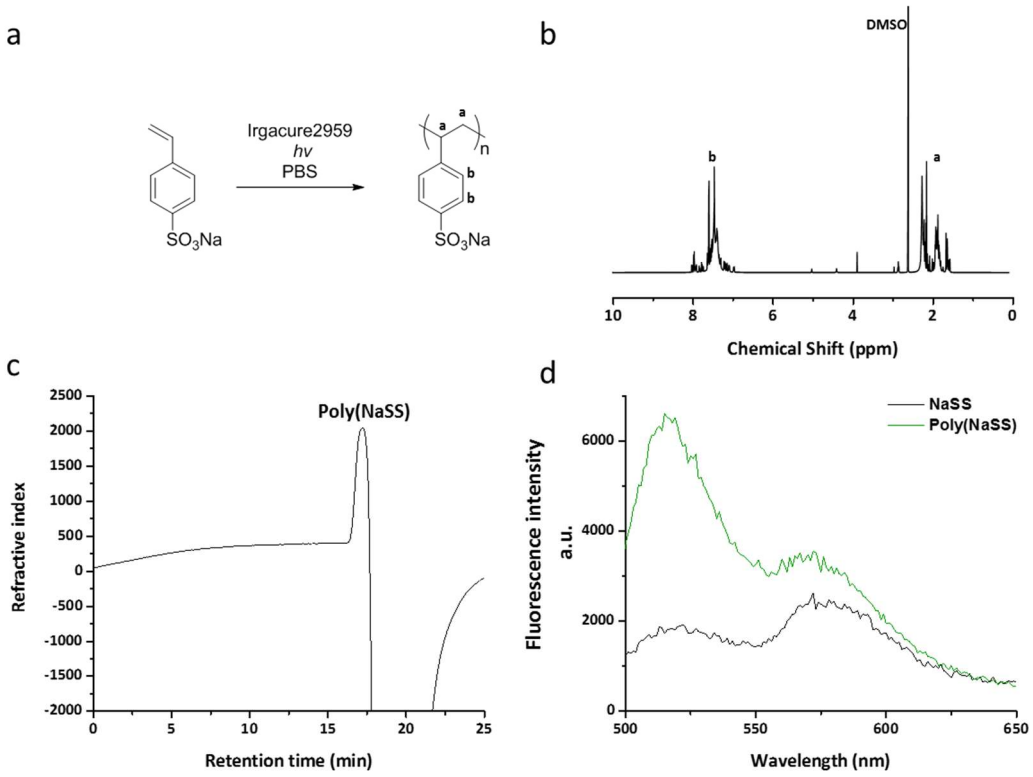

Figure 31. Photopolymerisation of NaSS in PBS with initiator Irgacure2959 (2 mM) and illumination at 365 nm for 5 min. The polymer was purified by dialysis and (b) analysed by ^{1}H NMR (in D_2O) and (c) GPC (eluted with DMF). GPC trace gave the molecular weights (and Đ) of poly(NaSS) as 5 kDa (1.0). (d) Emission spectrum (λ_{ex} = 480 nm) of solution of NaSS (50 mM) and initiator (2 mM) in PBS before (black line) and after (green line) photo-polymerisation (365 nm, 5 min) showing an increase in fluorescent intensity.

Polymerisation of NaSS was then carried out in Hela cells using the previously optimised conditions and the cells were analysed by confocal microscopy and flow cytometry (Figure 32). The "polymerised" cells were co-stained with a nuclear stain (Hoechst 33342, $\lambda_{ex/em}$ = 353/483 nm) and a plasma membrane stain (CellMask^{TM} Deep Red, $\lambda_{ex/em}$ = 649/666 nm) for confocal microscopy. The localisation of the *in situ* formed poly(NaSS) was confirmed to be homogeneously localised in the cytoplasma (Figure 32). When quantified by flow cytometry, the fluorescence increase (10-fold) of the whole cell population also confirmed that polymerisation happened intracellularly while controls (treated with monomer/initiator or illumination at 365 nm) showed negligible fluorescence increases.

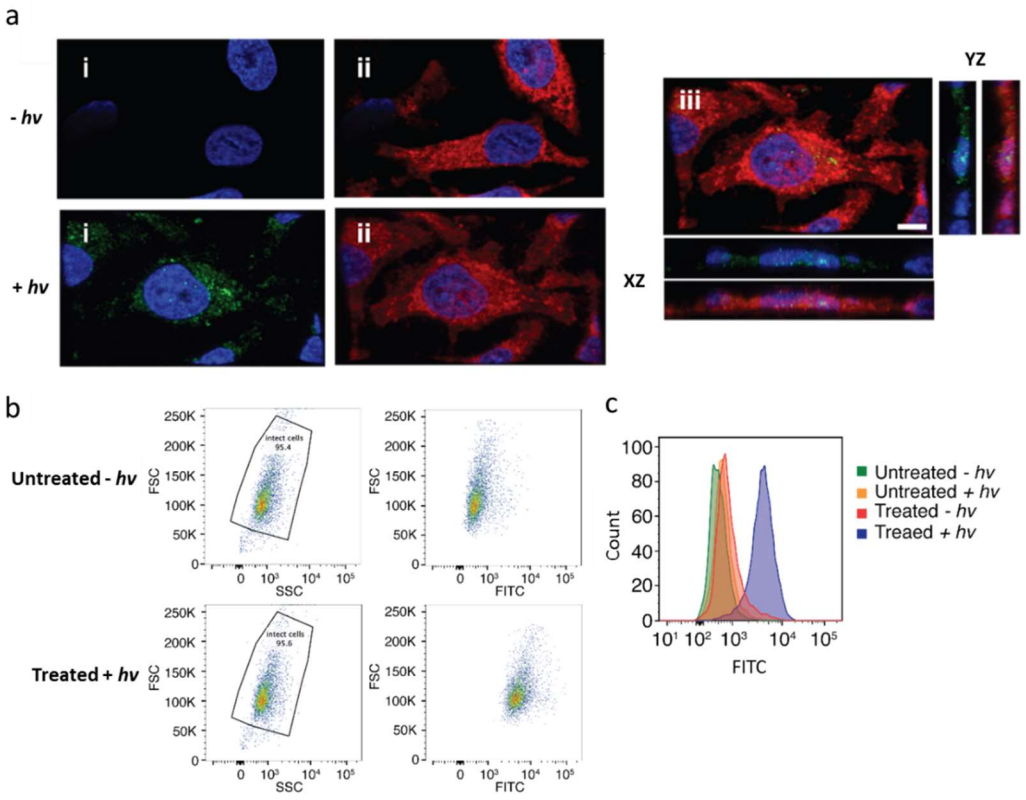

Figure 32. (a) Confocal fluorescence microscopy images of HeLa cells, with and without illumination, showing the intracellular polymerisation of NaSS. (i) Merged image of nucleus and NaSS or poly(NaSS), (ii) Merged image of nucleus and cell membrane; (iii) Merged image of all channels and 3D confocal image (Z-stacks projection) showing polymerised NaSS inside the cell with a vertical cross-section through the cells. Scale bar = 10 µm. (b) Dot plots of untreated and "polymerised" cells. (c) The population of cells shifted to higher intensity of fluorescence after polymerisation, but no difference was observed for untreated cells with and without illumination and treated cells without illumination. Poly(NaSS) was analysed ($\lambda_{ex/em}$ = 488/525 nm) with forward versus side scatter profiles used to gate intact cells. Flow cytometry analysis was based on analysis of 10,000 cells.

Similarly, the polymerisation of VAN were evaluated in PBS using the same polymerisation conditions as for poly(NaSS). ^{1}H NMR (7.18-6.15 ppm and 2.33-1.90 ppm) and the polymer peak in the GPC trace indicated the formation of the desired polymer while the fluorescence spectra confirmed the fluorescence intensity increase (3.7-fold) from the VAN monomer to the corresponding polymer (see Figure 33).

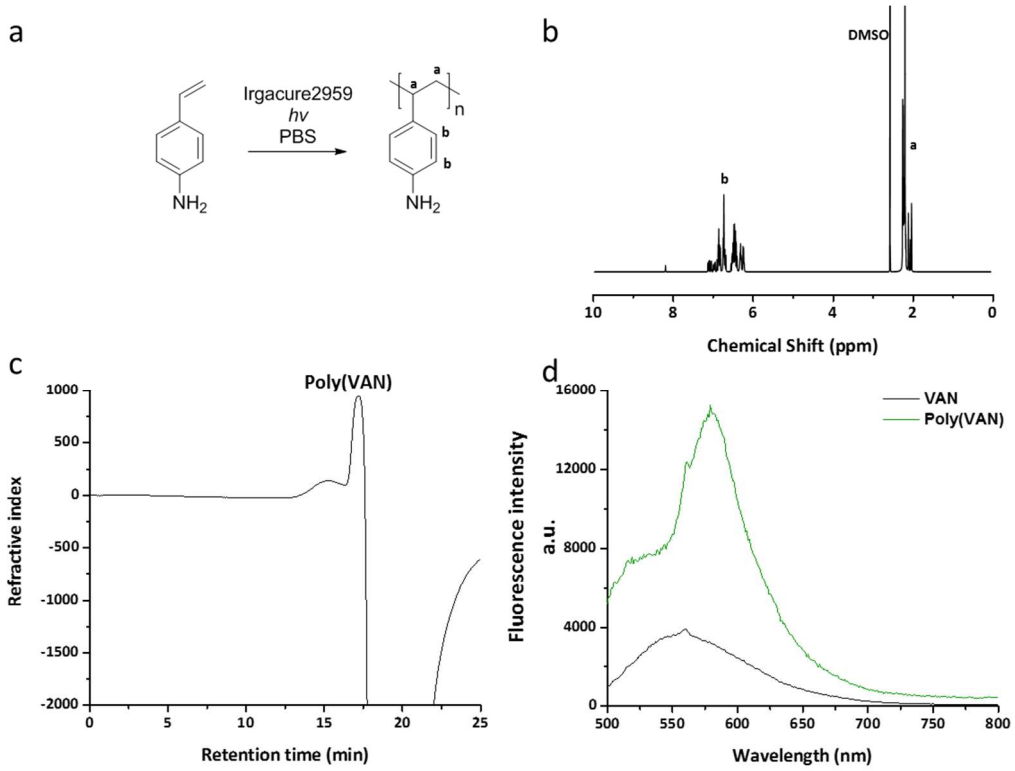

Figure 33. Photopolymerisation of VAN in PBS using the initiator Irgacure2959 (2 mM). The polymer was purified by dialysis and (b) analysed by ^{1}H NMR (in D_2O) and (c) GPC (eluted with DMF). The GPC trace gave the molecular weights (and Đ) of poly(NaSS) as 6 kDa (1.1). (d) Emission spectrum (λ_{ex} = 480 nm) of a solution of VAN (50 mM) and initiator (2 mM) in PBS before (black line) and after (green line) photo-polymerisation (365 nm, 5 min) showing an increase in fluorescent intensity.

The polymerisation of VAN also produced "fluorescent cells" as analysed by confocal microscopy (co-stained with Lysotracker red ($\lambda_{ex/em}$ = 577/590 nm) for lysosome staining and Hoechst 33342 ($\lambda_{ex/em}$ = 353/483 nm) for nucleus staining) and showed the localisation of poly(VAN) in the cellular lysosomes (Figure 34), probably directed by the protonation of the polyaniline moiety (pKa = 4.6).[93, 94] Quantification by flow cytometry showed a 9-fold increase

in fluorescence intensity of the "polymerised" cells comparing to the untreated cells. These observations further confirmed that the polymerisations were taken place inside the cells.

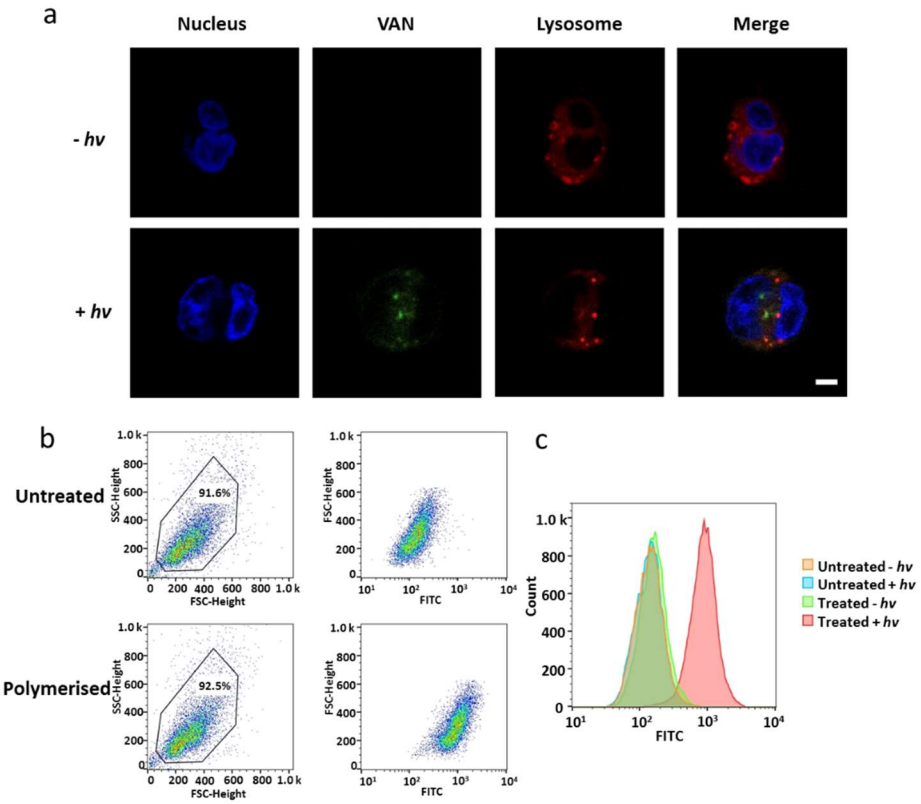

Figure 34. (a) Fluorescence microscopy images of HeLa cells treated with VAN (50 mM) and Irgacure2959 (2 mM) with and without illumination. (b) Histograms of untreated and "polymerised" Hela cells. (c) The population of cells shifted to higher intensity of fluorescence after polymerisation. Poly(VAN) was analysed ($\lambda_{ex/em}$ = 488/525 nm) with forward versus side scatter profiles used to gate intact cells. Flow cytometry analysis was based on analysis of 10,000 cells.

Despite the attractiveness of the *in situ* generation of fluorescent polymers, the overall fluorescence intensities were not sufficient for fluorescence studies over multiple cell passages. Thus, a bright fluorescent rhodamine based acrylic monomer AOTCRhB[95] (5 µM, IC_{50} = 20 µM, analysed by MTT assay, Table 1) was copolymerised with HPMA (20 mM) and Irgacure2959 (1 mM) in Hela cells. The low IC_{50} of AOTCRhB limited high concentration. The "polymerised cells" were analysed by fluorescent microscopy (Figure 35) and flow cytometry (Figure 36) for up to 5 passages (cells were passaged and analysed every 2 days). A

remarkably higher fluorescence intensity was observed in the "polymerised cells" compared to untreated cells (100-fold increase) directly after the polymerisation. The fluorescence intensity naturally decreased over passages, the "polymerised cells" exhibiting higher fluorescence intensities of 10 and 3-fold over untreated cells for passage 1 and passage 5, respectively as quantified by flow cytometry (Table 5). The long-term retention of fluorescence within the "polymerised cells" indicated that intracellular polymerisation is a viable strategy for creating long-term cellular tracking reporters, an important requirement in regenerative medicine where there is powerful need to track implanted cells.[89]

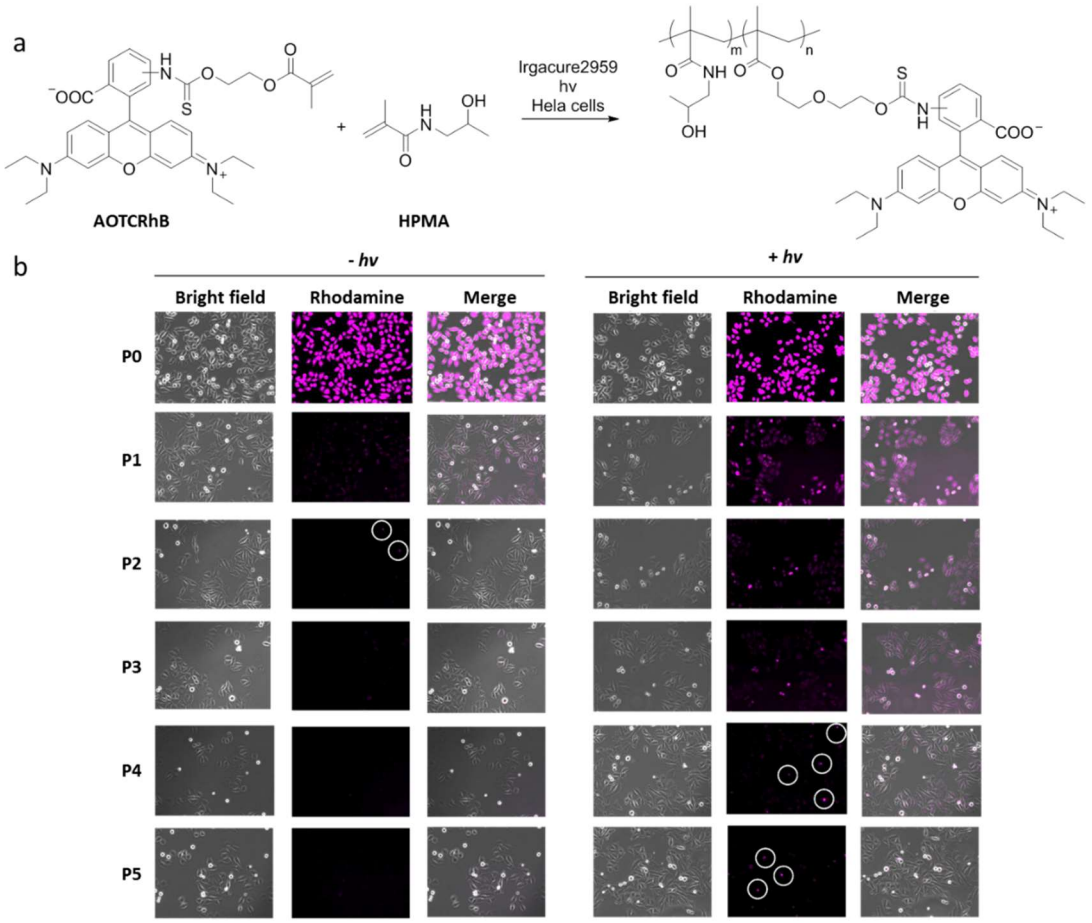

Figure 35. (a) Intracellular copolymerisation of HPMA and AOTCRhB. (b) Microscopy images of the HeLa cells with bright field, rhodamine (λ_{ex} = 527-563 nm, λ_{em} = 570-650 nm) and merged image. Cells were treated with HPMA (20 mM) and AOTCRhB (5 µM) and initiator (2 mM) with and without illumination (365 nm 5 min). Cells were then harvested for imaging over 5 passages every two days. No fluorescent cells were observed for the cells without polymerisation after 3 passages, but the fluorescent cells (in circles) were still observed after 5 passages for the "polymerised cells".

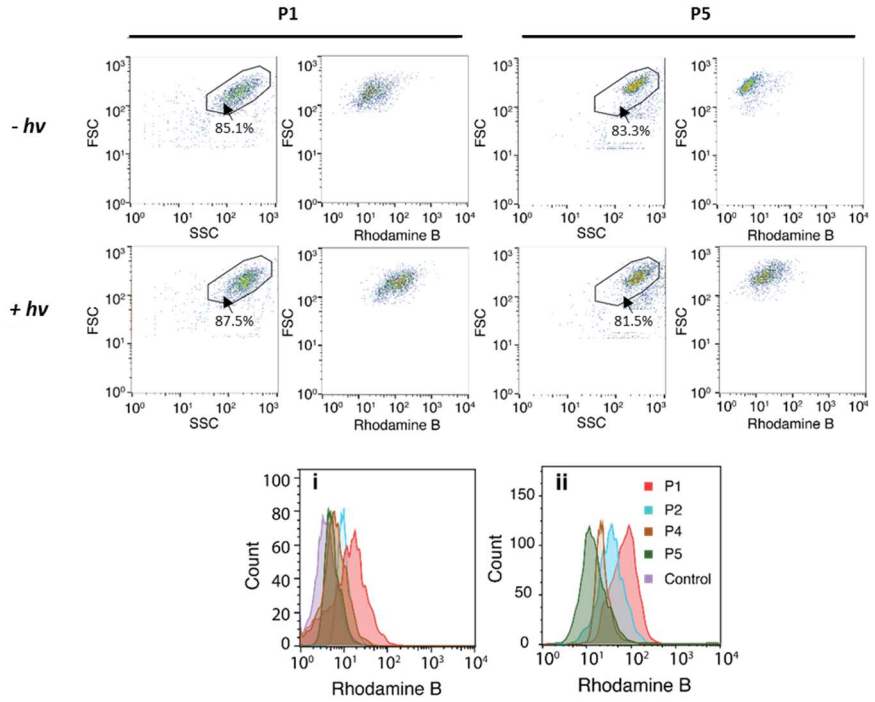

Figure 36. Analysis of cell passages (P1, P2, P4, and P5) following intracellular co-polymerisation of HPMA and AOTCRhB by flow cytometry. Poly(HPMA-*co*-AOTCRhB) was analysed using the rhodamine B channel ($\lambda_{ex/em}$ = 536/617 nm). Forward versus side scatter profiles were used to gate intact cellular materials. Flow cytometry analysis was based on analysis of 10,000 cells. P1 and P5 for treated cells with and without illumination are shown. P1, P2, P3 and P5 are summarised as histograms in (i) with no illumination and (ii) with illumination (5 min illumination). The population of "polymerised cells" still retained their higher fluorescence intensity after 5 passages when compared to cells without polymerisation. Cells at P0 saturated the detector at the same settings and was not shown.

Table 5. Fluorescence intensities of Hela cells after 1, 2, 4 and 5 passages following polymerisation (cells treated with/without AOTCRhB (5 µM), HPMA (20 mM) and Irgacure2959 (1 mM), with/without illumination (365 nm)). Fluorescence intensity quantified by flow cytometry ($\lambda_{ex/em}$ = 536/617 nm).

AOTCRhB concentration	**Illumination**	**Fluorescence intensity (a.u.)**			
		P1	P2	P4	P5
5 µM	Yes	147	57	30	20
5 µM	No	14	10	8	7
0	Yes	8	7	7	7
0	No	8	7	7	7

3.2.8. Polymerisation Induced Intracellular Polymer Aggregation

Polymerisation induced nanoparticle formation is of interest because monomers and in polymer nanoparticles would have different accessibility to cellular organelles and could affect cellular functions. Ferrocene based polymers and nanoparticles (*e.g.* poly(FMMA) and ferrocene functionalised polyethyleneimine) have been found in the cytoplasm but shown no accessibility to the nucleus, whereas ferrocene conjugated small molecules, *e.g.* anthracene–ferrocene with a M_n of 388 Da was used for the *in situ* detection of reactive oxygen species in Hela cells and was found to be nucleus accessible.[96-99]

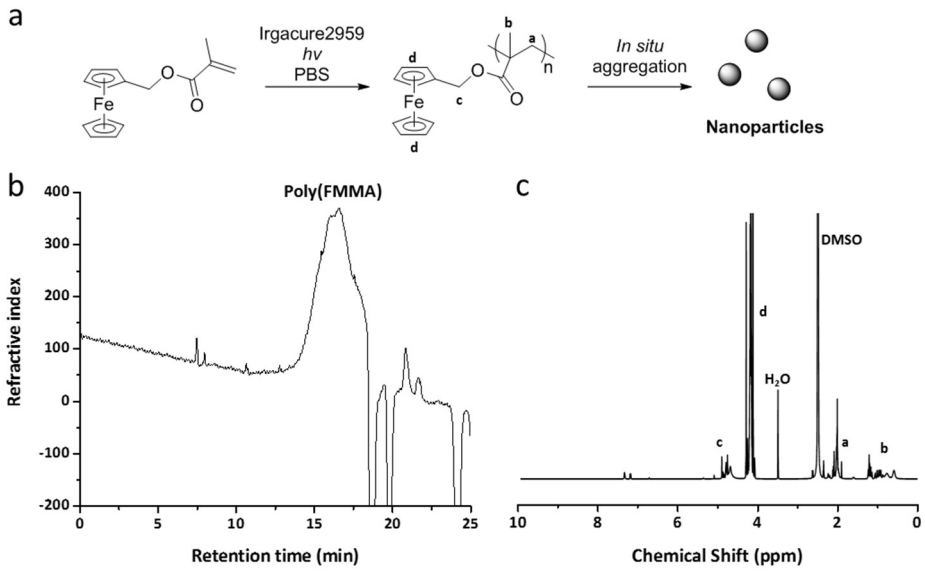

Figure 37. (a) Photo-polymerisation of FMMA (20 mM) in the presence of initiator Irgacure2959 (1 mM) was followed by self-aggregation to form nanoparticles in PBS. The nanoparticles were collected by centrifugation and washed with PBS. (b) GPC trace (partially dissolved and eluted with DMF) of the isolated poly(FMMA) giving a M_n = 8 kDa with Đ = 2.2. (c) ^{1}H NMR of poly(FMMA) in d_6-DMSO.

To investigate the aggregation behaviour of poly(FMMA), the polymerisation was initially conducted in PBS as a proof of concept (Figure 37). Because of the solubility of the monomer FMMA, 20 mM was used for photopolymerisation with Irgacure2959 (1 mM) as initiator. The polymer precipitated while being formed and allowed collection by centrifugation. The collected poly(FMMA) was analysed by ^{1}H NMR and showed representative polymer

resonance peaks while the GPC trace gave a molecular weight of 8 kDa with a dispersity of 2.2 (see Figure 37).

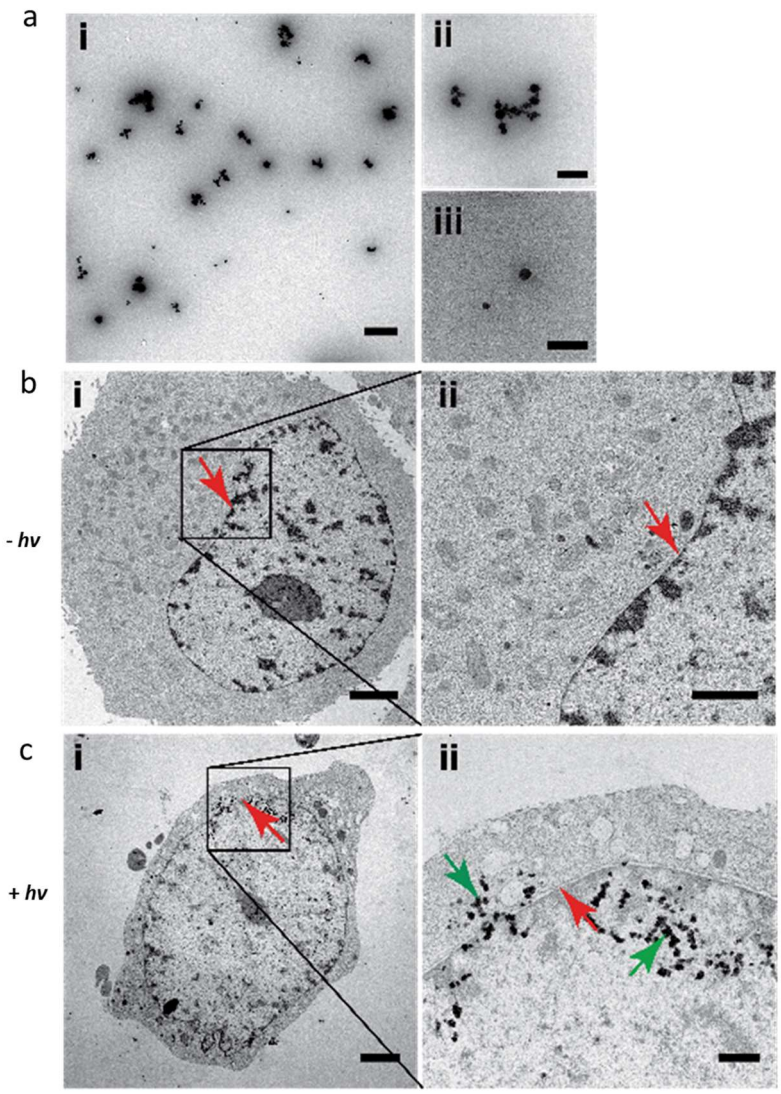

Figure 38. (a) (i) TEM image of ferrocene polymeric nanoparticles formed *in vitro*, showing both individual and small clusters of particles; (ii) Clusters of nanoparticles; (iii) Individual nanoparticles. Scale bars = (i) 1 µm; (ii) and (iii) 500 nm. (b) and (c) TEM images of "polymerised" HeLa cells and untreated cells, respectively. The cells were fixed, sliced, and treated with uranyl acetate to stain membranes and lead citrate to stain the nucleus. Red arrows show the nuclear membrane and green arrows ferrocene nanoparticles. (i) A single cell and (ii) magnification of nuclear membrane. Scale bars: (b) (i) = 2 µm, (ii) = 500 nm; (c) (i) = 1 µm, (ii) = 500 nm.

To investigate the polymerisation of FMMA induced nanoparticle formation in cells, the ferrocene monomer (10 mM) was polymerised in Hela cells (with 1 mM Irgacure2959). TEM analysis of fixed cells showed 50–70 nm diameter nanoparticles in the cytoplasm and the nucleus after polymerisation (Figure 38b), which were not present in cells treated with FMMA but without illumination (Figure 38a). Control polymerisations in PBS showed similar nanostructures, suggesting that the formation of nanoparticles was driven by the polymerisation.

In situ formation of precipitations intracellularly using the monomer without a metal can be achieved using HEMA and *O*-HPMA, which are water soluble monomers that can polymerise as water insoluble polymers inducing the formation of polymeric nanoparticles.[100, 101] As a proof of concept, the polymerisations were initially performed in PBS (with monomer concentration of 50 mM) and the polymers were purified by dialysis. Similar to other monomers, representative polymer peaks were observed in both the ^{1}H NMR spectra and GPC traces, indicating good polymerisation reactivity (see Figure 39).

Intracellular formation of polymeric nanoparticles of HEMA and *O*-HPMA were carried out in HeLa cells. Although both monomers showed cytotoxicity to Hela cells above 10 mM (MTT assay, Figure 39), the monomers were taken up by the cells (quantified by extraction of monomers by DCM followed by HPLC analysis, Figure 39) and nanoparticles were observed via TEM after the photopolymerisation. (Figure 40). The images of “polymerised cells” showed nanoparticles in aggregates localised mainly on the plasma membrane and nuclear envelope while no similar structures were observed in non-illuminated cells.

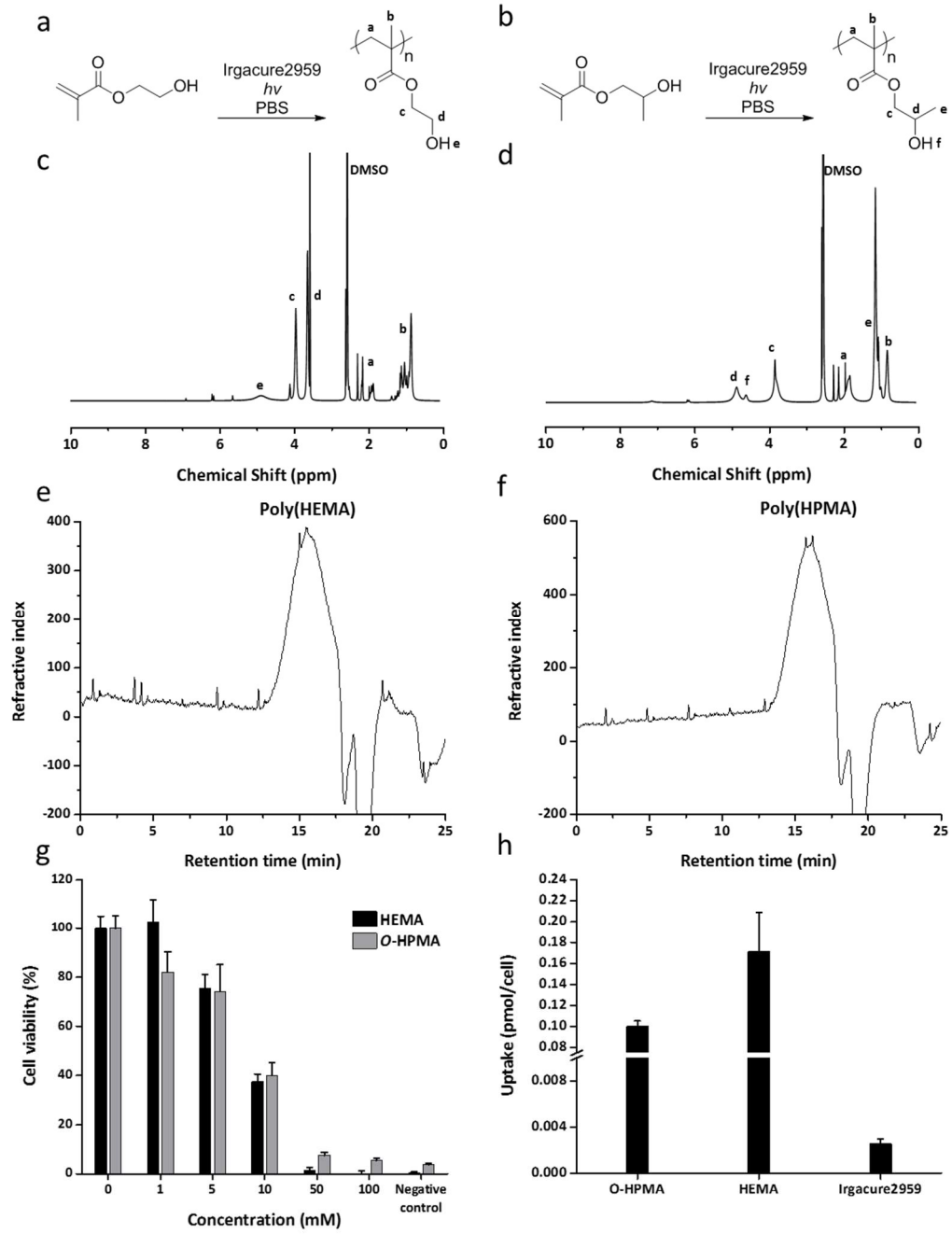

Figure 39. (a) and (b) Photopolymerisation of HEMA and *O*-HPMA in PBS, respectively. The resulting polymers were purified by dialysis. (c) and (d) ^{1}H NMR spectra (in d_6-DMSO) of poly(HEMA) and poly(*O*-HPMA) in d^6-DMSO, respectively. (e) and (f) GPC traces (eluted with DMF) of poly(HEMA) and poly(*O*-HPMA) gave the molecular weights (and Đ) of 14 kDa (2.0) and 11 kDa (1.78), respectively. (g) Evaluation of cell viability of HEMA and *O*-HPMA using an MTT assay with cells incubated for 48 h, n = 6. As a negative control, the cells were treated with 50% DMSO in DMEM. (h) Concentrations of monomer/initiator recovered from cell lysate after 4 h incubation with 50 mM *O*-HPMA or HEMA and 2 mM Irgacure2959. Compounds were extracted by DCM and quantified by HPLC.

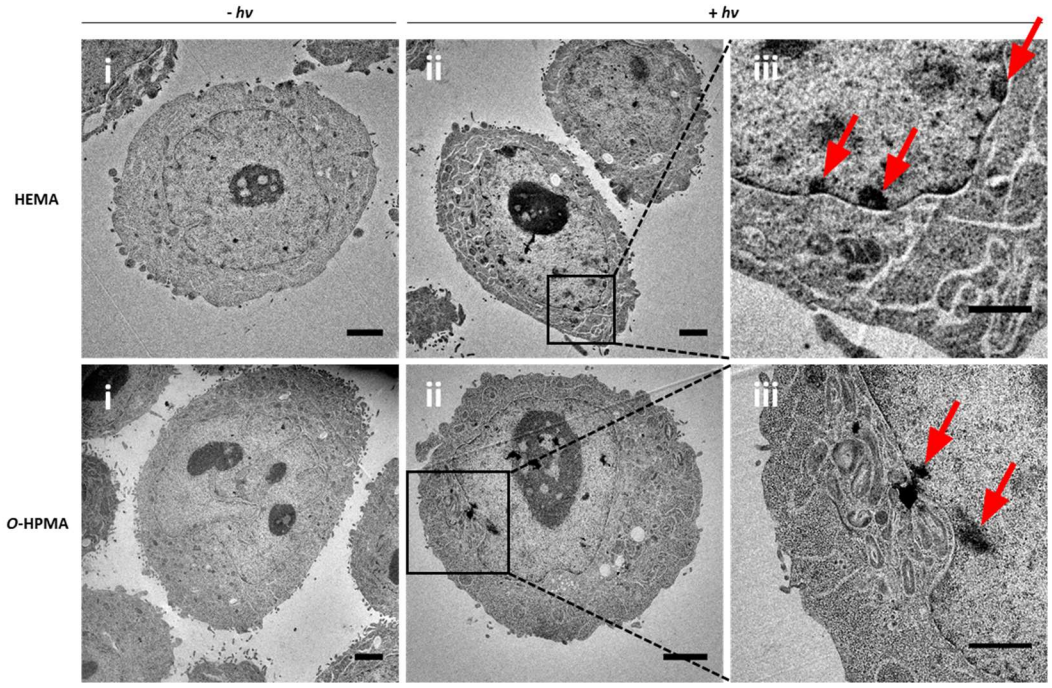

Figure 40. TEM images of HeLa cells treated with HEMA (50 mM) or *O*-HPMA (50 mM) and polymerised. The cells treated with monomer/initiator without illumination were used as controls. The cells were fixed, sliced, and treated with uranyl acetate to stain membranes and lead citrate to stain the nucleus. The precipitated polymers found in cells are highlighted within red arrows. Scale bar = 2 µm for (i) and (ii) and 1 µm for (iii). Cell were fixed directly after the polymerisation because of the monomer toxicity.

3.3. Conclusions and Outlook

A strategy of photo-induced free radical polymerisation in an intracellular microenvironment was developed utilising a series of biocompatible functional acrylic and styrene monomers. The free radical mechanism of the polymerisation process was confirmed and the radical initiating the polymer chain propagation was proven not to be influenced by the radical scavenging species in cells. The successful polymerisation was confirmed by characterisation of the isolated polymers from cells. In addition, the optimised polymerisation allowed the manipulation, tracking and tuning of cellular behaviour by the generation of unnatural macromolecules. Basic cell functions including cell viability, proliferation ability, cell cycle, cell migration and cytoskeleton structures were evaluated and found to be affected by intracellular polymerisation. The intracellular polymerisation processes were observed to

have negligible effects on cell viability and the cell proliferation activity. However, the synthesis of HPMA based polymers in cells induced delay of the cells to access the S-phase of the cell cycle. The generation of polymers were also found to alter the cell mobility by restricting their movements, while the generation of polymers with larger molecular weights induced greater reduction of cell movement rates. The cytoskeleton structures of the "polymerised" cells were observed to be more anisotropic than the "untreated" cells with the actin fibres more parallel to each other and the cellular structure more "elongated". Moreover, various polymers with different functions were generated intracellularly. Fluorescent polymers were synthesised from non-fluorescent monomers and fluorescent copolymers were generated with the elongated cellular retention time. Nanostructures were induced by *in situ* precipitation of polymers from water soluble monomers. The potential power of the approach allow us to begin to understand the free radical chemistries in cells and explore new biocompatible chemistries and control cellular functions.

As this is the first time that biocompatible intracellular photopolymerisation has been reported, many improvements can be made to further optimise the polymerisation process. For example, less harmful visible light (> 400 nm) could be utilised as a light source potentially allowing efficient polymerisation with less cytotoxicity. More chemically robust living polymerisations, *e.g.* RAFT or ATRP, could also be investigated which may contribute to more controlled polymer size/distribution and allow introduction of functional groups to individual polymer chains. Monomers carries more functionalities could be utilised in the polymerisation system such as norbornene methacrylates (see Chapter 4).

Other cells, such as stem cells and primary cells could be alternatives to the cancer cells used here to further broaden the application. For instance, it would be interesting to investigate how polymerisation affects the differentiation of stem cells and whether the polymerisation reaction can act as a stimuli to trigger stem cell differentiation in specific directions. In addition, the polymerisation in normal cells could be investigated to see whether the generation of polymers can induce resistance of the cells towards certain diseases, *e.g.* bacterial/viral infection.

The monomer "tool box" can be extended to more biocompatible monomers allowing the production of structurally and functionally diverse polymers. For instance, a protein binding monomer could be applied to the cells, following co-polymerisation with other

biocompatible monomers and crosslinkers, allowing rigidly solidified cells with permanently immobilised cellular organisms to be achieved without damaging cellular structures.

Chapter 4. Polymer–Protein Conjugates for Signal Amplification

4.1. Introduction

4.1.1. Signal Amplification in Biology

As a fundamental tool in biology and medical science,[86, 102] fluorescent imaging has become highly developed as demand for the detection and tracking of proteins, bacteria, viruses and cells has grown. This has benefited from the development of multiple fluorescent reporters established over the past few decades, including small molecule dyes,[103] nanoparticles (*e.g.* quantum dots),[104, 105] synthetic polymers (*e.g.* intrinsically fluorescent conjugated polymers),[106, 107] and fluorescent proteins (*e.g.* green fluorescent protein)[108]. However, the fluorescence intensity of many fluorophores are unsatisfactory, especially when being used *in vivo*, such as for cancer diagnostics[16, 104] which may result in poor sensitivities, high error rates and narrow ranges of detection, particularly with low abundance targets. Therefore, new amplification methods are required for enhanced fluorescence-based detection.

4.1.1.1. Chain Reaction Based Amplification

Since the first example of the polymerase chain reaction (PCR) reported in the 1980s,[109, 110] chain reaction based amplification methods have rapidly developed and are widely used in biology and medicine.[111-113] The exponential amplifications of target DNA or RNA sequences occurs as shown in Figure 41, where double-stranded DNA is melted to give single-stranded DNA, annealed with a primer (an oligonucleotide providing the starting point for DNA chain growth) and the nucleoside triphosphate monomers added sequentially onto the primer by a polymerase. Originally, PCR based amplifications required temperature cycling for single-stranded DNA formation and primer annealing. Now isothermal amplification methods have been developed, such as strand-displacement amplification, rolling circle amplification and helicase-dependent DNA amplification. In the strand-displacement amplification method, double-stranded DNAs are nicked enzymatically and the synthesis of new chains directly started at the nick point displacing the downstream strand during the polymerisation.[114] In

rolling circle amplification, the amplification starts from a circular template DNA, which is nicked at a desired position and a new DNA chain grows (requiring a DNA polymerases) from the nick point using the circular DNA as the template. This allows continuous growth of the DNA chain with copying of the circular DNA template.[115-117] The efficiency of amplifying long nucleic acids has been further improved by applying helicase-dependent DNA amplification methods, which utilises helicase for unwinding duplex DNA, improving the reaction rate and reactivity.[113, 118]

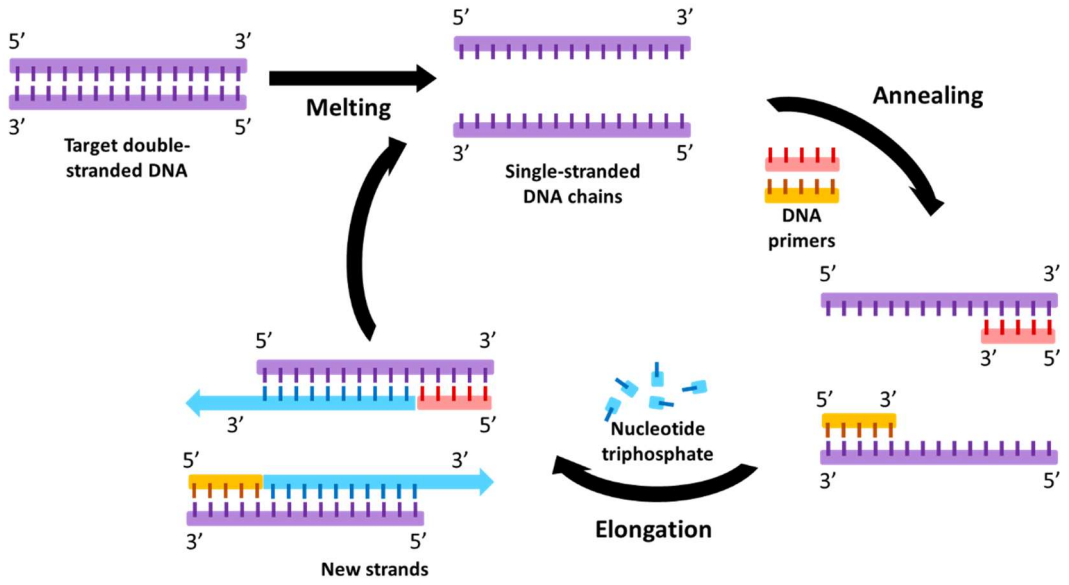

Figure 41. Principle of the standard polymerase chain reaction. The target double-stranded DNA is melted at 95 °C to give two separated strands and annealed with two DNA primers at 55 °C. From the primer, elongation takes place with the aid of a polymerase at 72 °C. The temperature cycling is repeated and gives an exponential increase in the number of DNA strands.

Although highly efficient, most enzyme-based amplification methods require specific substrates, costly materials, *e.g.* enzymes, and often require denaturing process. Hybridisation chain reaction based amplification has emerged as an alternative enzyme-free amplification technique that can be used under mild conditions.[16, 119, 120] Unlike other chain reaction based methods using nucleotide triphosphates for synthesising DNA chains, hybridisation based chain reactions use two species of DNA hairpins, triggered by an initiator to drive a cascade events leading to a nicked double-stranded DNA with multiple signal reporters (see Figure 42). Because of the unique mechanism, signal amplifications are not

achieved by multiplication of the template DNAs but through the introductions of multiple (tens to hundreds) of alternative DNA sequences to one DNA analyte (Figure 42).[121] Incorporating functional moieties such as fluorophores,[122] nanoparticles[123] and electrochemical reagents[124] to the DNA hairpins allows their detection with signal amplification of the analyte. However, challenges exists, such as the difficulties in designing and synthesising DNA hairpins and amplification of other analyte besides DNA or RNAs.

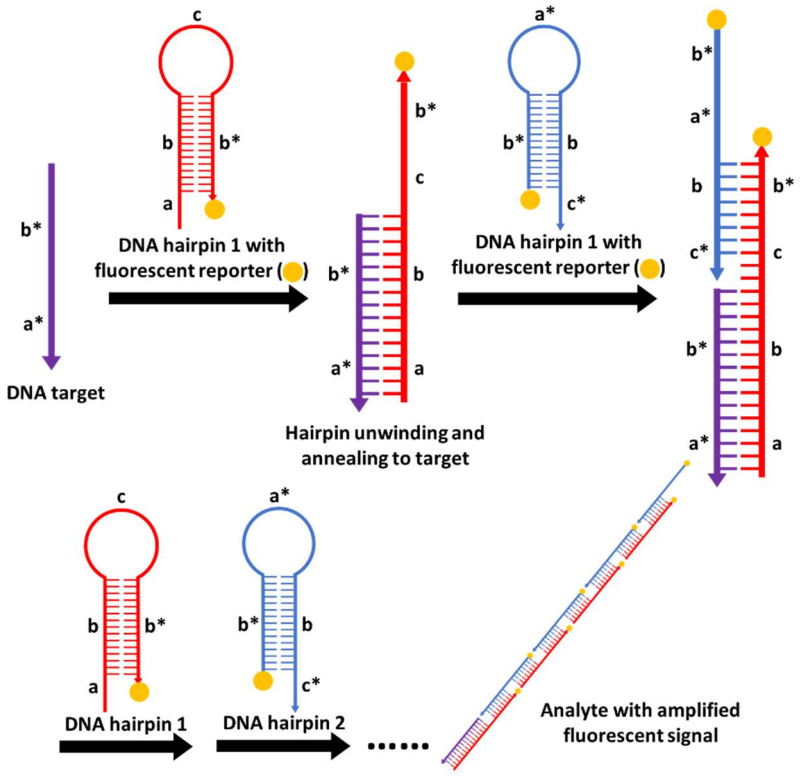

Figure 42. Principle of the hybridisation chain reaction. The introduction of the DNA target (**a***-**b***, as a primer) initiates the hybridisation chain reaction with sequence **a** of the **hairpin 1** recognising the DNA primer and producing the double-stranded complex and expose the **c**-**b*** domain. **Hairpin 2**, stably co-exists with **hairpin 1** without the primer. This thus opens **hairpin 2** and exposed the **a***-**b*** domain. The introduction of **hairpin 1** and **hairpin 2** can then be repeated automatically until the supply of the hairpins is exhausted.

Despite the power of these chain reactions for amplifications of analytes, the shortcomings are still obvious. For instance, amplification methodologies desired for nucleic acids are difficult to apply directly to other types of analytes. As a result, other signal amplification

strategies have emerged and have been successfully applied, including enzyme catalysed deposition based amplifications, and nanoparticle and polymer scaffold based amplifications.

4.1.1.2. Catalysed Reporter Deposition Amplification

Catalysed reporter deposition amplification, also known as tyramide signal amplification, was developed by Kerstens *et al*. in the 1990s[125] and widely used for detection of a range of biological analytes.[126] The amplification is achieved by deposition of multiple biotin labelled tyramides around horseradish peroxidase targeted to the analyte (Figure 43). Specifically, a DNA probe (for detection of selected DNA sequence) is labelled with biotin, which is then targeted by an anti-biotin antibody and a biotinylated secondary antibody. The exposed biotin is then labelled with a streptavidin tagged horseradish peroxidase, so that the peroxidase is bound to the DNA analyte with high specificity. The streptavidin labelled tyramide is subsequently activated by oxidation of the *in situ* generation of hydrogen peroxide which non-specifically reacts with surrounding proteins (the tyramide labelling is located at the target region due to the high reactivity of the activated tyramide). Fluorescently labelled biotin then binds to the streptavidin to achieve fluorescence amplification. Originally, this amplification method was established for signal amplification of fluorescence *in situ* hybridisation to reduce detection limits, but nowadays is used in many more areas such as detection of RNA,[127] bacteria,[128] and other immunohistochemistries[129].

To simplify the protocol, the technique has been developed. For example, streptavidin tagged horseradish peroxidise can be used to directly target the biotinylated DNA probe,[17] while conjugation of the peroxidase directly to the oligonucleotide probe provides an even simpler experimental procedures.[130] The peroxidase has also been replaced with alkaline phosphatase which catalyses the dephosphorylation of a soluble fluorophore to form an insoluble precipitate or allow visualisation of *in situ* generated fluorescent nanoparticles which displays a large Stokes shift ($\lambda_{ex/em}$ = 360/530 nm).[127] Application of such powerful amplification technology (together with *in situ* hybridisation) allows real time detection of multiple genes, proteins (by applying an protein targeting moiety to the peroxidase) and even cells in living organisms.[131, 132]

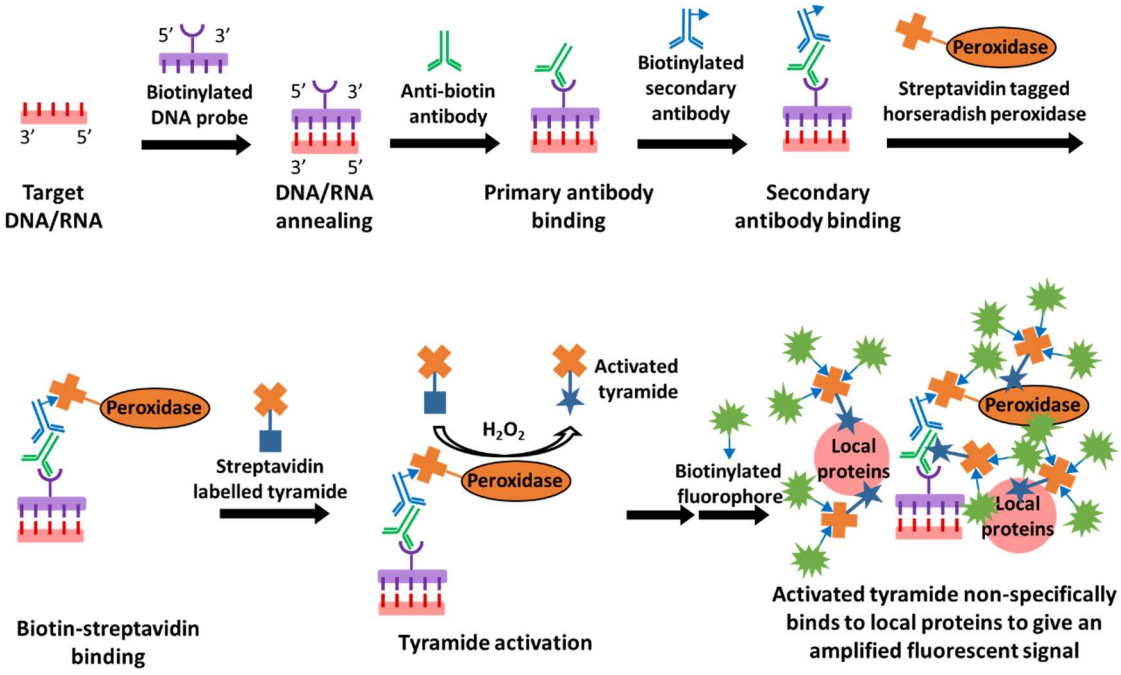

Figure 43. Principle of the original catalysed reporter deposition amplification. Streptavidin tagged horseradish peroxidase is introduced onto the target DNA/RNA analyte through a series of immunological reactions, which then *in situ* oxidation (activation) of the fluorescently labelled tyramide driving complex formation of the activated tyramide with local proteins to achieve fluorescence amplification.

4.1.1.3. Nanoparticle Assisted Amplification Technologies

The development of enzyme free amplification methods are still of interest and nanoparticle based amplification methods have emerged for signal amplification. Nanoparticles possess unique properties such as capacity for carrying multiple targeting motifs with plasma membrane accessibility. These may contribute to enhanced tumour targeting specificities with nanoparticles having been applied as an amplification platform for the detection of DNA, RNA, proteins and cells.

For example, CdSe nanoparticles loaded with RNA detection probes were utilised for detection of low abundant microRNAs. The targeted RNA sequences induced release of Cd^{2+} ions which subsequently "turned on" the fluorescence of Rhod-5N to achieve fluorescence amplifications with a detection limit of 35 fM.[133] WS_2 nanosheets, which specifically bind to single-strand oligonucleotide fragments, have been used for microRNA detection by selectively binding and quenching of oligo-DNA probes (which is linked to a fluorophore and

is fluorescent in solution) by the WS_2 nanosheets while leaving microRNA bound probes fluorescent (RNA analytes anneal to DNA probes to generate doubled-stranded structures that do not bind to WS_2).[134]

However, due to the cytotoxicity of heavy metals and the water solubility of the fluorophores (the fluorescent molecules were homogeneously distributed in solutions), such methodologies can only be applied for *in vitro* screening assays. Silica nanoparticles loaded with DNA probes have been developed for concentration of DNA analytes (prelabelled with a fluorophore) on their surfaces (by in situ hybridisation). Multiple intrinsically fluorescent conjugated polymers, acting as an Förster resonance energy transfer energy donor for the fluorophore on the analyte, were electrostatically absorbed onto the nanoparticle and amplified the fluorescent signal (>100-fold increase, compared to the free analyte in solution where no Förster resonance energy transfer occurred).[135] A polymer–bovine serum albumin (BSA) nanoparticle system with aggregation induced emission fluorophores (which only emit fluorescence in an aggregated state) doped inside the particles were applied for *in vivo* visualisation of tumour tissues. Targeting peptide sequences were attached to the particle surfaces to direct particles specifically to cancer cells.[136] Amplification was achieved by Förster resonance energy transfer between the conjugated polymers (energy donor) and the nanoparticles (with multiple aggregation induced emission accepters attached), where free aggregation induced emission fluorophores in solution was non-fluorescent and thus cannot obtain energy from the polymers.

4.1.1.4. Polymer–Protein Conjugates Based Amplification

One of the shortcome of nanoparticles is their relatively large size and the requirement for multiple targeting moieties labelling to allow stable target–probe conjugates. In comparison, targeting motifs such as antibodies tagged with functional polymer scaffold offer promising performance in fluorescence amplification. For example, an ATRP initiator was selectively attached to an antibody and used for controlled *in situ* polymerisation of a fluorescent copolymer, allowing fluorescent signal amplification for immune detection *in vitro*.[137] More recently, a dendrimer bearing multiple trans-cyclooctene moieties (M_n = 2 kDa) was conjugated to an antibody, allowing subsequent click chemistry with tetrazines carrying a radioligand to amplify radiative signals.[138] Signal amplification using a polymer scaffold provides a flexible platform for labelling various targeting moieties (*e.g.* DNAs, RNAs,

peptides and antibodies) with tuneable marker densities and signal intensities. (See detailed introduction of polymer-protein conjugates in Section 4.1.2.)

4.1.1.5. Other Amplification Technologies

Other amplification methods such as protein multimerisations showed promising efficiency in biological applications. Amplifications are achieved by recruitment of multiple fluorescent proteins (*e.g.* green fluorescent protein) to a targeting moiety (*e.g.* antibody and DNA) by gene transfection, so that the amplified fluorescence is introduced it. The probe with amplified fluorescent signals could be utilised for antigen and DNA detections.[85, 139-141] DNA binding proteins have been used to protect multiple fluorophore labelled DNA analytes from digestion (by a nuclease) with efficient Förster resonance energy transfer dequenching following cleavage.[142] Another Förster resonance energy transfer based amplification system was developed using a dendrimeric scaffold with multiple Dansyl motifs as the donor and a Dabsyl as a quencher. Upon enzyme cleavage of the linker between the donor and the accepter, the fluorescence was dequenched and amplified.[143-145]

4.1.1.6. Enzyme-Linked Immunosorbent Assay

Enzyme-linked immunosorbent assays (ELISA), are widely used for *in vitro* diagnostics in biological research and medicine and are highly specific, safe (compared to radioimmunoassay, another commonly used diagnostic method), to detect antigens at ultralow concentrations. As a powerful detection tool, many ELISAs have been commercialised and used for various applications. The first commercialised ELISA detection system developed and marketed by Organon Teknika was for the hepatitis B surface antigens, and more recently, the CUBE and SMART analysers were marketed by Eurolyser Diagnostica for clinically relevant analyte detections, such as biomarkers and bacteria.[146]

The principle of ELISA is to detect the analyte (often an antigen) using an enzyme immunoassay (see Figure 44). Specifically, antigens from the sample are anchored onto a solid support (*e.g.* a multi-well plate) directly (by physical adsorption) or by capture by an immobilised antibody (referred as a "sandwich ELISA"). The support surface is extensively washed to reduce biomolecules from non-specific binding and then treated with a blocking buffer (*e.g.* BSA in PBS) to block any unspecific binding site on the substrate. An enzyme labelled antibody (specific to the antigen) is introduced to deliver the enzyme to the antigen

to form an "immune complex". The enzyme specific substrate is incubated within the systems to allow the enzyme catalysed reaction and gives a detectible product and quantified by spectrometry.

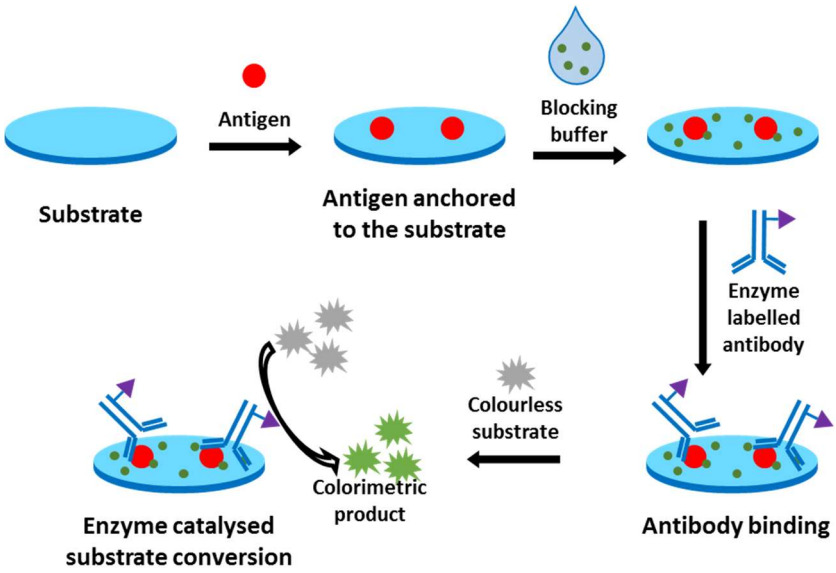

Figure 44. The principle of ELISA. The antigen is anchored to the substrate and treated with a blocking buffer. An antigen specific antibody with a labelled enzyme is then bound to the antigen. With the catalysis of the enzyme, the colourless substrate is converted to a coloured product and detected.

Driven by the huge market for ELISAs based applications, many developments have been reported to further improve its performance. For example, the antibody binding step can be divided into two steps to increase the specificity, where a primary antibody (targeting the antigen) is used initially and an enzyme labelled secondary antibody (target the primary antibody) is then applied to introduce the enzyme.[147] However, the use of antibodies have some potential issues including the relatively complicated and time-consuming approach, and their instability at room temperature or above. Several alternative targeting moieties have been developed such as aptamers (also known as "chemical antibodies"), which are single-stranded DNAs or RNAs that bind to a wide range of molecules with high specificity and affinity.[148] Successful applications of utilising aptamers in ELISA based assays have been reported to permit the detection of contaminants, *e.g.* arsenic, lead and toxic polymers in water,[149] and disease biomarkers, *e.g. T. cruzi* excreted secreted antigens in rats,[150] with

promising specificity. Another alternative to antibodies are so-called nanobodies, a single domain heavy chain antibody expressed without the light chains. In comparison to traditional antibodies, nanobodies have a simpler design, are readily expressed and engineered, and have been used for ELISA for the detection of natural mycotoxins (*e.g.* aflatoxin).[151]

Optimisations are also focused on the detection techniques and the enzyme based catalysts. For instance, electrochemical detection has been used for detection of *in situ* formed silver nanoparticles (by reduction of water soluble Ag^{+} ions by *p*-aminophenol, which was generated by alkaline phosphatase catalysed hydrolysis of *p*-aminophenyl phosphate), and used to detect H7N9 avian influenza virus achieving a single virus detection limit.[152] An enzyme-free version of the ELISA was reported by applying the specific and strong interaction between Fe^{3+} ions and poly(glutamic acid). Similar to other ELISAs, the antigen anchoring and antibody binding were performed initially, but the antibody was decorated with poly(glutamic acid) instead of an enzyme. The subsequent introduction of iron salt induced the formation of a deeply coloured iron complex. This approach showed an high sensitivity for detection of the microcystins-LR (12 pg/mL).[153]

4.1.2. Chemical Modification of Proteins with Polymers

As described in Chapter 1, proteins are extensively used in biology and medicine.[154, 155] However, shortcomings such as immunogenicity, poor stability, solubility and circulation time *in vivo* can limit their usefulness.[156] Since the first example of a polymer covalently conjugated to a protein in the 1970s,[157] the strategy of decorating native proteins with synthetic polymers has developed and shown potential to overcome some of these the limitations[158-160] while providing new functionalities such as cargo delivery, catalysis, diagnostics, and sensing to name but a few.[161-165]

Generally, there are three strategies for synthesising polymer–protein conjugates as shown in Figure 45.[158] The “graft from” approach is achieved by introducing an initiator or chain transfer agent to the protein and subsequent living polymerisation (*e.g.* ATRP and RAFT) directly from the protein.[166, 167] This strategy contributes to high grafting efficiency and simple purification benefiting from the significant molecular weight differences between the monomer and the polymer–protein conjugate. However, the complex 3D structure of proteins and the steric issue leads to lower polymerisation reactivity (*e.g.* monomers cannot

easily reach the initiating moieties buried inside the protein structure and the radicals tend to transfer to be quenched by hydroxyls or amides on the protein). Less controlled polymerisation and thus broader distributions compare to the same polymerisations in solution are resulted. The polymerisation condition and monomer used also has to fulfil many criteria for sensitive proteins to avoid denaturation.[158]

The "graft to" approach directly conjugates preformed polymers to proteins, provides accessibility to most of the polymerisation methods with a wide screen of functional monomers. However the yield of the conjugation step is often low due to the steric hindrance between two macromolecules, and multiple purification steps are often required to isolate the product from the macromolecular reactants.[159]

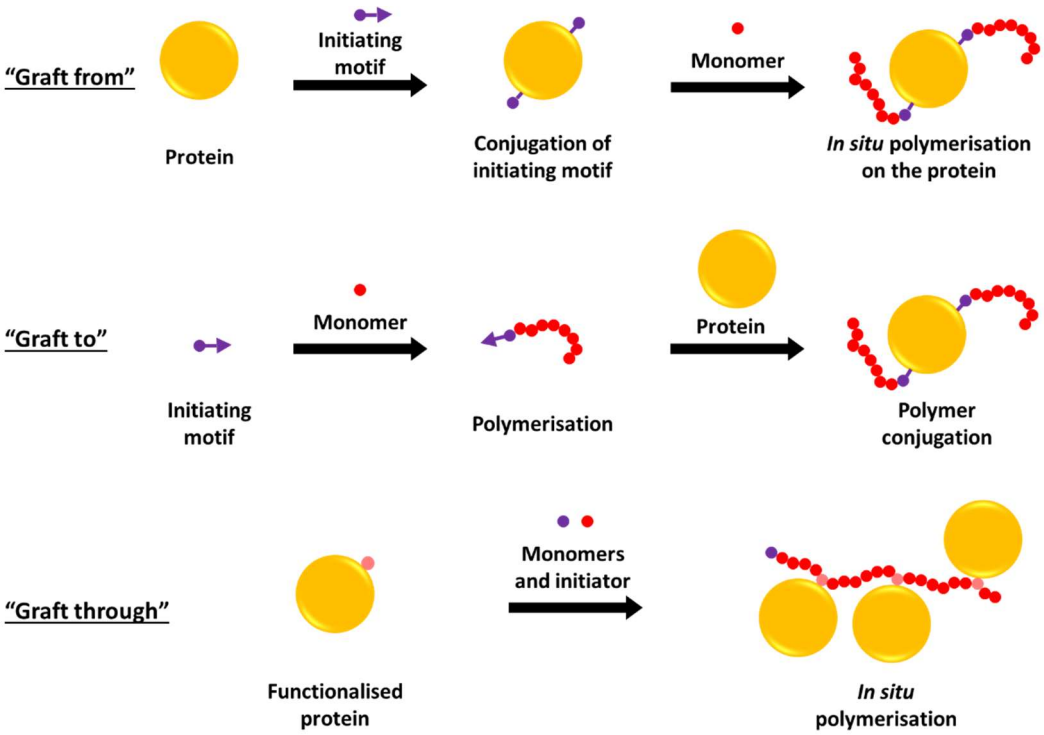

Figure 45. Strategies for fabricating polymer–protein conjugates. (top) The "graft from" approach requires initiating motifs to be introduced onto the protein surfaces and subsequent *in situ* polymerisation gives controlled polymer chains conjugated to the proteins. (middle) The "graft to" approach requires polymer chains to be initially synthesised with a terminal functional group allowing coupling reactions to the protein. (bottom) The "graft through" requires the protein molecules to be functionalised with a polymerisable moiety which allowing copolymerisation with other monomer(s) to give multiple protein conjugated polymers.

The third method is often referred as the "graft through" approach, which chemically modifies proteins with polymerisable motifs and conducts the polymerisation to obtain comb-shaped polymer structure with multiple proteins present.[158] Due to limited polymerisation reactivity, yields of the "graft through" polymers are low and the number of reported examples and applications are limited. In summary, to achieve high quality polymer–protein conjugates, it is essential to consider the conjugation strategy, the type of protein and polymer utilised, the chemical reaction for the coupling reactions and key issues such as purifications.

4.1.2.1. "Graft from" approach

The "graft from" method, which directly grows polymer chain from the protein, has gained increasing attention because of its high yield and ease of purification since the early 2000s.[166, 168] Incorporating the initiating motif to the protein of interest is key and will directly affect the reactivity of the *in situ* polymerisation and the properties and dispersity of the resulting conjugates. The most widely used conjugation strategy is to conduct coupling reactions at the site of native reactive centres *e.g.* lysines or cysteines on the protein surfaces with various available reactive moieties, such as active esters, isocyanates, maleimides and halogenides.[156, 159] The general coupling reactions included active ester–amine coupling, thiol–maleimide 1,4-addition and thiol–disulfide exchange, which covalently conjugate the initiating motifs to proteins.[169-173] However, because of the presence of multiple lysines and cysteines on proteins, such conjugation may result in heterogeneous conjugates with undetermined numbers and locations of the conjugations, with the risk of changing the solubility and/or loss of biofunction.[166, 174] Introducing unnatural amino acids or replacing reactive lysines or cysteines with other amino acids by mutagenesis allows site specific modifications at desired site. However, such methods suffer from complicated designs and needs to synthesise the desired mutants and limits the choice of coupling reactions. Other site specific modifications such as α-amine selective coupling using optimised conditions (typically by tuning pH) also show good selectivity and efficiency, but required precise optimisation for individual protein candidates and are difficult to translate to different protein structures.[175]

From the initiator proteins, polymerisations can be conducted to generate polymer chains directly on the protein. To date, only a few polymerisation approaches (most commonly,

ATRP[176] and RAFT polymerisation[177]) with a limited number of monomers (*e.g. N*-isopropylacrylamide, PEG methacrylate and *N*,*N*-dimethyl acrylamide) have been possible. This is due to the need to preserve the native protein structures and carry out the chemistry in aqueous solution at mild pH and low temperature. ATRP was initially applied with *in situ* polymerisation on proteins using Cu(I) as the catalyst.[166-168] The successful introduction of ATRP initiators onto proteins, *e.g.* BSA, streptavidin, lysosome, trypsin and the P22 capsid. This is achieved with marcoinitiator formation strategies including biotin–streptavidin interaction, thiol–maleimide 1,4-addition and thiol–disulfide exchange, which permitted subsequent controlled polymerisations of monomers such as *N*-isopropylacrylamide, PEG methacrylate, 2-aminoethyl methacrylate, acrylamide, *N*,*N*-dimethyl acrylamide and *N*,*N*-dimethylaminoethyl methacrylate, (Figure 46). This has given desired polymer–protein conjugates that have shown enhanced protein stabilisation.[166-168, 178, 179]

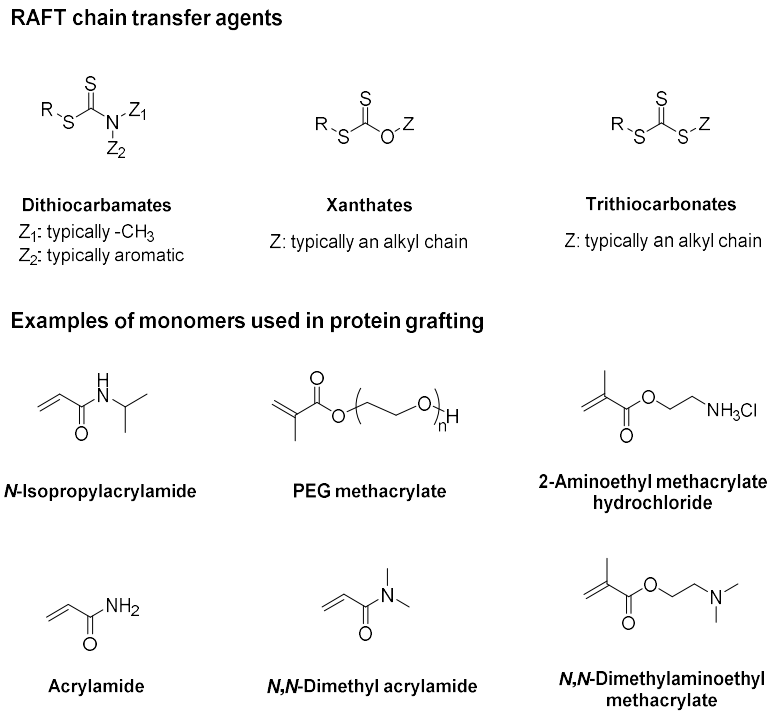

Figure 46. Structures of the RAFT agents and examples of monomers used to graft onto proteins directly.

However, ATRP requires a heavy metal catalyst and the residue left may limit applications of the product. Another living polymerisation technique, RAFT polymerisation, has also been explored avoiding the use of heavy metal catalysis using unique RAFT reactive centres, *e.g.* dithiocarbamates, trithiocarbonates and xanthates, see Figure 46. These are proved to have high reactivity and robustness in aqueous solutions.[170, 171, 174, 180] The subsequent polymerisation under mild conditions allows the *in situ* growth of the polymer chains on the proteins with the desired chain length and density of function groups. For example, RAFT agents were covalently conjugated to the target proteins, *e.g.* BSA and lysosome followed by RAFT polymerisation of *N*-isopropylacrylamide and gave controlled polymer–protein conjugates in high yield without affecting protein activity.[169-171, 174]

It is worth noting that synthetic polypeptides can be decorated with polymers using this "graft from" method in an even simpler procedure than natural proteins. Some examples that have shown success including coupling of RAFT agent to the synthesised polypeptide directly on the solid supports via different coupling chemistries, *e.g.* Cu catalysed alkyne–azide cycloaddition and carboxylic acid–amine coupling. Subsequent living polymerisations gave well-tuned polymer–peptide conjugates.[181-183]

4.1.2.2. "Graft to" approach

Different from the "graft from" method, where an *in situ* polymerisation process is required in the presence of the fragile proteins, the "graft to" approach requires only one step chemical reaction with the target protein substrate (using the presynthesised polymers). The first example using this method was introduced by Abuchowski in the 1970s, where activated PEGs were covalently introduced onto lysine residues on BSA or bovine liver catalase and showed loss of immunogenicity.[157, 184] Although showing poor coupling efficiency, this conjugation method is used in various applications because of the available functional polymers and the straight forward synthesis procedure.[158, 165]

The most widely used polymer for protein conjugation is poly(ethylene glycol). For example, PEGylation of proteins protect the proteins from enzymatic degradation and reduced the immunological uptake by the phagocyte system (e.g. macrophages). Several PEG-protein products have been developed and approved by the Food and Drug Administration for

therapeutic uses (e.g. PEG-asparaginase (Oncaspar) and PEG-growth hormone receptor antagonist (Somavert)).[185, 186]

Other terminal functionalised polymer scaffolds are accessible through diverse synthetic strategies, *e.g.* free radical polymerisation (with chain transfer agent), living radical polymerisations, ring open polymerisations, anionic polymerisations and post functionalisation of commercial polymers.[165] The polymer scaffolds generated can be directly used for conjugation or further modified with "clickable" functional groups.

The conjugation step, which links the polymer chain to the protein, is a key step. As described above, amine and thiol groups are the most common reactive centres for incorporation of artificial motifs to proteins. Active esters are widely used for amine coupling, and has been applied for polymer–protein conjugation by coupling poly(*N*-isopropylacrylamide-*co*-*N*-acryloxysuccinimide) to a series of proteins (egg lysozyme, horse myoglobin, human haemoglobin, human serum albumin and bovine γ-globulin), and used for studying the aggregation properties of the conjugates.[187] Interestingly, most of the reported examples showed negligible influence on the polymer conjugated proteins (with undefined number of unspecific binding sites), whereas some even showed increased enzymatic activities such as the trypsin upon poly(*N*-isopropylacrylamide) addition.[188] Some alternatives to *N*-hydroxy succinimide esters, such as 2,4,5-trichlorophenol ester[189] and pentafluorophenyl ester,[190, 191] have also been established and used for conjugation of comb shaped PEG polymers and *N*-isopropylacrylamide copolymers to proteins, *e.g.* collagen and anti-p24 IgG antibody with high yields.

In comparison to highly abundant lysines on protein surfaces, free cysteines are much rarer especially for those accessible (not buried inside the 3D structures). Therefore, modification of proteins with only one available free thiol group allows site selective conjugation. Similar to the initiator coupling reaction used in the "graft from" approach, thiol–maleimide 1,4-addition and thiol–disulfide exchange have been commonly used for polymer conjugations with thiols.[165, 192] For example, maleimide terminated poly(*N*-isopropylacrylamide)s was synthesised by RAFT polymerisation with a set of different molecular weights (10-30 kDa) and were coupled to a small molecular weight DNA binding protein (rcSso7d, 7 kDa). The systematic increase in molecular weight dramatically varied the folding structure and contributed to a well organised 3D structure in bulk which was rare for the wild type

protein.[193] Similarly, a maleimide terminated poly(*N*-isopropylacrylamide) was conjugated to a green fluorescent protein derivative amilFP497 via thiol–maleimide 1,4-addition which self-assembled with the anticancer drug doxorubicin, permitting the thermal controlled release of drug molecules with the ability of simultaneously tracing the degree of release by fluorescence life time microscopy.[194] A pyridyl disulfide (as an activated disulphide bond) functionalised poly(2-hydroxyethyl methacrylate) was synthesised by ATRP and conjugated to the model protein BSA in high yield.[195] Because of the reduction cleavable nature of the disulfides in biological systems, the resulting conjugates may be utilised for targeted cargo release applications.

However, despite the rapid kinetics and high selectivity of the thiol–maleimide 1,4-addition in aqueous environment, the instability of the thiosuccinimides (thiol–maleimide adduct) caused by oxidation[196] or *retro*-1,4-addition[197] reactions dramatically limit its application *in vivo* and are therefore not favourable for conjugation chemistries.[198] In addition, the disulphide bonds formed by thiol–disulfide exchange are unstable to reduction and not suitable for permanent linkages *in vivo*.

Benefiting from the rapid development of bioorthogonal chemistry over the past two decades,[33] many unnatural functional groups have been introduced into protein structures chemically or genetically and have opened a new field of site specific protein labelling via click chemistries (Figure 47). The most commonly used functional groups introduced onto protein structures include azides,[199] aldehydes (ketones),[200] strained alkenes[201] and alkynes[202] which provide the potential for rapid and selective conjugation of functionalised polymers to proteins within biological relevant environments in high yields, although real examples of such applications are still rare.[158]

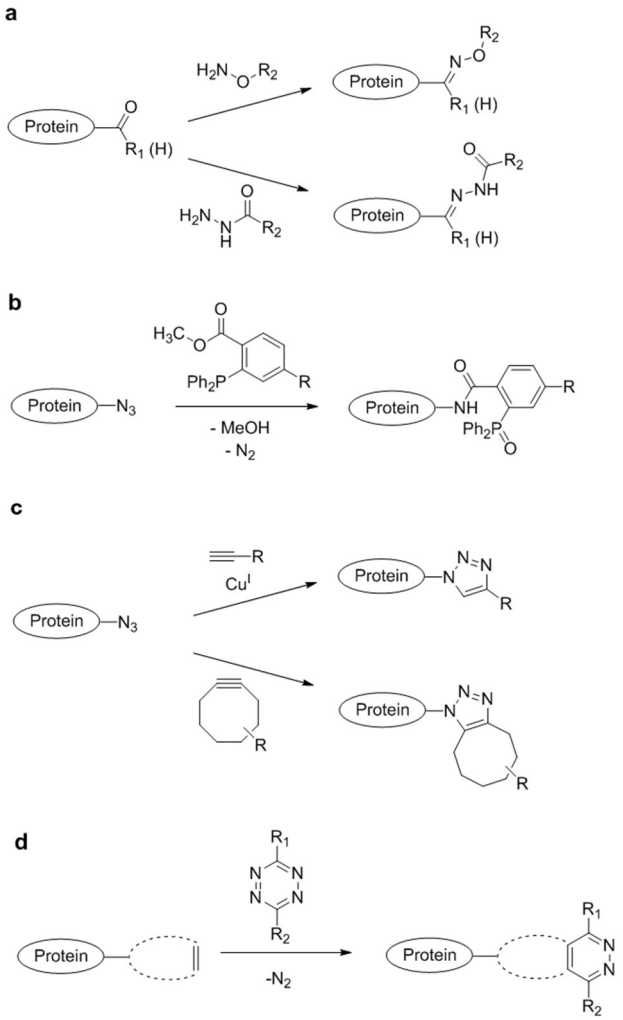

Figure 47. Typical bioorthogonal reactions used for protein labelling. (a) Ketones (aldehydes) condense with a hydroxylamine derivative or a hydrazide; (b) An azide undergoes a trapping Staudinger ligation with a triarylphosphine; (c) Azides reacts with a terminal alkyne through a copper catalysed cycloaddition or reacts with a strained alkyne; and (d) A strained alkene undergoes an inverse electron demand Diels–Alder cycloaddition with an 1,2,4,5-tetrazine.

Some supramolecular interaction based conjugation methods, *e.g.* biotin–streptavidin interactions and metal chelation have also been reported. For example, a biotinylated poly(*N*-isopropylacrylamide) was synthesised via RAFT polymerisation and conjugated to a fluorescent streptavidin and was used for protein–protein conjugations with BSA.[203] Nitrilotriacetic acid functionalised polymers, *e.g.* polystyrene, poly(*N*-acryloylmorpholine-*co*-*N*-acryloxysuccinimide) and pyridylthiourea-grafted polyethylenimine have enabled immobilisation of Ni^{2+} ions onto the polymer with recognition and binding to hexahistidine

tags on target proteins, *e.g.* GFP and streptavidin, permitting enzyme immobilisation, *in vivo* imaging and drug delivery.[204-206]

4.1.3. Purification Techniques for Polymer–Protein Vonjugates

The yield of the aforementioned polymer–protein conjugation methods rarely reach 100% and purification steps are usually required to isolate the conjugation product from the macromolecular reactants.[207] Dialysis is the most commonly used method and works well when separating small molecules from large proteins, although it lacks efficiency when separating mixtures of proteins, *e.g.* isolation of polymer modified proteins from unreacted proteins. For more precise separation of proteins, protein chromatography techniques have been developed,[208, 209] which allow separation of proteins based on their size, charge, affinity and hydrophobicity, *e.g.* size exclusion, ion-exchange, affinity and hydrophobic interaction chromatographies.[210]

4.1.3.1. Size Dependent Chromatography Purification

Size dependent chromatography, *e.g.* gel permeation, size exclusion and molecular sieve chromatographies, separate macromolecules depending on their hydrodynamic volume (relates to their molecular weight) (Figure 48). It is the most widely used separation method for polymer–protein conjugates due to the significant change of the protein molecular weights before and after polymer addition.[88, 194, 211, 212] When eluting through the porous stationary phase matrix (also referred as a gel), high molecular weight molecules elute first because they are excluded from the pores in the matrix while the small molecules are retained longer due to their accessibility into the larger volume within the porous matrix.[213] Benefiting from this mechanism, polymer–protein conjugates can be isolated from the reactant mixture (with the presence of unreacted protein and polymer fragments, coupling agents, catalysts and inorganic salts).[88, 211, 212] However, due to the limited resolution of the technique, it is challenging to provide highly pure products in high yields if aiming for clinical/industrial application.[213]

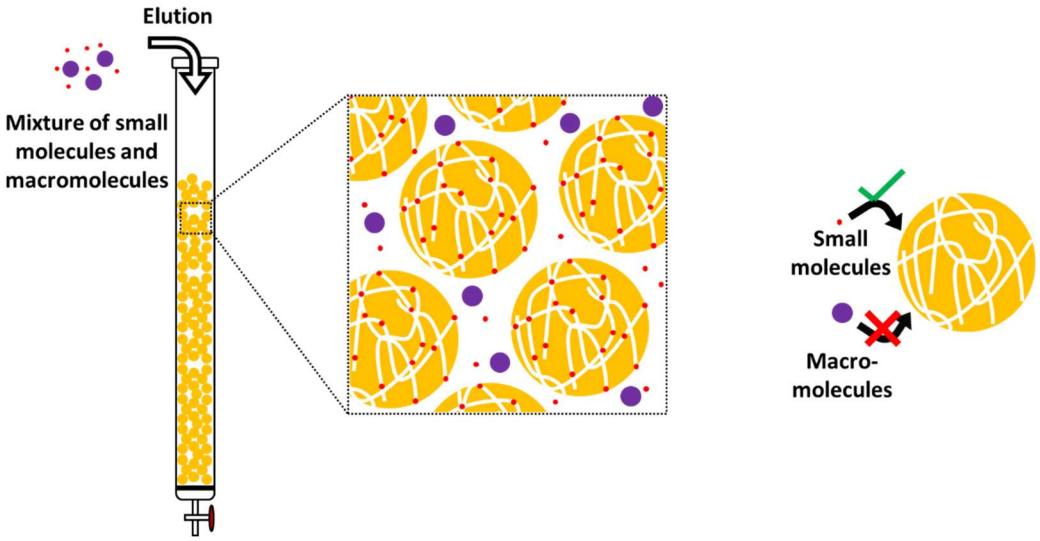

Figure 48. Mechanism of size dependent chromatography. The porous stationary matrix only allows small molecules into their internal pores, so that they have a greater "free volume" to go through and therefore are retained for a longer time in the column, while the macromolecules can only go through the voids between matrix particles and thus retained for a shorter elusion time. However, the method has very limited resolving power as fractions are not usually well separated.

4.1.3.2. Affinity chromatography purification

The development of scalable and simple purification methods are of great interest to avoid costly chromatography equipment and complicated purification procedures. Affinity chromatography was established for isolating target molecules from complex biological mixtures aided by specific interactions (*e.g.* antibody–antigen interaction, cofactor binding, lectin–carbohydrate interaction and metal chelation) between the target and the stationary support. Although usually referred as affinity chromatography, a loaded and optimised column is not always needed for such techniques with magnetic particles, a widely used alternative to columns, providing a simpler purification procedure.[214]

Metal chelation based methods, *i.e.* immobilised metal ion affinity chromatography, immobilise target proteins onto an insoluble support (by metal ion chelation with ligands on the protein), with elution of the protein from the solid support by a low pH buffer or a competitive displacement to give purified proteins in high purity.[215] The best known application is the purification of hexahistidine tagged proteins by Ni^{2+} loaded affinity resins, ranging from a bench scale to an industrial scale.[216-219] Specifically, a chelating ligand, *e.g.*

nitrilotriacetic acid, the most commonly used tetradentate ligand, is introduced onto a solid support (*e.g.* agarose gel, silica particle, polymeric resin and/or magnetic particles) and the metal ions (normally Ni^{2+} with coordination number of 6) chelated to the ligand with two water binding sites displaced by the protein.[220] When eluting through or incubated with the support, the hexahistidine tagged protein is selectively bound and isolated from other biomolecules by simple filtration and washing of the solid support (the washing buffer usually contains inorganic salt, *e.g.* NaCl, and/or detergents to minimise unspecific ionic or hydrophobic interactions). The loaded proteins are eluted from the solid support at the optimised condition (or through a gradient eluting buffer) to elute fractions with different affinities. The target protein can be obtained in high quality and high yield while the matrix can be reused by simple washings and reloading of metal ions.[216]

Examples of successful application of the immobilised metal ion affinity chromatography can be found in many areas. An enzymatically cleavable histidine tag can be genetically introduced to a set of protein mutants which permitted the efficient isolation of target proteins in one chromatography step and was used for purification of Fab fragments[221] and antibodies[222]. Naturally occurring polyhistidine motifs on protein surfaces, *e.g.* growth hormone, prolactin and recombinant human feron γ, have been used for the direct isolation of proteins although the existence of these kind of proteins are not common in nature.[223-225] In addition, introducing hexahistidine tags into the heavy chain of antibodies enables immobilised metal ion affinity chromatography purification without affecting antigen binding properties.[226-230] However, little attention has been paid to applying such a powerful purification technique for chemically modified proteins. To the best of our knowledge, there have not been any examples reported using affinity chromatography for isolating polymer–protein conjugates, although it may overcome the problem of generating high quality conjugation products.

4.1.4. Tetrazine Quenched "Turn on" Probes

Fluorescent imaging is widely used in diagnostics, permitting the visualisation of a target of interest by specific labelling with fluorophores. However it has to face the barrier of non-specific bindings and may need extra washing steps to minimise background fluorescence. An alternative strategy is to use fluorogenic reporters, which are quenched and only fluoresce after undergoing a specific reaction or a change in environment, permitting wash-

free *in vivo* diagnostics with high efficiency and specificity. As a bioorthogonal reactive group as well as a fluorescence quencher, tetrazine quenched fluorophores have drawn many attentions.

The general strategy for designing tetrazine based fluorogenic markers were to covalently conjugate fluorophores to tetrazine cores to allow efficient quenching of the fluorescence. Because of the unique electron structure (high electron affinity)[231] and the absorbance spectra of tetrazines, fluorescence quenching of tetrazine based fluorogenic markers can be achieved through the "through bond energy transfer mechanism",[232] the photoinduced electron transfer mechanism[233] or the Förster resonance energy transfer mechanism[234]. Boron dipyrromethenes (BODIPY) are lipophilic fluorophores with high fluorescence intensities, and are conjugated to tetrazines to give fluorogenic fluorophores (see examples in Figure 49).[233] Other tetrazine quenched green fluorogenic fluorophores have also been reported (*e.g.* tetrazine-Oregon Green 488, Figure 49). [233, 235]

Many efforts have been made to develop tetrazine based fluorogenic reporters with emission across the full visible spectrum. Recent work by Park *et al.* report the synthesis of tetrazine quenched fluorophores from green to red using an emission tuneable Seoul-Fluor fluorescent core skeleton (see Figure 49b), which gives a general strategy for synthesising predictable fluorogenic markers through a relatively simple route.[234]

The flexible spacer (shown in red in Figure 49) between the tetrazine, *i.e.* the tetrazine not directly conjugated to the fluorescent core, and fluorescent moieties may not be able to effectively facilitate the quenching and results in limited fluorescence increases upon activation.[236] To further optimise the performance of the fluorogenic reporters, several fluorophores (coumarin,[237] BODIPY,[236, 238] fluorescein,[238, 239] rhodamine,[239] phenoxazine[240] and cyanine,[241] see Figure 49) have been conjugated to the tetrazine core with improved "through bond energy transfer" efficiency and showed improved fluorescence dequenching.

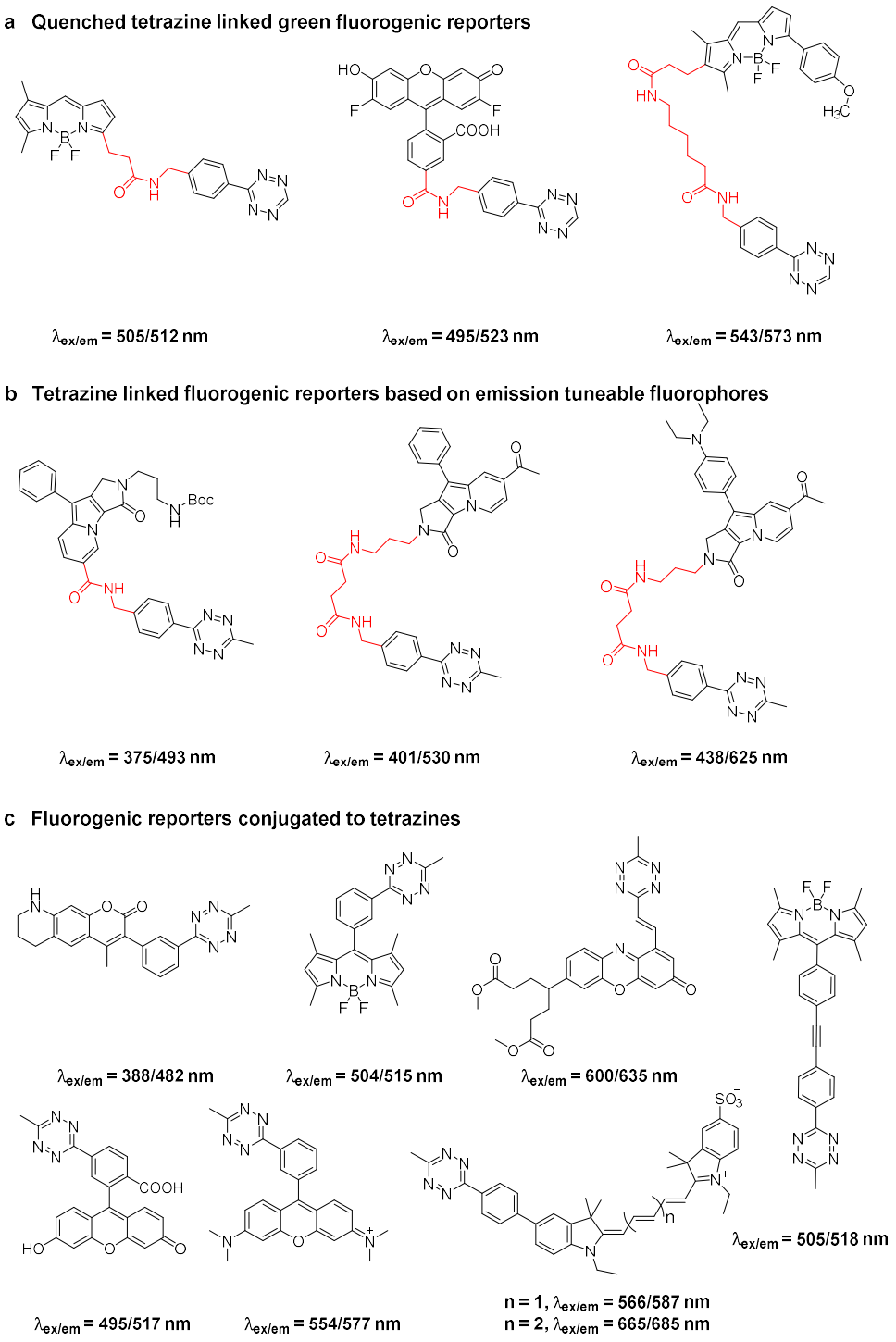

Figure 49. Examples of tetrazine quenched fluorogenic reporters. (a) Green tetrazine linked (quenched) fluorophores (b) Tetrazine linked (quenched) fluorophores based on an emission tuneable Seoul-Fluor fluorescent core. The substitution of the fluorescent core contributes to various emission wavelength (493, 530 and 625 nm). (c) Fluorogenic fluorophores conjugated to tetrazines.

Taking advantages of these “turn on” fluorogenic reporters, wash-free *in vivo* diagnostics has been achieved. However, few examples has been reported to further amplify the fluorescent signal of the fluorogenic markers which may further improve the signal to background ratio.

In this chapter, the first strategy for simultaneous switch on and amplification of fluorescent signals is reported. A polymer scaffold providing reactive centres for inverse electron-demand Diels–Alder chemistry was synthesised with a hexahistidine tag handle for purification. This presynthesised polymer was covalently conjugated to the antibody Herceptin allowing specific cancer cell targeting. The dequenching of the tetrazine quenched fluorogenic fluorophore with the polymer–antibody conjugates took place on live cells to achieve simultaneous switch on and amplification of the fluorescent signal.

4.2. Results and Discussions

4.2.1. Synthesis of Polymer–Protein Conjugates Through a "Graft From" Approach

To synthesise the polymer scaffold, a "graft from" approach was initially applied (see Figure 50). As previously described, this approach offers a high yield and easy product isolation procedures. Thus as a proof of concept, a commercially available active ester functionalised RAFT chain transfer agent (RAFT agent) was conjugated to the lysine or N terminal amine of bovine serum albumin (BSA) through active ester-amine coupling reaction in PBS (giving **1**), followed by photoinduced electron transfer RAFT polymerisation using *N*,*N*-dimethylacrylamide (DMAA) to give the polymer–protein conjugate **2** (see Figure 50). The conjugation reaction was initially conducted in PBS at 37 °C to give the macro-RAFT agent and the successful conjugation was confirmed by MALDI-ToF mass spectrometry (Figure 50). The mass increase to BSA (of 1050 Da) implied the degree of substitution of the protein was 2.6, sufficient for the subsequent photoinduced electron transfer RAFT polymerisation from the protein. The macro-RAFT agent generated was purified and used directly for the RAFT polymerisation.

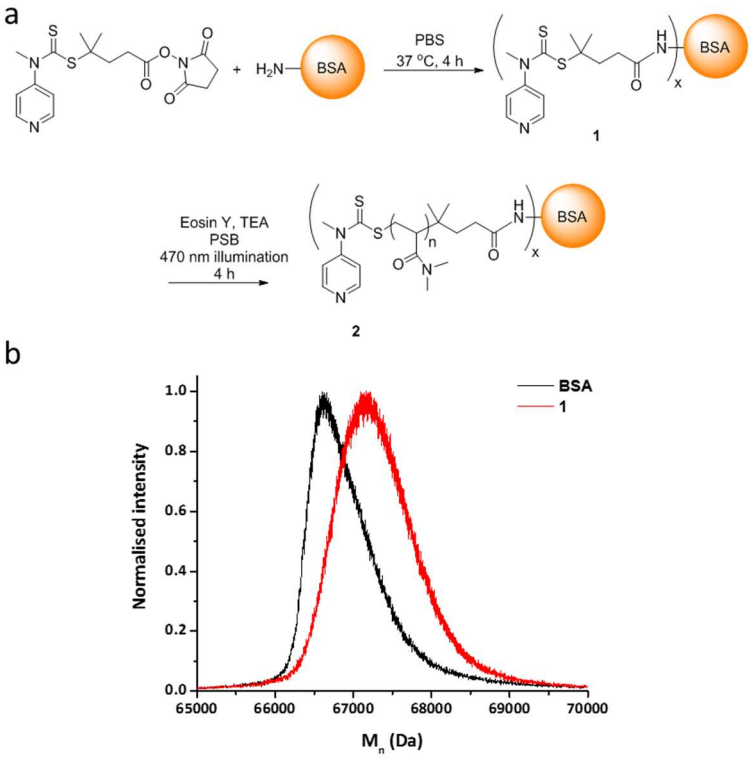

Figure 50. (a) Synthesis of polymer–protein conjugates through a "graft from" approach. The active ester functionalised RAFT agent was conjugated to BSA by reacting with the lysine motifs and/or the N terminus in PBA at 37 °C to give the "macro-RAFT agent" **1**. A photoinduced electron transfer RAFT polymerisation of DMAA was then conducted in PBS aided with Eosin Y as a photosensitiser, and triethylamine as an electron transfer agent and 470 nm illumination to give poly(DMAA) grafted BSA **2** in quantitative yield. (b) MALDI-ToF mass spectra of BSA (black) and macro-RAFT agent **1** (red), showing a difference of around 1050 Da. MALDI-ToF mass spectra were obtained using a linear reflective scan method with sinapinic acid as the matrix.

To optimise the polymerisation conditions, DMAA was used as a model monomer looking at a range of concentrations between 1 µM and 1 M with the concentration of the macro-RAFT agent **1** set at 100 µM with monomer conversions quantified by ^{1}H NMR (Table 6). No polymerisation was observed with monomer concentrations lower than 100 mM but polymer–BSA conjugates with molecular weights of 299 kDa and 860 kDa were found with DMAA concentrations of 100 mM and 1 M, respectively (M_n of BSA = 67 kDa). However, the molecular weights of the conjugates could not be easily controlled by tuning the monomer-RAFT agent ratio, and issued when aiming for small molecular weight conjugates. This is probably because of the low concentrations of the activated RAFT agents generated in the system[58] and were not able to initiate the polymerisation unless high concentration of

monomers were introduced to drive the reaction. The problem could be overcome by applying a higher concentration of the macro-RAFT agent but would be limited by the solubilities of the conjugates. The stability of the protein materials needs to be considered if concentrated reactants, *e.g.* monomers and fluorophores, has to be used, which can cause denaturation of proteins. As a result, an alternative "graft to" approach was explored.

Table 6. Optimisation of monomer concentration for the photoinduced electron transfer RAFT polymerisation. The DMAA (1 µM to 1 M), marco-RAFT agent **1** (100 µM), Eosin Y (200 µM) and triethylamine (10 mM) were dissolved in PBS (pH = 7.4) and illuminated for 4 h at 470 nm (monomer conversion was quantified by ^{1}H NMR by comparing the integration of the monomer peaks and the polymer peaks). The M_n of the polymer BSA conjugates were quantified by GPC.

Monomer concentration	1 µM	10 µM	100 µM	1 mM	10 mM	100 mM	1 M
Monomer conversion	<1%	<1%	<1%	<1%	<1%	65%	59%
M_n (kDa)	-	-	-	-	-	299	860

4.2.2. Synthesis of Polymer–Protein Conjugates Through a "Graft To" Approach

Another approach is to conjugate preformed functional polymers to proteins (the "graft to" approach) and to provide the opportunity of comparing polymer–protein conjugates with different polymer structures and molecular weights. However, the coupling efficiency between the two macromolecules is often low and requires tedious purification and typically provides low yields.[158] Histidine tagging and affinity chromatography is well developed and routinely applied in protein purification.[204, 242, 243] By combining the "graft to" polymer modification approach and affinity chromatography, polymers carrying a hexahistidine affinity tag offer the opportunity for ease of purification of the resulting polymer–protein conjugate.

4.2.2.1. RAFT Chain Transfer Agent Synthesis and Characterisation

A RAFT polymerisation approach, which was developed by Rizzardo in 1990s,[177, 244] was selected for the synthesis of polymer scaffolds. It is widely used in biology, *e.g.* protein conjugation, due to the precise control over molecular weight, topology structure and the negligible cytotoxicity of the RAFT process itself and the generated polymers.[158, 245, 246]

Here as a key part of the RAFT polymerisation, the new trithiocarbonate RAFT agent **8** bearing a hexahistidine tag was synthesised as shown in Figure 52. The trithiocarbonate moiety was chosen as a reactive centre for the RAFT polymerisation because of its good performance with acrylic monomers. In comparison to dithiocarbamates and xanthates, trithiocarbonates provide higher reactivity and better distribution control for acrylic monomers (as described previously) while the aliphatic tail contributes to better solubility in organic solvents.[247, 248] The hexahistidine tag and the ω-carboxylic acid moieties were directly incorporated into the RAFT agent in order to give even distribution of functional groups in individual polymers (one functional group per polymer). The functional RAFT agent **8** was synthesised using a solid phase synthesis strategy, which allows straight forward synthesis in high yield and again ease of purification.[182, 249]

The carboxylic acid functionalised RAFT agent **3** was synthesised according to published procedure (Figure 51).[250] Specifically, *n*-butanethiol was deprotonated by KOH and added to carbon disulphide to form the trithiocarbonate anion which was coupled to bromopropanoic acid to give **3** in 63% yield. The ^{1}H NMR spectrum shows representative peaks of the RAFT agent, *e.g.* the broad peak at 13.16 ppm showed the presence of the carboxylic acid, while HPLC showed the good purity of the compound (see Figure 51).

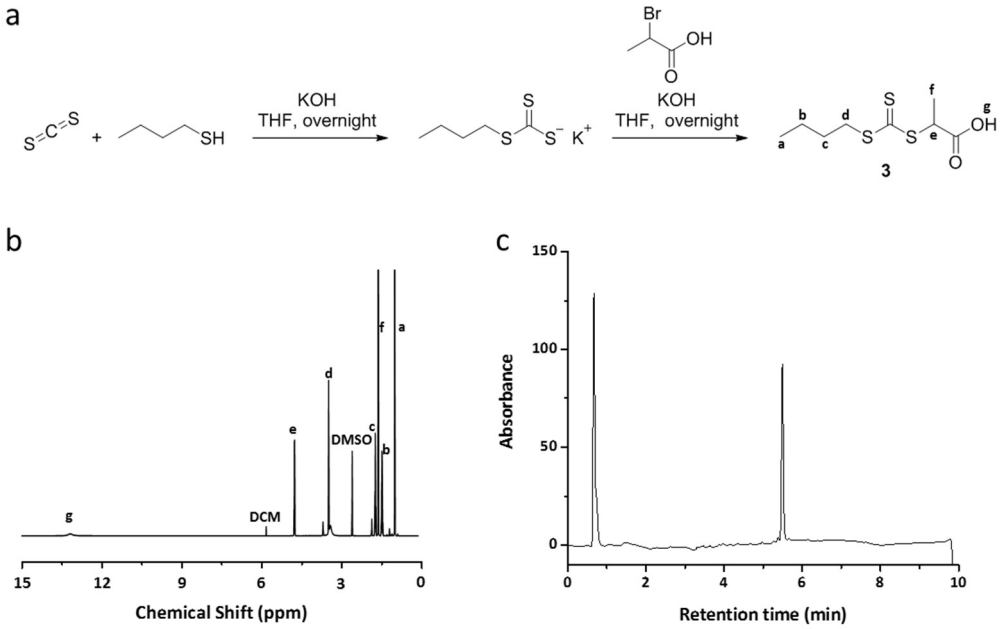

Figure 51. (a) Synthesis of carboxylic acid functionalised RAFT agent **3**. (b) ^{1}H NMR of **3** in d_6-DMSO with representative resonances shows the corresponding protons resonances. (c) HPLC trace of **3** with a peak at 5.49 min showing the presence of compound **3** (HPLC was performed using water/MeCN (with 0.1% formic acid) as the mobile phase and with UV detection at 254 nm).

Fmoc-aminohexanoic acid was coupled onto a chloro-2-chlorotrityl functionalised PS resin (giving **5** after Fmoc deprotection) (Figure 52). Six histidines (Fmoc-His(Trt)-OH) were then sequentially coupled to the amino acid sequence end (giving **6**) by standard amidation chemistry followed by coupling of the carboxylic acid functionalised RAFT agent **3** using the same reaction condition to give the hexahistidine tag bearing a RAFT initiating moiety **7**. This was cleaved using a mixture of TFA/water and was purified by reverse-phase column chromatography to give the target RAFT agent **8** in 63% overall yield. The compound was characterised by ^{1}H NMR, ^{13}C NMR (see Chapter 6), HRMS (see Chapter 6) and HPLC (see Figure 52). NMR analyses and high resolution MS demonstrated the successful synthesis of the target compound while HPLC indicated its high purity.

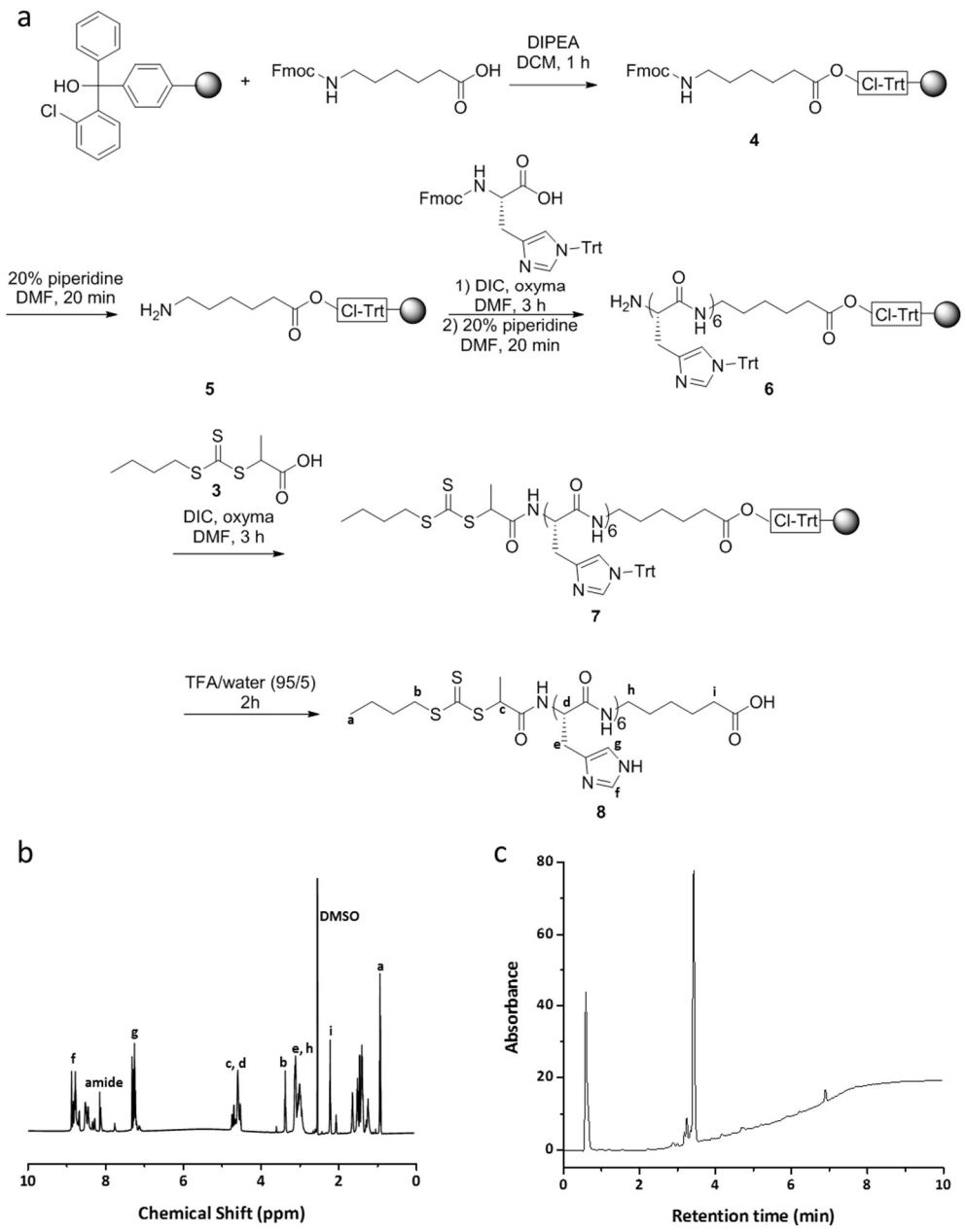

Figure 52. Synthesis of the hexahistidine tagged RAFT agent **8**. (b) ^{1}H NMR of **8** in d_6-DMSO. (c) HPLC trace of **8** with a peak at 3.42 min showing the presence of compound **8**.

4.2.2.2. Norbornene Acrylamide Monomer Synthesis and Characterisation

To introduce reactive centres for the inverse electron-demand Diels–Alder chemistry with the tetrazine quenched fluorophores, a norbornene acrylate monomer **11** was designed and

synthesised that could be incorporated into the polymer scaffolds (see Figure 53). In comparison to methacrylate or methacrylamide, acrylamide monomers typically show higher reactivity and undergo faster polymerisations.[245, 251] Importantly, having a similar chemical structure to DMAA (which provides good water solubility for the resulting polymers),[245, 252] the propagation rate of the norbornene monomer **11** should be similar to DMAA and results in relatively homogeneous copolymers with evenly distributed functional groups.

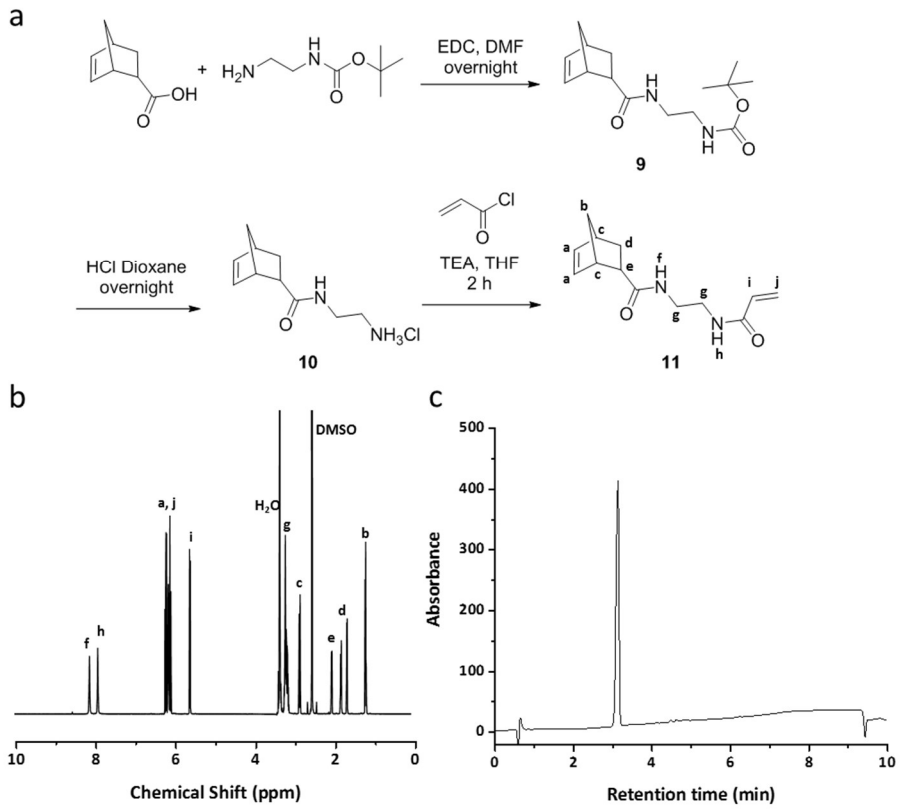

Figure 53. Synthesis of norbornene acrylamide monomer **11**. (b) ^{1}H NMR of **11** in d_6-DMSO. (c) HPLC trace of **1** with a peak at 3.12 min showing the presence of compound **11**.

The norbornene acrylamide monomer **11** was synthesised through a three step route (Figure 53). Specifically, a Boc-protected ethylene diamine was coupled to the *exo*-norbornene carboxylic acid through a standard anhydride-amine amidation coupling followed by Boc deprotection to give the primary amine terminated norbornene **10**. Acryloyl chloride was subsequently coupled onto the primary amine to give the norbornene acrylamide monomer

11 in 19% overall yield. The yield of the last step was only 22%, which was attributed to the competition of two possible reactions where the acid chloride could react with the primary amine to give an amide bond (the desired product), or a 1,4 addition of the primary amine forming a secondary amine as a side product. By silica gel chromatography, the norbornene acrylamide monomer **11** was effectively purified and indicated by ^{1}H NMR and HPLC (see Figure 53). Both the acrylamide double bond protons (at 6.19 ppm, 6.07 ppm and 5.58 ppm) and the norbornene double bond protons (6.12 ppm) were observed via the ^{1}H NMR spectrum. The clear HPLC trace showed only a single peak at 3.13 min demonstrating the high purity of the monomer.

4.2.2.3. Polymer Synthesis and Characterisation

In a standard RAFT polymerisation, three key components were required for the synthesis of a RAFT polymer: the radical initiator, the RAFT agent and the monomer(s).[58, 177] Here, AIBN was used as the thermal initiator (which generates free radicals at 60-90 °C) to initiate the polymerisation. The amount of the radical initiator AIBN was set at 0.1 equivalent to the RAFT agent to insure that all free radical could be deactivated by the RAFT agent to avoid free radical chain propagation. The ratio's used were set at DMAA:**11**:**8**:AIBN = 100:10:1:0.1 to control polymer size and the norbornene density. A solvent mixture of dioxane/water (95:5) (the addition of water accelerates the polymerisation) was used to allow the polymerisation process to be controlled, *i.e.* a high water content causes polymer precipitation and thus less controlled polymerisation.[58, 177] To avoid radical quenching by oxygen, the polymerisation was conducted under argon.

The monomer conversion was monitored by ^{1}H NMR with > 90% of the monomers consumed within 4 h (Figure 54). Uncontrolled chain transfer and termination leads to broad molecular weight distributions and typically happens with high radical-monomer ratios, *i.e.* when most of the monomers were consumed. To minimise this issue, the polymerisation time was set to 4 h (where the active monomers has not been fully consumed) and the polymerisation was quenched by freezing the reaction mixture in liquid nitrogen and thawed in the presence of air to allow the oxygen to quench any active radicals.

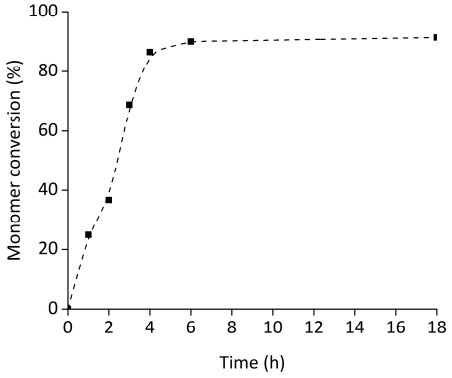

Figure 54. Plot of monomer conversion (for both norbornene acrylamide **11** and DMAA) versus time. Polymerisation was carried out under argon at 70 °C. Aliquots of reaction mixtures were taken every hour, diluted in d_6-DMSO and analysed by ^{1}H NMR. The conversions were quantified by comparing the integration of the monomer and polymer peaks.

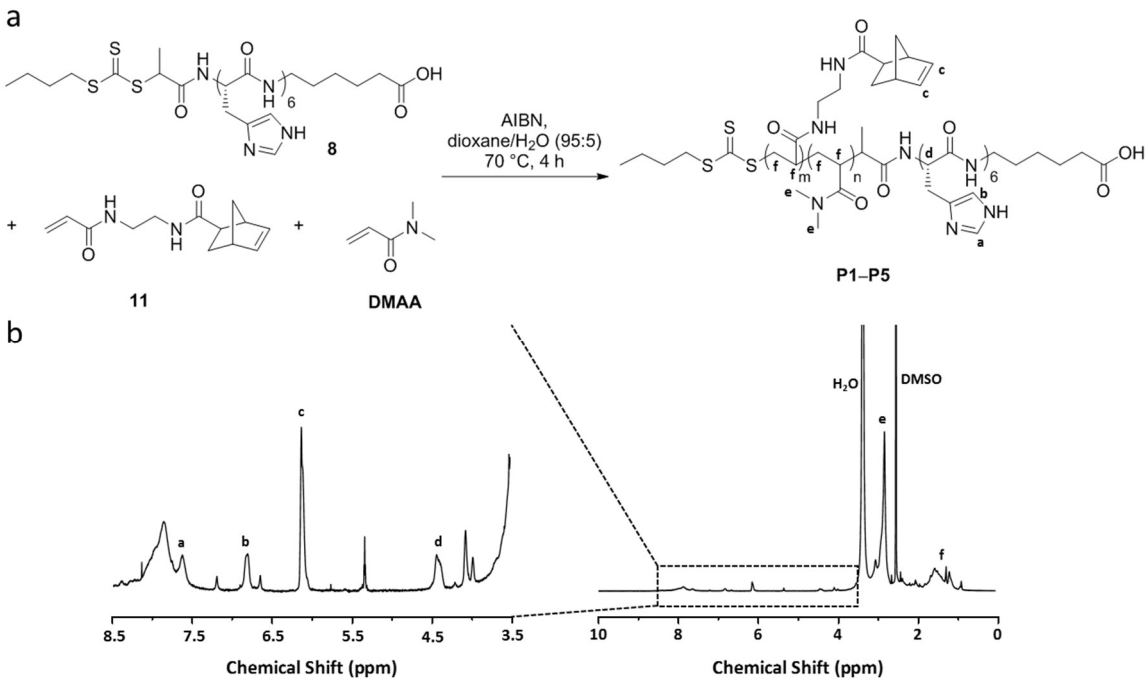

Figure 55. (a) Synthesis of the functional polymers **P1** to **P5**. (b) ^{1}H NMR spectrum of polymer **P1** in d_6-DMSO.

In order to evaluate how the polymer composition affects conjugation efficiency and the activity of the resulting polymer–protein conjugates, five polymers with different molecular

weights (**P1**, **P2** and **P3**) and densities of reactive centres (**P1**, **P4** and **P5**) were synthesised using the optimised polymerisation condition described above (Table 7). Conversions of all polymers were over 89% after 4 h except **P5** (78%), which may be attributed to the bulky norbornene functional group, resulting in less reactive radicals and therefore slower reaction. The molecular weights of the polymers were confirmed by GPC and ^{1}H NMR, which matched well the theoretical values, indicating the well-controlled polymerisation process. This was further confirmed by the narrow dispersity from the GPC traces. The chemical composition, *i.e.* the monomer ratio in the copolymers and the presence of the hexahistidine moiety, were established by ^{1}H NMR (Figure 55). The presence of aromatic resonances at 6.80 ppm and 7.86 ppm confirmed the presence of the histidine moiety and the integration ratios at 6.80/4.41 ppm (RAFT agent), 6.12 ppm (norbornene monomer), 2.58-3.15 ppm (DMAA monomer) and 0.68-1.85 ppm (polymer backbone) indicating the polymer composition.

Table 7. Characterisations of the functional polymers **P1** to **P5**. Synthesis shown in Figure 55. The conversions of monomer mixtures were quantified by ^{1}H NMR by comparing the integration of the monomer peaks and the polymer peaks. Theoretical M_n of polymers were calculated by addition of all molecular weights of the components (RAFT agent and monomers, assuming all converted monomers were in the polymers). M_n of polymers were determined by GPC (DMF), and ^{1}H NMR (by comparing the integration of the representative monomer peaks (in polymers) and the RAFT agent peaks).

Polymer	**8**:**11**:DMAA (Experimental)	**8**:**11**:DMAA (^{1}H NMR)	Conversion [a]	M_n (kDa) (Theoretical)	M_n (kDa) (^{1}H NMR)	M_n (kDa) (GPC)	Đ
P1	1:10:100	1:8.0:101	90%	13	13	14	1.5
P2	1:4.0:40	1:3.3:57	91%	6.1	7.6	7.1	1.2
P3	1:25:250	1:21:240	89%	32	23	30	1.8
P4	1:4.0:100	1:2.8:107	96%	12	12	11	1.4
P5	1:25:100	1:18:89	78%	17	14	16	1.7

[a] Calculated for the monomer mixture.

4.2.2.4. Polymer to protein conjugation

The polymer scaffolds **P1** to **P5** were covalently conjugated to the protein via an active ester coupling reaction with the surface amines, which is efficient and widely used in bioconjugation as discussed above.[165, 170, 171, 174] Specifically, the ω-carboxylic acid in the polymers was firstly activated using EDC and NHS to give the NHS active ester terminated polymers **PA1** to **PA5** that were isolated by precipitation. Activated polymer scaffolds **PA1**, **PA2** and **PA3** (700 µM) were reacted with BSA (140 µM) (as a model protein) in PBS to give the corresponding polymer–BSA conjugates **P1-BSA**, **P2-BSA** and **P3-BSA**, respectively (Figure 56).

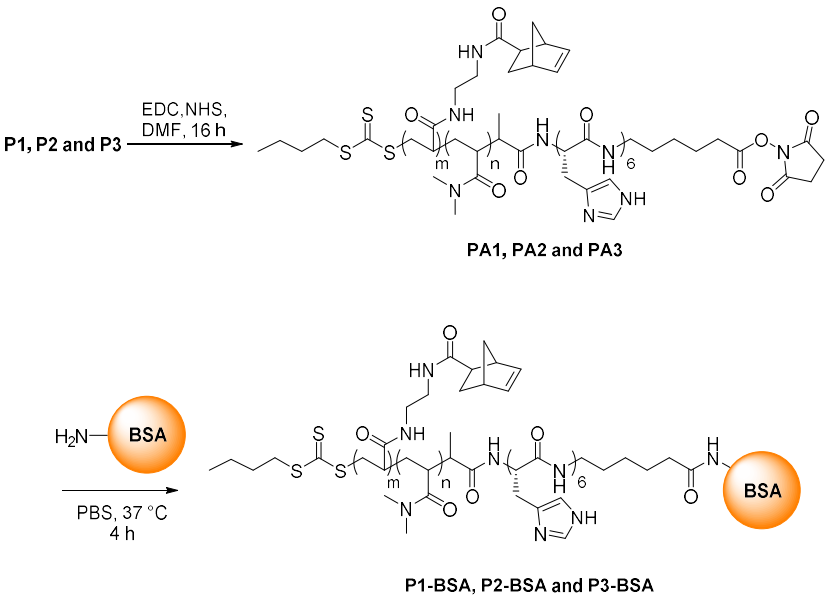

Figure 56. Polymer **P1**, **P2** and **P3** were activated by EDC and NHS and conjugated BSA and purified by dialysis (to remove the excess polymers) to give polymer–BSA conjugates **P1-BSA**, **P2-BSA** and **P3-BSA**.

As described above, the conjugation of two macromolecules often results in low yields and requires the removal of excess of polymer or unreacted protein.[158] The excess of polymer (if small) can be efficiently removed by dialysis benefitted from the molecular weight differences between the polymers and the polymer–protein conjugates, but unreacted proteins cannot be removed by dialysis and thus other purification methods are needed. Immobilised metal-affinity chromatography was used in this study due to its high efficiency,

compatibility with proteins and simple operation (Figure 57). Thus the polymer–protein conjugate was concentrated to 200 µL, shaken with the affinity chromatography resin to allow the polymer–protein conjugates to be loaded onto the resin. The resin was washed and, finally, the polymer–protein conjugates were eluted from the resin using an elution buffer (containing the optimised concentration of imidazole, pH = 8.0, see Figure 58 for optimisation).

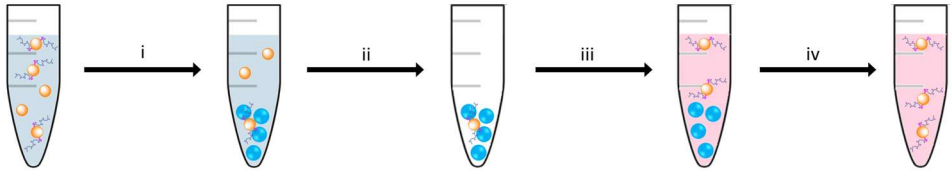

Figure 57. Purification/isolation of the polymer–protein conjugates. i) Conjugated proteins were bound to the Ni(II)-charged immobilised metal-affinity chromatography resin;[242] ii) Unmodified proteins were removed by washing; iii) Polymer–protein conjugates were eluted; iv) polymer–protein conjugates were isolated.

To optimise the elution buffer, **P1-BSA** was loaded onto the resin as described above and eluted using a series of buffers with a 10 mM to 500 mM gradient concentration of imidazole. The samples eluted from the resins were collected by filtration and concentrated followed by sodium dodecyl sulfate-polyacrylamide gel electrophoresis (SDS-PAGE) analysis (Figure 58). The loading showed no obvious polymer–protein conjugates bands from the column flow in the washing step (lane 3). The polymer conjugated BSA began to be competed off by imidazole at a concentration of 100 mM (lane 7) and was completed at an imidazole concentration of 200 mM (lane 8). In order to collect all the proteins from the resin, the concentration of imidazole was chosen as 500 mM as no additional protein bands were observed at such a concentration (lane 9).

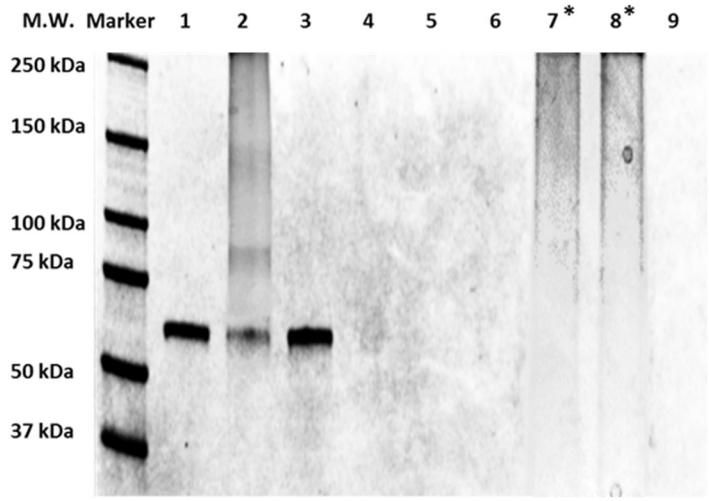

Figure 58. Optimisation of the elution condition for immobilised metal-affinity chromatography. SDS-PAGE of BSA conjugated to polymer **P1** (**P1-BSA**) showing protein eluting from the affinity chromatography resin using different concentrations of imidazole. Markers: Precision Plus Protein™ Kaleidoscope™ Prestained Protein Standards, 10-250 kDa; Lane 1 unmodified BSA; Lane 2 **P1-BSA** before purification; Lane 3 column flow; Lane 4 elution buffer with 10 mM imidazole; Lane 5 elution buffer with 20 mM imidazole; Lane 6 elution buffer with 50 mM imidazole; Lane 7***** elution buffer with 100 mM imidazole ("smear" showed polymer–BSA conjugates); Lane 8***** elution buffer with 200 mM imidazole ("smear" showed polymer–BSA conjugates); Lane 9 elution buffer with 500 mM imidazole. Staining was carried out with Coomassie blue (0.1% *w*/*v* in 1:4:5 acetic acid/water/MeOH for 2 h) and destained using a mixture of 1:7:2 acetic acid/water/MeOH for 24 h. Bright field images of the gel was taken using a Universal Hood II Gel Doc System (Bio-Rad).

The optimised purification approach was applied for the polymer BSA conjugates (**P1-BSA**, **P2-BSA** and **P3-BSA**), which were analysed by SDS-PAGE and GPC with the data shown in Table 8, Figure 59 and Figure 60. As quantified by measuring the absorbance of the protein conjugate solutions at 280 nm, the yield for the conjugation reaction after the purification was 42% for **P1-BSA** and 52% for **P2-BSA**. However, the conjugation of **P3** to BSA gave only a 15% yield, which may be attributed to the poor reactivity of the coupling reaction due to the steric hindrance of the longer polymer chain.[158] The power of the hexahistidine tags enabled efficient removal of unreacted protein fractions from the mixture, which was confirmed by electrophoresis. Comparing lane 2 to lane 3, and lane 4 to lane 5, and lane 6 to lane 7 (Figure 59), unmodified protein was not visible after the purification. This was further confirmed by water phase GPC with the native BSA bands not visible in the GPC trace (Figure 60, top). The obvious broad weight distributions of the polymer–protein conjugates are due to both the

inherent polydispersity of the polymer scaffold and the various degrees of substitution of the protein, which is common for such synthetic polymer–protein conjugates.[166, 174]

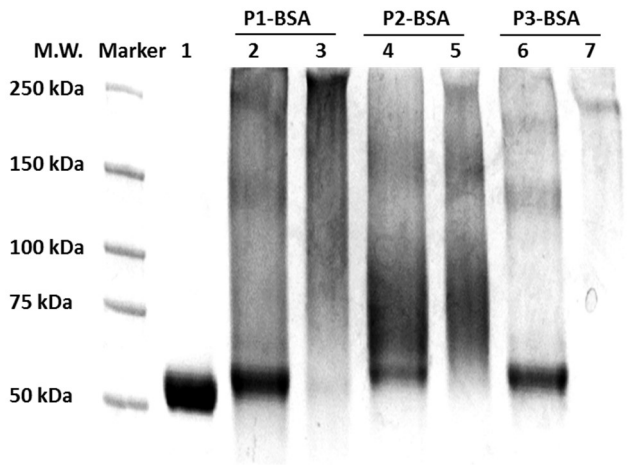

Figure 59. SDS-PAGE of polymers conjugated to BSA before and after metal-affinity chromatography based-purification. Markers: Precision Plus Protein™ Kaleidoscope™ Prestained Protein Standards, 10-250 kDa; Lane 1 BSA; Lane 2 **P1-BSA** (before purification); Lane 3 **P1-BSA** (after purification); Lane 4 **P2-BSA** (before purification); Lane 5 **P2-BSA** (after purification); Lane 6 **P3-BSA** (before purification); Lane 7: **P3-BSA** (after purification) (the faint "smear" is due to low yield of the conjugation). Staining was carried out with Coomassie blue (0.1% *w*/*v* in 1:4:5 acetic acid/water/MeOH for 2 h) and destained using a mixture of 1:7:2 acetic acid/water/MeOH for 24 h. Bright field image of the gel was taken using a Universal Hood II Gel Doc System.

Table 8. Synthesised polymer–protein conjugates.

Conjugate	Protein	Polymer	Yield[a]
P1-BSA	BSA	**P1**	42%
P2-BSA	BSA	**P2**	52%
P3-BSA	BSA	**P3**	15%

[a] Yield quantified by UV spectroscopy at λ = 280 nm

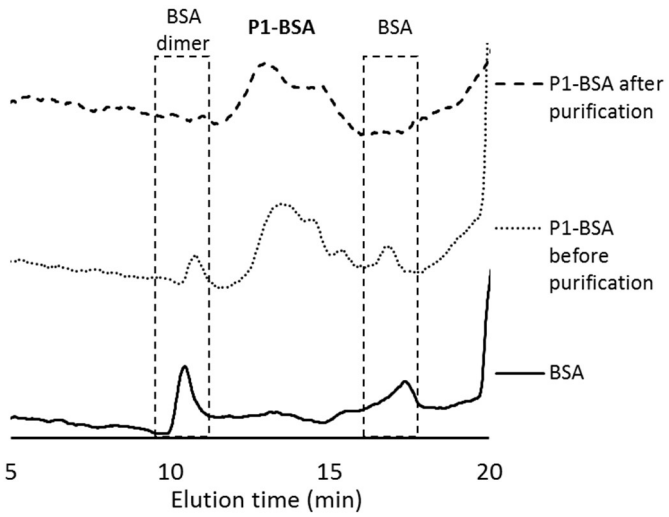

Figure 60. GPC traces of unmodified **BSA** (lower trace), **P1-BSA** before purification (middle trace) and **P1-BSA** after purification (top trace). The GPC was run using H_2O as an eluent at 40 °C at 1 mL/min with an RI detector.

4.2.2.5. Synthesis of Polymer–Antibody Conjugates

Herceptin (Her) is an antibody developed for the treatment of breast cancers, which selectively binds to and facilitate degradation of the tyrosine kinase receptor HER2 (overexpressed in some breast cancers) and causes cancer cell death. The conjugation methodology (Figure 56) was applied to Herceptin to give polymer–antibody conjugates **P1-Her** to **P5-Her** (Figure 61a) and the same purification strategy (Figure 57) was applied to remove the unconjugated antibody, and the purified antibody conjugates were analysed by SDS-PAGE (Figure 61b). In a similar manner to the polymer–BSA conjugates, the Herceptin conjugates showed additional high molecular weight bands by SDS-PAGE with widely dispersed bands implying uneven substitution. The light chain fragments, which are essential for antibody activity, were still clearly present, suggesting that the amidation coupling reaction mainly happened on the heavy chains, minimising the influence on the antibody binding affinity.

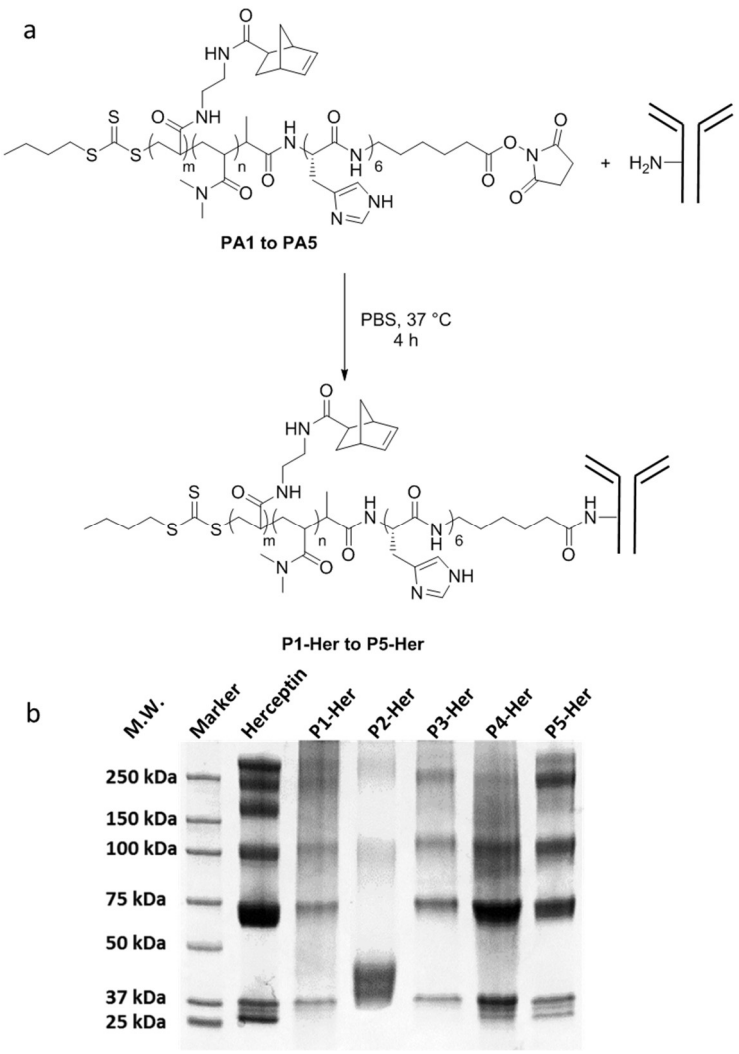

Figure 61. (a) Synthesis of polymer–antibody conjugates. Activated polymers **PA1** to **PA5** (685 µM) were treated with Herceptin (137 µM) in PBS at 37 °C for 4 h and purified by dialysis and affinity chromatography to give the purified polymer–antibody conjugates **P1-Her** to **P5-Her**. (b) SDS-PAGE of purified polymer–antibody conjugates and the native antibody. Marker: Precision Plus Protein™ Kaleidoscope™ Prestained Protein Standards, 10-250 kDa. Staining was carried out with Coomassie blue (0.1% *w*/v in 1:4:5 acetic acid/water/MeOH for 2 h) and destained using a mixture of 1:7:2 acetic acid/water/MeOH for 24 h. The bright field image of the gel was taken using a Universal Hood II Gel Doc System.

The conjugation yields were quantified by UV-*vis* spectroscopy and are given in Table 9. In comparison to BSA (M_n = 67 kDa with roughly 20 lysine residuals), Herceptin has a larger molecular weight (146 kDa) and more lysine moieties (approximately 90).[253, 254] For the smaller polymer **P2** (7 kDa), the conjugation yields for the antibody were similar to BSA (45% and 52%, respectively). As described above, the large polymer **P3** (30 kDa) was not efficiently

conjugated to BSA (15% yield). However, when Herceptin was used, the coupling efficiency was greatly improved (88% yield), which may be attributed to the higher number of accessible lysines on the antibody surfaces. When polymers with similar molecular size (**P1**, 14 kDa and **P4**, 11 kDa) were used for the antibody conjugation, similar yields were obtained (72% and 73%, respectively), although conjugation of **P5** (16 kDa) gave decreased yields (56%), which may due to the higher steric hindrance and the hydrophobicity of the polymer due to increased norbornene density.

Table 9. Details of the synthesised polymer–antibody conjugates.

Conjugate	Protein	Polymer	Yield[a]
P1-Her	Herceptin	**P1**	72%
P2-Her	Herceptin	**P2**	45%
P3-Her	Herceptin	**P3**	88%
P4-Her	Herceptin	**P4**	73%
P5-Her	Herceptin	**P5**	56%

[a] Yield quantified by UV spectroscopy at λ = 280 nm. The yield was calculated by comparing the amount of the polymer–protein conjugate to the protein used for conjugation.

4.2.3. "Switch on" of Tetrazine Quenched Fluorophore (with A. Gambardella)

To simultaneously "turn on" and amplify a fluorescent signal using the polymer–protein conjugates, the tetrazine quenched BODIPY fluorophore **Tz1** was synthesised.[238] The reactivity of the tetrazine ligation towards norbornene was evaluated by monitoring the time-dependent fluorescence increase (over 0.5, 1 and 2 h) of the reaction mixture. (Figure 62 and 63).

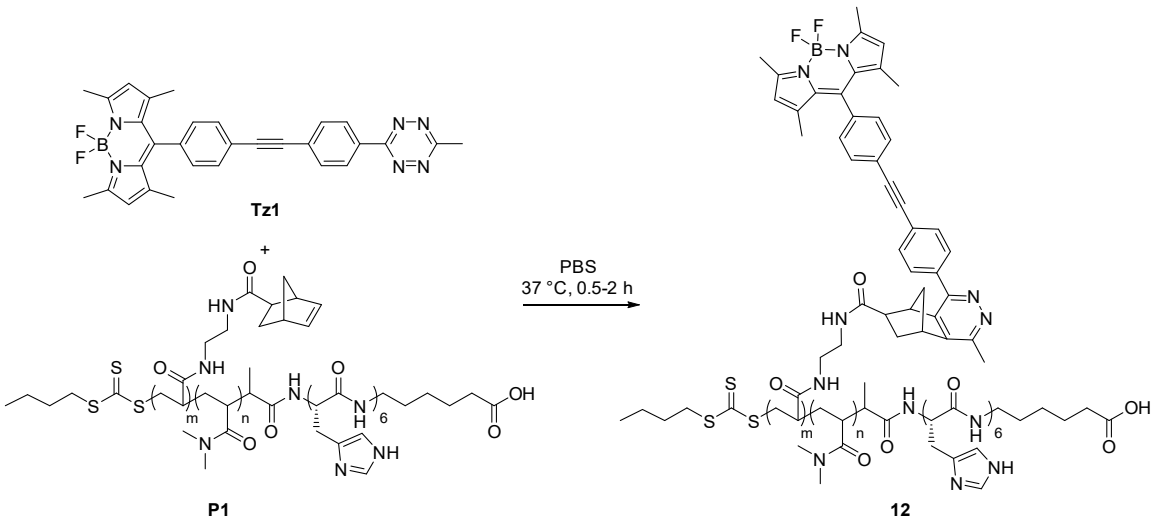

Figure 62. "Switch on" of the tetrazine quenched fluorophore **Tz1** ($\lambda_{ex/em}$ = 488/512 nm) by reacting with norbornene decorated polymer **P1**. **P1** and **Tz1** were dissolved in PBS and incubated at 37 °C for 0.5, 1 or 2 h and analysed on a fluorescence spectrometer.

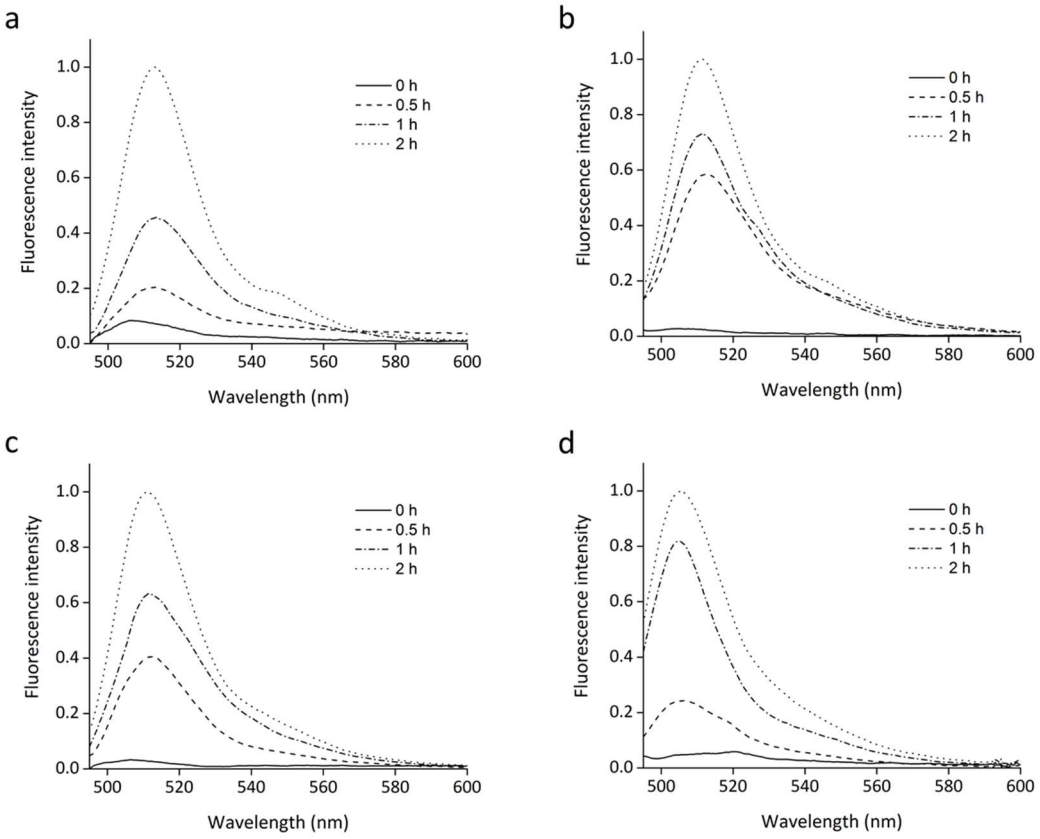

Figure 63. Fluorescence spectra of **Tz1** (a) 0.5 µM, (b) 1 µM, (c) 2 µM and (d) 5 µM incubated with polymer **P1** (12 µM) at 0, 0.5, 1 and 2 h. Fluorescence measurements were carried out on a FluoroMax-3 fluorimeter (λ_{ex} = 488 nm) using a quartz cuvette. Fluorescence intensities were normalised to the intensity after 2 h.

The reactions of norbornene bearing polymer **P1** (with an average of 8 norbornenes per polymer chain, 12 µM) with four concentrations (0.5, 1, 2, 5 µM) of the tetrazine BODIPY **Tz1** were evaluated by fluorescence spectrometry. The fluorescence intensity increased over time over the first two hours with the reaction rate increasing with higher concentration of **Tz1** (Figure 63) and the fold increases of fluorescence intensities of **Tz1** (compared to the fluorescence intensity of **Tz1** at 0 h) were calculated (see Table 10). For application in biological systems, both a fast reaction rate and high signal to noise ratio are required.

Table 10. Fold increase of fluorescence intensity of **Tz1** over time. **Tz1** (0.5-5 µM) was incubated with polymer **P1** (12 µM) for 0.5, 1 and 2 h and the fluorescence recorded. The fluorescence intensities were monitored at $\lambda_{ex/em}$ = 488/511 nm and compared to the intensity before incubation (t_0) to calculate the fold increase.

Tz1 concentration	**Incubation time**		
	0.5 h	1 h	2 h
0.5 µM	3	6	13
1 µM	24	30	41
2 µM	15	23	36
5 µM	4	12	16

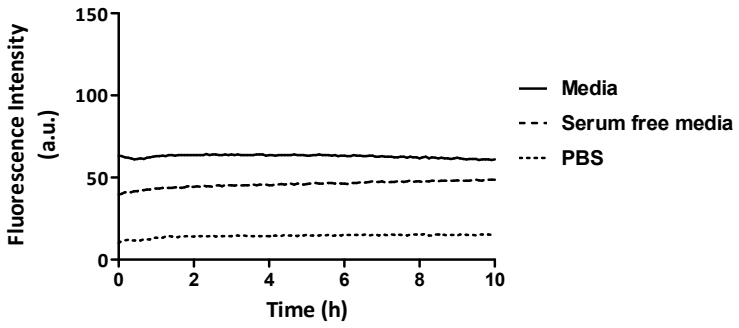

Figure 64. Stability studies of **Tz1** in PBS, serum-free media, cell culture media (10% FBS, *v*/*v*) conducted in a black 96-well plate with 1 µM solutions of **Tz1**. The fluorescence intensities monitored using a multimode plate reader (λ_{ex}=465-505 nm, λ_{em}=508-548 nm), with readings taken every 5 min at 37 °C.

In order to investigate the stability of the tetrazine quenched fluorophore under biologically relevant conditions, the fluorescence intensities of **Tz1** were monitored over time in PBS, cell culture media (containing 10% *v*/*v* serum) and serum free media (Figure 64). Only negligible increases in fluorescence were observed during 10 h incubation indicating the stability of **Tz1**. This is important as many tetrazines are not stable under such conditions.

The fluorescence dequenching of **Tz1** was evaluated on the model polymer–protein conjugate **P1-BSA** (Figure 65). **P1-BSA** (2.5 µM) was treated with excess amount of **Tz1** (25 µM) for 4 h and analysed by SDS-PAGE (Figure 65b) to demonstrate the compatibility and selectivity of the polymer–protein conjugates. Clear fluorescence was observed in lane 4 (**P1-BSA** treated with **Tz1**) while no fluorescence was seen in lane 2 (where native BSA was treated with **Tz1** at the same conditions as the control). This indicated the selectivity of the tetrazine quenched fluorophore between the polymer labelled BSA and the corresponding unmodified variant.

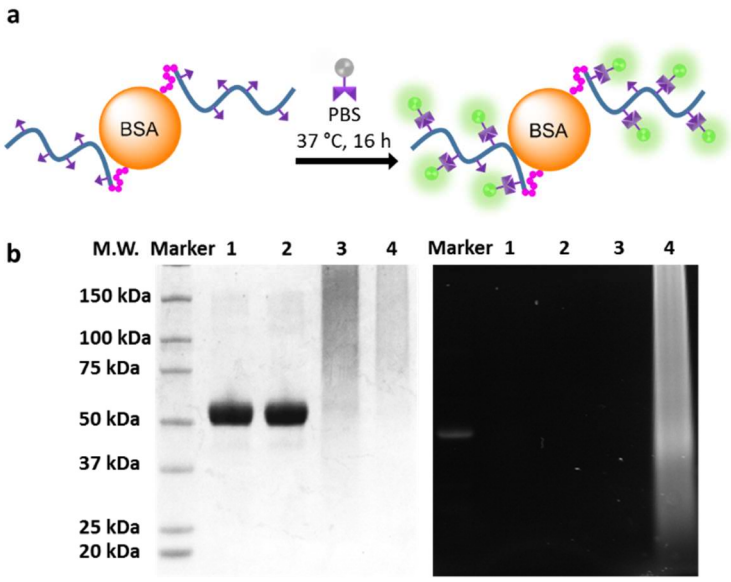

Figure 65. (a) Fluorescence of the polymer conjugated BSA with **Tz1** giving **BODIPY-P1-BSA**; (b) SDS-PAGE of the resulting fluorescent BSA conjugate **BODIPY-P1-BSA**. MW Markers: Precision Plus Protein™ Kaleidoscope™ Prestained Protein Standards, 10-250 kDa; Lane 1 BSA; Lane 2 BSA (2.5 µM) incubated with **Tz1** (25 µM); Lane 3 **P1-BSA;** Lane 4 **P1-BSA** (2.5 µM) incubated with **Tz1** (25 µM)**.** Staining was carried out with Coomassie blue (0.1% *w*/*v* in 1:4:5 acetic acid/water/MeOH for 2 h). Staining was carried out with Coomassie blue (0.1% *w*/v in 1:4:5 acetic acid/water/MeOH for 2 h) and destained using a mixture of 1:7:2 acetic acid/water/MeOH for 24 h. Bright field and fluorescent images (λ_{ex} = 365 nm, λ_{em} = 520 ± 30 nm) of gels were taken using a Universal Hood II Gel Doc System.

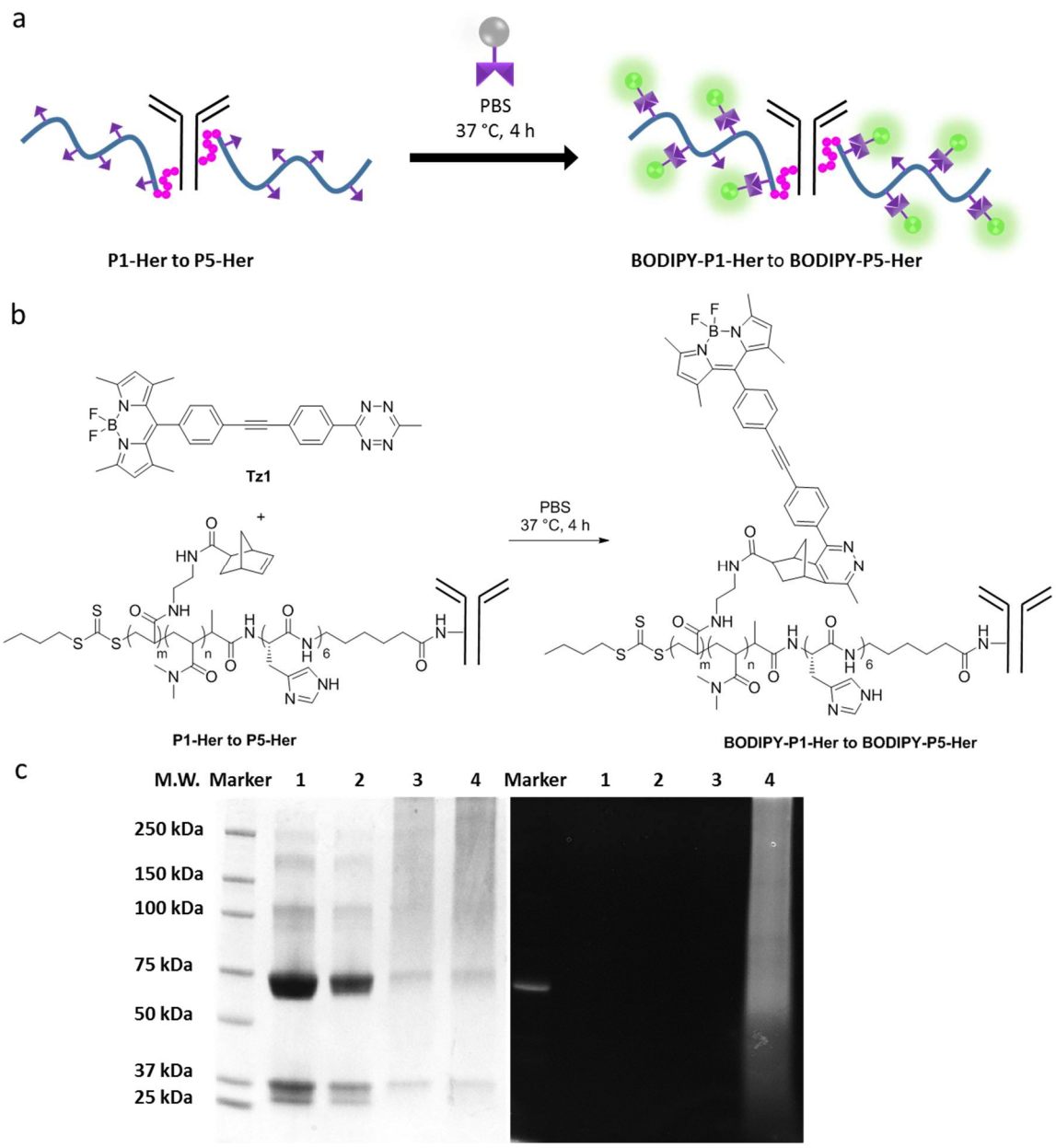

Figure 66. (a) and (b) Fluorescence of the polymer conjugated Herceptin treated with **Tz1** giving **BODIPY-P1-Her** to **BODIPY-P5-Her**. The tetrazine quenched BODIPY **Tz1** was incubated with norbornene bearing polymer antibody conjugates **P1-Her** to **P5-Her** in PBS (pH = 7.4) at 37 °C for 4 h and purified by dialysis to give **BODIPY-P1-Her** to **BODIPY-P5-Her**. (c) SDS-PAGE of the resulting fluorescent Herceptin conjugate **BODIPY-P1-Her**. MW Markers: Precision Plus Protein™ Kaleidoscope™ Prestained Protein Standards, 10-250 kDa; Lane 1 Herceptin; Lane 2 Herceptin (2.5 µM) incubated with **Tz1** (25 µM); Lane 3 **P1-Her;** Lane 4 **P1-Her** (2.5 µM) incubated with **Tz1** (25 µM)**.** Staining was carried out with Coomassie blue (0.1% *w*/v in 1:4:5 acetic acid/water/MeOH for 2 h) and destained using a mixture of 1:7:2 acetic acid/water/MeOH for 24 h. Bright field and fluorescent images (λ_{ex} = 365 nm, λ_{em} = 520 ± 30 nm) of gels were taken using a Universal Hood II Gel Doc System.

The same *in situ* dequenching strategy was applied to the antibody conjugate **P1-Her** to investigate the reactivity and selectivity of **Tz1** to the antibody conjugate (Figure 66). Similar to the BSA conjugates, a clear but broad fluorescent smear was observed on the gel for the polymer–antibody conjugate treated with **Tz1** (lane 4, Figure 66c). No non-specific binding of the fluorophores to the native antibody was observed (Figure 66c).

4.2.4. Polymer Conjugation Affects the Antibody Binding Rate but not Affinity (with Dr M. Ucuncu)

As described previously, the clinically used antibody Herceptin selectively binds to tyrosine kinase receptor HER2 and was used here as the targeting moiety for the polymer based fluorescent probes. The HER2 receptor positive cancer cell line SK-BR-3 was selected and used for immunological studies, while a HER2 receptor negative cancer cell line MCF-7 was used as a negative control.

To investigate the binding kinetics of antibody to HER2 receptors and optimise the incubation conditions, *e.g*. antibody concentration and incubation time, an NHS functionalised BODIPY fluorophore **12**^{255} was coupled to the antibody Herceptin to give a fluorescently labelled antibody **BODIPY-Her** (see Figure 67) and this enabled analysis of binding rates by flow cytometry. The concentration of antibody was optimised by analysing the fluorescence intensity change of cell populations with increasing concentrations of the fluorescent antibody **BODIPY-Her**. In comparison to untreated cells, a fluorescence increase was observed with different concentrations of the **BODIPY-Her** with 1.7, 3.2 and 3.2 fold increases for 1, 10 and 50 nM, respectively. There were no significant differences in fluorescence intensity when 10 nM and 50 nM of **BODIPY-Her** was used, indicating saturation of the HER2 receptors.

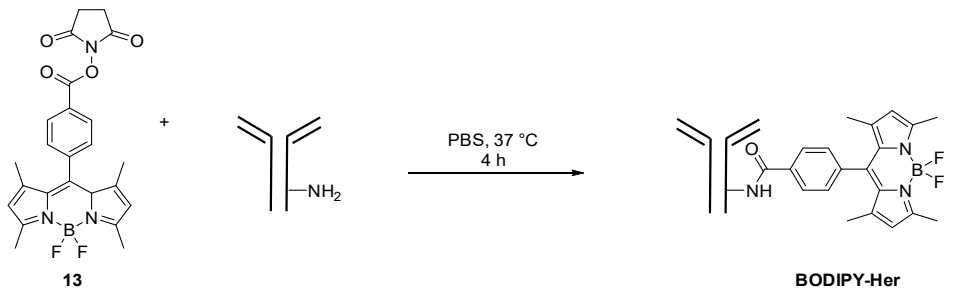

Figure 67. Synthesis of the fluorescently labelled antibody **BODIPY-Her**. Herceptin (137 µM) was treated with the active ester functionalised BODIPY **13** (1.4 mM) at 37 °C for 4 h in PBS (pH = 7.4) and purified by dialysis.

The optimal incubation time was evaluated using a similar strategy, with the fluorescently labelled antibody **BODIPY-Her** (10 nM) incubated with SK-BR-3 cells for 0.5, 1, 2, 4 and 6 h before analysis by flow cytometry. The fluorescence intensities were normalised to the fluorescence saturated cells (after 6 h incubation) and shown in Figure 68. The fluorescence was saturated within 2 h with a $t_{1/2}$ of 18 min.

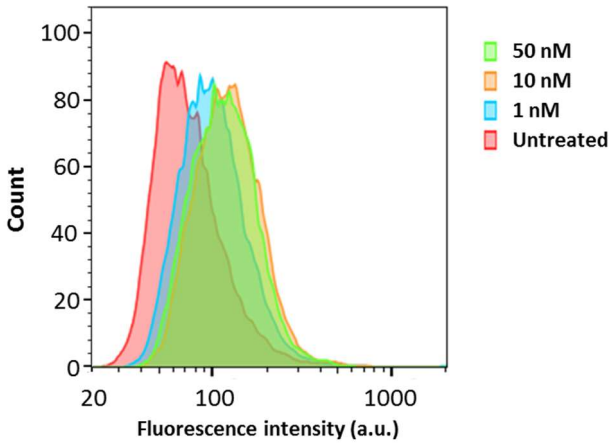

Figure 68. Flow cytometry histograms of antibody concentration optimisation on SK-BR-3 cells. Cells were treated with **BODIPY-Her** at various concentrations: 1 nM (blue), 10 nM (orange) and 50 nM (green), with untreated cells (red) used as a control.

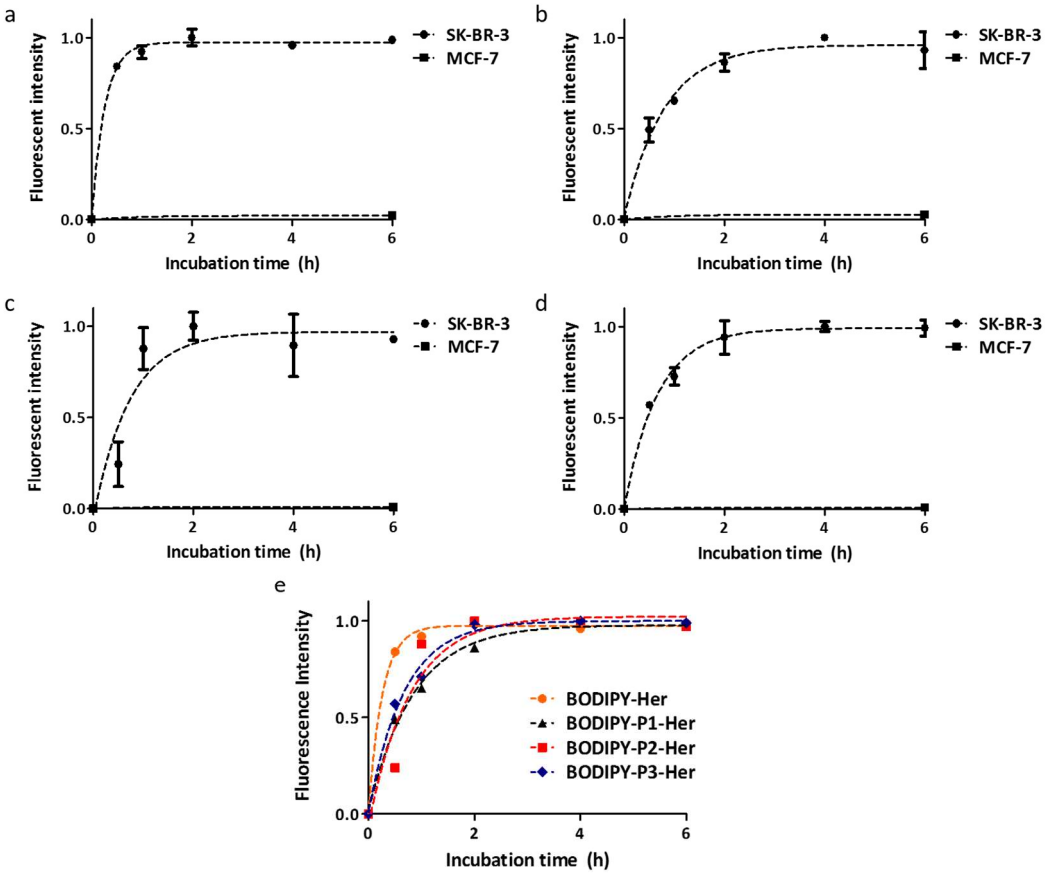

Figure 69. Kinetics of binding of antibody conjugates (a) **BODIPY-Her**; (b) **P1-Her**; (c) **P2-Her** and (d) **P3-Her** to the HER2 expressing cell line SK-BR-3 and the non-HER2 expressing cell line MCF-7 (quantified by flow cytometry with an antibody concentrations of 10 nM, $\lambda_{ex/em}$ = 488/525 nm). (e) Comparison of binding affinities. Fluorescence intensity normalised to the intensity of fluorescence saturated cells (6 h incubation), n = 3.

To investigate how chemical modification of antibodies with different molecular weight polymers affected the antibody binding affinity, the kinetics of the polymer–antibody conjugates **P1-Her**, **P2-Her** and **P3-Her** binding to the HER2 receptor was evaluated. The tetrazine BODIPY fluorophore **Tz1** was used to pre-label the polymer–antibody conjugates *in vitro* (see Figure 66) to enable fluorescent analysis by flow cytometry (Figure 69). As the molecular weight of the polymers increases (**P2**, 7 kDa, **P1**, 14 kDa and **P3**, 30 kDa), the binding rates of the antibody conjugates decreased (**BODIPY-P2-Her** $t_{1/2}$ = 38 min, **BODIPY-P1-Her** $t_{1/2}$ = 44 min, and **BODIPY-P3-Her** $t_{1/2}$ = 52 min). Although the polymer conjugation induced a small delay in fluorescence saturation time, receptor saturation with all polymer–antibody conjugates took place within 4 h, while the saturation time of the small

molecule labelled antibody **BODIPY-Her** was approximately 2 h. As a result, the incubation time of the polymer–antibody conjugates was set at 4 h. For the HER2 receptor negative cells MCF-7, no significant fluorescence increase in cell populations were observed when treated under the same conditions (6 h) (Figure 69), indicating the specificity of the antibody conjugate based fluorescent probes.

4.2.5. Cytotoxicity of the Antibody Conjugates and the Tetrazine BODIPY Fluorophore

Before moving onto the next step of applying the polymer–antibody conjugates to cells, the biocompatibility of these materials was evaluated utilising an MTT assay (Figure 70). For the native antibody Herceptin, the viability of cells were over 90% at concentrations lower than 20 nM, but dropped to 81% at 50 nM (Figure 70a), in agreement with the literature.[256] The chemically modified antibodies (**P1-Her** to **P5-Her** and **BODIPY-Her**, 1-50 nM) showed high viability (>90%) at all tested concentrations (0.5-50 nM, Figure 70), indicating that modification of the antibody may slightly affect the degradation rate or the degradation mechanism of the HER2 receptor.[257] SK-BR-3 cells treated with **Tz1** showed over 90% viability up to 2 μM.

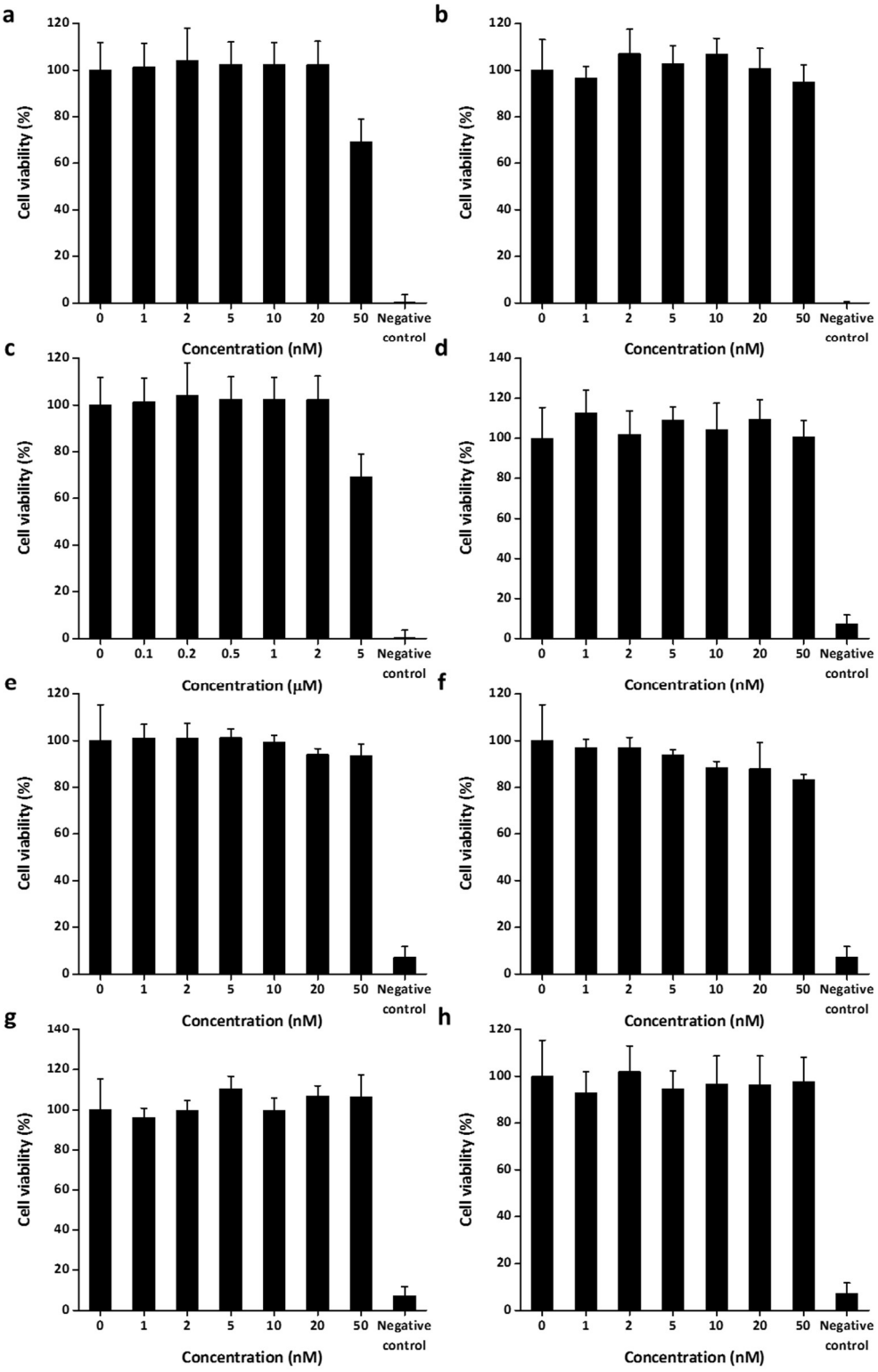

Figure 70. SK-BR-3 cell viability against: (a) **Herceptin**; (b) **BODIPY-Her**, (c) **Tz1** and (d) to (h) **P1-Her** to **P5-Her**. The viabilities were measured using a standard MTT assay (4 h incubation with diphenyltetrazolium bromide) with cells incubated with the compounds for 24 h, n = 3. As a negative control, cells were treated with 50% DMSO in DMEM).

Considering the reactivity of the tetrazine with norbornene and the cytotoxicity of **Tz1**, the concentrations of polymer–antibody conjugates **P1-Her** to **P5-Her** and **Tz1** were set at 10 nM and 1 µM, respectively, for cell based experiments.

4.2.6. *In Cellulo* Fluorescence Switch on and Amplification

To demonstrate fluorescence "switch-on" and amplification, HER2 receptor positive SK-BR-3 cells were treated with the polymer–antibody conjugates **P1-Her** to **P5-Her** (10 nM) for 4 h followed by addition of the tetrazine quenched BODIPY fluorophore **Tz1** (1 µM) for 30 min, and the cells analysed by fluorescent microscopy and flow cytometry (Figure 71 and 72). As controls, SK-BR-3 cells were treated with ether the antibody conjugates or the quenched fluorophore individually, which all gave negligible fluorescence. In comparison to the cells treated with small molecule fluorophore labelled antibody **BODIPY-Her** (10 nM), remarkable fluorescence intensity increases were observed (see Figure 72). The fold increase in the fluorescence intensities (compared to **BODIPY-Her** treated cells as the control) were quantified by flow cytometry (Table 11), which showed fluorescence increases greater than 80-fold for **P3-Her** and **P5-Her**.

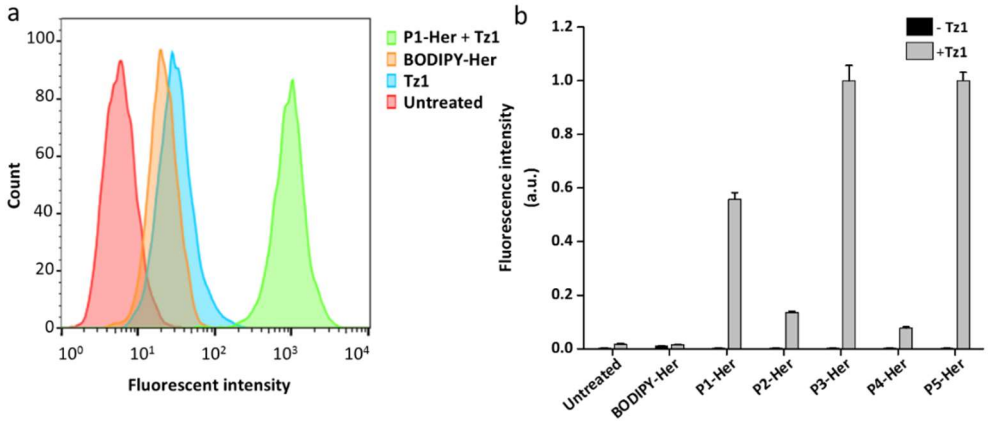

Figure 71. Flow cytometry histograms of SK-BR-3 cells treated with the BODIPY labelled Herceptin (**BODIPY-Her**, 10 nM orange), **Tz1** (1 µM, blue), and the polymer–antibody conjugates (**P1-Her**, 10nM) followed by **Tz1** (1 µM, green), (untreated control cells are shown in red) and the data plotted as fluorescence intensity normalised to the highest intensity (cells treated with **P3-Her** (10 nM) followed by **Tz1** (1 µM)), $\lambda_{ex/em}$ = 488/525 nm);

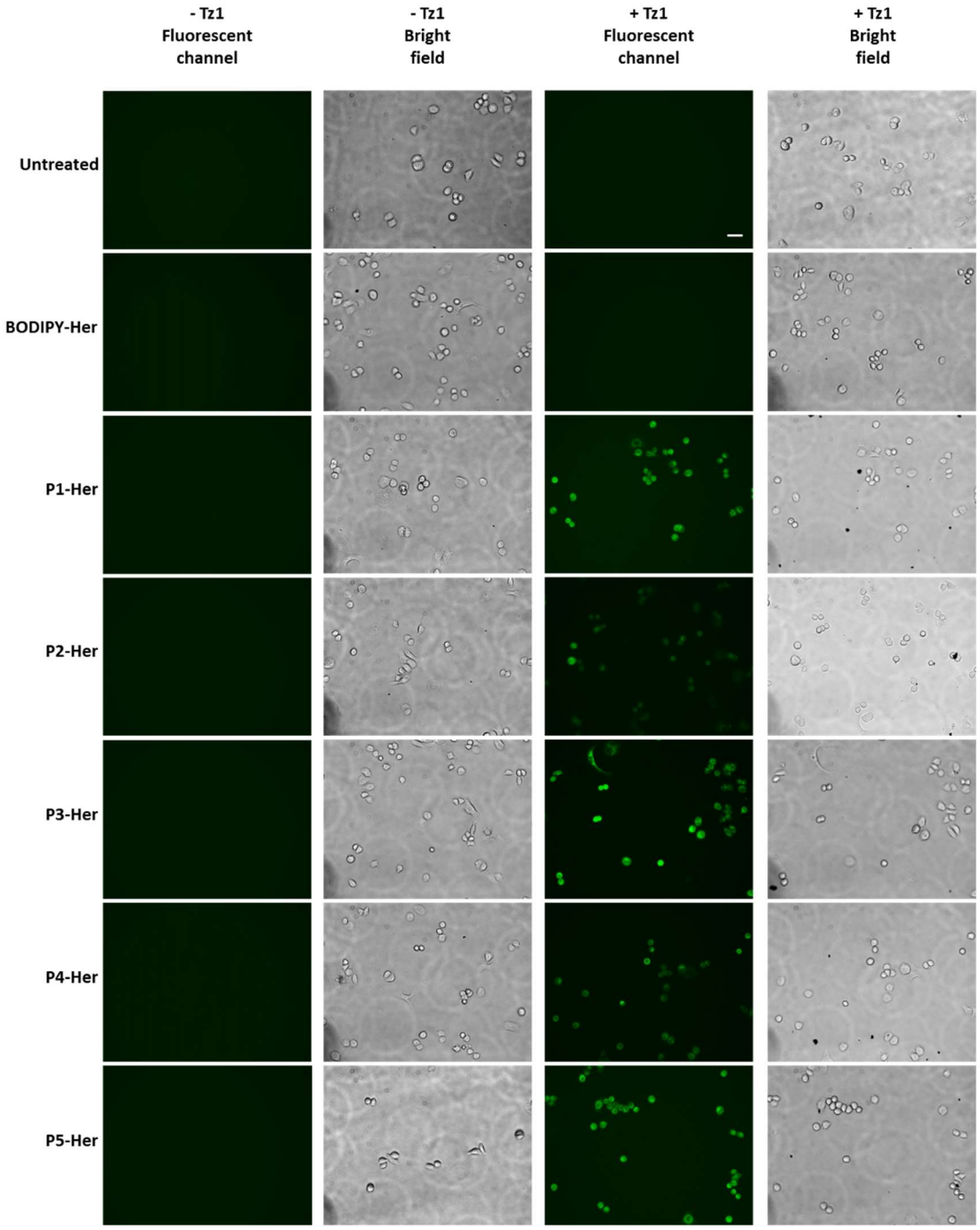

Figure 72. Fluorescent and bright field images taken using a Zeiss AxioVert 200M fluorescence Microscope (λ_{ex}=447-494 nm, λ_{em}=500-554 nm). Cells were treated with or without **BODIPY-Her** (10 nM) or the polymer–antibody conjugates (10 nM) for 4h followed by addition of the quenched tetrazine fluorophore **Tz1** (30 min at 1 µM) (scale bar: 50 µm).

The fluorescence intensity could be tuned by ether changing the length of the polymer scaffold (**P1-Her**, **P2-Her** and **P3-Her**) or changing the functional group densities (**P1-Her**, **P4-Her** and **P5-Her**) (see Table 11). Confocal microscopy analysis showed antibody conjugates both in the cytoplasm and on the plasma membranes (Figure 73), in agreement with the localisation of the small molecule labelled antibody **BODIPY-Her**. Different degrees of fluorescent increases were observed when using polymer–antibody conjugates with different number of reactive centres (see different brightness of BODIPY channel in Figure 73).

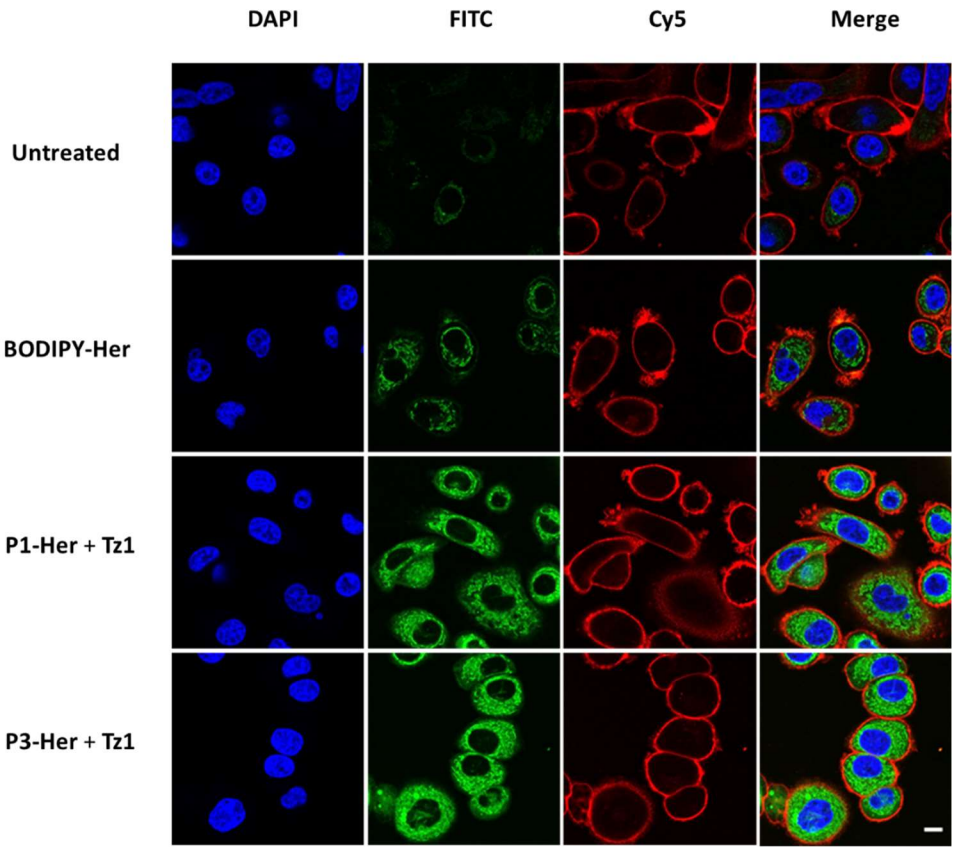

Figure 73. Confocal fluorescence microscopy images of SK-BR-3 cells treated with BODIPY labelled Herceptin (**BODIPY-Her**, 10 nM), polymer-antibody conjugates (**P1-Her** and **P3-Her**, 10 nM) followed by **Tz1** (1 μM) and untreated cells as a control. Cell nuclei were stained with Hoechst 33342 (blue, $\lambda_{ex/em}$ = 353/483 nm), and the plasma membrane stained with CellMask^{TM} Deep Red (red, $\lambda_{ex/em}$ = 649/666 nm), **Tz1** (green, $\lambda_{ex/em}$ = 488/512 nm). Scale bar = 10 μm.

Table 11. Properties of the polymers and the fold increase in fluorescence intensity of SK-BR-3 cells treated with the polymer–antibody conjugates **P1-Her** to **P5-Her** (10 nM) and subsequent addition of **Tz1** (1 μM) in comparison to **BODIPY-Her** treated cells.

polymer–antibody conjugates	P1-Her	P2-Her	P3-Her	P4-Her	P5-Her
Polymer M_n (kDa)	14	7.1	30	11	16
DMAA:**7** (molar ratio in polymers)	100:8	100:6	100:9	100:3	100:20
Fold increase of fluorescence intensity	47	11	84	7	84

4.3. Conclusions and Outlook

With the development of modern medical science, various therapeutic technologies have been developed for treating cancers, where surgery remains the most efficient therapy. Fluorescent imaging techniques have been developed for cancer diagnostics and for image guided surgery, but these techniques would benefit from amplification technologies to visualise tumours with high resolution and signal to background ratios. Here, a polymer–antibody conjugate based fluorescent probe was developed and applied for cancer cell imaging. The polymer scaffolds bearing a norbornene reactive centre and a hexahistidine tag purification handle were synthesised through RAFT polymerisation and covalently conjugated to a clinically used antibody to give the fluorescent probe. With easy purification by affinity column chromatography, the polymer–antibody conjugates with different molecular weights and reactive centre densities were obtained in high quality. A tetrazine quenched fluorophore was applied for *in situ* "switch on" and amplification of fluorescent signals by undergoing an inverse electron-demand Diels–Alder reaction with norbornene moieties on the polymer–antibody conjugates. When applied in cell imaging, the fluorescence was dequenched *in situ* and amplified with up to an 80-fold increase in comparison to a traditional fluorophore labelled antibody. Such improvement may contribute to the improvement of fluorescence-guided surgery of cancers and other biomedical applications.

The application of such polymer scaffold antibody conjugates is not limited to fluorescent signal amplifications, but can be applied for loading cargo in other biological systems. For example, MRI agents or heavy metals cores could be loaded onto the antibody conjugates to amplify signals for MRI or radiation-therapy; while cleavable drug molecules could be loaded to the antibody conjugates to enable drug release. In addition, the reactive centres are not limited to norbornene, but could be other reactive groups that fulfil the bioorthogonality such as strained alkynes, azides and aminooxy groups. The terminal trithiocarbonate could be incorporated into a peptide, another polymer chain, an additional targeting moiety or a fluorophore to track the probe.

Although highly efficient and selective, this antibody based fluorescent amplification method still has some shortcomings. The polymer–antibody conjugation was based on an active ester-amine coupling reaction using the lysine residues (and the N terminus amine), thus the degree of substitution will be variable while the substitution may change the hydrophobicity of the proteins. As previously indicated, genetic incorporation of orthogonal reactive centres into protein structures has been reported[258] and may overcome such shortcomings but the substitution position will need to be optimised for both the reactivity and the protein activity. The BODIPY dye used here was a "green fluorophore" ($\lambda_{ex/em}$ = 488/512 nm), which may not be ideal for biological applications especially for *in vivo* studies due to the strong autofluorescence of tissues. A red or near infrared fluorophore might provide even higher signal to noise ratios and may also improve the penetration depth.

Chapter 5. Experimental

5.1. General Information

Anhydrous solvents were purchased from Sigma Aldrich and used under a N_2 atm using Schlenk techniques. Culture-Insert 2 Well µ-Dishes were obtained from Ibidi. Hoechst 33342, CellMask™ Deep Red plasma membrane stain, Alexa Fluor™ phalloidin (488), RIPA cell lysis buffer, and Dynabeads™ MyOne™ Streptavidin T1 were purchased from Thermo Fisher Scientific. Acryloxyethyl thiocarbamoyl rhodamine B was purchased from Polysciences Inc. All other chemicals were purchased from Acros Organics, Alfa Aesar, Fisher Scientific or Sigma Aldrich and used without further purification, unless otherwise indicated. A Blak-Ray B-100 UV lamp was used as the light source and had a measured intensity of 5 mW cm^{-2}. 2-Chlorotrityl polystyrene resin was purchased from GL Biochem (Shanghai) Ltd. 4-20% Mini-PROTEAN TGX precast protein gels, 2 × Laemmli Sample Buffer, and Ni-charged Profinity™ IMAC Resin were purchased from Bio-Rad. Dialysis membrane (molecular weight cut off 7000 Da) was purchased from Medicell Membranes Ltd. Reverse phase chromatography was carried out on an Isolera™ Spektra One system (Biotage) equipped with a Biotage® SNAP Ultra C18 column. SDS-PAGE was performed using a Bio-Rad Laboratories Mini-Protean® 3 Cell System (Bio-Rad).

^{1}H and ^{13}C NMR spectra were recorded on a Bruker AVA500 spectrometer (500 and 125 MHz, respectively) or a Bruker AVA600 spectrometer (600 and 150 MHz, respectively) at 298 K in deuterated solvents. Chemical shifts for proton and carbon spectra are reported on the δ scale in ppm. All coupling constants (*J* values) were measured in Hz. ES mass spectra were recorded using a VG Platform Quadrupole Electrospray Ionisation mass spectrometer. Reverse phase analytical HPLC (RP-HPLC) was performed using an Agilent 1100 ChemStation, with a Kinetex 5u XB-C18 (50 × 4 × 60 mm) column, eluting with 5% ACN in water to 95% ACN in water over 10 min (both with 0.1% formic acid).at a flow rate of 1 mL/min with evaporative light scattering detection (ELSD) (Polymer Lab PL-ELS 1000) with simultaneous detection at 220, 254, 260, 282 and 495 nm. All solvents used were HPLC grade. Flow cytometry analysis was carried out on a Becton Dickinson (BD) FACScan XP5 using FlowJo software for data

analysis. The absorbance of 96-well plates was read on a BioTek HT Synergy multimode reader at 570 nm using the Microplate manager 4.0 software. Transmission Electron Microscope (TEM) analysis was conducted on a JEOL JEM-1400 Plus and representative images were collected on a GATAN OneView camera. Fluorescence spectra were recorded on a SPEX Fluoromax, using 1 cm path length fused quartz cuvettes. HeLa and SK-BR-3 cells were monitored using a 20x objective (Leica fluorescence microscope) under brightfield and 488 nm excitation. Confocal images were taken on a Leica SP5 confocal microscope and Zeiss 510 Meta software was used for digital acquisition. Polymers were analysed by gel permeation chromatography (GPC) using two PLgel MIXED-C columns (200-2,000,000 g mol^{-1}, 5 µm) using DMF with 0.1% *w/v* LiBr at 60 °C at 1 mL min^{-1} as an eluent or an Agilent 1100 GPC equipped with an PL aquagel-OH 30 column (8 µm) and one PL aquagel-OH MIXED-H column (8 µm) using H_2O as an eluent at 40 °C at 1 mL/min. Molecular weights obtained were relative to narrow dispersity poly(methyl methacrylate) and poly ethylene glycol standards. The number of repeating units in a polymer was determined by ^1H NMR (using the integrals of the initiator and the vinyl moiety to calculate the molecular weight of the polymers). Matrix-assisted laser desorption/ionization-Time of Flight (MALDI-TOF) mass spectroscopy was carried out on Bruker UltraflexExtreme MALDI-TOF, with sinapinic acid (SA) or 2-(4'-hydroxybenzeneazo)benzoic acid (HABA) as matrices. UV-Vis spectra of protein samples were recorded on a NanoDrop® ND-1000 UV-Vis spectrophotometer (Thermo Fisher Scientific). Stability studies were carried out recording the fluorescence spectra on a BioTek HT Synergy multi-mode reader.

5.2. Small Molecule Synthesis

Biotin-PEG-methacrylate

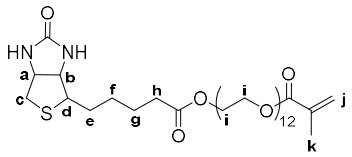

A mixture of biotin (1.0 g, 4.1 mmol), PEG-monomethacrylate (1.5 g, 4.1 mmol, average molecular weight = 500), EDC (0.78 g, 4.1 mmol), 4-DMAP (0.05 g, 0.22 mmol) were dispersed in DMF (50 mL) and stirred for 24 h. The solvent was removed *in vacuo* and the crude product was re-dissolved in DCM and washed with 5% $NaHCO_3$ aqueous solution, 1% HCl and saturated brine (three times each). The solvent was removed *in vacuo* and the product was purified by column chromatography eluting with DCM/MeOH (from100:2 to 100:10), to give 0.75 g of the product (yield 30%).

^{1}H NMR (500 MHz, $CDCl_3$): δ = 6.15 (s, 1H, H_j), 5.60 (s, 1H, H_j), 4.55 (m, 1H, H_a), 4.15 (m, 1H, H_b), 3.80–3.50 (m, 48H, H_i), 3.12 (dt, J = 8.4, 4.4 Hz, 1H, H_d), 2.89 (m, 1H, H_c), 2.72 (m, 1H, H_c), 2.34 (t, *J* = 7.6 Hz, 2H, H_h), 1.68 (s, 3H, H_k), 1.54–1.37 (m, 4H, H_e, H_g); 1.29 (m, 2H, H_g).

^{13}C NMR (500 MHz, $CDCl_3$): δ = 173.5, 167.4, 162.7, 136.2, 125.7, 70.6, 69.1, 64.1, 63.9, 63.5, 61.8, 60.0, 55.2, 50.9, 40.5, 33.7, 28.2, 24.7, 18.3;

IR λ_{max} (cm^{-1}) 3350, 2868, 1703, 1456, 1298, 1254, 1101, 952;

MS ($C_{40}H_{72}N_2O_{17}S$): $[M+H]^+$: 885.16, found: 885.20.

Data was in agreement with the literature.[69]

Carboxylic acid tagged RAFT agent 3

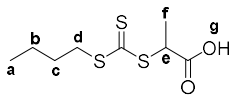

To a suspension of potassium hydroxide (9.0 g, 0.16 mol) in tetrahydrofuran (150 mL), a solution of 1-butanethiol (16 g, 0.18 mol) in THF (50 mL) was added and stirred for 30 minutes followed by addition of carbon disulfide (17 g, 0.23 mol) in THF (50 mL). The resulting mixture was stirred overnight and then concentrated *in vacuo* to 50 mL. The crude product was used without purification.

A solution of tetrapropylammonium bromide (22 g, 0.15 mol) in THF (50 mL) was added dropwise and the resulting solution was stirred 24 hours before concentrated onto silica gel (200 g) *in vacuo* and purified by flash column chromatography (eluted with DCM) to give the title compound as a bright yellow solid (22 g, 63%).

^{1}H NMR (600 MHz, DMSO-d_6): δ/ppm 13.16 (s, 1H, H_g), 4.69 (q, J = 7.4 Hz, 1H, H_e), 3.40 (t, J = 6.8 Hz, 2H, H_d), 1.64 (tt, J = 8.6, 6.8 Hz, 2H, H_c), 1.52 (d, J = 7.4 Hz, 3H, H_f), 1.46–1.31 (m, 2H, H_b), 0.90 (t, J = 7.4 Hz, 3H, H_a).

^{13}C NMR (150 MHz, DMSO-d_6): δ/ppm 222.9, 172.0, 48.6, 36.7, 30.1, 21.9, 17.2, 13.9.

HRMS (ESI) for $C_8H_{14}O_2S_3$ $[M+H]^+$: *calcd.*: 239.0229; *found*: 239.0242.

R_f = 0.41 (DCM/EtOAc, 9:1).

Data was in agreement with the literature.[250]

(Fmoc-amino)hexanoic acid linker bound resin 4

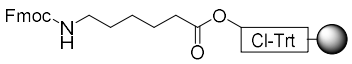

In an SPE filter cartridge (12 mL, fitted with a polyethylene frit with 20 µm porosity, Sigma-Aldrich), thionyl chloride (40 µL, 0.55 mmol) was added to preswollen (in anhydrous DCM) 2-chlorotrityl chloride resin (500 mg, loading 0.95 mmol/g, GL Biochem) in anhydrous DCM under a N_2 atm, and the reaction mixture was shaken for 1 h. The solvent was drained and the resin was washed with anhydrous DCM (3 × 5 mL) and anhydrous DMF (3 × 5 mL). The activated resin was swollen in anhydrous DCM for 10 min, followed by the addition of Fmoc-Ahx-OH (237 mg, 1.8 mmol) and DIPEA (275 µL, 1.7 mmol) in anhydrous DMF (5 mL) and shaken for 1 h. The resin was drained and washed sequentially with anhydrous DCM (3 × 5 mL), anhydrous DMF (3 × 5 mL) and then treated twice with DCM/MeOH/DIPEA (80:15:5, 5 mL) and washed with DCM (3 × 5 mL) and DMF (3 × 5 mL). The coupling reactions were monitored by a ninhydrin test[259].

6-Aminohexanoic acid linker bound resin 5

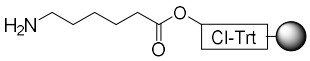

To the hexanoic acid linker bound resin **4** (500 mg, pre-swollen in DCM), piperidine (5 mL, 20% *v*/*v* in DMF) was added and the resin was shaken for 20 min. The solvent was drained and the resin was washed with DCM (3 × 5 mL), DMF (3 × 5 mL), MeOH (3 × 5 mL) and diethyl ether (3 × 5 mL). The coupling reactions were monitored by a ninhydrin test[259].

Hexahistidine tag resin 6

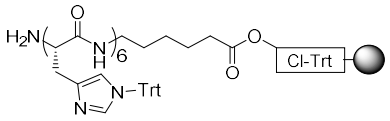

Fmoc-His(Trt)-OH (930 mg, 1.5 mmol) and ethyl cyano(hydroxyimino) acetate (213 mg, 1.5 mmol) were dissolved in DMF (5 mL) and stirred for 10 min. *N*,*N*′-Diisopropylcarbodiimide (232 µL, 1.5 mmol) was added and stirred for further 2 min. The mixture was added to the 6-aminohexanoic acid linker bound resin **5** (500 mg, pre-swollen in DCM) and shaken for 3 h. The solution was drained and the resin washed with DCM (3 × 5 mL) and DMF (3 × 5 mL). The resulting resin was swollen in DCM and piperidine (5 mL, 20% *v*/*v* in DMF) was added and shaken for 20 min, before the solvent was drained and the resin was washed with DCM (3 × 5 mL), DMF (3 × 5 mL), MeOH (3 × 5 mL) and Et_2O (3 × 5 mL). This procedure was repeated 6 times to build the hexahistidine tag moiety. The coupling reactions were monitored by a ninhydrin test[259].

Hexahistidine tagged RAFT agent bound resin 7

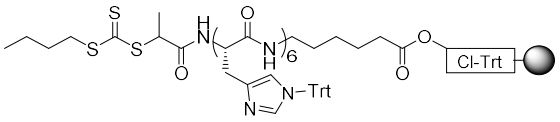

2-{[(butylsulfanyl)carbonothioyl]sulfanyl} propanoic acid **3**[250] (358 mg, 1.5 mmol), and ethyl cyano(hydroxyimino) acetate (213 mg, 1.5 mmol) were dissolved in DMF (5 mL) and stirred for 10 min. *N*,*N*′-diisopropylcarbodiimide (232 µL, 1.5 mmol) was added and stirred for further 2 min. The mixture was added to the hexahistidine tag resin **6** (500 mg, pre-swollen in DCM) and reaction mixture was shaken for 3 h. The solution was drained and the resin was washed with DCM (3 × 5 mL) and DMF (3 × 5 mL). The coupling reactions were monitored by a ninhydrin test[259].

Hexahistidine tagged RAFT agent 8

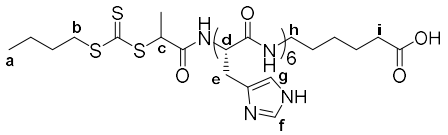

The hexahistidine tagged RAFT agent bound resin **7** (500 mg, pre-swollen in DCM) was shaken in TFA/water (95:5, *v*/*v*, 5 mL) for 2 h. The filtrate was collected and the resin was washed with TFA/water (3 × 5 mL). The solutions were combined and evaporated *in vacuo*. The crude product was purified by reverse phase column chromatography using a gradient of acetonitrile (5% to 95% over 10 min, *v*/*v*, with 0.1% formic acid) in water as the eluent (170 mg, 63%).

^{1}H NMR (600 MHz, DMSO-d_6): δ/ppm 8.97–8.73 (m, 6H, H_f), 8.68–8.13 (m, 7H, H_{amide}), 7.42–7.08 (m, 6H, H_g), 4.81–4.41 (m, 7H, H_c, H_d), 3.34 (t, *J* = 7.4, 2H, H_b), 3.16–2.81 (m, 14H, H_e, H_h), 2.18 (t, *J* = 7.4, 2H, H_i), 1.61–1.13 (m, 13H, -CH_2- and -CH-CH_3), 0.88 (t, *J* = 7.4 Hz, 3H, H_a).

^{13}C NMR (150 MHz, DMSO-d_6): δ/ppm 223.1, 174.9, 170.6, 170.5, 170.4, 170.4, 170.2, 170.1, 170.0, 159.6, 159.3, 159.1, 158.9, 134.4, 134.3, 130.3, 130.2, 130.0, 129.9, 120.5, 118.5, 117.3, 117.2, 117.1, 116.5, 114.6, 52.6, 52.5, 52.5, 52.3, 50.1, 49.8, 39.0, 38.7, 36.6, 35.8, 34.1, 30.0, 29.0, 27.6, 26.4, 26.3, 25.5, 24.7, 24.6, 21.8, 18.5, 18.0, 13.9.

HRMS (ESI) for $C_{50}H_{67}N_{19}O_9S_3$ $[M+H]^+$: *calcd.*: 1174.4604; *found*: 1174.4599.

HPLC t_R= 1.49 min. (Purity >98% by ELSD).

***Exo*-2-*tert*-butoxycarbamatoethyl-carboxamidonorborn-5-ene 9**

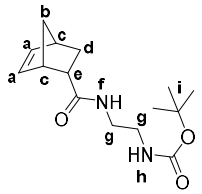

To a solution of *N*-Boc-ethylenediamine (3.6 g, 23 mmol) and *exo*-5-norbornenecarboxylic acid (2.8 g, 20 mmol) in DMF (50 mL), *N*-(3-dimethylaminopropyl)-*N*'-ethylcarbodiimide hydrochloride (4.2 g, 22 mmol) was added and the reaction mixture was stirred overnight. The solvent was removed *in vacuo* and the crude product was purified by flash column chromatography (eluting with EtOAc/DCM, 2:8) to give compound **9** as a white solid (5.0 g, 89%).

^{1}H NMR (600 MHz, DMSO-d_6): δ/ppm 7.83 (t, *J* = 5.7 Hz, 1H, H_f), 6.77 (t, *J* = 5.7 Hz, 1H, H_h), 6.16–6.09 (m, 2H, H_a), 3.07–2.98 (m, 4H, H_g), 2.83 (m, 2H, H_c), 2.02 (m, 1H, H_e), 1.78 (m, 1H, H_d), 1.62 (m, 1H, H_d), 1.38 (s, 9H, H_i), 1.20–1.11 (m, 2H, H_b).

^{13}C NMR (150 MHz, DMSO-d_6): δ/ppm 175.2, 156.1, 138.2, 136.7, 78.1, 47.3, 46.1, 43.5, 41.4, 30.2, 28.7.

HRMS (ESI) for $C_{15}H_{24}N_2O_3$ $[M+H]^+$: *calcd.*: 281.1860; *found*: 281.1859.

R_f = 0.10 (DCM/EtOAc, 9:1).

Data was in agreement with the literature.[260]

***Exo*-2-aminoethyl-carboxamidonorborn-5-ene hydrochloride 10**

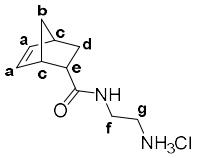

To a solution of Boc-protected amino norbornene **9** (3.6 g, 12.8 mmol) in 1,4-dioxane (5 mL), 4 M HCl in 1,4-dioxane (25 mL) was added and the mixture was stirred overnight. The solvent was removed *in vacuo* to give the titled compound as a white solid (2.3 g, 98%).

^{1}H NMR (600 MHz, DMSO-d_6): δ/ppm 6.17–6.09 (m, 2H, H_a), 3.35–3.28 (m, 4H, H_f, H_g), 2.85 (m, 2H, H_c), 2.07 (m, 1H, H_e), 1.83–1.62(m, 2H, H_d), 1.23–1.15 (m, 2H, H_b).

^{13}C NMR (150 MHz, DMSO-d_6): δ/ppm 175.8, 138.3, 136.7, 47.2, 46.2, 43.6, 41.5, 39.1, 37.1, 30.3.

HRMS (ESI) for $C_{10}H_{16}N_2O$ $[M+H]^+$: *calcd.*: 181.1335; *found*: 181.1330.

R_f = 0.16 (9:1, CH_2Cl_2/CH_3OH).

Data was in agreement with the literature.[260]

***Exo*-2-acrylamidoethyl-carboxamidonorborn-5-ene 11**

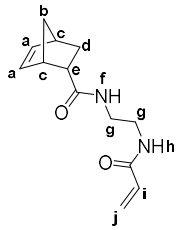

To a solution of **S2** (2.3 g, 13mmol) and triethylamine (2.7 mL, 19 mmol) in anhydrous THF (20 mL), acryloyl chloride (1.2 mL, 14 mmol) in anhydrous THF (10 mL) was added dropwise at 0 °C. The reaction mixture was stirred for 2 h, concentrated *in vacuo* and purified by column chromatography (eluting with EtOAc/DCM, 4:6) to give **11** as a white solid (0.8 g, 22%).

^{1}H NMR (600 MHz, DMSO-d_6): δ/ppm 8.11 (t, J = 5.1 Hz, 1H, H_f), 7.91 (t, J = 5.3 Hz, 1H, H_h), 6.19 (m, 1H, H_j), 6.13 (m, 2H, H_a), 6.07 (m, 1H, H_j), 5.58 (m, 1H, H_i), 3.22–3.12 (m, 5H, H_g, H_c), 2.86–2.78 (m, 1H, H_c), 2.35 (m, 1H, H_e), 1.79 (m, 1H, H_d), 1.63 (m, 1H, H_d), 1.17 (m, 2H, H_b).

^{13}C NMR (150 MHz, DMSO-d_6): δ/ppm 175.3, 165.3, 138.2, 136.8, 132.3, 125.5, 47.3, 46.1, 43.5, 41.4, 39.0, 38.9, 30.2.

HRMS (ESI) for $C_{13}H_{18}N_2O_2$ $[M+H]^+$: *calcd.*: 235.1447; *found*: 235.1445.

R_f = 0.49 (DCM/MeOH, 9:1).

5.3. Polymer Synthesis

Poly(HPMA)

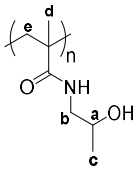

N-(2-Hydroxypropyl) methacrylamide (7.2 mg, 50 µmol) and initiator Irgacure2959 (0.4 mg, 2 µmol) were added to PBS (1 mL) and the mixture illuminated at 365 nm for 5 min. The polymer was purified by dialysis against water for 72 h (2.5 L, exchanged twice every 24 h, molecular weight cut off 1000 Da) and freeze dried (42% yield).

^{1}H NMR (500 MHz, DMSO-d_6): δ/ppm 3.68 (H_a), 2.91 (H_b), 1.68 (H_e), 1.21–0.91 (H_d), 0.82 (H_c).

^{13}C NMR (125 MHz, DMSO-d_6): δ/ppm 171.40, 92.89, 58.91–53.38, 28.94, 20.69.

See GPC data in Figure 17 and Table 4.

Poly(HPMA-*co*-biotin-PEGMA)

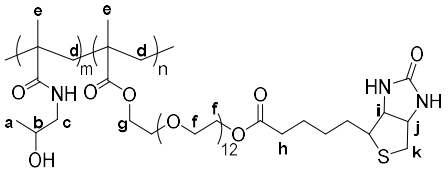

N-(2-Hydroxypropyl) methacrylamide (7.2 mg, 50 µmol), biotin-PEGMA (4.2 mg, 5 µmol) and initiator Irgacure2959 (0.4 mg, 2 µmol) were added to PBS (1 mL) and the mixture illuminated at 365 nm for 5 min. The polymer was purified by dialysis against water for 72 h (2.5 L, exchanged twice every 24 h, molecular weight cut off 1000 Da) and freeze dried (43% yield).

^{1}H NMR (500 MHz, Chloroform-*d*): δ/ppm 4.12–3.91 (H_i, H_j, H_g), 3.8–3.45 (H_f), 3.22 (H_c), 2.58–2.28 (H_d, H_k, H_h), 1.63 (H_a, H_e).

^{13}C NMR (125 MHz, Chloroform-*d*): δ/ppm 169.39, 139.73, 132.43, 119.96, 114.20, 70.59, 67.67, 47.18, 28.71, 21.09, 18.67.

GPC (DMF) M_n=9 kDa, Đ = 1.7.

Poly(NaSS)

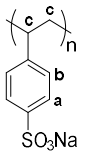

Sodium 4-styrenesulfonate (10.3 mg, 50 µmol) and initiator Irgacure2959 (0.4 mg, 2 µmol) were added to PBS (1 mL) and the mixture illuminated at 365 nm for 5 min. The polymer was purified by dialysis against water for 72 h (2.5 L, exchanged twice every 24 h, molecular weight cut off 1000 Da) and freeze dried (56% yield).

^{1}H NMR (500 MHz, DMSO-d_6): δ/ppm 7.85–6.97 (H_a, H_b), 2.36–1.63 (H_c).

^{13}C NMR (125 MHz, DMSO-d_6): δ/ppm 164.59, 147.89, 70.26, 59.69–54.65, 50.19.

GPC (DMF) M_n=5 kDa, Đ = 1.0.

Poly(VAN)

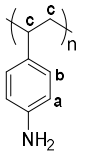

4-Vinylaniline (6.0 mg, 50 µmol) and initiator Irgacure2959 (0.4 mg, 2 µmol) were added to PBS (1 mL) and the mixture illuminated at 365 nm for 5 min. The polymer was purified by dialysis against water for 72 h (2.5 L, exchanged twice every 24 h, molecular weight cut off 1000 Da) and freeze dried (62% yield).

^{1}H NMR (500 MHz, DMSO-d_6): δ/ppm 7.18–6.15 (H_a, H_b), 2.33–1.90 (H_c).

^{13}C NMR (125 MHz, DMSO-d_6): δ/ppm 173.80, 155.34, 146.13, 60.26–52.69.

GPC (DMF) M_n=6 kDa, Đ = 1.1.

Poly(FMMA)

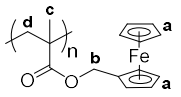

Ferrocenylmethyl methacrylate (5.7 mg, 20 µmol) and initiator Irgacure2959 (0.4 mg, 2 µmol) were added to PBS (1 mL) and the mixture illuminated at 365 nm for 5 min. The polymer was purified by dialysis against water for 72 h (2.5 L, exchanged twice every 24 h, molecular weight cut off 1000 Da) and freeze dried (25% yield).

^{1}H NMR (500 MHz, DMSO-d_6): δ/ppm 4.98–4.60 (H_a), 4.38–4.03 (H_b), 2.18–1.85 (H_d), 1.33–0.47 (H_c).

^{13}C NMR (125 MHz, DMSO-d_6) δ 176.50, 162.53, 136.42, 133.72, 130.07, 126.20, 82.03, 69.68, 68.90, 63.03, 18.50.

GPC (DMF) M_n=8 kDa, Đ = 2.2.

Poly(HEMA)

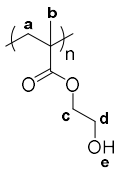

2-Hydroxyethyl methacrylate (6.5 mg, 50 µmol) and initiator Irgacure2959 (0.4 mg, 2 µmol) were added to PBS (1 mL) and the mixture illuminated at 365 nm for 5 min. The polymer was purified by dialysis against water for 72 h (2.5 L, exchanged twice every 24 h, molecular weight cut off 1000 Da) and freeze dried (42% yield).

^{1}H NMR (500 MHz, DMSO-d_6): δ/ppm 5.09–4.23 (H_e), 4.16–3.38 (H_c, H_d), 2.33–1.71 (H_a), 1.44–0.48 (H_b).

^{13}C NMR (125 MHz, DMSO-d_6): δ/ppm 179.13, 70.26, 66.67, 58.93, 26.80.

GPC (DMF) M_n=14 kDa, Đ = 2.0.

Poly(*O*-HPMA)

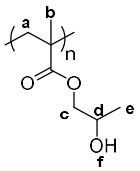

O-2-Hyroxypropyl methacrylate (7.2 mg, 50 µmol) and initiator Irgacure2959 (0.4 mg, 2 µmol) were added to PBS (1 mL) and the mixture illuminated at 365 nm for 5 min. The polymer was purified by dialysis against water for 72 h (2.5 L, exchanged twice every 24 h, molecular weight cut off 1000 Da) and freeze dried (43% yield).

^{1}H NMR (500 MHz, DMSO-d_6): δ/ppm 4.72 (H_d, H_f), 4.08–3.53 (H_c), 2.31–1.53 (H_a), 1.30–0.89 (H_e), 0.88–0.68 (H_b).

^{13}C NMR (126 MHz, DMSO-d_6): δ/ppm 175.10, 70.26, 64.14, 61.20, 20.63.

GPC (DMF) M_n=11 kDa, Đ = 1.8.

Hexahistidine tagged poly(*exo*-2-acrylamidoethyl-carboxamidonorborn-5-ene-*co*-*N*,*N*'dimethylacrylamide) P1 to P5

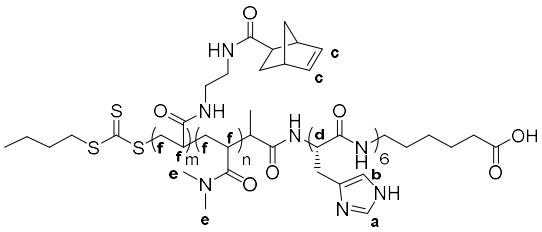

N,*N*'-dimethylacrylamide (103 µL, 41 µL, 258 µL, 103 µL and 103 µL for **P1** to **P5**, respectively), norbornene acrylamide **11** (23 mg, 9.4 mg, 59 mg, 9.4 mg, 59 mg for **P1** to **P5**, respectively), RAFT agent **8** (12 mg, 10 µmol) and 2,2'-azobis(2-methylpropionitrile) (0.16 mg, 1.0 µmol) was dissolved in 1,4-dioxane (1 mL) and degassed by freeze-pump-thaw cycling. The polymerisation solution was stirred at 70 °C under Ar atm for 4 h and subsequently quenched by freezing in liquid nitrogen and thawed in the presence of air. The solvent was removed *in vacuo* and the resulting polymer was purified by dialysis (2.5 L, exchanged twice every 24 h, molecular weight cut off 30 kDa) against deionised water for 3 days (water changed every 12 h).

P1 (90% yield):

^{1}H NMR (600 MHz, DMSO-d_6): δ/ppm 8.32–7.45 (H_a), 6.81 (H_b), 6.11 (H_c), 4.42 (H_d), 3.15–2.58 (H_e), 1.85–0.68 (H_f).

^{13}C NMR (150 MHz, DMSO-d_6): δ/ppm 38.7–37.3, 33.4.

GPC (DMF) M_n=14 kDa, Đ = 1.5.

P2 (91% yield):

^{1}H NMR (600 MHz, DMSO-d_6): δ/ppm 8.35–7.50 (H_a), 6.80 (H_b), 6.19 (H_c), 4.36 (H_d), 3.02–2.61 (H_e), 1.85–0.66 (H_f).

^{13}C NMR (150 MHz, DMSO-d_6): δ/ppm 38.7–37.3, 33.2.

GPC (DMF) M_n=7 kDa, Đ = 1.2.

P3 (88% yield):

^{1}H NMR (600 MHz, DMSO-d_6): δ/ppm 8.34–7.41 (H_a), 6.78 (H_b), 6.21 (H_c), 4.39 (H_d), 3.24–2.43 (H_e), 1.96–0.62 (H_f).

^{13}C NMR (150 MHz, DMSO-d_6): δ/ppm 39.1–37.2, 33.0.

GPC (DMF) M_n=30 kDa, Đ = 1.8.

P4 (91% yield):

^{1}H NMR (600 MHz, DMSO-d_6): δ/ppm 8.33–7.48 (H_a), 6.69 (H_b), 6.02 (H_c), 4.33 (H_d), 3.05–2.50 (H_e), 1.82–0.57 (H_f).

^{13}C NMR (150 MHz, DMSO-d_6): δ/ppm 38.9–37.2, 33.4.

GPC (DMF) M_n=11 kDa, Đ = 1.4.

P5 (78% yield):

^{1}H NMR (600 MHz, DMSO-d_6): δ/ppm 8.44–7.38 (H_a), 6.79 (H_b), 6.11 (H_c), 4.39 (H_d), 3.18–2.61 (H_e), 1.80–0.56 (H_f).

^{13}C NMR (150 MHz, DMSO-d_6): δ/ppm 39.0–37.7, 33.0.

GPC (DMF) M_n=16 kDa, Đ = 1.7.

Polymer NHS esters PA1 to PA5

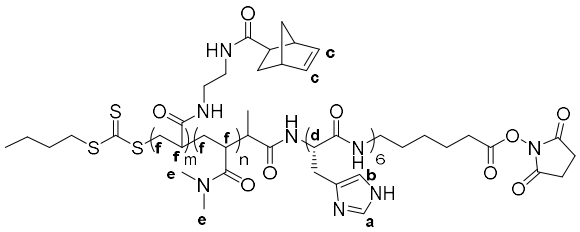

Polymers **P1** to **P5** (1 equivalent, 10 mg) and 10 equivalent of *N*-hydroxysuccinimide (0.88 mg, 1.5 mg, 0.50 mg, 0.93 mg, 0.80 mg for **PA1** to **PA5**, respectively) were dissolved in anhydrous DMF and stirred for 5 min, followed by addition of 10 equivalent *N*-(3-dimethylaminopropyl)-*N*'-ethylcarbodiimide hydrochloride (1.5 mg, 2.5 mg, 0.83 mg, 1.5 mg, 1.3 mg for **PA1** to **PA5**, respectively). The reaction mixture was stirred under a N_2 atm. for 16 h and the product precipitated from Et_2O (50 mL). The polymer active esters were redissolved in the minimum amount of DMF and precipitated from Et_2O a further 3 times before drying *in vacuo*.

PA1 (> 95% yield):

^{1}H NMR (600 MHz, DMSO-d_6): δ/ppm 8.19–7.64 (H_a), 6.79 (H_b), 6.09 (H_c), 4.40 (H_d), 3.12–2.79 (H_e), 1.85–0.62 (H_f).

^{13}C NMR (150 MHz, DMSO-d_6): δ/ppm 38.7–37.3, 33.4.

GPC (DMF) M_n=16 kDa, Đ = 1.6.

PA2 (> 95% yield):

^{1}H NMR (600 MHz, DMSO-d_6): δ/ppm 8.21–7.66 (H_a), 6.80 (H_b), 6.11 (H_c), 4.36 (H_d), 3.12–2.62 (H_e), 1.65–0.72 (H_f).

^{13}C NMR (150 MHz, DMSO-d_6): δ/ppm 38.8–37.3, 33.2.

GPC (DMF) M_n=7 kDa, Đ = 1.2.

PA3 (> 95% yield):

^{1}H NMR (600 MHz, DMSO-d_6): δ/ppm 8.11–7.61 (H_a), 6.79 (H_b), 6.11 (H_c), 4.39 (H_d), 3.14–2.51 (H_e), 1.96–0.62 (H_f).

^{13}C NMR (150 MHz, DMSO-d_6): δ/ppm 39.1–37.2, 33.1.

GPC (DMF) M_n=32 kDa, Đ = 1.7.

PA4 (> 95% yield):

^{1}H NMR (600 MHz, DMSO-d_6): δ/ppm 8.16–7.64 (H_a), 6.89 (H_b), 6.22 (H_c), 4.51 (H_d), 3.15–2.60 (H_e), 1.72–0.66 (H_f).

^{13}C NMR (150 MHz, DMSO-d_6): δ/ppm 38.9–37.2, 33.1.

GPC (DMF) M_n=11 kDa, Đ = 1.6.

PA5 (> 95% yield):

^{1}H NMR (600 MHz, DMSO-d_6): δ/ppm 8.09–7.58 (H_a), 6.88 (H_b), 6.23 (H_c), 4.40 (H_d), 3.19–2.58 (H_e), 1.80–0.67 (H_f).

^{13}C NMR (150 MHz, DMSO-d_6): δ/ppm 39.0–37.7, 33.5.

GPC (DMF) M_n=15 kDa, Đ = 1.6.

5.4. Synthesis of Protein Conjugates

Macro-RAFT agent 1

To BSA (9 mg, 140 nmol) in PBS (1 mL, pH = 7.4), 1-succinimidyl-4-cyano-4-[*N*-methyl-*N*-(4-pyridyl) carbamothioylthio] pentanoate (140 µL, 10 mM solution in DMSO) was added and

the mixture was stirred at 37 °C for 4 h. The solution was diluted with PBS (2 mL) and dialysed against water (2.5 L, exchanged twice every 24 h, molecular weight cut off 12,000 Da) for 24 h and freeze dried to give the titled compound in quantitative yield. The macro-RAFT agent was stored at 4 °C.

Poly(DMAA) grafted BSA 2

Macro-RAFT agent **1** (2.7 mg, 50 nmol), *N*,*N*'-dimethylacrylamide (1 nmol to 1 mM), Eosin Y (130 µg, 200 nmol) and triethylamine (1.4 µL, 10 µmol) were mixed in PBS and illuminated at 470 nm for 4 h. The crude was dialysed against water (2.5 L, exchanged twice every 24 h, molecular weight cut off 12,000 Da) for 24 h and freeze dried to give poly(DMAA) grafted BSA **2** in quantitative yield. The poly(DMAA) grafted BSA was stored at 4 °C.

P1-BSA, P2-BSA and P3-BSA

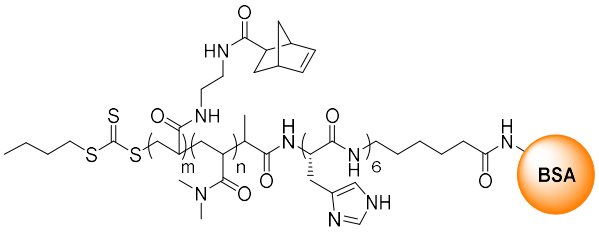

To BSA (0.9 mg, 14 nmol) in PBS (100 µL, pH = 7.4), 10 eq. polymer active ester **PA1** to **PA3** (1.8 mg, 1.0 mg, 3.2 mg for **P1-BSA, P2-BSA** and **P3-BSA**, respectively) were added and the mixtures stirred at 37 °C for 4 h. The solution was diluted with PBS (5 mL) before being concentrated to 100 µL using an Amicon Ultra-15 centrifugal filter unit (molecular weight cut off 30 kDa, 30 kDa, 100 kDa for **P1-BSA**, **P2-BSA** and **P3-BSA**, respectively) and the dilution and concentration were repeated 10 times. The protein conjugate solutions were stored at 4 °C.

P1-Her to **P5-Her**

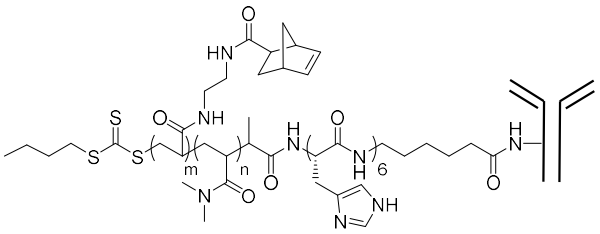

To Herceptin (20 mg/mL, 137 μM, 20 μL) in PBS, 10 eq. of the polymer active esters **PA1** to **PA5** (0.4 mg, 0.2 mg, 0.7 mg, 0.4 mg, 0.4 mg for **P1-Her** to **P5-Her**, respectively) were added and stirred at 37 °C for 4 h. The solution was diluted with PBS (5 mL, pH = 7.4) and concentrated to 100 μL using an Amicon Ultra-15 centrifugal filter units (molecular weight cut off 100 kDa) and the dilution and concentration were repeated for 10 times. The protein conjugate solutions were stored at 4 °C.

Purification for polymer–protein conjugates

The polymer–protein conjugates were purified using an immobilised metal-affinity chromatography resin following the manufacturer's instructions. Specifically, Ni-charged Profinit IMAC Resin slurry (500 μL) was transferred to a SPE filter cartridge (12 mL with a polyethylene frit with 20 μm porosity, Sigma-Aldrich) and washed with deionised water (3 × 5 mL) and drained. The polymer–protein conjugates (20 μL, 14 μM) were solvent exchanged into the washing buffer (50 mM sodium phosphate, 300 mM NaCl, 5 mM imidazole, pH = 8.0) using an Amicon Ultra-15 centrifugal filter unit (molecular weight cut off 30 kDa), concentrated to 200 μL, and added to the immobilised metal-affinity chromatography resin. The resin slurry was shaken for 30 min, the solvent drained, and the resin washed with the washing buffer (3 × 5 mL) and then treated with optimised elution buffer (3 × 5 mL, 50 mM sodium phosphate, 300 mM NaCl and 500 mM imidazole, pH = 8.0, see optimisation below) The solution was collected by filtration before concentrated to 100 μL using an Amicon Ultra-15 centrifugal filter units (molecular weight cut off 30 kDa) and washed with PBS (pH = 7.4) 10 times. The protein conjugate yields were determined by measuring the absorbance of the protein samples at 280 nm using a NanoDrop® ND-1000 UV-Vis Spectrophotometer and calibrated with 5 concentrations of the native corresponding protein solutions (sample volume = 1 μL, n = 3). The polymer–protein solutions were stored at 4 °C.

The imidazole concentration in the elution buffer was optimised by loading **P1-BSA** to the immobilised metal-affinity chromatography resin (using the same protocol as mentioned above) and eluted with a set of elution buffers (3 × 5 mL, 50 mM sodium phosphate, 300 mM NaCl and a gradient concentration of 10, 20, 50, 100, 200 and 500 mM imidazole, pH = 8.0). The elution was analysed using SDS-PAGE (see Figure 58). Staining was carried out with Coomassie blue (0.1% *w*/*v* in 1:4:5 acetic acid/water/MeOH for 2 h). Protein markers used were Precision Plus Protein™ Kaleidoscope™ Prestained Protein Standards, 10-250 kDa (Bio-Rad). Bright field and fluorescent images (λ_{ex} = 365 nm, λ_{em} = 520 ± 30 nm) of gels were taken using a Universal Hood II Gel Doc System (Bio-Rad).

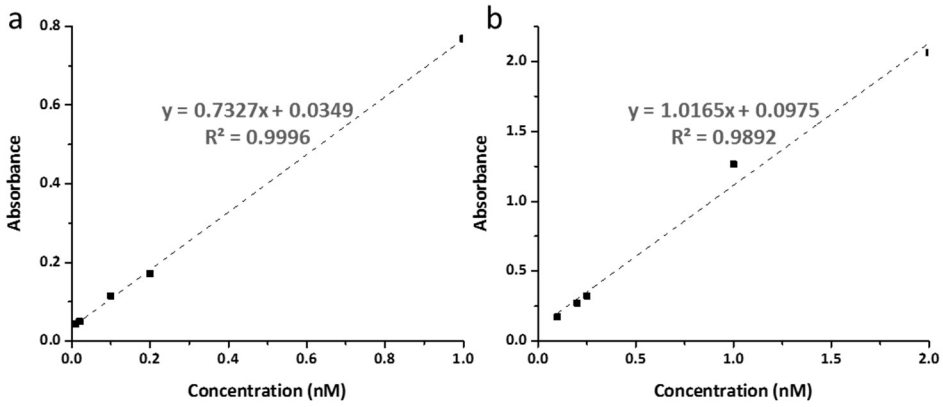

Figure 74. Protein yield calibration curve of (a) BSA and (b) Herceptin with absorbance at 280 nm using a NanoDrop® ND-1000 UV-Vis Spectrophotometer.

Table 12. Protein yields calibrated using a UV-Vis Spectrophotometer. The absorbance of the polymer–protein conjugate solutions at 280 nm was recorded and compared to the calibration curve to give the molar concentration. The yield was calculated by comparing the amount of the polymer–protein conjugate to the protein used for conjugation. The data is presented as a mean ± standard deviation (n = 3 for each group).

Polymer-protein conjugates	Absorbance	Concentration (nM)	Yield (%)
P1-BSA	0.59 ± 0.02	0.76 ± 0.01	42 ± 1
P2-BSA	0.73 ± 0.01	0.95 ± 0.01	52 ± 1
P3-BSA	0.23 ± 0.01	0.27 ± 0.01	15 ± 1
P1-Her	1.72 ± 0.04	1.59 ± 0.04	72 ± 2
P2-Her	1.12 ± 0.01	1.00 ± 0.01	45 ± 1
P3-Her	2.07 ± 0.03	1.94 ± 0.03	88 ± 2
P4-Her	1.73 ± 0.04	1.61 ± 0.04	73 ± 1
P5-Her	1.35 ± 0.01	1.24 ± 0.01	56 ± 1

Synthesis of the BODIPY labelled antibody BODIPY-Her

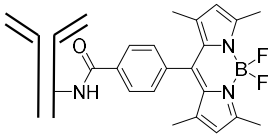

To Herceptin in PBS (pH = 7.4, 20 µL, 137 µM), NHS ester functionalised BODIPY **13** in DMSO (2 µL, 14 mM) was added and mixture was stirred at 37 °C for 4 h. The mixture was diluted with PBS (5 mL) and concentrated to 100 µL using an Amicon Ultra-15 centrifugal filter unit (molecular weight cut off 30 kDa), and the dilution and concentration repeated 10 times. The labelled-antibody solutions were stored at 4 °C.

In vitro BODIPY labelling of polymer–antibody conjugates

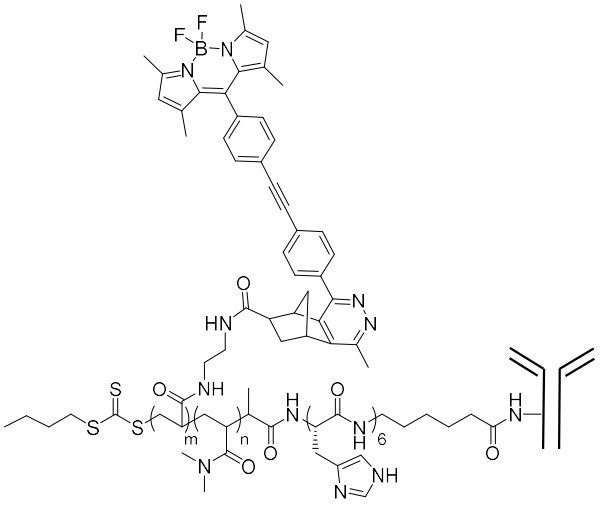

To the polymer antibody conjugates **P1-Her**, **P2-Her** and **P3-Her** in pH 7.4 PBS (10 µL, 2.7 µM, pH = 7.4), **Tz1** in DMSO (1 µL, 274 µM) was added and the mixture was shaken at 37 °C for 4 h. The mixture was diluted with PBS (5 mL) and concentrated to 100 µL using an Amicon Ultra-15 centrifugal filter units (molecular weight cut off 30 kDa), and the dilution and concentration were repeated for 10 times to give **BODIPY-P1-Her**, **BODIPY-P2-Her** and **BODIPY-P3-Her**.

5.5. Biology

Cell culture

HeLa, human adipogenesis mesenchymal stem, SK-BR-3 and MCF-7 cells were maintained in 25 cm^3 tissue culture flasks (Corning) in DMEM, supplemented with 10 % (*v*/*v*) FBS, L-glutamine (100 U, Gibco) and penicillin/streptomycin (100 U/mL, Sigma), in a cell incubator (37 °C and 5 % CO_2). Cell passaging was conducted by treating cells with trypsin (1% in PBS, *v*/*v*, 1 mL). The detached cells were diluted with fresh media (4 mL) to deactivate the trypsin and 20% cells were transferred to a new flask with fresh media (4 mL) added. The process was repeated every 2 days.

General procedure for intracellular polymerisation

HeLa cells were seeded in a 96-well plate at a density of 1×10^4 cells per well (5×10^4 cells per well in a 24-well plate and 5×10^5 cells per well in a 6-well plate) and cultured overnight. The cells were then treated with monomer HPMA (50 mM) and Irgacure2959 (2 mM) for 4 h. The cells were washed with PBS (3 × 200 µL) and fresh medium added (200 µL). Polymerisation was initiated by illumination at 365 nm for 5 min, with the lamp fixed 5 cm above the plate. The cells were incubated at 37 °C. Polymerisation of other monomers typically followed the same procedure. Untreated cells were used as control, unless otherwise stated.

Cytotoxicity studies

HeLa or SK-BR-3 cells were seeded in a 96-well plate at a density of 1×10^4 cells per well and incubated overnight. The cells were then treated with a series of concentrations of monomer or initiator and incubated for 48 h at 37 °C (n = 3). To test illumination cytotoxicity, the lamp was fixed at the height of 5 cm above the plate and illuminated at 365 nm for 5 min, 10 min and 15 min and followed by 48 h incubation at 37 °C.

MTT assay

Cells (Hela, human adipogenesis mesenchymal stem, SK-BR-3 or MCF-7) seeded in 96-well plate (1×10^4 cells per well) were incubated with 100 µL of 3-(4,5-dimethylthiazol-2-yl)-2,5-diphenyltetrazolium bromide (MTT) solution (0.7 mg/mL) in PBS/media (7:3) for 4 h at 37 °C. Then 100 µL of solubilising solution (9:1 Triton-X 100/Isopropanol, pH = 1) were added to each well. The plate was shaken horizontally for 60 min to dissolve the formazan crystals. The absorbance at 570 nm was measured by a plate reader. Cell viability was calculated compared to untreated cells. All of the experiments were repeated three times.

Table 13. HeLa cell viability after illumination at 365 nm for 5, 10 and 15 min. Viability was measured using an MTT assay. The data is presented as a mean ± standard deviation (n = 3 for each group).

Illumination time (min)	Absorbance (a.u.)	Viability (%)
0	1.54 ± 0.26	100 ± 17
5	1.49 ± 0.20	97 ± 13
10	1.29 ± 0.25	84 ± 16
15	0.62 ± 0.17	40 ± 11

Table 14. HeLa cell viability after incubation with Irgacure2959 (1 mM, 2 mM, 5 mM, 10 mM, 20 mM and 50 mM) for 48 h. Viability was measured using an MTT assay. The data is presented as a mean ± standard deviation (n = 6 for each group).

Concentration (mM)	Absorbance (a.u.)	Viability (%)
0	1.76 ±1.17	100 ± 10
1	1.95 ± 0.14	111 ± 8
2	1.49 ± 0.10	85 ± 6
5	1.37 ± 0.12	78 ± 7
10	1.20 ± 0.16	68 ± 9
20	0.14 ± 0.08	8 ± 4
50	0.01 ± 0.03	1 ± 2

Table 15. HeLa cell viability after incubation with BABO-ONa (0.1 mM, 0.5 mM, 1 mM, 2 mM, 5 mM and 10 mM) for 48 h. Viability was measured using an MTT assay. The data is presented as a mean ± standard deviation (n = 6 for each group).

Concentration (mM)	Absorbance (a.u.)	Viability (%)
0	0.68 ± 0.04	100 ± 6
0.1	0.83 ± 0.03	121 ± 4
0.5	0.84 ± 0.03	122 ± 2
1	0.85 ± 0.02	124 ± 2
2	0.78 ± 0.01	115 ± 1
5	0.68 ± 0.07	100 ±10
10	0.49 ± 0.05	72 ± 7

Table 16. HeLa cell viability after incubation with *N*-(2-hydroxypropyl) methacrylamide (HPMA) (1 mM, 3 mM, 10 mM, 30 mM, 100 mM and 250 mM) for 48 h. Viability was measured using an MTT assay. The data is presented as a mean ± standard deviation (n = 6 for each group).

Concentration (mM)	Absorbance (a.u.)	Viability (%)
0	0.50 ± 0.04	100 ± 8
1	0.54 ± 0.04	108 ± 8
3	0.54 ± 0.07	107 ± 4
10	0.47 ± 0.04	93 ± 8
30	0.47 ±0.08	93 ± 15
100	0.38 ±0.07	77 ± 14
250	0.25 ± 0.07	50 ± 14

Table 17. HeLa cell viability after incubation with sodium 4-styrenesulfonate (NaSS) (1 mM, 3 mM, 10 mM, 30 mM, 100 mM and 250 mM) for 48 h. Viability was measured using an MTT assay. The data is presented as a mean ± standard deviation (n = 6 for each group).

Concentration (mM)	Absorbance (a.u.)	Viability (%)
0	0.50 ± 0.05	100 ± 10
1	0.65 ± 0.09	130 ± 19
5	0.64 ± 0.09	127 ± 18
10	0.70 ± 0.01	138 ± 1
20	0.48 ± 0.02	95 ± 4
50	0.51 ± 0.07	102 ± 14
100	0.06 ± 0.02	11 ± 4

Table 18. HeLa cell viability after incubation with 4-vinylaniline (VAN) ((1 mM, 5 mM, 10 mM, 20 mM, 50 mM and 100 mM) for 48 h. Viability was measured using an MTT assay. The data is presented as a mean ± standard deviation (n = 6 for each group).

Concentration (mM)	Absorbance (a.u.)	Viability (%)
0	2.35 ± 0.27	100 ± 12
1	2.50 ± 0.04	107 ± 2
5	2.67 ± 0.20	114 ± 9
10	2.78 ± 0.52	118 ± 22
20	2.20 ± 0.21	94 ± 9
50	1.13 ± 0.09	48 ± 4
100	0.81 ± 0.27	35 ± 12

Table 19. HeLa cell viability after incubation with ferrocenylmethyl methacrylate (FMMA) (1 mM, 5 mM, 10 mM, 20 mM, 50 mM and 100 mM) for 48 h. Viability was measured using an MTT assay. The data is presented as a mean ± standard deviation (n = 6 for each group).

Concentration (mM)	Absorbance (a.u.)	Viability (%)
0	0.63 ± 0.08	100 ± 12
1	0.60 ± 0.06	95 ± 9
5	0.46 ± 0.01	72 ± 1
10	0.41 ± 0.02	65 ± 3
20	0.34 ± 0.02	54 ± 3
50	0.30 ± 0.04	47 ± 6
100	0.29 ± 0.05	46 ± 8

Table 20. HeLa cell viability after incubation with biotin-PEGMA (0.1 mM, 0.5 mM, 1 mM, 2 mM, 5 mM and 10 mM) for 48 h. Viability was measured using an MTT assay. The data is presented as a mean ± standard deviation (n = 6 for each group).

Concentration (mM)	Absorbance (a.u.)	Viability (%)
0	2.07 ± 0.79	100 ± 13
1	1.97 ± 0.11	95 ± 6
5	1.63 ± 0.13	79 ± 6
10	1.19 ± 0.11	57 ± 5
20	0.23 ± 0.06	11 ± 3
50	0.23 ± 0.08	11 ± 4
100	0.21 ±0.01	10 ± 1

Table 21. HeLa cell viability after incubation with 2-hydroxyethyl methacrylate (HEMA) ((1 mM, 5 mM, 10 mM, 20 mM, 50 mM and 100 mM) for 48 h. Viability was measured using an MTT assay. The data is presented as a mean ± standard deviation (n = 6 for each group).

Concentration (mM)	Absorbance (a.u.)	Viability (%)
0	2.40 ± 0.13	100 ± 5
1	2.10 ± 0.17	82 ± 8
5	1.78 ± 0.26	74 ± 11
10	0.96 ± 0.13	40 ± 5
20	0.31 ± 0.04	12 ± 2
50	0.18 ± 0.03	8 ± 1
100	0.13 ± 0.02	5 ± 1

Table 22. HeLa cell viability after incubation with *O*-2-hydroxypropyl methacrylate (*O*-HPMA) ((1 mM, 5 mM, 10 mM, 20 mM, 50 mM and 100 mM) for 48 h. Viability was measured using an MTT assay. The data is presented as a mean ± standard deviation (n = 6 for each group).

Concentration (mM)	Absorbance (a.u.)	Viability (%)
0	2.19 ±0.02	100 ± 10
1	2.26 ± 0.20	103 ± 9
5	2.12 ± 0.17	97 ± 8
10	1.65 ± 0.12	76 ± 6
20	0.82 ± 0.07	38 ± 3
50	0.11 ± 0.05	5 ± 2
100	0.03 ± 0.02	2 ± 1

Table 23. HeLa cell viability after "polymerisation" (The cells were treated with HPMA, (1 mM, 3 mM, 10 mM, 30 mM, 100 mM and 250 mM), and Iggacure2959 (2 mM) for 4 h and illuminated at 365 nm for 5 min) and incubation in fresh media for further 48 h. Viability was measured using an MTT assay. The data is presented as a mean ± standard deviation (n = 6 for each group).

Concentration (mM)	Absorbance (a.u.)		Viability (%)	
	- hv	*+ hv*	*- hv*	*+ hv*
0	0.51 ± 0.08	0.91 ± 0.13*	100 ± 16	96 ± 15*
1	0.65 ± 0.09	0.82 ± 0.03	130 ± 19	90 ± 3
3	0.64 ± 0.09	0.86 ± 0.14	127 ± 18	94 ± 15
10	0.70 ± 0.07	0.86 ± 0.11	138 ± 1	94 ± 12
30	0.48 ± 0.02	0.73 ± 0.04	95 ± 4	81 ± 6
100	0.51 ± 0.07	0.70 ± 0.03	102 ± 14	79 ± 5
250	0.06 ± 0.02	0.59 ± 0.01	14 ± 4	66 ± 2

* Hela cells without 365 nm illumination was used as a control with their viability set as 100%.

Table 24. Human adipogenesis mesenchymal stem cell viability after "polymerisation" (The cells were treated with HPMA, (1 mM, 3 mM, 10 mM, 30 mM, 100 mM and 250 mM), and Iggacure2959 (2 mM) for 4 h and illuminated at 365 nm for 5 min) and incubation in fresh media for further 48 h. Viability was measured using an MTT assay. The data is presented as a mean ± standard deviation (n = 6 for each group).

Concentration (mM)	Absorbance (a.u.)		Viability (%)	
	- hv	*+ hv*	*- hv*	*+ hv*
0	0.36 ± 0.03	0.33 ± 0.02*	100 ± 9	90 ± 6*
1	0.34 ± 0.01	0.35 ± 0.01	95 ± 1	98 ± 4
3	0.33 ± 0.01	0.37 ± 0.01	91 ± 4	101 ± 3
10	0.29 ± 0.03	0.35 ± 0.01	81 ± 9	96 ± 4
30	0.30 ± 0.03	0.31 ± 0.01	82 ± 9	87 ± 3
100	0.23 ± 0.02	0.27 ± .0.02	64 ± 5	76 ± 6
250	0.01 ± 0.01	0.00 ± 0.00	1 ± 1	0 ± 0

* Hela cells without 365 nm illumination was used as a control with their viability set as 100%.

CellTiter-Glo

HeLa cells were seeded in opaque-walled 96-well plates at a density of 1×10^4 cells per well and incubated overnight. The cells were then treated with HPMA (50 mM), NaSS (50 mM), VAN (50 mM), FMMA (20 mM) and biotin-PEGMA (2 mM) and Irgacure2959 (2 mM) for 4 h. The medium was replaced with fresh medium followed by illumination at 365 nm for 6 min. After 7 d incubation, the well plate was equilibrated for 30 minutes and 100µl of CellTiter-Glo® 2.0 reagent was added directly to the culture media and the content was mixed for 2

minutes on an orbital shaker followed by 10 min incubation. The luminescence was measured on a plate reader. Cell viability was calculated compared to untreated cells.

Table 25. HeLa cell viability after "polymerisation" Viability measured using a CellTiter-Glo assay. The data is presented as a mean ± standard deviation (n = 6 for each group).

Monomer	Luminescence (a.u.)		Viability (%)	
	- hv	*+ hv*	*- hv*	*+ hv*
Control	449000 ± 37000	498000 ± 36000*	100 ± 8	111 ± 7*
HPMA (50 mM)	413000 ± 15000	542000 ± 20000	92 ± 24	121 ± 4
NaSS (50 mM)	471000 ± 68000	545000 ± 11000	105 ± 15	121 ± 2
VAN (50 mM)	64000 ± 13000	409000 ± 85000	14 ± 3	91 ± 17
FMMA (20 mM)	500000 ± 15000	493000 ± 30000	111 ± 3	110 ± 6
Biotin-PEGMA (2 mM)	456000 ± 93000	512000 ± 34000	102 ± 21	114 ± 7

* Hela cells without 365 nm illumination was used as a control with their viability set as 100%.

Cell proliferation

Hela cells (5×10^4) were incubated with monomers (HPMA, NaSS or FMMA, 50 mM) and initiators (Irgacure2959 or BAPO-ONa, 2 mM) for 4 h, washed and illuminated 5 min at 365 nm. The cells were then incubated at 37 °C for 7 d and analysed by the Click-iT EdU flow cytometry assay. Specifically, the cells were incubated with EdU for 2 h, and harvested. The cells were pelleted by centrifugation and washed with PBS (1mL) for 3 times and fixed using paraformaldehyde (4% in PBS, *w*/*v*). The cells were then pelleted and washed with PBS (1mL) for 3 times and incubated with a saponin solution (1% in PBS, *v*/*v*) to remove the cell membrane. The cells were labelled with an Alexa Fluor 488 azide probe in a "Click it" buffer (from the manufacturer) and analysed by flow cytometry ($\lambda_{ex/em}$ = 488/525 nm). Forward versus side scatter profiles were used to gate intact cellular materials. All flow cytometry analyses are based on analysis of 10,000 cells.

Table 26. Hela cell proliferation quantified by flow cytometry. Intact cells were gated using forward versus side scatter profiles.

Monomer + initiator	Intact cells (%)		Proliferating cells (%)	
	- hv	*+ hv*	*- hv*	*+ hv*
Control	88 ± 2	92 ± 1	36 ± 3	33 ± 1
HPMA + Irgacure2959	91 ± 2	92 ± 1	32 ± 1	28 ± 1
HPMA + BAPO-ONa	92 ± 0	89 ± 1	33 ± 2	27 ± 1
NaSS + Irgacure2959	89 ± 2	92 ± 1	34 ± 2	30 ± 1
VAN + Irgacure2959*****	17 ± 9	9 ± 2	-	-
FMMA + Irgacure2959	89 ± 5	92 ± 0	33 ± 7	30 ± 7

* 4-Vinylaniline treated cells showed a significant reduction in the number of intact cells and therefore the proliferation assay could not be carried out.

Cellular uptake

For the measurement of cellular uptake of monomer and initiator, calibrations were first established by HPLC. A series of concentrations of monomers (from 0.1 mM to 5 mM) and initiator (from 0.1 mM to 5 mM) in ACN were made up and analysed by HPLC and the calibration curves were then plotted (Figure 75 to 82).

Hela cells were then seeded in 24-well plate at a density of 1×10^4 cells per well and incubated overnight. Monomers and initiator were added to the medium at a final concentration of 50 mM and 2 mM, respectively. After incubation for 2, 3 or 4 h, HeLa cells were collected, washed (× 3) and lysed using RIPA cell lysis buffer. After mixing by pipetting 20 times, MeOH was added and the precipitated proteins were removed by centrifugation (at 4 °C and 12,000 rpm for 10 min). The supernatant was collected and dried under a flow of nitrogen before re-solubilisation of the residue in ACN and HPLC analysis. HPLC was performed using a reverse phase column with 10 µL injections, using water/MeCN (95:5 to 5:95 over 10 min, *v*/*v*, with 0.1% formic acid) as the mobile phase and UV detection at 254 nm.

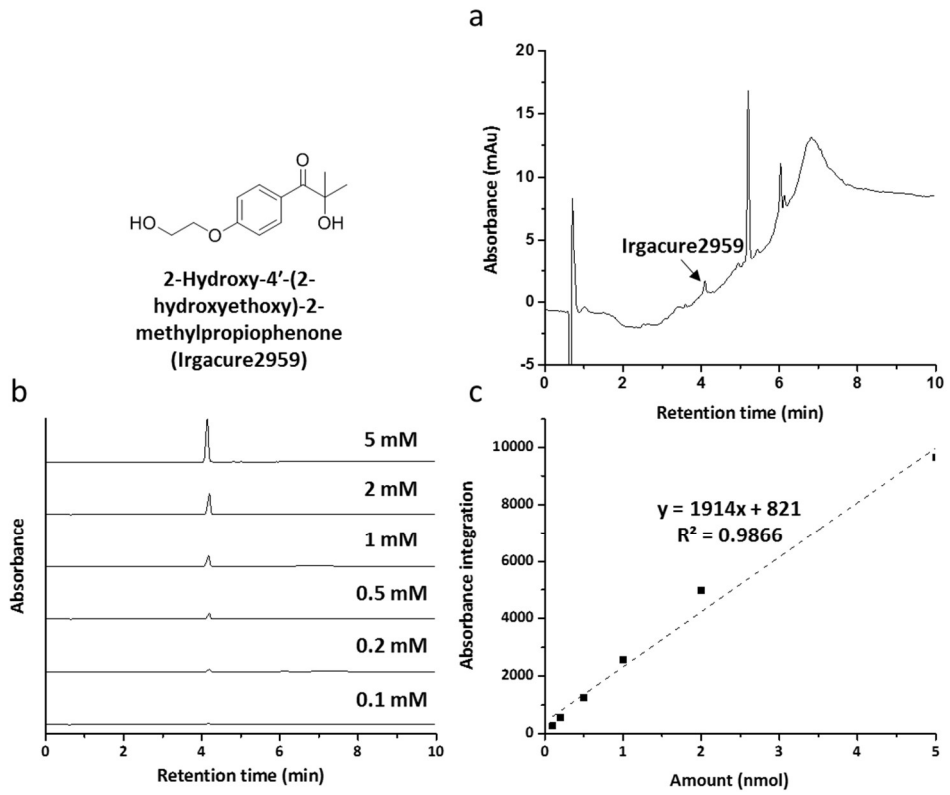

Figure 75. (a) HPLC trace of the initiator Irgacure2959 (2 mM) recovered from Hela cells after 4 h incubation with the compound. (b) HPLC traces of Irgacure2959 at 0.1 mM, 0.2 nM, 0.5 mM, 1 mM, 2 mM and 5 mM. The peak at 4.06 min represents Irgacure2959. (c) Calibration curve of Irgacure2959, amounts were plotted against integration of the peaks on the HPLC.

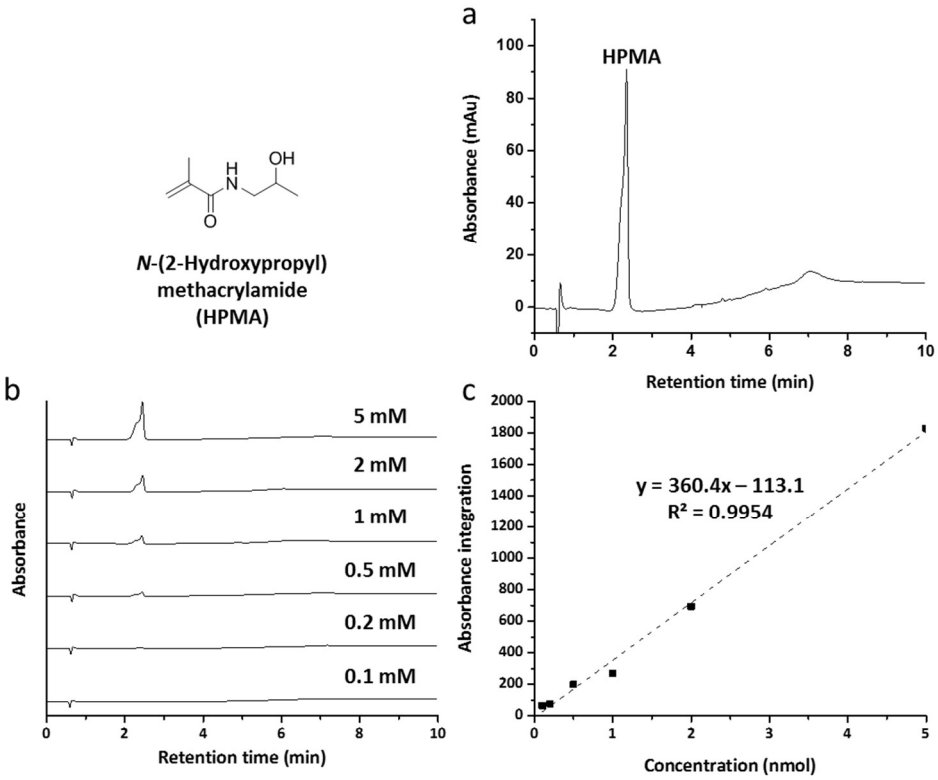

Figure 76. (a) HPLC trace of the monomer HPMA (50 mM) recovered from Hela cells after 4 h incubation with the compound. (b) HPLC traces of HPMA at 0.1 mM, 0.2 nM, 0.5 mM, 1 mM, 2 mM and 5 mM. The peak at 2.11 min represents HPMA. (c) Calibration curve of HPMA, amounts were plotted against integration of the peaks on the HPLC.

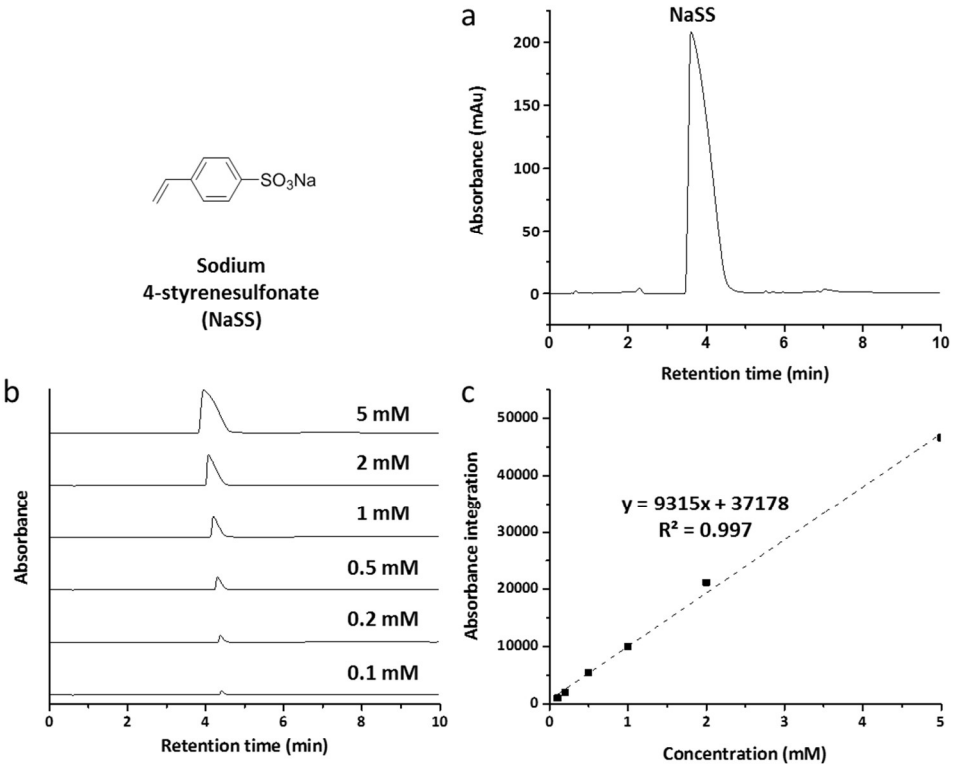

Figure 77. (a) HPLC trace of the monomer NaSS (50 mM) recovered from Hela cells after 4 h incubation with the compound. (b) HPLC traces of NaSS at 0.1 mM, 0.2 nM, 0.5 mM, 1 mM, 2 mM and 5 mM. The peak at 3.67 min represents NaSS. (c) Calibration curve of NaSS, amounts were plotted against integration of the peaks on the HPLC.

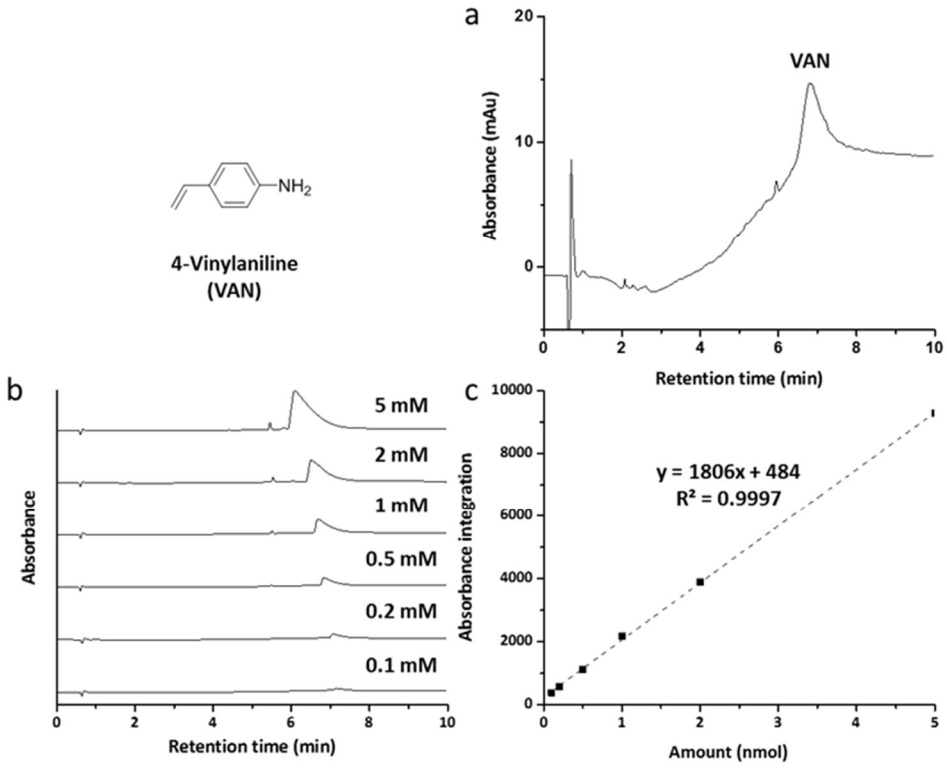

Figure 78. (a) HPLC trace of the monomer VAN (50 mM) recovered from Hela cells after 4 h incubation with the compound. (b) HPLC traces of VAN at 0.1 mM, 0.2 nM, 0.5 mM, 1 mM, 2 mM and 5 mM. The peak at 7.06 min represents VAN. (c) Calibration curve of VAN, amounts were plotted against integration of the peaks on the HPLC.

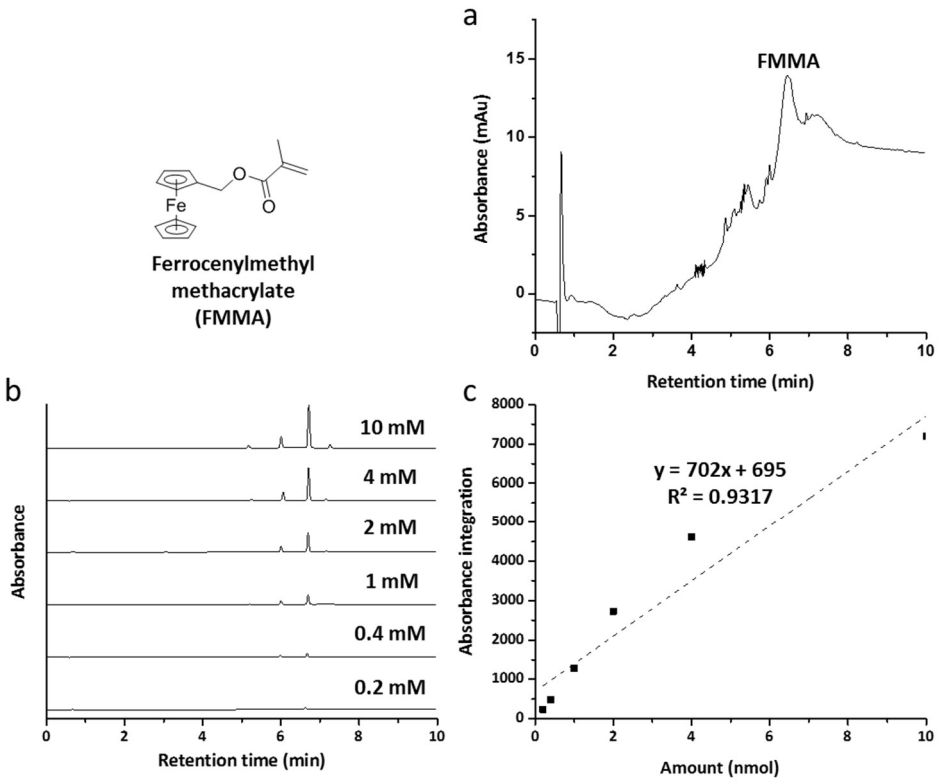

Figure 79. (a) HPLC trace of the monomer FMMA (20 mM) recovered from Hela cells after 4 h incubation with the compound. (b) HPLC traces of FMMA at 0.2 mM, 0.4 nM, 1 mM, 2 mM, 4 mM and 10 mM. The peak at 6.71 min represents FMMA. (c) Calibration curve of FMMA, amounts were plotted against integration of the peaks on the HPLC.

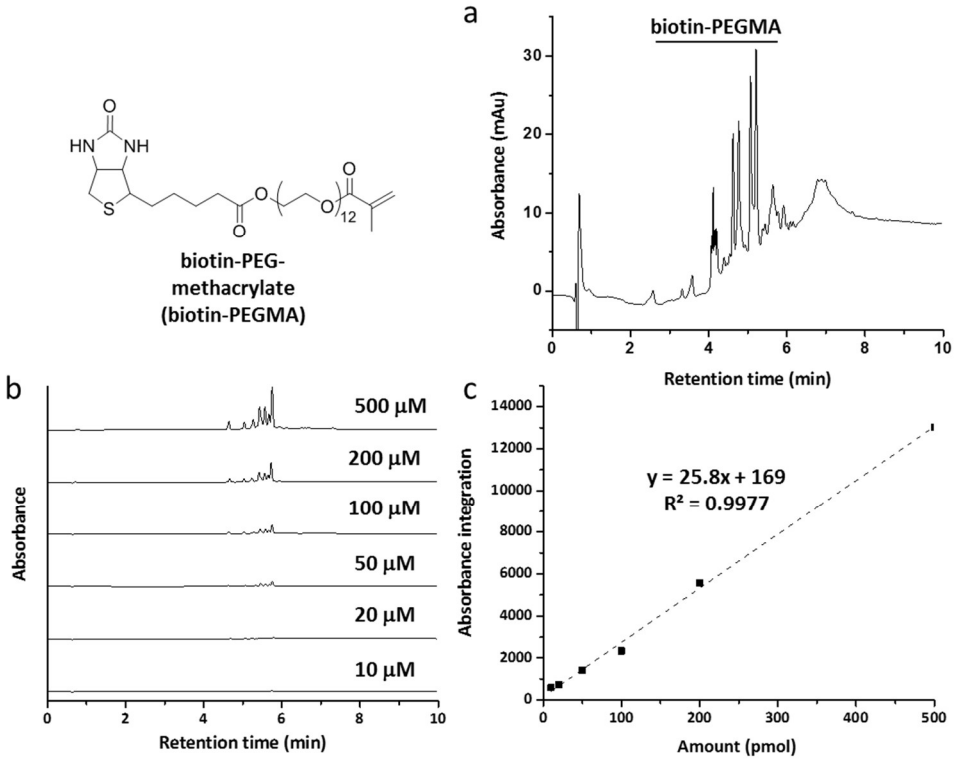

Figure 80. (a) HPLC trace of the monomer biotin-PEGMA (2 mM) recovered from Hela cells after 4 h incubation with the compound. (b) HPLC traces of biotin-PEGMA at 0.01 mM, 0.02 nM, 0.05 mM, 0.1 mM, 0.2 mM and 0.5 mM. The peaks at 4.61 to 5.75 min represents biotin-PEGMA. (c) Calibration curve of biotin-PEGMA, amounts were plotted against integration of the peaks on the HPLC.

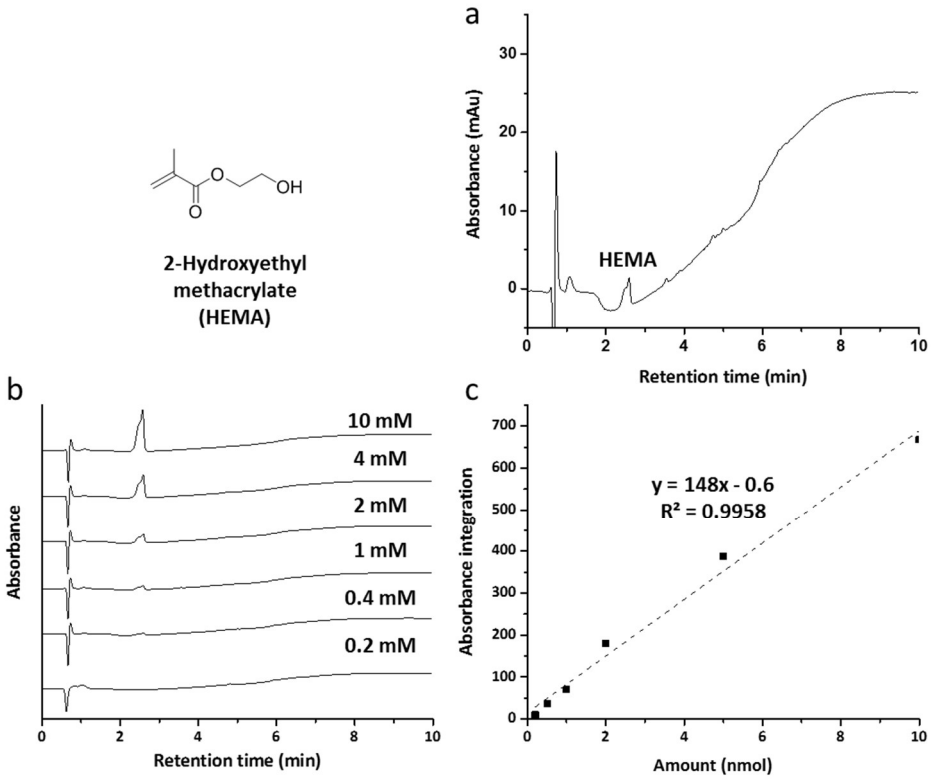

Figure 81. (a) HPLC trace of the monomer HEMA (50 mM) recovered from Hela cells after 4 h incubation with the compound. (b) HPLC trace of HEMA at 0.2 mM, 0.4 nM, 1 mM, 2 mM, 4 mM and 10 mM. The peak at 2.58 min represents HEMA. (c) Calibration curve of HEMA, amounts were plotted against integration of the peaks on the HPLC.

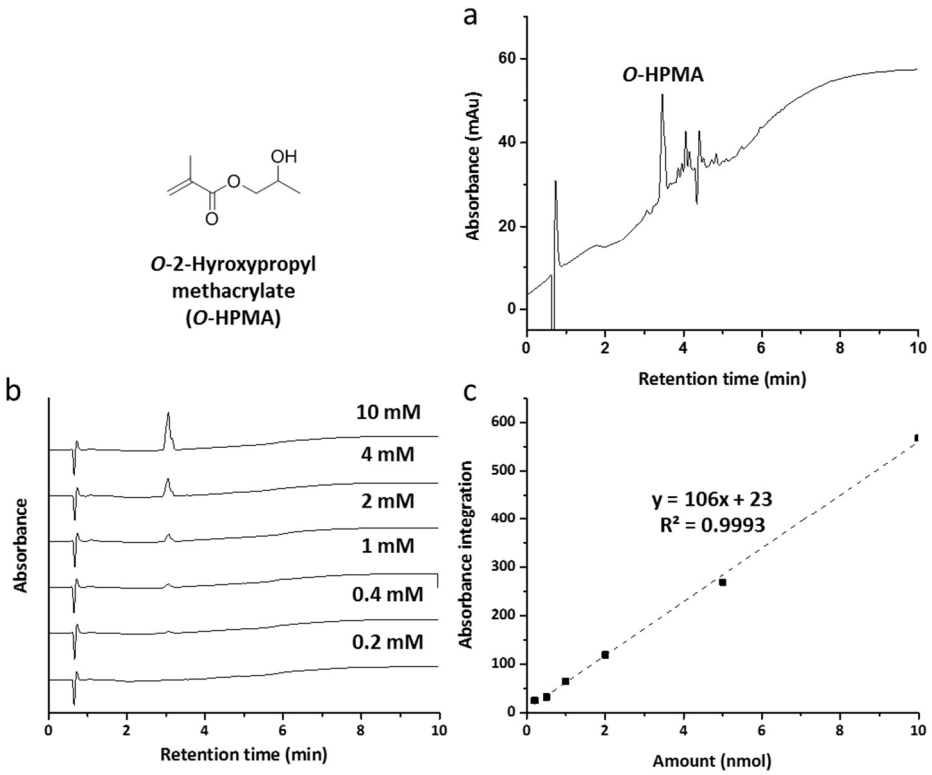

Figure 82. (a) HPLC trace of the monomer *O*-HPMA (50 mM) recovered from Hela cells after 4 h incubation with the compound. (b) HPLC trace of *O*-HPMA at 0.2 mM, 0.4 nM, 1 mM, 2 mM, 4 mM and 10 mM. The peak at 3.01 min represents *O*-HPMA. (c) Calibration curve of *O*-HPMA, amounts were plotted against integration of the peaks on the HPLC.

Table 26. Intracellular initiator/monomer concentration determined after 4 h incubation. Uptakes (molar concentration) were determined by comparing the absorbance integration of compounds to their calibration curves. Cellular concentration was calculated by the equation below: (Amount of compound was calculated from the calibration curves. sample volume = 1 mL, injection volume = 10 µL)

$$Uptake = \frac{amount\ of\ compound \times sample\ volume}{injection\ volume \times number\ of\ cells \times dilution\ factor}$$

Initiator/Monomer	Absorbance integration	Number of cells	Dilution factor	Uptake (pmol/cell)
Irgacure2959	1200 ± 300	5×10^4	2	0.01 ± 0.00
HPMA	135 ± 9	1×10^4	5	0.26 ± 0.01
NaSS	89000 ± 13000	1×10^4	5	0.82 ±0.11
VAN	360 ± 40	1×10^4	5	0.10 ± 0.01
FMMA	61 ± 9	1×10^4	10	0.20 ± 0.03
Biotin-PEGMA	40 ± 2	1×10^5	20	0.03 ± 0.00
HEMA	48 ± 8	1×10^4	5	0.17 ± 0.04
O-HPMA	29 ± 2	1×10^4	5	0.10 ± 0.01

Identification of free radicals and ROS in cells

Hela cells were seeded at a density of 50,000 cells per well in a 24-well plate and incubated overnight. Then the medium was changed with fresh medium without phenol red and serum. Cells were incubated with HPMA (50 mM) and/or initiator (2 mM) for 3.5 h before the addition of 2',7'-dichlorodihydrofluorescein diacetate (DCFH-DA) (10 µM) and incubated for

another 30 min following 5 min illumination at 365 nm. The cells were gently washed with PBS (3 times) and treated with trypsin for 5 min before suspending in 500 µL of phenol red free medium. The cell suspensions were analysed by flow cytometry using a FITC filter ($\lambda_{ex/em}$ = 488/525 nm).

Extraction of polymer from cells

HeLa cells were seeded in 6-well plates at a density of 5×10^5 cells per well (16 wells in total) and incubated overnight. BiotinPEGMA, HPMA and initiator Irgacure2959 were added to media at a final concentration of 5 mM, 50 mM and 2 mM, respectively. After incubation for 4 h, cells were washed and photo-polymerised by illumination at 356 nm for 5 min. The cells were washed three times with PBS and harvested. The collected cells were lysed using RIPA cell lysis buffer and the polymer extracted from the cell lysate with Dynabeads™ M-280 Strepavidin according to the manufacturer's protocol, summarised as follows:

Cell lysate was added to the washed Dynabeads™ magnetic beads in a centrifuge tube (15 mL, Flacon) and incubated for 30 min at RT with slow end-over-end mixing. The tube was placed in a magnet for 5 min and the supernatant was removed. The beads were washed three times with washing buffer and water and re-suspended in water and incubated at 40°C for 10 min. The supernatant was collected and another portion of water was added and incubated at 40°C for another 10 min. The supernatant was collected combined with the previous portion and freeze-dried. The releasing steps were repeated at 60°C, 80°C and 97°C. The collected samples were characterised by ^{1}H NMR (see Figure 83).

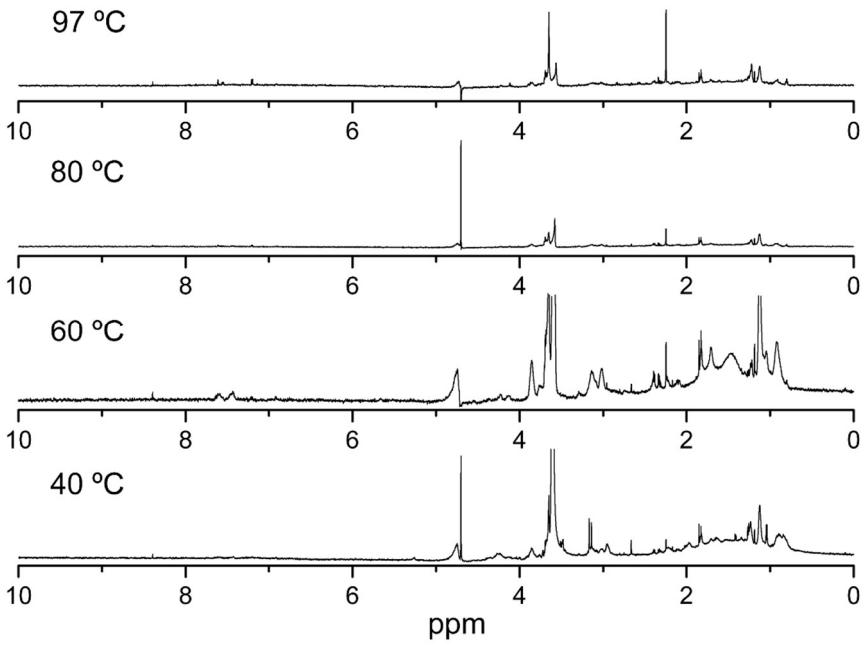

Figure 83. ^{1}H NMR spectra (in D_2O) of poly(HPMA-co-biotinPEGMA) isolated from cells using magnetic beads and the polymer released at 40 °C, 60 °C, 80 °C and 97 °C.

Table 27. Recovery of poly(HPMA-*co*-biotin-PEGMA) (mass percentage of the total amount of polymers collected) from the nanoparticles.

Incubation temperature (°C)	Mass of polymer (mg)	Recovery (%)
40	< 0.1	< 1
60	1.9	83
80	0.4	17
97	< 0.1	< 1

Cell cycle study

HeLa cells were seeded in a 24-well plate at a density of 5×10^4 cells per well and incubated at 37 °C overnight. To each well, HPMA (50 mM) and Irgacure2959 (2 mM) were added and incubated at 37 ˚C for 4 h, followed by washing and polymerisation as described above. The cells were then incubated at 37 ˚C for 48 h. The media was removed and the cells were gently washed twice with PBS. The cells were treated with 1% trypsin (200 µL) for 10 min and the detached cells were suspended in fresh media (800 µL) and transferred to test tubes. To each tube, Vybrant® DyeCycle™ Green (2 µL of a 5 mM stock solution) was added and incubated for 30 min in dark. The samples were analysed on a flow cytometer using a FITC filter (λ_{ex} = 488 nm).

Cell migration study

HeLa cells were seeded in Ibidi® Culture-Insert 2 Well µ-Dish at a density of 1.5×10^4 cell per well (in 70 µL media) and incubated at 37 °C overnight. To each well, HPMA (3.5 µmol) and Irgacure2959 (0.14 µmol) was added and incubated at 37 ˚C for 4 h, followed by gentle washing with PBS (3 × 70 µL). Fresh media (70 µL) was added and the plate with cells was illuminated for 5 min from the top. The media was removed and the cells were gently washed three times with PBS. The PBS was decanted and the insert modes were removed, followed by addition of fresh media (2 mL) to the dish. Microscopy images were taken using the bright field channel every 24 h and the diameter of the void between cells measured using ImageJ with the Wound Healing Tool plugin, using the variance method.

The influence of polymer size over cell mobility was determined by applying different concentration s of HPMA (50 mM, 100 mM and 250 mM) with Irgacure2959 concentration set as 2 mM. The wound closure assay was carried out using the same protocol as described above (Table 29).

Table 28. "Wound" area remaining in the wound healing assay. HPMA and Irgacure2959 concentrations were set at 50 mM and 2 mM respectively. Percentage of area remaining was calculated by comparing the remaining areas to the area at time 0.

Monomer/ Initiator	Time (h)	Area remaining		Percentage of area remaining (%)	
		365 nm	No illumination	365 nm	No illumination
Yes	0	283000 ± 6000	346000 ± 3000	100 ± 2	100 ± 1
Yes	24	189000 ± 11000	218000 ± 21000	67 ± 4	63 ± 6
Yes	48	130000 ± 8000	35000 ± 14000	46 ± 3	10 ± 4
Yes	72	82000 ± 6000	0 ± 0	29 ± 2	0 ± 0
No	0	346000 ± 3000	400000 ± 8000	100 ± 4	100 ± 2
No	24	218000 ± 21000	268000 ± 16000	63 ± 6	67 ± 4
No	48	35000 ± 14000	56000 ± 12000	10 ± 4	14 ± 3
No	72	0 ± 0	0 ± 0	0 ± 0	0 ± 0

Table 29. "Wound" area remaining in the wound healing assay. HPMA concentrations were set at 50 mM, 100 mM and 250 mM with Irgacure2959 concentration set at 2 mM. Percentage of area remaining was calculated by comparing the remaining areas to the area at time 0.

HPMA concentration (mM)	Incubation Time (h)	Area remaining	Percentage of area remaining (%)
0	0	406000 ± 13000	100 ± 3
50	0	409000 ± 12000	67 ± 3
100	0	400000 ± 20000	18 ± 0
250	0	361000± 15000	0 ± 0
0	24	272000 ± 12000	100 ± 3
50	24	286000 ± 16000	70 ± 4
100	24	272000 ± 16000	49 ± 5
250	24	303000 ± 14000	25 ± 2
0	48	73000 ± 4000	100 ± 5
50	48	201000 ± 20000	68 ± 4
100	48	168000 ± 24000	42 ± 6
250	48	292000 ± 18000	29 ± 1
0	72	0 ± 0	100 ± 4
50	72	102000 ± 8000	84 ± 4
100	72	116000 ± 4000	81 ± 5
250	72	223000 ± 47000	62 ± 3

Actin staining and measurement of actin filament orientation

HeLa cells were seeded Ibidi® 8 Well μ-Slide at a density of 1×10^4 cells per well and incubated overnight. HPMA (50 mM) and Irgacure2959 (2 mM) were added to the medium and the cells were incubated at 37 °C for 4 h, followed by washing and polymerisation as described above. After 48 h and 72 h incubation at 37 °C, cells were washed three times with PBS and fixed by 4% PFA following permeabilisation with 0.1% Triton™ X-100 in PBS for 15 minutes. The cells were stained with Alexa Fluor™ 488 Phalloidin (10 μg/mL) for 30 min at RT, and images (λ_{ex} = 475 nm, λ_{em} = 509 nm) were taken by confocal laser scanning microscopy. The images of cells with fluorescently labelled actin filaments were analysed using ImageJ with OrientationJ plugin and the anisotropy of actin was quantified using FibrilTool. **Measurement of actin area.** Images of fluorescently labelled cells were smoothed using a Gaussian filter in ImageJ, followed by removal of the background using a 20 μm diameter rolling ball. The images were then thresholded and the actin microdomains were analysed to obtain the area.

Synthesis of fluorescent polymers (poly(NaSS) and poly(VAN)) in cells

Hela cells were seeded in 24-well plate at a density of 5×10^4 cells per well and incubated overnight. Monomer sodium 4-vinylbenzenesulfonate (NaSS) (50 mM) or 4-vinylaniline (VAN) (50 mM) and initiator (2 mM) were added to each well. After incubation for 4 h, cells were washed and the medium replaced, followed by 5 min illumination at 365 nm. Subsequently, the nuclei and plasma membrane were stained with Hoechst 33342 and CellMask™ Deep Red Plasma Membrane Stain, and the stained samples were imaged by confocal laser scanning microscope (CLSM) and quantified buy flow cytometry.

Cell passage study

HeLa cells were seeded in a 6-well plate at a density of 1×10^5 cells per well and incubated at 37 °C overnight. To each well, acryloxyethyl thiocarbamoyl rhodamine B (50 μM), HPMA (20 mM) and Irgacure2959 (2 mM) was added and incubated at 37 °C for 4 h, followed by washing and polymerisation as described above. For each passage analysis, cells were treated with 1% trypsin/EDTA (500 μL) for 10 min and the detached cells were suspended in fresh

media. ¾ cell suspensions were transferred to cytometry tubes and analysed on a flow cytometer using a PI filter ($\lambda_{ex/em}$ = 488/586 nm). The rest of the cells were seeded back into new well plate (1 × 10^5 cells per well) and incubated at 37 °C. The trypsinisation process, microscopy imaging and flow cytometry analysis were repeated every 48 h for 5 passages.

FMMA polymerisation in cells

HeLa cells were seeded in 6-well plates at a density of 1 × 10^5 cells per well and incubated overnight (16 wells in total). FMMA and initiator were added to the medium at a final concentration of 10 mM and 1 mM, respectively. After incubation for 4 h, the medium was replaced with fresh medium followed by 5 min illumination. Subsequently, the cells were washed three times with cold PBS and harvested for TEM analysis. Untreated cells were used as the negative control.

For TEM analysis, photo-polymerised HeLa cells were fixed with 3% glutaraldehyde in 0.1 M sodium cacodylate buffer (pH 7.3) for 2 hours and washed in 0.1 M sodium cacodylate (three times 10 min). Specimens were then post-fixed in 1% osmium tetroxide in 0.1M sodium cacodylate for 45 min, then washed with 0.1 M sodium cacodylate buffer (three times 10 min). The samples were then dehydrated in 50%, 70%, 90% and 100% ethanol (three times) for 15 min each, then two times (10 min each) in propylene oxide. Samples were then embedded in TAAB 812 resin. Sections (1µm thick) were cut on a Leica Ultracut ultramicrotome, stained with toluidine Blue, and viewed in a light microscope to select suitable areas for investigation. Ultrathin sections, 60 nm thick, were cut from selected areas, stained with uranyl acetate and lead citrate and viewed in a JEOL JEM-1400 Plus TEM. (Conducted by Dr S. Mitchell)

Sodium dodecyl sulfate–polyacrylamide gel electrophoresis (SDS-PAGE)

SDS-PAGE was performed with a Bio-Rad Laboratories Mini-Protean 3 Cell System using a 4-20% Mini-PROTEAN TGX precast protein gel at 100 V and 95 mA for 90 min. Samples were dissolved in PBS (10 µL, 1.37 µM, pH = 7.4), mixed with 2 × Laemmli Sample Buffer (10 µL)[261] and heated at 95 °C for 5 min before loading. Staining was carried out with Coomassie blue

(0.1% *w*/*v* in 1:4:5 acetic acid/water/MeOH for 2 h). Protein markers used were Precision Plus Protein™ Kaleidoscope™ Prestained Protein Standards, 10-250 kDa (Bio-Rad). Bright field and fluorescent images (λ_{ex} = 365 nm, λ_{em} = 520 ± 30 nm) of gels were taken using a Universal Hood II Gel Doc System (Bio-Rad).

Kinetics of Herceptin binding

Binding kinetics were followed by measuring the rate of fluorescence intensity increase in individual cells over time by flow cytometry. An BODIPY-NHS ester[255] (10 eq.) was incubated with Herceptin to give **BODIPY-Her** as a model of the native antibody (details see above). Polymer protein conjugates **P1-Her**, **P2-Her** and **P3-Her** were treated with **Tz1** (10 eq.) to give fluorescent conjugates. The four antibody samples were incubated with SK-BR-3 cells for different time points and the fluorescence intensity recorded by flow cytometry. The fluorescence intensities were normalised to the intensity of saturated cells. Each of the antibody samples was incubated MCF-7 cells as a negative control.

SK-BR-3 cells was seeded in 24 well plates (5×10^4 cells/well in 500 µL DMEM) 24 h prior to the experiments. The BODIPY labelled antibody **BODIPY-Her** (10 nM) and the BODIPY labelled polymer antibody conjugates **BODIPY-P1-Her**, **BODIPY-P2-Her** and **BODIPY-P3-Her** (all at 10 nM) were added to the cells and incubated for different period of time (0.5, 1, 2, 4 and 6 h). The cells were washed with PBS (3 × 1 mL, pH = 7.4), harvested, and the fluorescence intensity was analysed by flow cytometry, Becton Dickinson (BD) FACSAria™, laser excitation at 488 nm and emission filter of 530/30 nm).

Table 30. Kinetics of **BODIPY-Her** binding. Fluorescence intensities were measured using flow cytometry. Fluorescence intensity normalised to the intensity of fluorescence saturated cells (n = 3). Untreated cells were used as a control.

Incubation Time (h)	Fluorescence intensity (a.u.)	Normalised fluorescence intensity
0.5 (untreated cells)	4 ± 0	-
4 (untreated cells)	4 ± 0	-
0.5	22 ± 1	0.88 ± 0.02
1	24 ± 1	0.95 ± 0.03
2	26 ± 1	1.01 ± 0.04
4	25 ± 0	0.98 ± 0.01
6	26 ± 0	1.00 ± 0.00

Table 31. Kinetics of **P1-Her** binding. Fluorescence intensities were measured using flow cytometry. Fluorescence intensity normalised to the intensity of fluorescence saturated cells (n = 3).

Incubation Time (h)	Fluorescence intensity (a.u.)	Normalised fluorescence intensity
0.5	850 ± 50	0.82 ± 0.05
1	920 ± 10	0.88 ± 0.01
2	1010 ± 40	0.97 ± 0.03
4	1070 ± 10	1.03 ± 0.01
6	1040 ± 70	1.00 ± 0.07

Table 32. Kinetics of **P2-Her** binding. Fluorescence intensities were measured using flow cytometry. Fluorescence intensity normalised to the intensity of fluorescence saturated cells (n = 3).

Incubation Time (h)	Fluorescence intensity (a.u.)	Normalised fluorescence intensity
0.5	220 ± 6	0.88 ± 0.02
1	250 ± 5	0.99 ± 0.02
2	260 ± 10	1.01 ± 0.05
4	250 ± 20	0.99 ± 0.09
6	252 ± 0	1.00 ± 0.00

Table 33. Kinetics of **P3-Her** binding. Fluorescence intensities were measured using flow cytometry. Fluorescence intensity normalised to the intensity of fluorescence saturated cells (n = 3).

Incubation Time (h)	Fluorescence intensity (a.u.)	Normalised fluorescence intensity
0.5	1620 ± 10	0.87 ± 0.00
1	1710 ± 30	0.92 ± 0.01
2	1830 ± 50	0.98 ± 0.03
4	1860 ± 20	1.00 ± 0.01
6	1860 ± 20	1.00 ± 0.01

Fluorescence switching on and amplification

SK-BR-3 cells were seeded in 24-well plates (5×10^4 cells/well in 500 µL DMEM) 24 h prior to the experiments. The BODIPY labelled antibody **BODIPY-Her** (10 nM) and the polymer antibody conjugates **P1-Her**, **P2-Her**, **P3-Her**, **P4-Her** and **P5-Her** (10 nM) were added to the cells and incubated for 4 h. The cells were washed with PBS (3 × 1 mL, pH = 7.4) and treated with/without **Tz1** (1 µM) for 30 min before washing with PBS (3 × 1 mL, pH = 7.4). The cells were analysed by flow cytometry (Becton Dickinson (BD) FACSAria™, laser excitation at 488 nm and emission filter of 530/30 nm). For confocal microscopy, the cell nuclei were stained with Hoechst 33342 (blue, $\lambda_{ex/em}$ = 353/483 nm), the plasma membrane stained with CellMask™ Deep Red (red, $\lambda_{ex/em}$ = 649/666 nm) and the cells were imaged using Zeiss LSM 880 Airyscan confcocal microscope with a 40x / 1.3 oil immersion objective.

Table 34. Signal amplification on SK-BR-3 cells. Fluorescence intensities were measured using flow cytometry (n = 3). Untreated cells and **BODIPY-Her** treated cells were used as controls.

Polymer–protein conjugates	**Tz1**	Fluorescence intensity (a.u.)
Untreated cells	No	6 ± 0
Untreated cells	Yes	32 ± 6
BODIPY-Her	No	22 ± 1
BODIPY-Her	Yes	28 ± 2
P1-Her	No	6 ± 0
P1-Her	Yes	1040 ± 50
P2-Her	No	6 ± 0
P2-Her	Yes	250 ± 10
P3-Her	No	7 ± 0
P3-Her	Yes	1860 ± 110
P4-Her	No	6 ± 0
P4-Her	Yes	140 ± 10
P5-Her	No	6 ± 0
P5-Her	Yes	1860 ± 60

Chapter 6. References

1. W. A. Marston, J. Hanft, P. Norwood and R. Pollak, The efficacy and safety of Dermagraft in improving the healing of chronic diabetic foot ulcers: results of a prospective randomized trial, *Diabetes Care*, 2003, **26**, 1701-1705.
2. Organogenesis Inc., *Chronic, stalled wound biology: Adding Dermagraft helps to reestablish the dermal bed*, (http://www.dermagraft.com/composition, 2013).
3. N. H. Attenello and C. S. Maas, Injectable fillers: review of material and properties, *Facial Plast. Surg.*, 2015, **31**, 029-034.
4. Galderma Laboratories L.P., *What Is Sculptra® Aesthetic?*, (https://www.sculptraaesthetic.com/about, 2017).
5. Evonik Nutrition & Care GmbH, *Biomaterials. For pharmaceuticals and medical devices.*, (https://healthcare.evonik.com/product/health-care/en/products/biomaterials/pages/biomaterials.aspx).
6. T. Lammers, F. Kiessling, W. E. Hennink and G. Storm, Drug targeting to tumors: principles, pitfalls and (pre-) clinical progress, *J. Control. Release*, 2012, **161**, 175-187.
7. F. Chen, P. W. Tillberg and E. S. Boyden, Expansion microscopy, *Science*, 2015, **347**, 543-548.
8. A. T. Wassie, Y. Zhao and E. S. Boyden, Expansion microscopy: principles and uses in biological research, *Nat. Methods*, 2018, **16**, 33-41.
9. R. Gao, S. M. Asano, S. Upadhyayula, I. Pisarev, D. E. Milkie, T.-L. Liu, V. Singh, A. Graves, G. H. Huynh, Y. Zhao, B. John, C. Jennifer, M. O. Carolyn, Z. Christopher, T. Susan, R. Alfredo, R. M. Kishore, S. Shu-Hsien, P. H. Amalia, P. Song, X. C. Shan, M. S. G., H. Harald, L.-S. Jennifer, H. Adam, R. G. M., K. Tom, S. Stephan, A. Yoshinori, B. E. S. and B. Eric, Cortical column and whole-brain imaging with molecular contrast and nanoscale resolution, *Science*, 2019, **363**, 8302-8318.
10. E. Abbe, Beiträge zur Theorie des Mikroskops und der mikroskopischen Wahrnehmung, *Archiv für mikroskopische Anatomie*, 1873, **9**, 413-418.
11. B. Huang, H. Babcock and X. Zhuang, Breaking the diffraction barrier: super-resolution imaging of cells, *Cell*, 2010, **143**, 1047-1058.
12. B. Huang, W. Wang, M. Bates and X. Zhuang, Three-dimensional super-resolution imaging by stochastic optical reconstruction microscopy, *Science*, 2008, **319**, 810-813.
13. R. Kellner, C. Baier, K. Willig, S. Hell and F. Barrantes, Nanoscale organization of nicotinic acetylcholine receptors revealed by stimulated emission depletion microscopy, *Neuroscience*, 2007, **144**, 135-143.
14. J. J. Sieber, K. I. Willig, C. Kutzner, C. Gerding-Reimers, B. Harke, G. Donnert, B. Rammner, C. Eggeling, S. W. Hell and H. Grubmüller, Anatomy and dynamics of a supramolecular membrane protein cluster, *Science*, 2007, **317**, 1072-1076.
15. D. Greenfield, A. L. McEvoy, H. Shroff, G. E. Crooks, N. S. Wingreen, E. Betzig and J. Liphardt, Self-organization of the Escherichia coli chemotaxis network imaged with super-resolution light microscopy, *PLoS Biol.*, 2009, **7**, 1-11.

16. Q. Zhou, H. Yan, F. Ran, J. Cao, L. Chen, B. Shang, H. Chen, J. Wei and Q. Chen, Ultrasensitive enzyme-free fluorescent detection of VEGF 165 based on target-triggered hybridization chain reaction amplification, *RSC Adv.*, 2018, **8**, 25955-25960.

17. B. F. Schmidt, J. Chao, Z. Zhu, R. L. DeBiasio and G. Fisher, Signal amplification in the detection of single-copy DNA and RNA by enzyme-catalyzed deposition (CARD) of the novel fluorescent reporter substrate Cy3. 29-tyramide, *J. Histochem. Cytochem.*, 1997, **45**, 365-373.

18. A. G. Walton, *Biopolymers*, Academic Press, 1973.

19. C. S. Tsai, *Biomacromolecules: Introduction to Structure, Function and Informatics*, Wiley, 2007.

20. R. L. Adams, *The biochemistry of the nucleic acids*, Springer Science & Business Media, 2012.

21. T. G. Wolfsberg, J. McEntyre and G. D. Schuler, Guide to the draft human genome, *Nature*, 2001, **409**, 824-826.

22. P. G. Higgs, RNA secondary structure: physical and computational aspects, *Q. Rev. Biophys.*, 2000, **33**, 199-253.

23. T. E. Creighton, *Proteins: structures and molecular properties*, Macmillan, 1993.

24. S. Dumitriu, *Polysaccharides: structural diversity and functional versatility*, CRC press, 2004.

25. D. J. Adams, Fungal cell wall chitinases and glucanases, *Microbiology*, 2004, **150**, 2029-2035.

26. J. A. Prescher and C. R. Bertozzi, Chemistry in living systems, *Nat. Chem. Biol.*, 2005, **1**, 13-21.

27. Y. Zhu, W. Huang, S. S. Lee and W. Xu, Crystal structure of a polyphosphate kinase and its implications for polyphosphate synthesis, *EMBO Rep.*, 2005, **6**, 681-687.

28. B. Kessler and B. Witholt, Factors involved in the regulatory network of polyhydroxyalkanoate metabolism, *J. Biotechnol.*, 2001, **86**, 97-104.

29. R. K. Iha, K. L. Wooley, A. M. Nystrom, D. J. Burke, M. J. Kade and C. J. Hawker, Applications of orthogonal “click” chemistries in the synthesis of functional soft materials, *Chem. Rev.*, 2009, **109**, 5620-5686.

30. J. Venugopal, L. Ma, T. Yong and S. Ramakrishna, In vitro study of smooth muscle cells on polycaprolactone and collagen nanofibrous matrices, *Cell Biol. Int.*, 2005, **29**, 861-867.

31. R. M. Yusop, A. Unciti-Broceta, E. M. Johansson, R. M. Sánchez-Martín and M. Bradley, Palladium-mediated intracellular chemistry, *Nat. Chem.*, 2011, **3**, 239-243.

32. J.-Z. Du, X.-J. Du, C.-Q. Mao and J. Wang, Tailor-made dual pH-sensitive polymer–doxorubicin nanoparticles for efficient anticancer drug delivery, *J. Am. Chem. Soc.*, 2011, **133**, 17560-17563.

33. E. M. Sletten and C. R. Bertozzi, Bioorthogonal chemistry: fishing for selectivity in a sea of functionality, *Angew. Chem. Int. Ed.*, 2009, **48**, 6974-6998.

34. S. Tasoglu and U. Demirci, Bioprinting for stem cell research, *Trends Biotechnol.*, 2013, **31**, 10-19.

35. K. Moharamzadeh, I. Brook and R. Van Noort, Biocompatibility of resin-based dental materials, *Materials*, 2009, **2**, 514-548.

36. X. Cui, K. Breitenkamp, M. Lotz and D. D'Lima, Synergistic action of fibroblast growth factor-2 and transforming growth factor-beta1 enhances bioprinted human neocartilage formation, *Biotechnol. Bioeng.*, 2012, **109**, 2357-2368.

37. T. Grix, A. Ruppelt, A. Thomas, A.-K. Amler, B. P. Noichl, R. Lauster and L. Kloke, Bioprinting Perfusion-Enabled Liver Equivalents for Advanced Organ-on-a-Chip Applications, *Genes*, 2018, **9**, 176-191.

38. G. L. Ying, N. Jiang, S. Maharjan, Y. X. Yin, R. R. Chai, X. Cao, J. Z. Yang, A. K. Miri, S. Hassan and Y. S. Zhang, Aqueous Two-Phase Emulsion Bioink-Enabled 3D Bioprinting of Porous Hydrogels, *Adv. Mater.*, 2018, 5460-5469.

39. Z. Wu, X. Su, Y. Xu, B. Kong, W. Sun and S. Mi, Bioprinting three-dimensional cell-laden tissue constructs with controllable degradation, *Sci. Rep.*, 2016, **6**, 24474-24484.

40. A. P. Zhang, X. Qu, P. Soman, K. C. Hribar, J. W. Lee, S. Chen and S. He, Rapid fabrication of complex 3D extracellular microenvironments by dynamic optical projection stereolithography, *Adv. Mater.*, 2012, **24**, 4266-4270.

41. K. C. Hribar, D. Finlay, X. Ma, X. Qu, M. G. Ondeck, P. H. Chung, F. Zanella, A. J. Engler, F. Sheikh and K. Vuori, Nonlinear 3D projection printing of concave hydrogel microstructures for long-term multicellular spheroid and embryoid body culture, *Lab Chip.*, 2015, **15**, 2412-2418.

42. S. Suri, L.-H. Han, W. Zhang, A. Singh, S. Chen and C. E. Schmidt, Solid freeform fabrication of designer scaffolds of hyaluronic acid for nerve tissue engineering, *Biomed. Microdevices*, 2011, **13**, 983-993.

43. X. Ma, X. Qu, W. Zhu, Y.-S. Li, S. Yuan, H. Zhang, J. Liu, P. Wang, C. S. E. Lai and F. Zanella, Deterministically patterned biomimetic human iPSC-derived hepatic model via rapid 3D bioprinting, *Proc. Natl. Acad. Sci.*, 2016, **113**, 2206-2211.

44. P. Soman, P. H. Chung, A. P. Zhang and S. Chen, Digital microfabrication of user-defined 3D microstructures in cell-laden hydrogels, *Biotechnol. Bioeng.*, 2013, **110**, 3038-3047.

45. C. Cha, P. Soman, W. Zhu, M. Nikkhah, G. Camci-Unal, S. Chen and A. Khademhosseini, Structural reinforcement of cell-laden hydrogels with microfabricated three dimensional scaffolds, *Biomater. Sci.*, 2014, **2**, 703-709.

46. W. Zhu, X. Ma, M. Gou, D. Mei, K. Zhang and S. Chen, 3D printing of functional biomaterials for tissue engineering, *Curr. Opin. Biotechnol.*, 2016, **40**, 103-112.

47. J. Yang, J. Li, X. Li, X. Wang, Y. Yang, N. Kawazoe and G. Chen, Nanoencapsulation of individual mammalian cells with cytoprotective polymer shell, *Biomaterials*, 2017, **133**, 253-262.

48. S. H. Yang, S. M. Kang, K.-B. Lee, T. D. Chung, H. Lee and I. S. Choi, Mussel-inspired encapsulation and functionalization of individual yeast cells, *J. Am. Chem. Soc.*, 2011, **133**, 2795-2797.

49. P. De Vos, A. Hamel and K. Tatarkiewicz, Considerations for successful transplantation of encapsulated pancreatic islets, *Diabetologia*, 2002, **45**, 159-173.

50. H. Iwata, H. Amemiya, T. Matsuda, H. Takano, R. Hayashi and T. Akutsu, Evaluation of microencapsulated islets in agarose gel as bioartificial pancreas by studies of hormone secretion in culture and by xenotransplantation, *Diabetes*, 1989, **38**, 224-225.

51. G. M. Cruise, O. D. Hegre, F. V. Lamberti, S. R. Hager, R. Hill, D. S. Scharp and J. A. Hubbell, In vitro and in vivo performance of porcine islets encapsulated in interfacially photopolymerized poly (ethylene glycol) diacrylate membranes, *Cell Transplant.*, 1999, **8**, 293-306.

52. F. Lim and A. M. Sun, Microencapsulated islets as bioartificial endocrine pancreas, *Science*, 1980, **210**, 908-910.

53. T. M. S. Chang, Therapeutic applications of polymeric artificial cells, *Nature Reviews Drug Discovery*, 2005, **4**, 221.

54. J. Niu, D. J. Lunn, A. Pusuluri, J. I. Yoo, M. A. O'Malley, S. Mitragotri, H. T. Soh and C. J. Hawker, Engineering live cell surfaces with functional polymers via cytocompatible controlled radical polymerization, *Nat. Chem.*, 2017, **9**, 537-545.

55. J. Y. Kim, B. S. Lee, J. Choi, B. J. Kim, J. Y. Choi, S. M. Kang, S. H. Yang and I. S. Choi, Cytocompatible Polymer Grafting from Individual Living Cells by Atom-Transfer Radical Polymerization, *Angew. Chem. Int. Ed.*, 2016, **55**, 15306-15309.

56. E. P. Magennis, F. Fernandez-Trillo, C. Sui, S. G. Spain, D. J. Bradshaw, D. Churchley, G. Mantovani, K. Winzer and C. Alexander, Bacteria-instructed synthesis of polymers for self-selective microbial binding and labelling, *Nat. Mater.*, 2014, **13**, 748-755.

57. T. Davis, D. Haddleton and S. Richards, Controlled polymerization of acrylates and methacrylates, *J. Macromol. Sci. Rev., Macromol. Chem. Phys.*, 1994, **34**, 243-324.

58. W. A. Braunecker and K. Matyjaszewski, Controlled/living radical polymerization: Features, developments, and perspectives, *Prog. Polym. Sci.*, 2007, **32**, 93-146.

59. Y. Issa, D. Watts, P. Brunton, C. Waters and A. Duxbury, Resin composite monomers alter MTT and LDH activity of human gingival fibroblasts in vitro, *Dent. Mater.*, 2004, **20**, 12-20.

60. H. Schweikl, G. Spagnuolo and G. Schmalz, Genetic and cellular toxicology of dental resin monomers, *J. Dent. Res.*, 2006, **85**, 870-877.

61. G. Müller, M. Zalibera, G. Gescheidt, A. Rosenthal, G. Santiso-Quinones, K. Dietliker and H. Grützmacher, Simple One-Pot Syntheses of Water-Soluble Bis (acyl) phosphane Oxide Photoinitiators and Their Application in Surfactant-Free Emulsion Polymerization, *Macromol. Rapid Commun.*, 2015, **36**, 553-557.

62. N. E. Fedorovich, M. H. Oudshoorn, D. van Geemen, W. E. Hennink, J. Alblas and W. J. Dhert, The effect of photopolymerization on stem cells embedded in hydrogels, *Biomaterials*, 2009, **30**, 344-353.

63. C. G. Williams, A. N. Malik, T. K. Kim, P. N. Manson and J. H. Elisseeff, Variable cytocompatibility of six cell lines with photoinitiators used for polymerizing hydrogels and cell encapsulation, *Biomaterials*, 2005, **26**, 1211-1218.

64. J. Wang, S. Stanic, A. A. Altun, M. Schwentenwein, K. Dietliker, L. Jin, J. Stampfl, S. Baudis, R. Liska and H. Grützmacher, A highly efficient waterborne photoinitiator for visible-light-induced three-dimensional printing of hydrogels, *Chem. Commun.*, 2018, **54**, 920-923.

65. S. J. Bryant, C. R. Nuttelman and K. S. Anseth, Cytocompatibility of UV and visible light photoinitiating systems on cultured NIH/3T3 fibroblasts in vitro, *J. Biomater. Sci. Polym. Ed.*, 2000, **11**, 439-457.

66. A. M. Luciani, A. Rosi, P. Matarrese, G. Arancia, L. Guidoni and V. Viti, Changes in cell volume and internal sodium concentration in HeLa cells during exponential growth and following lonidamine treatment, *Eur. J. Cell Biol.*, 2001, **80**, 187-195.

67. S.-I. Choi, J. S. Lee, S. Lee, J.-H. Lee, H.-S. Yang, J. Yeo, J.-Y. Kim, B.-Y. Lee, I.-J. Kang and O.-H. Lee, Radical scavenging-linked anti-adipogenic activity of Alnus firma extracts, *Int. J. Mol. Med.*, 2018, **41**, 119-128.

68. D. Armstrong, *Advanced protocols in oxidative stress II*, Springer, 2010.

69. S. Aleksanian, B. Khorsand, R. Schmidt and J. K. Oh, Rapidly thiol-responsive degradable block copolymer nanocarriers with facile bioconjugation, *Polym. Chem.*, 2012, **3**, 2138-2147.

70. K. H. Kim and J. M. Sederstrom, Assaying cell cycle status using flow cytometry, *Curr. Protoc. Mol. Biol.*, 2015, **111**, 1-11.

71. W. P. Roos and B. Kaina, DNA damage-induced cell death by apoptosis, *Trends Mol. Med.*, 2006, **12**, 440-450.

72. J. D. Hood and D. A. Cheresh, Role of integrins in cell invasion and migration, *Nat. Rev. Cancer*, 2002, **2**, 91-100.

73. A. J. Ridley, M. A. Schwartz, K. Burridge, R. A. Firtel, M. H. Ginsberg, G. Borisy, J. T. Parsons and A. R. Horwitz, Cell migration: integrating signals from front to back, *Science*, 2003, **302**, 1704-1709.

74. D. Mizuno, C. Tardin, C. F. Schmidt and F. C. MacKintosh, Nonequilibrium mechanics of active cytoskeletal networks, *Science*, 2007, **315**, 370-373.

75. P. Roca-Cusachs, V. Conte and X. Trepat, Quantifying forces in cell biology, *Nat. Cell Biol.*, 2017, **19**, 742-751.

76. S. Tommasi, A. Mangia, R. Lacalamita, A. Bellizzi, V. Fedele, A. Chiriatti, C. Thomssen, N. Kendzierski, A. Latorre and V. Lorusso, Cytoskeleton and paclitaxel sensitivity in breast cancer: the role of β-tubulins, *Int. J. Cancer*, 2007, **120**, 2078-2085.

77. M. Tamura, J. Gu, K. Matsumoto, S.-i. Aota, R. Parsons and K. M. Yamada, Inhibition of cell migration, spreading, and focal adhesions by tumor suppressor PTEN, *Science*, 1998, **280**, 1614-1617.

78. K. Rottner and T. E. Stradal, Actin dynamics and turnover in cell motility, *Curr. Opin. Cell Biol.*, 2011, **23**, 569-578.

79. M. G. Poirier and J. F. Marko, Effect of internal friction on biofilament dynamics, *Phys. Rev. Lett.*, 2002, **88**, 1-4.

80. E. Blotnick, A. Sol and A. Muhlrad, Histones bundle F-actin filaments and affect actin structure, *PLoS One*, 2017, **12**, 1-18.

81. D. R. Talbert, K. R. Doherty, P. B. Trusk, D. M. Moran, S. A. Shell and S. Bacus, A multi-parameter in vitro screen in human stem cell-derived cardiomyocytes identifies ponatinib-induced structural and functional cardiac toxicity, *Toxicol. Sci.*, 2014, **143**, 147-155.

82. D. Riveline and P. Nurse, 'Injecting'yeast, *Nat. Methods*, 2009, **6**, 513-515.

83. J. Tremoleda, E. Schoevers, T. Stout, B. Colenbrander and M. Bevers, Organisation of the cytoskeleton during in vitro maturation of horse oocytes, *Mol. Reprod. Dev.*, 2001, **60**, 260-269.

84. A. Boudaoud, A. Burian, D. Borowska-Wykręt, M. Uyttewaal, R. Wrzalik, D. Kwiatkowska and O. Hamant, FibrilTool, an ImageJ plug-in to quantify fibrillar structures in raw microscopy images, *Nat. Protoc.*, 2014, **9**, 457-463.

85. M. E. Tanenbaum, L. A. Gilbert, L. S. Qi, J. S. Weissman and R. D. Vale, A protein-tagging system for signal amplification in gene expression and fluorescence imaging, *Cell*, 2014, **159**, 635-646.

86. R. Weissleder and M. J. Pittet, Imaging in the era of molecular oncology, *Nature*, 2008, **452**, 580-589.

87. J. Zhang, R. E. Campbell, A. Y. Ting and R. Y. Tsien, Creating new fluorescent probes for cell biology, *Nat. Rev. Mol. Cell Biol.*, 2002, **3**, 906-918.

88. D. Duret, Z. Haftek-Terreau, M. Carretier, T. Berki, C. Ladavière, K. Monier, P. Bouvet, J. Marvel, Y. Leverrier, M.-T. Charreyre and A. Favier, Labeling of native proteins with fluorescent RAFT polymer probes: application to the detection of a cell surface protein using flow cytometry, *Polym. Chem.*, 2018, **9**, 1857-1868.

89. Z. Wang, S. Chen, J. W. Lam, W. Qin, R. T. Kwok, N. Xie, Q. Hu and B. Z. Tang, Long-term fluorescent cellular tracing by the aggregates of AIE bioconjugates, *J. Am. Chem. Soc.*, 2013, **135**, 8238-8245.

90. M. D. Major and J. M. Torkelson, Fluorescence of vinyl aromatic polyelectrolytes: effects of conformation, concentration, and molecular weight of sodium poly (styrene sulfonate), *Macromolecules*, 1986, **19**, 2801-2806.

91. J. J. Yan, Z. K. Wang, X. S. Lin, C. Y. Hong, H. J. Liang, C. Y. Pan and Y. Z. You, Polymerizing nonfluorescent monomers without incorporating any fluorescent agent produces strong fluorescent polymers, *Adv. Mater.*, 2012, **24**, 5617-5624.

92. J. Bridges and R. Williams, The fluorescence of indoles and aniline derivatives, *Biochem. J.*, 1968, **107**, 225-237.

93. L. E. Gerweck and K. Seetharaman, Cellular pH gradient in tumor versus normal tissue: potential exploitation for the treatment of cancer, *Cancer Res.*, 1996, **56**, 1194-1198.

94. D. E. Johnson, P. Ostrowski, V. Jaumouillé and S. Grinstein, The position of lysosomes within the cell determines their luminal pH, *J. Cell Biol.*, 2016, **212**, 677-692.

95. C. Wang, M. Podgórski and C. N. Bowman, Monodisperse functional microspheres from step-growth "click" polymerizations: preparation, functionalization and implementation, *Mater. Horiz.*, 2014, **1**, 535-539.

96. K. Kumar, G. Vulugundam, P. Kondaiah and S. Bhattacharya, Co-liposomes of redox-active alkyl-ferrocene modified low MW branched PEI and DOPE for efficacious gene delivery in serum, *J. Mater. Chem. B*, 2015, **3**, 2318-2330.

97. R. Vankayala, P. Kalluru, H.-H. Tsai, C.-S. Chiang and K. C. Hwang, Effects of surface functionality of carbon nanomaterials on short-term cytotoxicity and embryonic development in zebrafish, *J. Mater. Chem. B*, 2014, **2**, 1038-1047.

98. S. Chen, J. Lu, C. Sun and H. Ma, A highly specific ferrocene-based fluorescent probe for hypochlorous acid and its application to cell imaging, *Analyst*, 2010, **135**, 577-582.

99. T. K. Goswami, S. Gadadhar, M. Roy, M. Nethaji, A. A. Karande and A. R. Chakravarty, Ferrocene-conjugated copper (II) complexes of L-methionine and phenanthroline bases: Synthesis, structure, and photocytotoxic activity, *Organometallics*, 2012, **31**, 3010-3021.

100. M. F. Refojo, Hydrophobic interaction in poly (2-hydroxyethyl methacrylate) homogeneous hydrogel, *J. Polym. Sci., Part A: Polym. Chem.*, 1967, **5**, 3103-3113.

101. A. Blanazs, A. Ryan and S. Armes, Predictive phase diagrams for RAFT aqueous dispersion polymerization: effect of block copolymer composition, molecular weight, and copolymer concentration, *Macromolecules*, 2012, **45**, 5099-5107.

102. J. Zhang, R. E. Campbell, A. Y. Ting and R. Y. Tsien, Creating new fluorescent probes for cell biology, *Nat. Rev. Mol. Cell Biol.*, 2002, **3**, 906-918.

103. N. K. Devaraj, R. Upadhyay, J. B. Haun, S. A. Hilderbrand and R. Weissleder, Fast and sensitive pretargeted labeling of cancer cells through a tetrazine/trans-cyclooctene cycloaddition, *Angew. Chem.*, 2009, **121**, 7147-7150.

104. J. B. Haun, N. K. Devaraj, S. A. Hilderbrand, H. Lee and R. Weissleder, Bioorthogonal chemistry amplifies nanoparticle binding and enhances the sensitivity of cell detection, *Nat. Nanotechnol.*, 2010, **5**, 660-665.

105. D. Ding, K. Li, W. Qin, R. Zhan, Y. Hu, J. Liu, B. Z. Tang and B. Liu, Conjugated polymer amplified far-red/near-infrared fluorescence from nanoparticles with aggregation-induced emission characteristics for targeted in vivo imaging, *Adv. Healthc. Mater.*, 2013, **2**, 500-507.

106. F. Feng, F. He, L. An, S. Wang, Y. Li and D. Zhu, Fluorescent conjugated polyelectrolytes for biomacromolecule detection, *Adv. Mater.*, 2008, **20**, 2959-2964.

107. S. W. Thomas, G. D. Joly and T. M. Swager, Chemical sensors based on amplifying fluorescent conjugated polymers, *Chem. Rev.*, 2007, **107**, 1339-1386.

108. A. Y. Yong, S. Shabahang, T. M. Timiryasova, Q. Zhang, R. Beltz, I. Gentschev, W. Goebel and A. A. Szalay, Visualization of tumors and metastases in live animals with bacteria and vaccinia virus encoding light-emitting proteins, *Nat. Biotechnol.*, 2004, **22**, 313-320.

109. R. K. Saiki, T. L. Bugawan, G. T. Horn, K. B. Mullis and H. A. Erlich, Analysis of enzymatically amplified β-globin and HLA-DQα DNA with allele-specific oligonucleotide probes, *Nature*, 1986, **324**, 163-166.

110. S. J. Scharf, G. T. Horn and H. A. Erlich, Direct cloning and sequence analysis of enzymatically amplified genomic sequences, *Science*, 1986, **233**, 1076-1078.

111. R. Steffan and R. Atlas, Polymerase chain reaction: applications in environmental microbiology, *Annu. Rev. Microbiol.*, 1991, **45**, 137-161.

112. B. Schweitzer and S. Kingsmore, Combining nucleic acid amplification and detection, *Curr. Opin. Biotechnol.*, 2001, **12**, 21-27.

113. Y.-J. Jeong, K. Park and D.-E. Kim, Isothermal DNA amplification in vitro: the helicase-dependent amplification system, *Cell. Mol. Life Sci.*, 2009, **66**, 3325-3336.

114. G. T. Walker, M. S. Fraiser, J. L. Schram, M. C. Little, J. G. Nadeau and D. P. Malinowski, Strand displacement amplification—an isothermal, in vitro DNA amplification technique, *Nucleic Acids Res.*, 1992, **20**, 1691-1696.

115. A. Fire and S.-Q. Xu, Rolling replication of short DNA circles, *Proc. Natl. Acad. Sci.*, 1995, **92**, 4641-4645.

116. M. Liu, C. Y. Hui, Q. Zhang, J. Gu, B. Kannan, S. Jahanshahi-Anbuhi, C. D. Filipe, J. D. Brennan and Y. Li, Target-induced and equipment-free DNA amplification with a simple paper device, *Angew. Chem.*, 2016, **128**, 2759-2763.

117. Q. Xue, Z. Wang, L. Wang and W. Jiang, Sensitive detection of proteins using assembled cascade fluorescent DNA nanotags based on rolling circle amplification, *Bioconjug. Chem.*, 2012, **23**, 734-739.

118. M. Vincent, Y. Xu and H. Kong, Helicase-dependent isothermal DNA amplification, *EMBO Rep.*, 2004, **5**, 795-800.

119. R. M. Dirks and N. A. Pierce, Triggered amplification by hybridization chain reaction, *Proceedings of the National Academy of Sciences*, 2004, **101**, 15275-15278.

120. C. R. Park, S. J. Park, W. G. Lee and B. H. Hwang, Biosensors Using Hybridization Chain Reaction-Design and Signal Amplification Strategies of Hybridization Chain Reaction, *Biotechnol. Bioprocess Eng.*, 2018, **23**, 355-370.

121. S. Bi, S. Yue and S. Zhang, Hybridization chain reaction: a versatile molecular tool for biosensing, bioimaging, and biomedicine, *Chem. Soc. Rev.*, 2017, **46**, 4281-4298.

122. S. Bi, M. Chen, X. Jia, Y. Dong and Z. Wang, Hyperbranched hybridization chain reaction for triggered signal amplification and concatenated logic circuits, *Angew. Chem. Int. Ed.*, 2015, **54**, 8144-8148.

123. P. Liu, X. Yang, S. Sun, Q. Wang, K. Wang, J. Huang, J. Liu and L. He, Enzyme-free colorimetric detection of DNA by using gold nanoparticles and hybridization chain reaction amplification, *Anal. Chem.*, 2013, **85**, 7689-7695.

124. T. Hou, W. Li, X. Liu and F. Li, Label-free and enzyme-free homogeneous electrochemical biosensing strategy based on hybridization chain reaction: A facile, sensitive, and highly specific microRNA assay, *Anal. Chem.*, 2015, **87**, 11368-11374.

125. H. Kerstens, P. J. Poddighe and A. Hanselaar, A novel in situ hybridization signal amplification method based on the deposition of biotinylated tyramine, *J. Histochem. Cytochem.*, 1995, **43**, 347-352.

126. E. C. Stack, C. Wang, K. A. Roman and C. C. Hoyt, Multiplexed immunohistochemistry, imaging, and quantitation: a review, with an assessment of Tyramide signal amplification, multispectral imaging and multiplex analysis, *Methods*, 2014, **70**, 46-58.

127. V. B. Paragas, Y.-Z. Zhang, R. P. Haugland and V. L. Singer, The ELF-97 alkaline phosphatase substrate provides a bright, photostable, fluorescent signal amplification method for FISH, *J. Histochem. Cytochem.*, 1997, **45**, 345-357.

128. A. Pernthaler, J. Pernthaler and R. Amann, Fluorescence in situ hybridization and catalyzed reporter deposition for the identification of marine bacteria, *Appl. Environ. Microbiol.*, 2002, **68**, 3094-3101.

129. I. Buchwalow, V. Samoilova, W. Boecker and M. Tiemann, Multiple immunolabeling with antibodies from the same host species in combination with tyramide signal amplification, *Acta Histochem.*, 2018, **12**, 405-414.

130. M. P. van de Corput, R. W. Dirks, R. P. van Gijlswijk, E. Van Binnendijk, C. M. Hattinger, R. A. De Paus, J. E. Landegent and A. K. Raap, Sensitive mRNA detection by fluorescence in situ hybridization using horseradish peroxidase-labeled oligodeoxynucleotides and tyramide signal amplification, *J. Histochem. Cytochem.*, 1998, **46**, 1249-1259.

131. D. Kosman, C. M. Mizutani, D. Lemons, W. G. Cox, W. McGinnis and E. Bier, Multiplex detection of RNA expression in Drosophila embryos, *Science*, 2004, **305**, 846-846.

132. B. Navarro-Domínguez, F. J. Ruiz-Ruano, J. P. M. Camacho, J. Cabrero and M. D. López-León, Transcription of a B chromosome CAP-G pseudogene does not influence normal Condensin Complex genes in a grasshopper, *Sci. Rep.*, 2017, **7**, 17650-17666.

133. J. Li, S. Schachermeyer, Y. Wang, Y. Yin and W. Zhong, Detection of microRNA by fluorescence amplification based on cation-exchange in nanocrystals, *Anal. Chem.*, 2009, **81**, 9723-9729.

134. Q. Xi, D.-M. Zhou, Y.-Y. Kan, J. Ge, Z.-K. Wu, R.-Q. Yu and J.-H. Jiang, Highly sensitive and selective strategy for microRNA detection based on WS2 nanosheet mediated fluorescence quenching and duplex-specific nuclease signal amplification, *Anal. Chem.*, 2014, **86**, 1361-1365.

135. Y. Wang and B. Liu, Silica nanoparticle assisted DNA assays for optical signal amplification of conjugated polymer based fluorescent sensors, *Chem. Commun.*, 2007, 3553-3555.

136. D. Ding, K. Li, W. Qin, R. Zhan, Y. Hu, J. Liu, B. Z. Tang and B. Liu, Conjugated polymer amplified far-red/near-infrared fluorescence from nanoparticles with aggregation-induced emission characteristics for targeted in vivo imaging, *Adv. Healthc. Mater.*, 2013, **2**, 500-507.

137. L. Zhang, W. Zhao, X. Liu, G. Wang, Y. Wang, D. Li, L. Xie, Y. Gao, H. Deng and W. Gao, Site-selective in situ growth of fluorescent polymer–antibody conjugates with enhanced antigen detection by signal amplification, *Biomaterials*, 2015, **64**, 2-9.

138. B. E. Cook, R. Membreno and B. M. Zeglis, Dendrimer scaffold for the amplification of in vivo pretargeting ligations, *Bioconjug. Chem.*, 2018, **29**, 2734-2740.

139. J. Coller and M. Wickens, *Tethered function assays: an adaptable approach to study RNA regulatory proteins*, Elsevier, 2007.

140. E. Bertrand, P. Chartrand, M. Schaefer, S. M. Shenoy, R. H. Singer and R. M. Long, Localization of ASH1 mRNA particles in living yeast, *Mol. Cell*, 1998, **2**, 437-445.

141. C. Wang, B. Han, R. Zhou and X. Zhuang, Real-time imaging of translation on single mRNA transcripts in live cells, *Cell*, 2016, **165**, 990-1001.

142. X. Liu, L. Ouyang, X. Cai, Y. Huang, X. Feng, Q. Fan and W. Huang, An ultrasensitive label-free biosensor for assaying of sequence-specific DNA-binding protein based on amplifying fluorescent conjugated polymer, *Biosens. Bioelectron.*, 2013, **41**, 218-224.

143. M. Ternon and M. Bradley, Assay amplification-multiple valent fluorophores, *Chem. Commun.*, 2003, 2402-2403.

144. M. Ternon, J. J. Díaz-Mochón, A. Belsom and M. Bradley, Dendrimers and combinatorial chemistry—tools for fluorescent enhancement in protease assays, *Tetrahedron*, 2004, **60**, 8721-8728.

145. J. M. Ellard, T. Zollitsch, W. J. Cummins, A. L. Hamilton and M. Bradley, Fluorescence enhancement through enzymatic cleavage of internally quenched dendritic peptides: A sensitive assay for the AspN endoproteinase, *Angew. Chem.*, 2002, **114**, 3367-3370.

146. G. Wolters, L. Kuijpers, J. Kacaki and A. Schuurs, Enzyme-immunoassay for HbsAg, *The Lancet*, 1976, **308**, 690-690.

147. S. K. Vashist and J. H. Luong, *Enzyme-Linked Immunoassays*, Elsevier, 2018.

148. S. Y. Toh, M. Citartan, S. C. Gopinath and T.-H. Tang, Aptamers as a replacement for antibodies in enzyme-linked immunosorbent assay, *Biosens. Bioelectron.*, 2015, **64**, 392-403.

149. H. Fukata, H. Miyagawa, N. Yamazaki and C. Mori, Comparison of ELISA-and LC-MS-based methodologies for the exposure assessment of bisphenol A, *Toxicol. Mech. Methods*, 2006, **16**, 427-430.

150. R. Nagarkatti, F. F. de Araujo, C. Gupta and A. Debrabant, Aptamer based, non-PCR, non-serological detection of Chagas disease biomarkers in Trypanosoma cruzi infected mice, *PLoS Negl. Trop. Dis.*, 2014, **8**, 1-10.

151. T. He, Y. Wang, P. Li, Q. Zhang, J. Lei, Z. Zhang, X. Ding, H. Zhou and W. Zhang, Nanobody-based enzyme immunoassay for aflatoxin in agro-products with high tolerance to cosolvent methanol, *Anal. Chem.*, 2014, **86**, 8873-8880.

152. Z. Wu, W.-J. Guo, Y.-Y. Bai, L. Zhang, J. Hu, D.-W. Pang and Z.-L. Zhang, Digital Single Virus Electrochemical Enzyme-Linked Immunoassay for Ultrasensitive H7N9 Avian Influenza Virus Counting, *Anal. Chem.*, 2018, **90**, 1683-1690.

153. J. Wu, Y. Xianyu, X. Wang, D. Hu, Z. Zhao, N. Lu, M. Xie, H. Lei and Y. Chen, Enzyme-Free Amplification Strategy for Biosensing Using Fe3+–Poly (glutamic acid) Coordination Chemistry, *Anal. Chem.*, 2018, **90**, 4725-4732.

154. B. Leader, Q. J. Baca and D. E. Golan, Protein therapeutics: a summary and pharmacological classification, *Nat. Rev. Drug Discov.*, 2008, **7**, 21-39.

155. S. J. Benkovic and S. Hammes-Schiffer, A perspective on enzyme catalysis, *Science*, 2003, **301**, 1196-1202.

156. W. Zhao, F. Liu, Y. Chen, J. Bai and W. Gao, Synthesis of well-defined protein–polymer conjugates for biomedicine, *Polymer*, 2015, **66**, 1-10.

157. A. Abuchowski, T. Van Es, N. Palczuk and F. Davis, Alteration of immunological properties of bovine serum albumin by covalent attachment of polyethylene glycol, *J. Biol. Chem.*, 1977, **252**, 3578-3581.

158. Y. Wang and C. Wu, Site-specific conjugation of polymers to proteins, *Biomacromolecules*, 2018, **19**, 1804-1825.

159. K. L. Heredia and H. D. Maynard, Synthesis of protein–polymer conjugates, *Org. Biomol. Chem.*, 2006, **5**, 45-53.

160. S. L. Kuan, Y. Wu and T. Weil, Precision biopolymers from protein precursors for biomedical applications, *Macromol. Rapid Commun.*, 2013, **34**, 380-392.

161. C. Boyer, X. Huang, M. R. Whittaker, V. Bulmus and T. P. Davis, An overview of protein–polymer particles, *Soft Matter*, 2011, **7**, 1599-1614.

162. E. M. Pelegri-O'Day, E.-W. Lin and H. D. Maynard, Therapeutic protein–polymer conjugates: advancing beyond PEGylation, *J. Am. Chem. Soc.*, 2014, **136**, 14323-14332.

163. R. Duncan, The dawning era of polymer therapeutics, *Nat. Rev. Drug Discov.*, 2003, **2**, 347-360.

164. A. N. Zelikin, C. Ehrhardt and A. M. Healy, Materials and methods for delivery of biological drugs, *Nat. Chem.*, 2016, **8**, 997-1007.

165. I. Cobo, M. Li, B. S. Sumerlin and S. Perrier, Smart hybrid materials by conjugation of responsive polymers to biomacromolecules, *Nat. Mater.*, 2015, **14**, 143-159.

166. K. L. Heredia, D. Bontempo, T. Ly, J. T. Byers, S. Halstenberg and H. D. Maynard, In situ preparation of protein−"smart" polymer conjugates with retention of bioactivity, *J. Am. Chem. Soc.*, 2005, **127**, 16955-16960.

167. D. Bontempo and H. D. Maynard, Streptavidin as a macroinitiator for polymerization: in situ protein− polymer conjugate formation, *J. Am. Chem. Soc.*, 2005, **127**, 6508-6509.

168. B. S. Lele, H. Murata, K. Matyjaszewski and A. J. Russell, Synthesis of uniform protein−polymer conjugates, *Biomacromolecules*, 2005, **6**, 3380-3387.

169. H. Li, M. Li, X. Yu, A. P. Bapat and B. S. Sumerlin, Block copolymer conjugates prepared by sequentially grafting from proteins via RAFT, *Polym. Chem.*, 2011, **2**, 1531-1535.

170. J. Liu, V. Bulmus, D. L. Herlambang, C. Barner-Kowollik, M. H. Stenzel and T. P. Davis, In situ formation of protein–polymer conjugates through reversible addition fragmentation chain transfer polymerization, *Angew. Chem. Int. Ed.*, 2007, **46**, 3099-3103.

171. P. De, M. Li, S. R. Gondi and B. S. Sumerlin, Temperature-regulated activity of responsive polymer− protein conjugates prepared by grafting-from via RAFT polymerization, *J. Am. Chem. Soc.*, 2008, **130**, 11288-11289.

172. F. Xu, K. Neoh and E. Kang, Bioactive surfaces and biomaterials via atom transfer radical polymerization, *Prog. Polym. Sci.*, 2009, **34**, 719-761.

173. D. Bontempo, R. C. Li, T. Ly, C. E. Brubaker and H. D. Maynard, One-step synthesis of low polydispersity, biotinylated poly (N-isopropylacrylamide) by ATRP, *Chem. Commun.*, 2005, 4702-4704.

174. C. Boyer, V. Bulmus, J. Liu, T. P. Davis, M. H. Stenzel and C. Barner-Kowollik, Well-defined protein− polymer conjugates via in situ RAFT polymerization, *J. Am. Chem. Soc.*, 2007, **129**, 7145-7154.

175. O. Kinstler, G. Molineux, M. Treuheit, D. Ladd and C. Gegg, Mono-N-terminal poly (ethylene glycol)–protein conjugates, *Adv. Drug Del. Rev.*, 2002, **54**, 477-485.

176. M. Kato, M. Kamigaito, M. Sawamoto and T. Higashimura, Polymerization of methyl methacrylate with the carbon tetrachloride/dichlorotris-(triphenylphosphine) ruthenium (II)/methylaluminum bis (2, 6-di-tert-butylphenoxide) initiating system: possibility of living radical polymerization, *Macromolecules*, 1995, **28**, 1721-1723.

177. J. Chiefari, Y. Chong, F. Ercole, J. Krstina, J. Jeffery, T. P. Le, R. T. Mayadunne, G. F. Meijs, C. L. Moad and G. Moad, Living free-radical polymerization by reversible addition− fragmentation chain transfer: the RAFT process, *Macromolecules*, 1998, **31**, 5559-5562.

178. S. Carmali, H. Murata, K. Matyjaszewski and A. J. Russell, Tailoring Site Specificity of Bioconjugation Using Step-Wise Atom-Transfer Radical Polymerization on Proteins, *Biomacromolecules*, 2018, **19**, 4044-4051.

179. S. L. Baker, A. Munasinghe, H. Murata, P. Lin, K. Matyjaszewski, C. M. Colina and A. J. Russell, Intramolecular Interactions of Conjugated Polymers Mimic Molecular Chaperones to Stabilize Protein–Polymer Conjugates, *Biomacromolecules*, 2018, **19**, 3798-3813.

180. C. L. McCormick, B. S. Sumerlin, B. S. Lokitz and J. E. Stempka, RAFT-synthesized diblock and triblock copolymers: thermally-induced supramolecular assembly in aqueous media, *Soft Matter*, 2008, **4**, 1760-1773.

181. S. Dehn, V. Castelletto, I. W. Hamley and S. b. Perrier, Altering peptide fibrillization by polymer conjugation, *Biomacromolecules*, 2012, **13**, 2739-2747.

182. J. Hentschel, K. Bleek, O. Ernst, J.-F. Lutz and H. G. Börner, Easy access to bioactive peptide− polymer conjugates via RAFT, *Macromolecules*, 2008, **41**, 1073-1075.

183. C. Chen, F. Kong, X. Wei and S. H. Thang, Syntheses and effectiveness of functional peptide-based RAFT agents, *Chem. Commun.*, 2017, **53**, 10776-10779.

184. A. Abuchowski, J. R. McCoy, N. C. Palczuk, T. van Es and F. F. Davis, Effect of covalent attachment of polyethylene glycol on immunogenicity and circulating life of bovine liver catalase, *J. Biol. Chem.*, 1977, **252**, 3582-3586.

185. P. J. Trainer, W. M. Drake, L. Katznelson, P. U. Freda, V. Herman-Bonert, A.-J. van der Lely, E. V. Dimaraki, P. M. Stewart, K. E. Friend and M. L. Vance, Treatment of

acromegaly with the growth hormone–receptor antagonist pegvisomant, *New Engl. J. Med.*, 2000, **342**, 1171-1177.

186. M. L. Graham, Pegaspargase: a review of clinical studies, *Adv. Drug Del. Rev.*, 2003, **55**, 1293-1302.

187. J. P. Chen, H. J. Yang and A. S. Huffman, Polymer-protein conjugates: I. Effect of protein conjugation on the cloud point of poly (N-isopropylacrylamide), *Biomaterials*, 1990, **11**, 625-630.

188. Z. Ding, G. Chen and A. S. Hoffman, Unusual properties of thermally sensitive oligomer–enzyme conjugates of poly (N-isopropylacrylamide)–trypsin, *J. Biomed. Mater. Res.*, 1998, **39**, 498-505.

189. P. Theato, J.-U. Kim and J.-C. Lee, Controlled radical polymerization of active ester monomers: Precursor polymers for highly functionalized materials, *Macromolecules*, 2004, **37**, 5475-5478.

190. K. T. Wiss, O. D. Krishna, P. J. Roth, K. L. Kiick and P. Theato, A versatile grafting-to approach for the bioconjugation of polymers to collagen-like peptides using an activated ester chain transfer agent, *Macromolecules*, 2009, **42**, 3860-3863.

191. D. Roy, B. J. Nehilla, J. J. Lai and P. S. Stayton, Stimuli-responsive polymer-antibody conjugates via RAFT and tetrafluorophenyl active ester chemistry, *ACS Macro Lett.*, 2013, **2**, 132-136.

192. P. S. Stayton, T. Shimoboji, C. Long, A. Chilkoti, G. Ghen, J. M. Harris and A. S. Hoffman, Control of protein–ligand recognition using a stimuli-responsive polymer, *Nature*, 1995, **378**, 472-474.

193. J. M. Paloni, E. A. Miller, H. D. Sikes and B. D. Olsen, Improved Ordering in Low Molecular Weight Protein–Polymer Conjugates Through Oligomerization of the Protein Block, *Biomacromolecules*, 2018, **19**, 3814-3824.

194. C. K. Wong, A. J. Laos, A. H. Soeriyadi, J. Wiedenmann, P. M. Curmi, J. J. Gooding, C. P. Marquis, M. H. Stenzel and P. Thordarson, Polymersomes prepared from thermoresponsive fluorescent protein–polymer bioconjugates: capture of and report on drug and protein payloads, *Angew. Chem. Int. Ed.*, 2015, **54**, 5317-5322.

195. D. Bontempo, K. L. Heredia, B. A. Fish and H. D. Maynard, Cysteine-reactive polymers synthesized by atom transfer radical polymerization for conjugation to proteins, *J. Am. Chem. Soc.*, 2004, **126**, 15372-15373.

196. N. Fishkin, E. K. Maloney, R. V. Chari and R. Singh, A novel pathway for maytansinoid release from thioether linked antibody–drug conjugates (ADCs) under oxidative conditions, *Chem. Commun.*, 2011, **47**, 10752-10754.

197. S. C. Alley, D. R. Benjamin, S. C. Jeffrey, N. M. Okeley, D. L. Meyer, R. J. Sanderson and P. D. Senter, Contribution of linker stability to the activities of anticancer immunoconjugates, *Bioconjug. Chem.*, 2008, **19**, 759-765.

198. J. F. Ponte, X. Sun, N. C. Yoder, N. Fishkin, R. Laleau, J. Coccia, L. Lanieri, M. Bogalhas, L. Wang and S. Wilhelm, Understanding how the stability of the thiol-maleimide linkage impacts the pharmacokinetics of lysine-linked antibody–maytansinoid conjugates, *Bioconjug. Chem.*, 2016, **27**, 1588-1598.

199. S. Averick, O. Karácsony, J. Mohin, X. Yong, N. M. Moellers, B. F. Woodman, W. Zhu, R. A. Mehl, A. C. Balazs and T. Kowalewski, Cooperative, Reversible Self-Assembly of Covalently Pre-Linked Proteins into Giant Fibrous Structures, *Angew. Chem. Int. Ed.*, 2014, **53**, 8050-8055.

200. H. Cho, T. Daniel, Y. J. Buechler, D. C. Litzinger, Z. Maio, A.-M. H. Putnam, V. S. Kraynov, B.-C. Sim, S. Bussell and T. Javahishvili, Optimized clinical performance of growth hormone with an expanded genetic code, *Proc. Natl. Acad. Sci.*, 2011, **108**, 9060-9065.

201. N. Krall, F. P. Da Cruz, O. Boutureira and G. J. Bernardes, Site-selective protein-modification chemistry for basic biology and drug development, *Nat. Chem.*, 2016, **8**, 103-113.

202. C. H. Kim, J. Y. Axup and P. G. Schultz, Protein conjugation with genetically encoded unnatural amino acids, *Curr. Opin. Chem. Biol.*, 2013, **17**, 412-419.

203. K. L. Heredia, G. N. Grover, L. Tao and H. D. Maynard, Synthesis of heterotelechelic polymers for conjugation of two different proteins, *Macromolecules*, 2009, **42**, 2360-2367.

204. V. Postupalenko, D. Desplancq, I. Orlov, Y. Arntz, D. Spehner, Y. Mely, B. P. Klaholz, P. Schultz, E. Weiss and G. Zuber, Protein delivery system containing a nickel-immobilized polymer for multimerization of affinity-purified his-tagged proteins enhances cytosolic transfer, *Angew. Chem. Int. Ed.*, 2015, **54**, 10583-10586.

205. H. Y. Cho, M. A. Kadir, B.-S. Kim, H. S. Han, S. Nagasundarapandian, Y.-R. Kim, S. B. Ko, S.-G. Lee and H.-j. Paik, Synthesis of well-defined (nitrilotriacetic acid)-end-functionalized polystyrenes and their bioconjugation with histidine-tagged green fluorescent proteins, *Macromolecules*, 2011, **44**, 4672-4680.

206. D. Duret, Z. Haftek-Terreau, M. Carretier, C. Ladavière, M.-T. Charreyre and A. Favier, Fluorescent RAFT polymers bearing a nitrilotriacetic acid (NTA) ligand at the α-chain-end for the site-specific labeling of histidine-tagged proteins, *Polym. Chem.*, 2017, **8**, 1611-1615.

207. Y. Zhang, K.-Y. Park, K. F. Suazo and M. D. Distefano, Recent progress in enzymatic protein labelling techniques and their applications, *Chem. Soc. Rev.*, 2018, **47**, 9106-9136.

208. E. A. Peterson and H. A. Sober, Chromatography of proteins. I. Cellulose ion-exchange adsorbents, *J. Am. Chem. Soc.*, 1956, **78**, 751-755.

209. A. B. Prescott, CERTAIN DISTINCT ADVANCES IN THE ANALYTICAL CHEMISTRY OF RECENT YEARS, *J. Am. Chem. Soc.*, 1893, **15**, 376-379.

210. D. Walls, R. McGrath and S. T. Loughran, *A digest of protein purification*, Springer, 2011.

211. M. Li, P. De, H. Li and B. S. Sumerlin, Conjugation of RAFT-generated polymers to proteins by two consecutive thiol–ene reactions, *Polym. Chem.*, 2010, **1**, 854-859.

212. S. Kulkarni, C. Schilli, B. Grin, A. H. Müller, A. S. Hoffman and P. S. Stayton, Controlling the aggregation of conjugates of streptavidin with smart block copolymers prepared via the RAFT copolymerization technique, *Biomacromolecules*, 2006, **7**, 2736-2741.

213. S. Tengattini, Chromatographic Approaches for Purification and Analytical Characterization of Extracellular Vesicles: Recent Advancements, *Chromatographia*, 2018, 1-10.

214. T. Yoshida, T. Ishidome and R. Hanayama, High Purity Isolation and Sensitive Quantification of Extracellular Vesicles Using Affinity to TIM4, *Curr. Protoc. Cell Biol.*, 2017, **77**, 1-18.

215. J. Porath, J. Carlsson, I. Olsson and G. Belfrage, Metal chelate affinity chromatography, a new approach to protein fractionation, *Nature*, 1975, **258**, 598-599.

216. R. C. F. Cheung, J. H. Wong and T. B. Ng, Immobilized metal ion affinity chromatography: a review on its applications, *Appl. Microbiol. Biotechnol.*, 2012, **96**, 1411-1420.

217. F. H. Arnold, Metal-affinity separations: a new dimension in protein processing, *Nat. Biotechnol.*, 1991, **9**, 151-156.

218. E. Sulkowski, The saga of IMAC and MIT, *Bioessays*, 1989, **10**, 170-175.

219. J. Porath, Immobilized metal ion affinity chromatography, *Protein Expression Purif.*, 1992, **3**, 263-281.

220. E. Hochuli, H. Döbeli and A. Schacher, New metal chelate adsorbent selective for proteins and peptides containing neighbouring histidine residues, *J. Chromatogr.*, 1987, **411**, 177-184.

221. Y. Zhao, L. Gutshall, H. Jiang, A. Baker, E. Beil, G. Obmolova, J. Carton, S. Taudte and B. Amegadzie, Two routes for production and purification of Fab fragments in biopharmaceutical discovery research: papain digestion of mAb and transient expression in mammalian cells, *Protein Expression Purif.*, 2009, **67**, 182-189.

222. S. Sakamoto, F. Taura, R. Tsuchihashi, W. Putalun, J. Kinjo, H. Tanaka and S. Morimoto, Expression, purification, and characterization of anti-plumbagin single-chain variable fragment antibody in Sf9 insect cell, *Hybridoma*, 2010, **29**, 481-488.

223. F. Maisano, S. A. Testori and G. Grandi, Immobilized metal-ion affinity chromatography of human growth hormone, *J. Chromatogr.*, 1989, **472**, 422-427.

224. Z. Zhang, K.-T. Tong, M. Belew, T. Pettersson and J.-C. Janson, Production, purification and characterization of recombinant human interferon γ, *J. Chromatogr.*, 1992, **604**, 143-155.

225. E. Ueda, P. Gout and L. Morganti, Ni (II)-based immobilized metal ion affinity chromatography of recombinant human prolactin from periplasmic Escherichia coli extracts, *J. Chromatogr.*, 2001, **922**, 165-175.

226. R. R. Prasanna and M. A. Vijayalakshmi, Characterization of metal chelate methacrylate monolithic disk for purification of polyclonal and monoclonal immunoglobulin G, *J. Chromatogr.*, 2010, **1217**, 3660-3667.

227. J. E. Hale and D. E. Beidler, Purification of humanized murine and murine monoclonal antibodies using immobilized metal-affinity chromatography, *AnBio*, 1994, **222**, 29-33.

228. J. Porath and B. Olin, Immobilized metal affinity adsorption and immobilized metal affinity chromatography of biomaterials. Serum protein affinities for gel-immobilized iron and nickel ions, *Biochemistry*, 1983, **22**, 1621-1630.

229. S. Jain and M. N. Gupta, Purification of goat immunoglobulin G by immobilized metal-ion affinity using cross-linked alginate beads, *Biotechnol. Appl. Biochem.*, 2004, **39**, 319-322.

230. G. Serpa, E. F. P. Augusto, W. M. S. C. Tamashiro, M. B. Ribeiro, E. A. Miranda and S. M. A. Bueno, Evaluation of immobilized metal membrane affinity chromatography for purification of an immunoglobulin G1 monoclonal antibody, *J. Chromatogr. B*, 2005, **816**, 259-268.

231. P. Audebert, F. Miomandre, G. Clavier, M. C. Vernieres, S. Badré and R. Meallet-Renault, Synthesis and properties of new tetrazines substituted by heteroatoms: towards the world's smallest organic fluorophores, *Chem. Eur. J.*, 2005, **11**, 5667-5673.

232. T. Kim, J. Castro, A. Loudet, J.-S. Jiao, R. Hochstrasser, K. Burgess and M. Topp, Correlations of structure and rates of energy transfer for through-bond energy-transfer cassettes, *J. Phys. Chem. A*, 2006, **110**, 20-27.

233. N. K. Devaraj, S. Hilderbrand, R. Upadhyay, R. Mazitschek and R. Weissleder, Bioorthogonal turn-on probes for imaging small molecules inside living cells, *Angew. Chem.*, 2010, **122**, 2931-2934.

234. Y. Lee, W. Cho, J. Sung, E. Kim and S. B. Park, Monochromophoric Design Strategy for Tetrazine-Based Colorful Bioorthogonal Probes with a Single Fluorescent Core Skeleton, *J. Am. Chem. Soc.*, 2017, **140**, 974-983.

235. J. Farinas and A. Verkman, Receptor-mediated targeting of fluorescent probes in living cells, *J. Biol. Chem.*, 1999, **274**, 7603-7606.

236. J. C. Carlson, L. G. Meimetis, S. A. Hilderbrand and R. Weissleder, BODIPY–tetrazine derivatives as superbright bioorthogonal turn-on probes, *Angew. Chem. Int. Ed.*, 2013, **52**, 6917-6920.

237. L. G. Meimetis, J. C. Carlson, R. J. Giedt, R. H. Kohler and R. Weissleder, Ultrafluorogenic Coumarin–Tetrazine Probes for Real-Time Biological Imaging, *Angew. Chem.*, 2014, **126**, 7661-7664.

238. A. Wieczorek, T. Buckup and R. Wombacher, Rigid tetrazine fluorophore conjugates with fluorogenic properties in the inverse electron demand Diels–Alder reaction, *Org. Biomol. Chem.*, 2014, **12**, 4177-4185.

239. A. Wieczorek, P. Werther, J. Euchner and R. Wombacher, Green-to far-red-emitting fluorogenic tetrazine probes–synthetic access and no-wash protein imaging inside living cells, *Chem. Sci.*, 2017, **8**, 1506-1510.

240. G. Knorr, E. Kozma, A. Herner, E. A. Lemke and P. Kele, New Red-Emitting Tetrazine-Phenoxazine Fluorogenic Labels for Live-Cell Intracellular Bioorthogonal Labeling Schemes, *Chem. Eur. J.*, 2016, **22**, 8972-8979.

241. G. Knorr, E. Kozma, J. M. Schaart, K. Németh, G. r. Török and P. t. Kele, Bioorthogonally Applicable Fluorogenic Cyanine-Tetrazines for No-Wash Super-Resolution Imaging, *Bioconjug. Chem.*, 2018, **29**, 1312-1318.

242. J. Schmitt, H. Hess and H. G. Stunnenberg, Affinity purification of histidine-tagged proteins, *Mol. Biol. Rep.*, 1993, **18**, 223-230.

243. J. Crowe, H. Dobeli, R. Gentz, E. Hochuli, D. Stiiber and K. Henco, *6xHis-ni-nta chromatography as a superior technique in recombinant protein expression/purification*, Springer, 1994.

244. G. Moad, E. Rizzardo and S. H. Thang, Living radical polymerization by the RAFT process, *Aust. J. Chem.*, 2005, **58**, 379-410.

245. C. Boyer, V. Bulmus, T. P. Davis, V. Ladmiral, J. Liu and S. Perrier, Bioapplications of RAFT polymerization, *Chem. Rev.*, 2009, **109**, 5402-5436.

246. D. Pissuwan, C. Boyer, K. Gunasekaran, T. P. Davis and V. Bulmus, In vitro cytotoxicity of RAFT polymers, *Biomacromolecules*, 2010, **11**, 412-420.

247. A. B. Lowe and C. L. McCormick, *RAFT polymerization in homogeneous aqueous media: initiation systems, RAFT agent stability, monomers and polymer structures*, Wiley, 2008.

248. G. Moad, E. Rizzardo and S. H. Thang, Radical addition–fragmentation chemistry in polymer synthesis, *Polymer*, 2008, **49**, 1079-1131.

249. R. B. Merrifield, Solid phase peptide synthesis. I. The synthesis of a tetrapeptide, *J. Am. Chem. Soc.*, 1963, **85**, 2149-2154.

250. C. J. Ferguson, R. J. Hughes, B. T. Pham, B. S. Hawkett, R. G. Gilbert, A. K. Serelis and C. H. Such, Effective ab initio emulsion polymerization under RAFT control, *Macromolecules*, 2002, **35**, 9243-9245.

251. T. Kelen and F. TÜd s, Analysis of the linear methods for determining copolymerization reactivity ratios. I. A new improved linear graphic method, *J. Macromal. Sci. A*, 1975, **9**, 1-27.

252. M. Schuster, C. Turecek, B. Kaiser, J. Stampfl, R. Liska and F. Varga, Evaluation of biocompatible photopolymers I: Photoreactivity and mechanical properties of reactive diluents, *J. Macromal. Sci. A*, 2007, **44**, 547-557.

253. H.-S. Cho, K. Mason, K. X. Ramyar, A. M. Stanley, S. B. Gabelli, D. W. Denney Jr and D. J. Leahy, Structure of the extracellular region of HER2 alone and in complex with the Herceptin Fab, *Nature*, 2003, **421**, 756-760.

254. K. A. Majorek, P. J. Porebski, A. Dayal, M. D. Zimmerman, K. Jablonska, A. J. Stewart, M. Chruszcz and W. Minor, Structural and immunologic characterization of bovine, horse, and rabbit serum albumins, *Mol. Immunol.*, 2012, **52**, 174-182.

255. A. B. Nepomnyashchii, A. J. Pistner, A. J. Bard and J. Rosenthal, Synthesis, photophysics, electrochemistry and electrogenerated chemiluminescence of PEG-modified BODIPY dyes in organic and aqueous solutions, *J. Phys. Chem. C Nanomater. Interfaces*, 2013, **117**, 5599-5609.

256. P.-H. Tseng, Y.-C. Wang, S.-C. Weng, J.-R. Weng, C.-S. Chen, R. W. Brueggemeier, C. L. Shapiro, C.-Y. Chen, S. E. Dunn and M. Pollak, Overcoming trastuzumab resistance in HER2-overexpressing breast cancer cells by using a novel celecoxib-derived phosphoinositide-dependent kinase-1 inhibitor, *Mol. Pharmacol.*, 2006, **70**, 1534-1541.

257. X. Bao, J. Duan, X. Fang and J. Fang, Chemical modifications of the (1→ 3)-α-D-glucan from spores of Ganoderma lucidum and investigation of their physicochemical properties and immunological activity, *Carbohydr. Res.*, 2001, **336**, 127-140.

258. J. D. Wallat, K. A. Rose and J. K. Pokorski, Proteins as substrates for controlled radical polymerization, *Polym. Chem.*, 2014, **5**, 1545-1558.

259. E. Kaiser, R. Colescott, C. Bossinger and P. Cook, Color test for detection of free terminal amino groups in the solid-phase synthesis of peptides, *Anal. Biochem.*, 1970, **34**, 595-598.

260. F. M. Pfeffer, P. E. Kruger and T. Gunnlaugsson, Anion recognition and anion-mediated self-assembly with thiourea-functionalised fused [3] polynorbornyl frameworks, *Org. Biomol. Chem.*, 2007, **5**, 1894-1902.

261. S. Cannon-Carlson and J. Tang, Modification of the Laemmli sodium dodecyl sulfate–polyacrylamide gel electrophoresis procedure to eliminate artifacts on reducing and nonreducing gels, *Anal. Biochem.*, 1997, **246**, 146-148.